

Technical Notes

Amperometric Sensing at High Temperature with a “Wired” Thermostable Glucose-6-phosphate Dehydrogenase from *Aquifex aeolicus*

Ramesh Iyer,[†] Valeri Pavlov,[‡] Ioanis Katakis,^{*,†} and Leonidas G. Bachas^{*,†}

Department of Chemistry, University of Kentucky, Lexington, Kentucky 40506-0055, and Bioengineering and Bioelectrochemistry Group, Chemical Engineering, Universitat Rovira i Virgili, Carretera de Salou s/n 43006 Tarragona, Spain

An amperometric enzyme sensor capable of operating at high temperatures was developed by utilizing a “wired” thermostable glucose-6-phosphate dehydrogenase (tG6PDH) from the hyperthermophilic bacterium *Aquifex aeolicus*. The response of the system was monitored through detection of the product of the enzymatic reaction, NADH, which was electrocatalytically reoxidized to NAD by a thermostable redox mediator, osmium (1,10-phenanthroline-5,6-dione)₂-poly(4-vinylpyridine), at $E_{app} = +150$ mV vs Ag/AgCl/KCl_{sat}. The enzyme was “wired” onto the surface of graphite electrodes by using an epoxy-based poly(ethylene glycol) diglycidyl ether cross-linker. The stability of the sensor at higher temperatures clearly surpassed the conventional system utilizing a mesophilic G6PDH (mG6PDH) from *Leuconostoc mesenteroides*. The mG6PDH-based system lost 26% of its response after 20 min at 50 °C. The response of the tG6PDH-based system remained unchanged under the same conditions. The tG6PDH-based system demonstrated excellent stability up to a temperature of 83 °C.

Enzymes isolated from thermophilic microorganisms, termed thermostable or thermophilic enzymes, have received a lot of attention because of their ability to catalyze biological reactions at high temperature.^{1–3} Thermostable enzymes not only withstand heat but also typically resist denaturation in the presence of organic solvents and detergents.⁴ From an application perspective, such thermostable enzymes are attractive because of their remarkable stability, thereby increasing the operational and storage stability of the devices that incorporate them. One of the most important advances in biotechnology during the last two decades is the development of the polymerase chain reaction

(PCR).^{5,6} *Thermus aquaticus* DNA polymerase (*Taq* DNA polymerase) was the first thermostable DNA polymerase characterized^{7,8} and facilitated the automation of PCR. Biosensors is another area that could greatly benefit from the availability of a stable biological component. For example, thermostable enzymes have been employed in biosensing systems for the determination of compounds such as phenol and asparagine using thermostable phenol hydroxylase and thermostable asparaginase, respectively,^{9,10} and for assaying analytes such as glucose and lactate by a coupled-enzyme system utilizing a thermostable soybean peroxidase.¹¹

Dehydrogenases are used in electrochemical biosensing systems for a wide variety of analytes. The detection of analytes in amperometric systems employing dehydrogenases is based on the signal generated by oxidation of the cofactor NADH or NADPH at the electrode surface. However, the direct electrochemical oxidation of NAD(P)H on conventional electrodes requires high overpotentials^{12,13} necessitating the use of “mediators” to facilitate the hydride transfer. This becomes more challenging with dehydrogenases from thermophilic sources, as they require a mediator capable of operating at elevated temperatures.

Thermostable glutamate dehydrogenase and a polymeric toluidine blue O mediator have been used for the amperometric detection of glutamate at temperatures up to 60 °C.¹⁴ The system was optimized using carbon paste electrodes in batch mode and further developed for flow injection analysis.¹⁵ The oxygen-

* Corresponding authors. (L.B.) Tel: 859-257-6350. Fax: 859-323-1069. E-mail: bachas@uky.edu. (I.K.) Tel: +34 977 55 9655. Fax: +34 977 55 9667. E-mail: ikatakis@etse.urv.es.

[†] University of Kentucky.

[‡] Universitat Rovira i Virgili.

(1) Adams, M. W. W.; Kelly, R. M. *Chem. Eng. News* **1995**, (51), 73, 32–42.
(2) Horikoshi, K. *Curr. Opin. Biotechnol.* **1995**, 6, 292–297.
(3) Hough, D. W.; Danson, M. J. *Curr. Opin. Chem. Biol.* **1999**, 3, 39–46.
(4) D'Auria, S.; Barone, R.; Rossi, M.; Nucci, R.; Barone, G.; Fessas, D.; Bertoli, E.; Tanfani, F. *Biochem. J.* **1997**, 323, 833–840.

(5) Saiki, R. K.; Gelfand, D. H.; Stoffel, S.; Scharf, S. J.; Higuchi, R.; Horn, G. T.; Mullis, K. B.; Erlich, H. A. *Science* **1988**, 239, 487–491.
(6) Mullis, K.; Faloona, F.; Scharf, S.; Saiki, R.; Horn, G.; Erlich, H. *Cold Spring Harbor Symp. Quantum Biol.* **1986**, 51, 263–273.
(7) Kaledin, A. S.; Sliusarenko, A. G.; Gorodetskii, S. I. *Biokhimiia* **1980**, 45, 644–651.
(8) Chien, A.; Edgar, D. B.; Trela, J. M. *J. Bacteriol.* **1976**, 127, 1550–1557.
(9) Li, J.; Wang, J.; Bachas, L. G. *Anal. Chem.* **2002**, 74, 3336–3341.
(10) Metzger, J.; Reiss, M.; Hartmeier, W. *Biosens. Bioelectron.* **1998**, 13, 1077–1082.
(11) Kenausis, G.; Chen, Q.; Heller, A. *Anal. Chem.* **1997**, 69, 1054–1060.
(12) Jaegfeldt, H. *J. Electroanal. Chem. Interfacial Electrochem.* **1980**, 110, 295–302.
(13) Samec, Z.; Elving, P. J. *J. Electroanal. Chem. Interfacial Electrochem.* **1983**, 144, 217–234.
(14) Jeffries, C.; Pasco, N.; Baronian, K.; Gorton, L. *Biosens. Bioelectron.* **1997**, 12, 225–232.

independent thermostable diaphorase from *Bacillus stearothermophilus* and thermostable NADH oxidase from *Thermus aquaticus* were used for amperometric NADH determination¹⁶ or were coupled with dehydrogenases in the design of sensing systems for a variety of analytes.^{17,18} The mediation was carried out by ferrocene-based compounds, but the sensors were not evaluated at temperatures of >25 °C. Although, there has been a considerable amount of research on mediators that can effectively recycle NADH/NADPH at the electrode surface,¹⁹ most currently available mediators have poor stability at elevated temperatures. Therefore, mediator stability is, presumably, one of the obstacles in the development of thermostable dehydrogenase based biosensor.

Herein, we report an amperometric enzyme electrode utilizing a “wired” thermostable glucose-6-phosphate dehydrogenase (tG6PDH) from *Aquifex aeolicus*, for the determination of glucose 6-phosphate. To address mediator stability, we have used a novel redox mediator, osmium (1,10-phenanthroline-5,6-dione)₂-poly(4-vinylpyridine) (Osphendione-PVP), for the electrocatalytic oxidation of NADH. The mediator was immobilized on oxidized graphite electrodes where the phendione moiety allows for shuttling electrons between the graphite electrode and NADH. Enzyme immobilization was achieved by cross-linking the amine groups of lysine residues with an epoxy-based poly(ethylene glycol) diglycidyl ether (PEGDGE) cross-linker. The performance of the system was compared to a system utilizing the glucose-6-phosphate dehydrogenase from the mesophilic microorganism *Leuconostoc mesenteroides*.

EXPERIMENTAL SECTION

Chemicals. Glucose-6-phosphate dehydrogenase from the mesophile, *L. mesenteroides* (mG6PDH), glucose 6-phosphate, and β-nicotinamide adenine dinucleotide (NAD) were purchased from Sigma (St. Louis, MO). PEGDGE and poly(4-vinylpyridine) (MW 40 000) were purchased from Polysciences (Warrington, PA). Graphite rods (3 mm in diameter) were purchased from Carbone of America (Bay City, MI). All other reagents were of analytical grade. Deionized distilled water was obtained from a Milli-Q system (Millipore, Milford, MA). The isolation and purification of tG6PDH from *A. aeolicus* is described elsewhere.²⁰ The synthesis of the bromoethylamine-modified poly(4-vinylpyridine) (binder polymer) has been published.²¹

Synthesis of Osmium (1,10-Phenanthroline-5,6-dione)₂-Poly(4-vinylpyridine) Mediator. The mediator was synthesized by refluxing a mixture of 80 mg of [Os(1,10-phenanthroline-5,6-dione)₂Cl₂] and 50 mg of poly(4-vinylpyridine) in 3 mL of ethylene glycol under argon in darkness for 1 h at 220 °C. The reaction mixture was cooled to room temperature and was added to 100 mL of aqueous 1 M NaCl over a period of 15 min. After cooling the mixture overnight at 4 °C, the resulting precipitate was filtered, washed with water, and air-dried. The UV spectrum of Osphen-

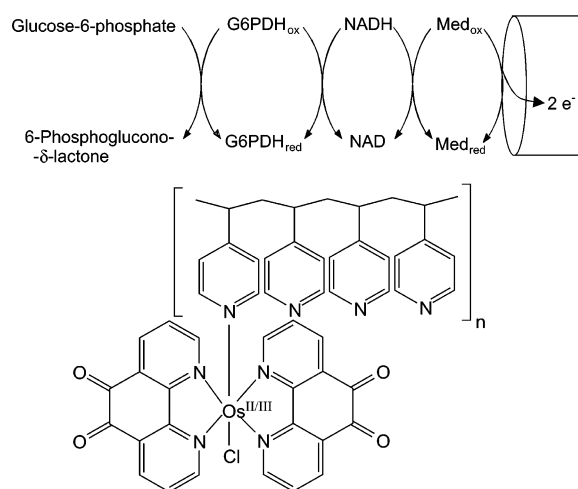


Figure 1. Reaction scheme for the mediated electrodes and chemical structure of the Osphendione-PVP mediator. The counterions necessary for charge balance are not shown (presumably, there is an additional one or two chlorine counterions depending on whether osmium is in the +2 or +3 oxidation state, respectively).

dione-PVP in ethylene glycol showed peaks due to the osmium complex at 361 and 467 nm and the pyridine backbone-dependent peaks at 250 and 298 nm. The proposed structure of the resulting redox polymer is shown in Figure 1. Anal. Calcd: C, 61.52%; H, 1.76%; N, 10.99%. Found: C, 61.71%; H, 1.70%; N, 10.7%.

Preparation of Electrodes. A graphite rod was wet polished on fine (grit 400 and 600) emery paper. The bars were cleaned by sonication for 5 min in water and oxidized by applying a potential of 1 V versus Ag/AgCl/KCl_{sat} during 30 s in 0.100 M NaH₂PO₄/HCl, 0.500 M NaCl, pH 7.00. The electrodes were washed with water and dried at 60 °C for 10 min. A volume of 1.0 μL of 1.8 mg/mL Osphendione-PVP in ethylene glycol was deposited per electrode and washed with 30 μL of ethylene glycol and plenty of water. The sensing layer was prepared by placing on each graphite electrode 5.0 μL of the mixture composed of 50 μL of 10 mg/mL binder polymer solution, 4.0 mg of NAD, 16.6 μL of 6.75 mg/mL PEGDGE aqueous solution, and 68 μL of tG6PDH (20 units/mL at 70 °C) or 83 μL of mesophilic G6PDH (40 units/mL at 25 °C) in 0.100 M NaH₂PO₄/HCl, 0.500 M NaCl, pH 7.00. The electrode was dried at room temperature under vacuum for 24 h.

Measurements. Electrochemical experiments were performed using a PAR 273 potentiostat and model 270 software (EG&G Princeton Applied Research, Princeton, NJ). All measurements were performed using a water-jacketed electrochemical cell in 2.0 mL of 0.100 M NaH₂PO₄/HCl, 0.500 M NaCl, pH 7.00. Cyclic voltammetry (CV) measurements were carried out in a conventional three-electrode electrochemical cell. Ag/AgCl/KCl_{sat} and a platinum wire served as reference and counter electrode, respectively. Chronoamperometry experiments were performed at an applied potential of +150 mV versus Ag/AgCl/KCl_{sat}. To evaluate the effect of temperature on biosensor response, the electrodes were heated from room temperature to 83 °C, while current densities were monitored at fixed intervals. All pH values are at room temperature, unless otherwise stated.

RESULTS AND DISCUSSION

Dehydrogenases are a class of enzymes that catalyze a wide variety of reactions that are useful in biosensors/diagnostics and

- (15) Pasco, N.; Jeffries, C.; Davies, Q.; Downard, A. J.; Roddick-Lanzilotta, A. D.; Gorton, L. *Biosens. Bioelectron.* **1999**, *14*, 171–178.
- (16) Compagnone, D.; McNeil, C. J.; Athey, D.; Ilio, C. D.; Guilbault, G. G. *Enzyme Microb. Technol.* **1995**, *17*, 472–475.
- (17) Antiochia, R.; Cass, A. E. G.; Palleschi, G. *Anal. Chim. Acta* **1997**, *345*, 17–28.
- (18) McNeil, C. J.; Spoor, J. A.; Cocco, D.; Cooper, J. M.; Bannister, J. V. *Anal. Chem.* **1989**, *61*, 25–29.
- (19) Katakis, I.; Dominguez, E. *Mikrochim. Acta* **1997**, *126*, 11–32.
- (20) Iyer, R. B.; Wang, J.; Bachas, L. G. *Extremophiles* **2002**, *6*, 283–289.
- (21) Katakis, I. Ph.D. Dissertation, The University of Texas, Austin, 1994.

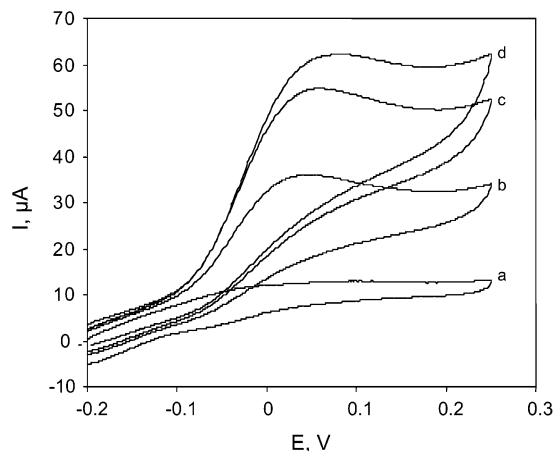


Figure 2. Cyclic voltammograms of immobilized Osphendione–PVP at 70 °C in 0.100 M $\text{Na}_2\text{HPO}_4/\text{HCl}$, 0.500 M NaCl, pH 7.00 containing (a) no NADH (b) 2.4 mM NADH (c) 4.7 mM NADH, and (d) 6.9 mM NADH. Scan rate 30 mV/s. Potentials vs Ag/AgCl/KCl_{sat}.

biotransformation applications. Industrial processes that require high temperature could benefit from the use of on-line sensors based on thermostable enzymes, which could potentially not only operate at elevated temperatures but also be resistant to organic solvents, detergents, and other denaturants. To establish the feasibility of using dehydrogenases from extremophiles in sensors, an amperometric biosensing system utilizing a thermostable glucose-6-phosphate dehydrogenase was employed. The system is based on the mediated oxidation of NADH, produced by G6PDH, by a thermostable mediator, osmium (1,10-phenanthroline-5,6-dione)₂–poly(4-vinylpyridine) immobilized on the electrode surface (Figure 1). For the purposes of comparison, parallel experiments were performed using a G6PDH from a mesophilic microorganism, *L. mesenteroides*.²²

The *gsdA* gene encoding for glucose-6-phosphate dehydrogenase from the hyperthermophilic bacterium, *A. aeolicus* was cloned and expressed as a fusion protein in *Escherichia coli*. The fusion protein contained a polyhistidine tail to facilitate purification to homogeneity by affinity chromatography. The characteristics of the recombinant enzyme have been previously described.²⁰ In brief, the enzyme has been found to be a dimer with a subunit molecular weight of 55 000. The enzyme exhibited dual coenzyme specificity, though it showed a preference in terms of k_{cat}/K_M of 20-fold for NADP over NAD at 40 °C and 5.7-fold at 70 °C. *A. aeolicus* G6PDH had an optimum temperature for catalytic activity at 90 °C.

Cyclic voltammograms of the mediator were pH dependent, with a formal standard potential of +38.7 mV versus Ag/AgCl/KCl_{sat} at pH 6.00. The peak-to-peak potential separation (ΔE_p) was 57.5 mV for the scan rate of 50 mV/s. The response of the mediator to increasing concentrations of NADH was studied at 70 °C (Figure 2). Cyclic voltammograms obtained showed a dramatic increase of the anodic peak currents in the presence of NADH at 70 °C, demonstrating the thermostability and strong electrocatalytic effect of the Osphendione complex.

The steady-state kinetics of the immobilized tG6PDH was measured amperometrically at a working potential of +150 mV versus Ag/AgCl/KCl_{sat} at 70 °C (Figure 3). The immobilized

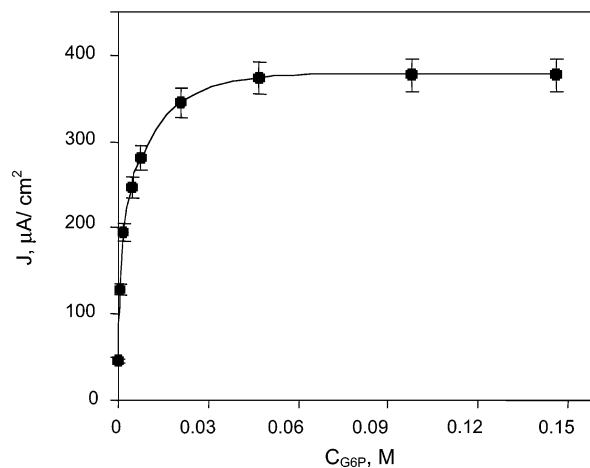


Figure 3. Calibration curve for tG6PDH-based biosensing system in 0.100 M $\text{Na}_2\text{HPO}_4/\text{HCl}$, 0.500 M NaCl containing 30 mM NAD, pH 6.80 at 70 °C. $E_{\text{app}} = +150$ mV vs Ag/AgCl/KCl_{sat}. Y-axis values represent current density, J .

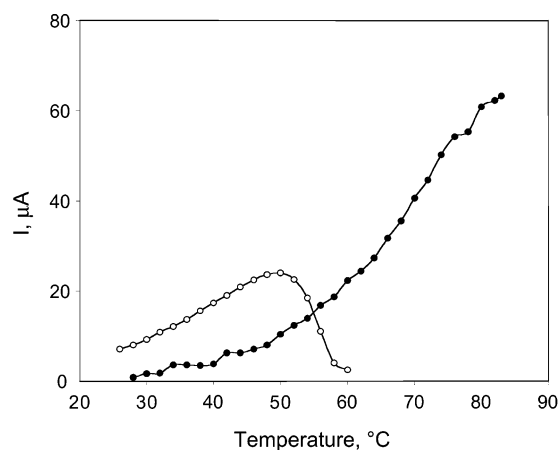


Figure 4. Response curve of tG6PDH (filled circles) and mG6PDH (open circles) biosensors as a function of temperature.

tG6PDH showed classic Michaelis–Menten kinetics with a K_M of 2.9 mM for glucose 6-phosphate ($K_M = 0.18$ mM in homogeneous solution).²⁰ The current densities, J , at 0.05 M glucose 6-phosphate reached a plateau of 390 $\mu\text{A}/\text{cm}^2$ at 70 °C. The mG6PDH-based system had an apparent K_M of 6.1 mM ($K_M = 0.069$ mM in homogeneous solution at 25 °C).²² Biosensors based on tG6PDH exhibited a detection limit of 2×10^{-4} M ($S/N = 3$) and had a working range of 6×10^{-4} – 2×10^{-2} M. Since the system showed maximum current densities at 0.05 M G6P concentration, this concentration was used for further stability studies.

The most important characteristic of thermostable enzymes is their ability to operate at higher temperatures for extended periods of time. Figure 4 shows the effect of temperature on the response for both electrodes. The biosensing system based on tG6PDH showed clear catalytic activity even at 83 °C. An Arrhenius plot of the data presented in Figure 4 for the immobilized enzyme gave an activation energy of 63.7 kJ/mol (40–80 °C). The system based on mG6PDH showed an optimum activity at 50 °C, after which there was a steady drop in current densities due to enzyme denaturation. The operational stability of the tG6PDH and mG6PDH systems was measured at 50 °C. The mG6PDH-based system lost 26% of response after 20 min at

(22) Lee, W. T.; Levy, H. R. *Protein Sci.* **1992**, *1*, 329–334.

50 °C, whereas the tG6PDH system retained 100% activity under the same conditions.

Although the osmium (1,10-phenanthroline-5,6-dione)₂-poly-(4-vinylpyridine) mediator appears to have higher than usual stability at elevated temperatures compared to other polymeric mediators, repetitive CVs at 60 °C demonstrated that a small amount of the osmium (less than 10%) was lost after repetitive scanning at this temperature. However, when CVs were taken before and after the sensor was exposed to NAD(H), the loss of the phenanthroline peak was higher. Therefore, it appears that loss in redox mediation is somehow linked to the presence of NAD(H) catalysis, probably due to side reactions with free radicals.²³ Despite this, when assembled as a biosensor, the tG6PDH system exhibited an operational half-life of 2 h at 60 °C, whereas the mG6PDH-based system showed no activity at this temperature.

(23) Pavlov, V.; Rincón, O.; Solé, S.; Narváez, A.; Domínguez, E.; Katakis, I., in preparation.

In conclusion, an amperometric biosensor for G6P based on a recombinant tG6PDH from *A. aeolicus* was developed. The sensor was based on the electrocatalytic oxidation of NADH at the electrode transducer using a thermostable Osphenanthroline-PVP mediator. The system showed excellent mediation at temperatures as high as 83 °C at a working potential of +150 mV versus Ag/AgCl/KCl_{sat}. The scheme of mediation reported here should be applicable to over 250 dehydrogenases that use the cofactors β -nicotinamide adenine dinucleotide and β -nicotinamide adenine dinucleotide phosphate (NADP).

Note Added after ASAP. The axis lettering on Figures 2–4 was misaligned. The figures were corrected, and the article was replaced on the Web on June 17, 2003.

Received for review November 9, 2002. Accepted April 29, 2003.

AC026298O

Professor Ioanis Katakis
Institute of Chemistry
Chemical Engineering School
University Rovira i Virgili
Campus Sescelades, Av. Paisos Catalans 26
43007 Tarragona, Spain
Tel +34 977 55 9655
Fax +34 977 55 9667
E-mail: ioanis.katakis@urv.net

January 15, 2005

Dear Prof. Murray,

We resubmit the full article "New Reagentless Glutamate Biosensors Based on Mesophilic and Thermophilic Glutamate Dehydrogenases" to Analytical Chemistry after changing its length.

The paper describes two general new methods for the fabrication of reagentless biosensors. These methods yielded glutamate biosensors based on NAD(P)(+) dependent mesophilic bovine glutamate dehydrogenase and thermophilic glutamate dehydrogenases from *Pyrococcus furiosus*. These biosensors were fully characterized and a mathematical kinetic model was developed and applied to determine the rate limiting step in their response to glutamate. Comparative operational stability studies of the biosensors based on mesophilic and thermophilic enzymes demonstrated the advantage of the thermophilic enzyme over the mesophilic one at elevated temperatures. The comparative shelf stability study also demonstrated the advantage of the usage of the thermophilic enzyme for the fabrication of biosensors.

A list of potential reviewers for the paper is enclosed.
Thank you in advance for your cooperation.

With best wishes,

Sincerely yours,

Ioanis Katakis

The list of potential reviewers:

List of potential reviewers

Professor Elisabeth Csoregi
Biotechnology and Analytical Chemistry
Lund University
S-221 00 Lund, Sweden
Tel: 46-46-222 4274
Fax: 46-46-222 4713
E-mail: Elisabeth.Csoregi@biotek.lu.se
E.Csoregi@biotek.lu.se

Name: Richard

Family name: Luxton
Faculty of Applied Sciences Frenchay Campus
University of the West of England
Coldharbour Lane Bristol BS16 1QY
United Kingdom
Tel: 0117 328 2472
Fax: 0117 328 2904
E-Mail: richard.luxton@uwe.ac.uk

Professor Paulino Tunon Blanco
Departamento de Quimica Fisica y Analitica,
Universidad de Oviedo
Oviedo, Asturias, Spain 33006
Phone: +34-985103480, 985103482 & 985103487.
Fax: +34-985103125.
E-mail: ptb@fluor.quimica.uniovi.es

Professor Ioanis Katakis
Institute of Chemistry
Chemical Engineering School
University Rovira i Virgili
Campus Sescelades, Av. Paisos Catalans 26
43007 Tarragona, Spain
Tel +34 977 55 9655
Fax +34 977 55 9667
E-mail: ioanis.katakis@urv.net

November 30, 2004

Dear Dr. David G. Whitten

Please find enclosed the paper entitled " The Use of the Lamellar Phase for the Construction of Reagentless Biosensors Based on NAD+ Dependent Glutamate Dehydrogenase" submitted as a full article to Langmuir.

The paper describes the synthesis of a new redox active surfactant for the electrochemical oxidation of NAD(P)H. This surfactant allowed to develop a new general method for the construction of reagentless electrochemical biosensors based on NAD(P)(+) dependent dehydrogenases. The method consists of the immobilization of the lamellar phase composed of the lipid 1,2-dioleoyl-sn-glycero-3-phosphatidylcholine, the redox surfactant, NAD+ and bovine glutamate dehydrogenase on graphite electrodes. As far as we are aware, this is the first example that demonstrates the use of the lamellar phase for the fabrication of reagentless electrochemical biosensors based on NAD(P)(+) dependent dehydrogenases.

We confirm that the manuscript, or its contents in some other form, has not been published previously by any of the authors and/or is not under consideration for publication in another journal at the time of submission.

We hope you will find this paper of interest for Langmuir.
A list of potential reviewers for the paper is enclosed.
Thank you in advance for your cooperation.

With best wishes,

Sincerely yours,

Ioanis Katakis

The list of potential reviewers

Professor Michael Gratzel
Dept de Chimie
Institut de Chimie Physique 2
CH-1015 Lausanne
Switzerland
Tel: +41 21 693 3112/55

Fax: +41 21 693 61 00/90
E-mail: michael.graetzel@epfl.ch

Professor Marco Mascini
Dipartimento Sanita Pubblica,
Epidemiologica e Analitica Ampientale
Sezione di Chimica Analitica
Universita di Firenze
Via Gino Capponi 9
50121 Firenze, Italy
Tel: +39 0552757274
Fax: +39 0552476972
E-mail: mascini@unifi.it

Professor Jean-Louis Marty
Centre of Phytopharmacy
University of Perpignan
URA 5054, 52 Av. de Villeneuve
66860
Perpignan Cedex
France
Tel: +33-4-68-66-22-54
Fax: +33-4-68-66-22-23
E-mail: jlmarty@univ-perp.fr

Dr. Renate Naumann
Max-Planck-Institute for Polymer Research
Ackermannweg 10
55128 Mainz, Germany
Tel: (+49) 6131-379-257
Fax: (+49) 6131-379-100
E-mail: naumannr@mpip-mainz.mpg.de

Professor Lo Gorton
Analytical Chemistry
Lund University
P. O. Box 124
SE-221 00 LUND
Sweden
Telephone: 046-222 75 82
Fax: +46 46 222 45 44
E-mail: lo.gorton@analykem.lu.se

Professor H Ti Tien
Membrane Biophysics Lab
Physiology (Giltner Hall)
Michigan State University
East Lansing, MI 48824
USA
Tel: +1 (517) 355 6475 Ext. 1273
Fax: +1(517) 355-5125
E-mail: tien@msu.edu and TIEN@PSL.MSU.EDU



ELSEVIER

Journal of Electroanalytical Chemistry 464 (1999) 208–214

JOURNAL OF
ELECTROANALYTICAL
CHEMISTRY

Electrocatalytic oxidation of NADH at graphite electrodes modified with osmium phenanthroline dione

Ionel Catalin Popescu^{a,*}, Elena Domínguez^a, Arántzazu Narváez^a, Valeri Pavlov^b, Ioanis Katakis^b

^a Departamento de Química Analítica, Universidad de Alcalá, E-28871 Alcalá de Henares, Madrid, Spain

^b Departament d'Enginyeria Química, Escola Tècnica Superior d'Enginyeria Química, Universitat Rovira i Virgili, E-43006 Tarragona, Catalonia, Spain

Received 5 May 1998; received in revised form 4 January 1999

Abstract

We report here a detailed study concerning the electrochemical behavior of Os(4,4'-dimethyl, 2,2'-bipyridine)₂(1,10-phenanthroline 5,6-dione) complex, adsorbed on spectrographic graphite, and about its electrocatalytic activity for NADH oxidation. Cyclic voltammetric measurements, performed in aqueous phosphate buffer solutions, at different scan rates and pH values, allowed us: (i) to relate the redox response of the *o*-quinone ligand (phendione) to that of the Os(II) central ion; (ii) to confirm that, in aqueous solutions, the phendione based redox process globally involves two electrons and two protons; (iii) to estimate the rate constant for the heterogeneous electron transfer corresponding to the phendione redox couple ($k_s \approx 20.1 \text{ s}^{-1}$). The second order rate constant for electrocatalytic oxidation of NADH ($k_{1,[\text{NADH}] = 0} = 1.9 \times 10^3 \text{ M}^{-1} \text{ s}^{-1}$, at pH 6.1) as well as its pH dependence (from pH 5.5 to 8.1) were evaluated from RDE experiments, using both Koutecky–Levich and Lineweaver–Burk data interpretations. © 1999 Elsevier Science S.A. All rights reserved.

Keywords: NADH; Electrocatalytic oxidation; Os-phendione; Modified electrode

1. Introduction

The mediated electro-oxidation of β -nicotinamide adenine dinucleotide (NADH) is interesting both from the theoretical and practical point of view. Thus, as it was summarized recently [1,2], it appears that depending on the mediator nature this reaction may: (i) involve the formation of an intermolecular complex between NADH and mediator, as in the case of redox dyes [3–9]; (ii) proceed through a net hydride transfer, as for *o*- and *p*-quinones and some aromatic diamines [10–18]; (iii) take place by two one-electron steps with

a proton transfer to the solvent, as for some polyoxometallates [19,20]. The efficient and reversible recycling of NADH is of particular interest in the construction of dehydrogenase based amperometric biosensors because more than 300 enzymes require nicotinamide co-enzymes as cofactors, and in the fine chemicals industry using NAD^+ -dependent biocatalysts.

Since the direct electro-oxidation of NADH on different conventional electrode materials requires high overpotentials [13,21,22], it is desirable to discover efficient electrocatalysts. The major electrochemical configurations already proposed for such catalytic recycling of NADH were examined critically in comprehensive works [1,2,5,23]. Among these mediating schemes, those based on tetracyanoquinodimethane (TCNQ) [24,25] and a phenoxazinium salt (Meldola blue) [3] gave the highest sensitivities and second order rate

* Corresponding author. Fax: +34-91-8854646.

E-mail address: prof.visit@alcala.es (I. Catalin Popescu)

¹ Permanent address. Department of Physical Chemistry, University 'Babes-Bolyai', RO-3400 Cluj-Napoca, Romania.

constants for the NADH mediated electro-oxidation. However, the TCNQ-modified electrode has as a major drawback the high value of applied potential (about +0.4 V vs. Ag | AgCl | KCl_(sat)), while the Meldola blue scheme has a low chemical stability, especially at high pH values.

In this work, based on some early results [26–28] showing that 1,10-phenanthroline-5,6-dione complexes of Os(II) exhibit electrocatalytic activity towards NADH oxidation, we report on a detailed study concerning the electrochemical behavior of Os(4,4'-dimethyl,2,2'-bipyridine)₂(1,10-phenanthroline-5,6-dione) complex (Os-phendione), adsorbed on spectrographic graphite. Thus, cyclic voltammetry, performed under different experimental conditions, was used to characterize the intrinsic electrochemical behavior of the adsorbed mediator. Then, the kinetics of the mediated electro-oxidation of NADH at an Os-phendione modified graphite electrode were investigated under defined mass transport conditions, using rotating disk electrode experiments.

2. Experimental

2.1. Chemicals

β -Nicotinamide adenine dinucleotide (NADH) was purchased from Sigma (St. Louis, MO, USA) as the disodium salt. Analytical grade, anhydrous acetonitrile was obtained from SDS (Peypin, France). All other reagents were of analytical grade and used as received. Water was obtained by means of a Milli-Q system (Millipore, Milford, MA, USA).

The Os(4,4'-dimethyl, 2,2'-bipyridine)₂(1,10-phenanthroline 5,6-dione) (Os-phendione) complex was synthesized according to procedures published earlier [26,29] and isolated finally as the PF₆⁻ salt form, which is insoluble in water.

2.2. Preparation of Os-phendione modified electrodes

A spectrographic graphite rod (Ringsdorff-Werke, GmbH, Bonn-Bad Godesberg, Germany), of ca. 3 mm diameter, was wet polished on fine (grit 400 and 600) emery paper (Buehler, Lake Bluff, IL, USA). Then, a graphite piece of suitable length was washed carefully with deionized water, dried, and finally press-fitted into a Teflon holder in order to obtain a graphite electrode having a flat circular surface of ca. 0.071 cm², in contact with the solution.

The modified graphite electrodes were obtained by spreading onto the electrode surface 1 μ l of 2 mM Os-phendione solution in acetonitrile, and leaving them for 20 min at room temperature to evaporate the solvent. Before immersion in the test solution the

modified electrodes were washed carefully with deionised water. For each electrode, the surface coverage was estimated from the under-peak areas (corresponding to the phendione ligand), recorded during the cyclic voltammetry measurements, and considering as 2 the number of exchanged electrons [30].

2.3. Electrochemical measurements

Cyclic voltammetry (CV) measurements were carried out in a conventional three electrode electrochemical cell. Ag | AgCl | KCl_(sat) and a coiled Pt wire served as reference and counter electrodes, respectively. The cell was connected to a computer-controlled BAS CV-50W voltammetric analyzer (Bioanalytical Systems, West Lafayette, IN, USA). As noticed, by changing the distance between the working and reference electrode, the uncompensated resistance in solution was negligible.

Steady state amperometric measurements at different rotating speeds of the working electrode were performed using a modulated speed rotator (model AMS-FRX, Pine, Grove City, PA, USA) and the same spectrographic graphite as the disk material. The current intensity-time data were collected using the already mentioned voltammetric analyzer. After the RDE experiments the surface coverage was checked by CV and found to be within $\pm 10\%$ of the initial value.

The supporting electrolyte was a 0.1 M phosphate buffer containing 0.15 M NaCl. The pH was adjusted in the interval 3 to 8 using the appropriate NaOH or H₃PO₄ solutions. For all measurements the solutions were deaerated by nitrogen bubbling for 15 min.

3. Results and discussion

3.1. Electrochemical behavior of the Os-phendione complex adsorbed on spectrographic graphite

The electrochemical behavior of free 1,10-phenanthroline 5,6-dione (phenidone) [26,30–32,35–37] as well as complexed with Ni(II), Co(II), Zn(II) [31–33] or with Cr(III), Fe(III), Ni(II), Co(II), Cu(I), Cu(II), Os(II) and Ru(II) [26,27,34–37] has retained the interest of many researchers. Globally, it has been established that the phendione voltammetric response presents one or two distinct, quasi-reversible and pH dependent waves, in protic or aprotic solvents, respectively [26,27,30–32,35–37], shows a positive shift of the half wave potential due to the divalent metal's complexation [26,31,33,37], exhibits a loss of ligand electroactivity due to the proton or metal cations binding to the pyridine nitrogen sites [35,36] and is affected strongly by the solubility and adsorption differences existing between oxidized and reduced forms of the free ligand and the complex [37].

In a protic solvent the two-electron two-proton reduction, characteristic of the quinone moiety, is evidenced on the corresponding voltammogram by a single wave [26,27,30–32]. In accordance with this, the cyclic voltammogram recorded in an aqueous phosphate buffer solution for the Os-phendione complex adsorbed on the surface of a graphite electrode (Fig. 1) presents also one wave for the phendione ligand, with a formal standard potential of +0.08 V versus $\text{Ag}|\text{AgCl}|\text{KCl}_{(\text{sat})}$ at pH 6.0. At a scan rate of 50 mV s^{-1} , the peak separation ($\Delta E_p = 54 \text{ mV}$), the ratio of the peak current intensities ($I_{\text{pa}}/I_{\text{pc}} = 1.02$) and the full width at half maximum ($E_{\text{FWHM}} = 100 \text{ mV}$ for the anodic peak and 120 mV for the cathodic one) indicate that it is a quasi-reversible voltammetric wave, and reveal the presence of some repulsive interactions between the adsorbed species [38,39]. Moreover, as expected for surface confined redox active species [40] the cyclic voltammograms recorded at low potential scan rates ($2\text{--}25 \text{ mV s}^{-1}$) showed a linear dependence of the peak currents, corresponding to the phendione wave, on the electrode potential scan rate.

The ratio between the phendione and Os(III/II) integrated peaks, corrected for the background current, offers an indirect way to estimate the number of electrons exchanged in the phendione oxido-reduction process. For example, at pH 7, these ratios, and consequently the number of electrons, were found 2.0 ± 0.2 and 2.1 ± 0.1 for the anodic and cathodic peaks, respectively (the results are the average of four independent measurements for the phendione wave, $E^{0'} = +0.032 \text{ V}$ vs. $\text{Ag}|\text{AgCl}|\text{KCl}_{(\text{sat})}$, and for the Os(III/II) wave, $E^{0'} = +0.703 \text{ V}$ vs. $\text{Ag}|\text{AgCl}|\text{KCl}_{(\text{sat})}$).

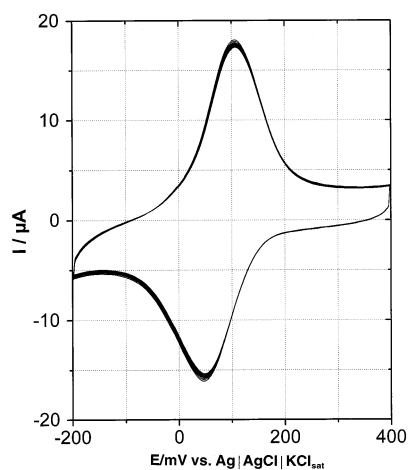


Fig. 1. Consecutive cyclic voltammograms for phendione of the Os-phendione complex, adsorbed on spectrographic graphite. Experimental conditions: starting potential, +400 mV vs. $\text{Ag}|\text{AgCl}|\text{KCl}_{(\text{sat})}$; scan rate, 50 mV s^{-1} ; deoxygenated, 0.1 M phosphate buffer, pH 6.0; number of cycles = 10.

In order to check the stability of the system, the potential of the modified electrode was cycled continuously over the range of -0.2 to $+0.4 \text{ V}$ and the resulting voltammograms were recorded (for convenience, in Fig. 1 only the first ten cycles are shown). A progressive decrease of the anodic and cathodic peak intensity was observed with a tendency towards a lower limit, while the voltammogram shape remained invariant. This behavior proves the good electrochemical stability of the Os-phendione complex, in the potential range used for the NADH recycling, and a relatively strong adsorption on the graphite surface.

As expected for the redox behavior of a compound containing a quinone moiety, the redox potential of the complexed phendione (estimated as the average of cathodic and anodic peak potentials) was pH-dependent, according to the reaction:



where OsQ, OsQH₂ denote the Os complexed phendione and its reduced form, respectively. The pH range explored was restricted deliberately to between 3 and 8 because of the phendione chemical instability [33] at pH values higher than 8, and of NADH hydrolysis in acid solutions [28,41]. The slope of the regression line, $E^{0'}/\text{V} = 0.383 - 0.049 \times \text{pH}$, ($r = 0.998$; $n = 11$), estimated from the experimental data in the pH range investigated, does not agree with the theoretical value for a redox process involving an equal number of electrons and protons. However, taking into account the acid–base behavior of the hydroquinone/quinone functionality of the phendione ligand, the best fit between the calculated and the experimental data was obtained when the corresponding pK_a value was taken as 6.3. Thus, the regression equation becomes: $E^{0'}/\text{V} = 0.429 - 0.0591 \times \text{pH} + 0.029 \times \log[1 + 10^{-(6.3 - \text{pH})}]$. In this context it is worth mentioning that from the pH dependence of the formal standard potential for the free phendione, dissolved in a partial aqueous solvent (50% dimethylsulfoxide), it was established [30] that the quinone form is unprotonated, while the hydroquinone one exhibits a pK_a of 9.0. This acid shift observed for the pK_a of complexed phendione is consistent with the positive shift (+185 mV, at pH 7) of the formal redox potential of the phendione induced by Os complexation, and with the similar behavior reported previously for divalent metals [26,31,33,37]. This phenomenon possibly also explains the higher stability of the phendione ligand when complexed, compared to the free ligand oxidation.

Using the treatment proposed by Laviron [42], from the variation of the peak potentials with the potential scan rate, the heterogeneous electron transfer rate constant (k_s) for the phendione redox process was estimated. Within experimental error, this rate constant appeared to be independent of pH, in the pH range

(6.5–8) used for NADH mediated electro-oxidation. At pH 6.5, the average value for k_s (20.1 s^{-1}) was higher than that reported for Meldola blue (10 s^{-1}) [3] and of the same order of magnitude as those measured recently for dihydroxybenzaldehyde redox active films [43,44]. Based on the electrochemical behavior of the graphite adsorbed Os-phendione complex, it is concluded that this is electrochemically a quasi-reversible redox couple, involving two electrons and two protons (at $\text{pH} < 6.3$) and having good chemical reversibility in aqueous solutions, a fact that makes it suitable for use as an NADH electro-oxidation catalyst.

3.2. Electrocatalytic oxidation of NADH at an Os-phendione modified graphite electrode

Many compounds containing quinone moieties have been shown previously to be active electrocatalysts for NADH oxidation (for a detailed discussion see [1,2,23,45]). However, it was stressed [1] that these mediators, due to their intrinsic reactivity, can be a source of side reactions that might eventually limit the efficiency and life time of the mediating system. Recently, a new strategy was demonstrated [26–28] that consists of the complexation of a quinoid structure with a transition metal. Due to the supposed higher stability of the radicals involved in the NADH oxidation with such complexes, an improved electrocatalytic activity and stability are expected to be achieved.

Fig. 2(A) shows the phendione cyclic voltammograms obtained for a graphite electrode modified with Os-phendione, in the absence and in the presence of NADH. A dramatic enhancement of the anodic peak currents, associated with the progressive diminishing of the cathodic one, when the NADH concentration was increased, proves the strong electrocatalytic effect of the Os-phendione complex. At pH 7, the catalytic peak was found at +60 mV versus $\text{Ag}|\text{AgCl}|\text{KCl}_{(\text{sat})}$, a significantly lower value compared to the uncatalyzed electro-oxidation of NADH, reported for bare graphite electrodes: +410 mV versus SCE [14] or +550 mV versus SCE [21,46]. Consequently, the decrease of the NADH electro-oxidation overvoltage, due to the electrocatalytic activity of the Os-phendione complex, is greater than 400 mV.

A qualitative estimation of the response rate and signal stability, due to the mediating configuration investigated, is furnished by the rotating disk electrode (RDE) results presented in Fig. 2(B). It can be noticed that, after a change of the electrode rotation speed, the new steady state is reached in less than 10 s.

The sensitivity of the Os-phendione-modified NADH sensor, for stationary ($13.2 \text{ mA M}^{-1} \text{ cm}^{-2}$) as well as for rotating disk electrode ($55.6 \text{ mA M}^{-1} \text{ cm}^{-2}$), estimated from the slope of the linear part of the current intensity versus NADH concentration plot, indicates

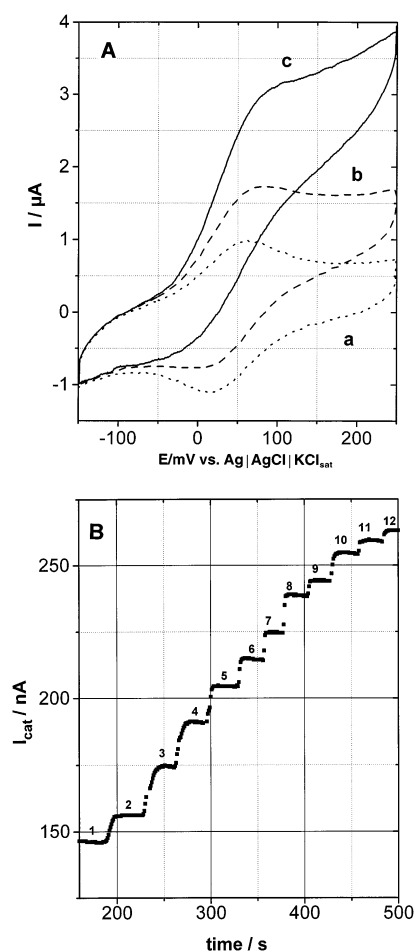


Fig. 2. Electrocatalytic oxidation of NADH on Os-phendione modified graphite electrode: (A) Cyclic voltammetry of modified electrodes: (a) in buffer; (b) in 0.5 mM of NADH; (c) in 2.0 mM of NADH. (B) Steady state current intensity response at increasing rotation speeds for an Os-phendione modified graphite rotating disk electrode. Experimental conditions: (A) surface coverage, $2.2 \times 10^{-10} \text{ mol cm}^{-2}$; scan rate, 10 mV s^{-1} ; starting potential, +250 mV vs. $\text{Ag}|\text{AgCl}|\text{KCl}_{(\text{sat})}$; deoxygenated, 0.1 M phosphate buffer, pH 7.0; (B) rotation speed; (1) 10 rpm; (2) 15 rpm; (3) 25 rpm; (4) 45 rpm; (5) 75 rpm; (6) 115 rpm; (7) 215 rpm; (8) 415 rpm; (9) 815 rpm; (10) 1615 rpm; (11) 2615 rpm; (12) 3615 rpm; surface coverage, $2.3 \times 10^{-10} \text{ mol cm}^{-2}$; applied potential, +200 mV vs. $\text{Ag}|\text{AgCl}|\text{KCl}_{(\text{sat})}$; 0.1 mM NADH; deoxygenated, 0.1 M phosphate buffer, pH 7.0.

that the Os-phendione/graphite configuration is among the most sensitive configurations for NADH detection (for comparison see table 1 from Ref. [1] and table 5 from Ref. [2]).

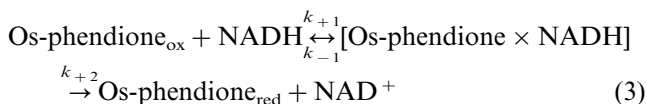
Kinetic measurements of NADH electrocatalytic oxidation at Os-phendione modified graphite electrodes were performed at different NADH concentrations and pH values, using the RDE technique. In all cases, in order to have a global electrode process controlled by the chemical reaction between NADH and the mediator, the applied potential was taken more positive by 120 mV [4] than the actual value of the formal standard potential of the Os-phendione mediator. The well behaved mixed control (diffusional–kinetic), characteris-

tic for the system investigated, is exemplified by the Levich plot (Fig. 3), obtained at pH 6.1, in the NADH concentration range from 0.04 to 2.28 mM, and for rotation speeds from 10 to 3615 rpm.

Based on the hypothesis that a substrate-mediator complex is involved in the mechanism of NADH electrocatalytic oxidation (Michaelis–Menten kinetic model), a general equation describing the dependence of the catalytic current (I_{cat}) on the experimental parameters was proposed [3,4]:

$$\frac{1}{I_{\text{cat}}} = \frac{1}{(nF\Gamma k_{+2})} + \left[\frac{K_{\text{M}}}{(nF\Gamma k_{+2})} + \frac{1}{(0.62nFAD^{2/3}\nu^{-1/6}\omega^{1/2})} \right] \frac{1}{(1/c_{\text{NADH}})} \quad (2)$$

where $K_{\text{M}} = (k_{-1} + k_{+2})/k_{+1}$, D ($\text{cm}^2 \text{s}^{-1}$) represents the diffusion coefficient of NADH, ν ($\text{cm}^2 \text{s}^{-1}$) the hydrodynamic viscosity, ω (rad s^{-1}) the rotational speed, and c_{NADH} (mol cm^{-3}) the NADH concentration. It is worth mentioning, that it is more convenient to replace the product $nF\Gamma$ by the coulometric charge, obtained experimentally as an average value from the integration of the anodic and cathodic peaks corresponding to the mediator voltammetric wave [44]. The rate constants, k_{-1} , k_{+1} and k_{+2} , appear in the following reaction scheme



In Table 1 are shown the results of the RDE measurements, treated according to both variants proposed [3–5] for the estimation of the relevant kinetic param-

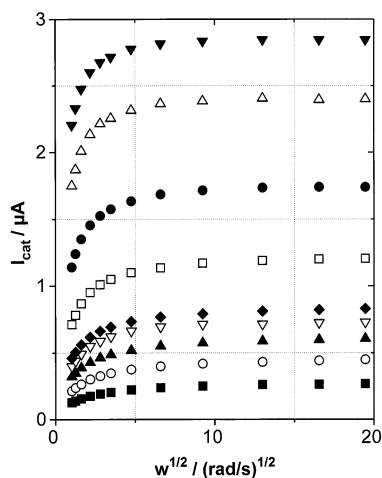


Fig. 3. Levich plot of the steady state electrocatalytic response for an Os-phendione modified graphite RDE at different NADH concentrations (0.04 mM (■), 0.08 mM (○), 0.12 mM (▲), 0.16 mM (▽), 0.20 mM (◆), 0.36 mM (□), 0.68 mM (●), 1.30 mM (△), 2.28 mM (▼). Experimental conditions: surface coverage, 2.6×10^{-10} mol cm^{-2} ; applied potential, +200 mV vs. Ag|AgCl|KCl_{sat.}; deoxygenated, 0.1 M phosphate buffer, pH 6.1.

eters K_{M} and k_{+2} : (i) the so called ‘Koutecky–Levich’ (KL) interpretation, in fact a $1/I_{\text{cat}}$ versus $\omega^{-1/2}$ plot at a constant NADH concentration; (ii) the so called ‘Lineweaver–Burk’ (LB) interpretation, which is a $1/I_{\text{cat}}$ versus $1/c_{\text{NADH}}$ plot at constant rotational speed.

In order to compare the values provided by the two variants of data treatment, the same experimental data set was used. It was not surprising to notice that both procedures gave practically the same result for k_{+2} , but different values for K_{M} (Table 1). The discrepancy can be explained if it is observed that, in the K_{M} calculation according to the KL treatment only the linear regression intercepts are involved, while in the LB procedure both linear regression parameters are used. Moreover, examining the partial results for both data treatments, shown in Table 1, it can be stated that due to the better precision, reflected by the smaller standard deviations of the linear regression parameters, the KL method of data treatment is preferable.

Because of the strong dependence of the second order reaction constant (k_1 , $\text{M}^{-1} \text{s}^{-1}$) for the NADH mediated electro-oxidation on the NADH concentration, defined for the above mentioned reaction scheme, it is unsuitable for a comparison of the catalytic efficiency for different mediating schemes. That is why it was proposed [3] to use its extrapolated value to zero NADH concentration ($k_{1,[\text{NADH}]=0}$), estimated as the k_{+2}/K_{M} ratio. In Table 2 are presented the $k_{1,[\text{NADH}]=0}$ calculated values for the Os-phendione based mediating configuration, measured at different pH values (from 5.5 to 7.0). As was reported previously for phenoxazine derivatives [5] and 3,4-dihydroxybenzaldehyde (3,4-DHB) electropolymerized films [44], the $k_{1,[\text{NADH}]=0}$ values decrease significantly as the pH increases. In our case the estimated value for $k_{1,[\text{NADH}]=0}$ at pH 7.0 is roughly 30 times lower than the corresponding value for Meldola blue ($2.7 \times 10^4 \text{ M}^{-1} \text{s}^{-1}$, at pH 7.0) [3] and a quarter of the value ($4.3 \times 10^3 \text{ M}^{-1} \text{s}^{-1}$, at pH 7.0) reported for a glassy carbon electrode covered by a 3,4-DHB film [44].

In this context, is it interesting to remark that, within experimental error and in spite of the inherent differences between the systems compared (for example the surface coverage of the electrodes), a surprisingly good agreement is observed between the heterogeneous electron transfer rate constants for the two mediators compared (Os-phendione $k_s = 20.1 \text{ s}^{-1}$, pH 6.5–8.0; 3,4-DHB $k_s = 25 \text{ s}^{-1}$, at pH 7.0). Moreover, it was observed that the linear correlation between E^0 and $\log k_{1,[\text{NADH}]=0}$, found by Gorton [5] for some phenoxazine derivatives, extends to the 3,4-DHB and Os-phendione mediators too (Fig. 4) [The corresponding linear regression equation is: $\log k_{1,[\text{NADH}]=0} = 2.97 + 0.0059 \times E^0$ with the correlation coefficient $r = 0.994$]. Once more, it appears that the electrocatalytic efficiency of different systems used for NADH oxidation is con-

Table 1
Results of data interpretation for electrocatalytic NADH oxidation at an Os-phendione modified RDE ($\Gamma = 2.6 \times 10^{-10}$ mol cm $^{-2}$; pH 6.1)

| [NADH]/mM | Linear regression parameters | | | k_{+2}/s^{-1} | K_M/mM | $10^6 D_{NADH}/cm^2 s^{-1}$ |
|---|------------------------------|-----------------------------|-----------|-------------------|-------------------|-----------------------------|
| | A/s_A | B/s_B | r/n^a | | | |
| <i>'Koutecky–Levich' interpretation</i> | | | | | | |
| 0.04 | $0.00353/3 \times 10^{-5}$ | $0.00457/6 \times 10^{-5}$ | 0.9992/12 | | | |
| 0.08 | $0.002101/7 \times 10^{-6}$ | $0.00264/2 \times 10^{-5}$ | 0.9998/12 | | | |
| 0.12 | $0.001582/7 \times 10^{-6}$ | $0.00159/1 \times 10^{-5}$ | 0.9996/12 | | | |
| 0.16 | $0.00128/1 \times 10^{-5}$ | $0.00123/3 \times 10^{-5}$ | 0.9980/12 | | | |
| 0.20 | $0.001153/3 \times 10^{-6}$ | $0.001042/6 \times 10^{-6}$ | 0.9998/12 | 0.80 ^b | 0.43 ^b | 4.2 ^c |
| 0.36 | $0.000792/5 \times 10^{-6}$ | $0.00061/1 \times 10^{-5}$ | 0.9982/12 | | | |
| 0.68 | $0.000554/3 \times 10^{-6}$ | $0.000322/8 \times 10^{-6}$ | 0.9972/12 | | | |
| 1.30 | $0.000403/3 \times 10^{-6}$ | $0.000171/6 \times 10^{-6}$ | 0.9930/12 | | | |
| 2.28 | $0.000342/2 \times 10^{-6}$ | $0.000110/4 \times 10^{-6}$ | 0.9918/12 | | | |
| <i>'Lineweaver–Burk' interpretation</i> | | | | | | |
| $\omega/rad s^{-1}$ | | | | | | |
| 1.05 | $0.00041/7 \times 10^{-5}$ | $0.254/6 \times 10^{-3}$ | 0.9982/9 | | | |
| 1.57 | $0.00038/6 \times 10^{-5}$ | $0.232/4 \times 10^{-3}$ | 0.9987/9 | | | |
| 2.62 | $0.00036/5 \times 10^{-5}$ | $0.206/4 \times 10^{-3}$ | 0.9985/9 | | | |
| 4.71 | $0.00035/4 \times 10^{-5}$ | $0.181/4 \times 10^{-3}$ | 0.9987/9 | | | |
| 7.85 | $0.00035/4 \times 10^{-5}$ | $0.165/3 \times 10^{-3}$ | 0.9986/9 | | | |
| 12.0 | $0.00035/4 \times 10^{-5}$ | $0.155/3 \times 10^{-3}$ | 0.9986/9 | | | |
| 22.5 | $0.00036/4 \times 10^{-5}$ | $0.141/3 \times 10^{-3}$ | 0.9982/9 | 0.75 ^d | 0.39 ^e | 6.1 ^e |
| 45.5 | $0.00036/4 \times 10^{-5}$ | $0.131/3 \times 10^{-3}$ | 0.9979/9 | | | |
| 85.3 | $0.00036/4 \times 10^{-5}$ | $0.124/3 \times 10^{-3}$ | 0.9979/9 | | | |
| 169.1 | $0.00038/4 \times 10^{-5}$ | $0.118/4 \times 10^{-3}$ | 0.9979/9 | | | |
| 273.8 | $0.00038/4 \times 10^{-5}$ | $0.116/3 \times 10^{-3}$ | 0.9970/9 | | | |
| 378.6 | $0.00038/4 \times 10^{-5}$ | $0.115/3 \times 10^{-3}$ | 0.9975/9 | | | |

^a r , Correlation coefficient; n , number of experiments.

^b Estimated from dependence of 'K–L' plot intercepts on $1/[NADH]$ $Y = 0.00034 + 0.146 \times [NADH]^{-1}$ ($r = 0.9961$; $n = 8$).

^c Estimated from dependence of 'K–L' plot slopes on $1/[NADH]$ $Y = 8.3 \times 10^{-6} + 0.204 \times [NADH]^{-1}$ ($r = 0.9976$; $n = 8$).

^d Estimated from the average (36.5 ± 1.2 nA $^{-1}$) of 'L–B' intercepts.

^e Estimated from the 'L–B.' slope dependence on $\omega^{-1/2}$. $Y = 0.1071 + 0.159 \times \omega^{-1/2}$ ($r = 0.9997$; $n = 11$).

trolled strongly by the thermodynamic driving force for electron exchange. This observation would point to the direction that the limits of molecular engineering for synthesis of more efficient NADH oxidation electrocatalysts have not been explored fully.

4. Conclusions

The Os(4,4'-dimethyl, 2,2'-bipyridine) $_2$ (1,10-phenanthroline 5,6-dione) complex is adsorbed strongly on graphite surfaces. Its quasi-reversible electrochemical behavior in aqueous solutions involves two electrons and two protons, with an apparent heterogeneous rate constant ($k_s \approx 20.1$ s $^{-1}$)

The adsorbed Os-phendione complex oxidises NADH reversibly and the electrochemical analysis provides evidence that a charge transfer complex is involved in the NADH oxidation mechanism that is apparently controlled by the thermodynamic driving force for electron exchange [5].

The electrocatalytic activity, a good electrochemical

stability and the high responses observed show that this is an advantageous strategy for NADH electrocatalytic oxidation. Taking into account that in our previous study [28] it was also shown that the resulting NAD $^+$ is enzymatically active, it can be stated that the Os-phendione based configuration fulfils well the expected conditions for a successful mediating scheme for the construction of NAD $^+$ -dependent dehydrogenase electrodes. For such electrodes to be reagentless, the coimmobilization of the enzymes, the Osphendione mediator and NAD $^+$ is now being attempted.

Table 2
pH dependence of the rate constant for the NADH electrocatalytic oxidation at an Os-phendione modified graphite electrode (Koutecky–Levich interpretation)

| 10^{10} Surface coverage/ mol cm $^{-2}$ | pH | $10^{-3}k_{1,[NADH]=0}/$ M $^{-1}$ s $^{-1a}$ |
|---|-----|--|
| 2.3 | 5.5 | 3.1 |
| 2.6 | 6.1 | 1.9 |
| 2.4 | 7.0 | 0.9 |

^a Extrapolated value for zero NADH concentration.

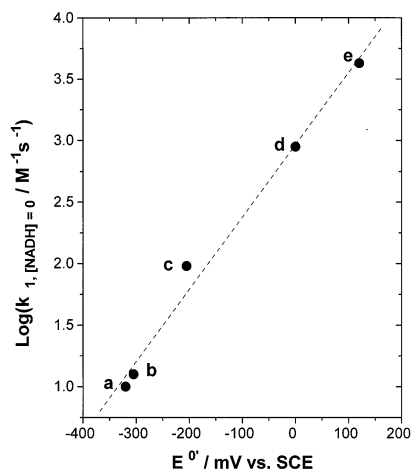


Fig. 4. Dependence of $\text{Log}(k_{1,[\text{NADH}]=0})$ on the formal standard potential (E^0) for some phenoxazine dyes: ethyl capri blue, methyl capri blue and galloycyanine (a–c) [5], Os-phendione (d) and 3,4-dihydroxybenzaldehyde electropolymerized film (e) [44]. The mediators were adsorbed on graphite (a–d), or deposited on glassy carbon (e). All rate constants were measured at pH 7. Dashed line represents the least-squares fit.

Acknowledgements

Financial support from CICYT (BIO97-1204-CO2) is acknowledged gratefully. I.C.P. acknowledges financial support from the University of Alcalá for a Visiting Professorship, and for a NATO scholarship. A.N. and V.P. acknowledge scholarships from the Spanish Ministry of Education and Culture (AP95 08986441), and the Department of Chemical Engineering of ‘Rovira i Virgili’ University, respectively.

References

- [1] I. Katakis, E. Domínguez, *Mikrochim. Acta* 126 (1997) 11.
- [2] M.J. Lobo, A.J. Miranda, P. Tuñón, *Electroanalysis* 9 (1997) 191.
- [3] L. Gorton, A. Torstensson, H. Jaegfeldt, G. Johansson, *J. Electroanal. Chem.* 161 (1984) 103.
- [4] L. Gorton, G. Johansson, A. Torstensson, *J. Electroanal. Chem.* 196 (1985) 81.
- [5] L. Gorton, *J. Chem. Soc. Faraday Trans. 1* 82 (1986) 1245.
- [6] F. Ni, H. Feng, L. Cotton, T.M. Cotton, *Langmuir* 6 (1990) 66.
- [7] B. Persson, *J. Electroanal. Chem.* 287 (1990) 61.
- [8] B. Persson, L. Gorton, *J. Electroanal. Chem.* 292 (1990) 115.
- [9] E. Katz, T. Lötzbeyer, D.D. Schlereth, W. Schuhmann, H.-L. Schmidt, *J. Electroanal. Chem.* 373 (1994) 189.
- [10] A. Kitani, Y.-H. So, L.L. Miller, *J. Am. Chem. Soc.* 103 (1981) 7636.
- [11] B.W. Carlson, L.L. Miller, *J. Am. Chem. Soc.* 107 (1985) 479.
- [12] L.L. Miller, J.R. Valentine, *J. Am. Chem. Soc.* 110 (1988) 3982.
- [13] H. Jaegfeldt, *J. Electroanal. Chem.* 110 (1980) 295.
- [14] H. Jaegfeldt, T. Kuwana, G. Johansson, *J. Am. Chem. Soc.* 105 (1983) 1805.
- [15] C.A. Coleman, J.G. Rose, C.J. Murray, *J. Am. Chem. Soc.* 114 (1992) 9755.
- [16] S. Fukuzumi, Y. Kando, T. Tanaka, *J. Chem. Soc. Perkin Trans. II* (1984) 673.
- [17] S. Fukuzumi, N. Nishizawa, T. Tanaka, *J. Org. Chem.* 49 (1984) 3571.
- [18] S. Fukuzumi, N. Ishikawa, T. Tanaka, *J. Chem. Soc. Perkin Trans. II* (1989) 1811.
- [19] K. Esssaadi, B. Keita, L. Nadjo, *J. Electroanal. Chem.* 367 (1994) 275.
- [20] B. Keita, K. Esssaadi, L. Nadjo, M. Desmadril, *Chem. Phys. Lett.* 237 (1995) 411.
- [21] J. Moiroux, P.J. Elving, *Anal. Chem.* 50 (1978) 1056.
- [22] Z. Samec, P.J. Elving, *J. Electroanal. Chem.* 144 (1983) 217.
- [23] P.N. Bartlett, P. Tebbutt, R.G. Whitaker, *Prog. React. Kinet.* 16 (1991) 55.
- [24] A.S.N. Murthy, A. Gupta, R.L. Gupta, *Bioelectrochem. Bioenerg.* 33 (1994) 71.
- [25] A.S.N. Murthy, A. Gupta, R.L. Gupta, *Anal. Chim. Acta* 289 (1994) 43.
- [26] C.A. Goss, H.D. Abruña, *Inorg. Chem.* 24 (1985) 4263.
- [27] Q. Wu, M. Maskus, F. Pariente, F. Tobalina, V.M. Fernández, E. Lorenzo, H.D. Abruña, *Anal. Chem.* 68 (1996) 3688.
- [28] M. Hedenmo, A. Narváez, E. Domínguez, I. Katakis, *Analyst* 121 (1996) 1891.
- [29] E. Amouyal, A. Homsí, J.-C. Chambron, J.-P. Sauvage, *J. Chem. Soc. Dalton Trans.* (1990) 1841.
- [30] D.H. Evans, D.A. Griffith, *J. Electroanal. Chem.* 134 (1982) 301.
- [31] T.S. Eckert, T.C. Bruice, J.A. Gainor, S.M. Weinreb, *Proc. Natl. Acad. Sci. USA* 79 (1982) 2533.
- [32] T.S. Eckert, T.C. Bruice, *J. Am. Chem. Soc.* 105 (1983) 4431.
- [33] D.H. Evans, D.A. Griffith, *J. Electroanal. Chem.* 136 (1982) 149.
- [34] G. Hilt, E. Steckhan, *J. Chem. Soc. Chem. Commun.* (1993) 1706.
- [35] Y. Lei, F.C. Anson, *J. Am. Chem. Soc.* 117 (1995) 9849.
- [36] Y. Lei, C. Shi, F.C. Anson, *Inorg. Chem.* 35 (1996) 3044.
- [37] M. Shi, F.C. Anson, *Anal. Chem.* 70 (1998) 1489.
- [38] E. Laviron, in: A.J. Bard (Ed.), *Electroanalytical Chemistry*, vol. 12, Marcel Dekker, New York, 1982, pp. 54–157.
- [39] R.W. Murray, in: A.J. Bard (Ed.), *Electroanalytical Chemistry*, vol. 13, Marcel Dekker, New York, 1984, pp. 191–368.
- [40] A.J. Bard, L.R. Faulkner, *Electrochemical Methods. Fundamental and Applications*, Wiley, New York, 1980, p. 521.
- [41] H.K. Chenault, G.M. Whitesides, *Appl. Biochem. Biotechnol.* 14 (1987) 147.
- [42] E. Laviron, *J. Electroanal. Chem.* 101 (1979) 19.
- [43] F. Pariente, F. Tobalina, M. Darder, E. Lorenzo, H.D. Abruña, *Anal. Chem.* 68 (1996) 3136.
- [44] F. Pariente, F. Tobalina, G. Moreno, L. Hernandez, E. Lorenzo, H.D. Abruña, *Anal. Chem.* 69 (1997) 4065.
- [45] P.N. Bartlett, P.R. Birkin, E.N.K. Wallace, *J. Chem. Soc. Faraday Trans.* 93 (1997) 1951.
- [46] A. Torstensson, L. Gorton, *J. Electroanal. Chem.* 130 (1981) 199.

°A Novel [Os(1,10-phenanthroline-5,6-dione)₂(PVP)₄Cl]Cl Redox Polymer for
Electrocatalytic Oxidation of NADH and its
Application to the Construction of Reagentless
 β -D-glucose Biosensors

*Valeri Pavlov,¹ Óscar Rincón,² Sonia Solé,¹ Arantzazu Narváez,² Elena Domínguez,² Ioanis Katakis^{*1}*

Bioanalysis and Bioelectrochemistry Group, Chemical Engineering, Universitat Rovira i Virgili, E-43006, Tarragona (Catalonia), Spain, and Departamento de Química Analítica, Universidad de Alcalá, E-28871 Alcalá de Henares (Madrid), Spain.

RECEIVED DATE

* To whom the correspondence should be addressed. E-mail: ioanis.katakis@urv.net, Tel: +34 977 55 9655. Fax: +34 977 55 9667.

¹Universitat Rovira i Virgili.

²Universidad de Alcalá.

ABSTRACT. The synthesis and study of the electrochemical behaviour of [Os(1,10-phenanthroline-5,6-dione)2-poly(4-vinylpyridine)4Cl]Cl redox polymer are reported. With cyclic voltammetry in aqueous phosphate buffer solutions at different scan rates and pH values, it was found that in aqueous solutions four protons and four electrons participate in the redox cycling of o-quinone (phendione) and the rate constant for the heterogeneous electron transfer of the phendione redox couple k_s is equal to $18 \pm 2 \text{ s}^{-1}$ at pH 6.0. The electrocatalytic oxidation of β -nicotinamide adenine dinucleotide (NADH) at graphite rotating disk electrodes modified with this redox polymer was studied and the second order rate constants for NADH oxidation $k_{[\text{NADH}] = 0}$ were determined to be $(1.9 \pm 0.2) \times 10^3 \text{ M}^{-1} \text{ s}^{-1}$ at pH 6.0 and $(3.4 \pm 0.3) \times 10^3 \text{ M}^{-1} \text{ s}^{-1}$ at pH 5.0. This novel electroactive polymer was used for the construction of reagentless glucose biosensors whereby NAD^+ and glucose dehydrogenase were immobilized on the graphite electrode surface. Such sensors showed operational lifetimes limited by leaching of NAD^+ .

KEYWORDS. glucose analysis, thermophilic, glutamate dehydrogenase, reagentless biosensors, NAD^+ .

More than 300 enzymes¹ use β -nicotinamide adenine dinucleotide (NAD^+) as a cofactor and therefore the development of methods for electrocatalytic oxidation of NADH attracts a great deal of theoretical and practical interest due to the possibility of applications to the design of biosensors, bioreactors and fuel cells. Despite the fact that the reversible potential for NADH/ NAD^+ couple is -0.56 V vs. SCE ³ direct electrooxidation of NADH at bare electrode surfaces is not convenient because it is not chemically reversible and requires high overpotentials.³

Different strategies to accelerate the kinetics of NADH oxidation were critically examined in comprehensive works,^{4,5} modification of the electrode surface, being one of them. First attempts to carry out such modification include an electrochemical pretreatment of carbon electrodes leading to the formation of surface hydroxyl and quinone groups.⁶ Another set of methods relies on covalent binding and adsorption on the electrode surface of different mediators for NADH oxidation such as *ortho*- and *para*-quinines,^{7,8} *ortho*- and *para*-phenylenediimines,⁹⁻¹⁰ organic conducting salts,¹¹ hydroxysubstituted

phenoxazine,¹² metal complexes containing *o*-quinone ligands.^{13,14} The electrodes modified with small molecules usually suffer from low surface coverage and leaching of the mediator to a bulk solution.

Modification of electrodes with redox polymers is preferable because it can decrease leaching. In addition the catalytic response of polymer-coated electrodes to NADH is much higher than this of a monolayer of immobilized small molecules since polymeric films contain the equivalent of many immobilized monomolecular layers and if all of them remain active, the number of electroactive sites is superior.¹⁵ Three major groups of NADH oxidizing polymers have been reported in the literature.

Polymers made from electropolymerization of monomers without intrinsic mediating properties such as poly(3-methylthiophene).¹⁶ Polymers produced by electropolymerization of monomers with intrinsic mediating properties, for example, poly(thionine),¹⁷ poly(3,4-dihydroxybenzaldehyde).¹⁸ Premade polymers into which mediating functionalities are covalently bound. For instance dopamine attached to poly(methacrylate),¹⁹ Toluidine Blue O connected through various spacers to polyalkane backbones,²⁰ In general most polymeric mediators showed lower rate constants of oxidation of NADH than the corresponding monomers because of “capping” by the polymer backbone of the active redox sites, oriented towards the electrode surface.²¹ The majority of monomeric and polymeric mediators has pH dependent redox potential and rate of interaction with NAD(P)H. Both of them increase when pH decreases because of protons participating in the redox conversion of $\text{NAD(P)}^+/\text{NAD(P)H}$ couple and many mediators facilitate hydride transfer to accepting groups of mediators.

Polymeric mediators proved to adhere more than small molecules to the electrode surface, but inherit from their corresponding monomers low chemical and operational stability. Almost all reported mediators for NAD(P)H oxidation can be used in pH range from 2 to 7 and showed the increased decomposition rate at the pH above 7.0 where the majority of the known NAD(P)^+ dependent dehydrogenases has optimal activity. The complexes of some transition metals with 1,10-phenanthroline-5,6-dione proved to be chemically more stable and more reversible in alkaline media.

The reaction of electrochemical oxidation of NAD(P)H can be coupled with the reaction of enzymatic oxidation by dehydrogenases to yield a great number of possible configurations applicable to the

construction of biosensors, bioreactors and fuel cells. Many electrodes operating in the presence of enzymes, cofactors and mediators in a sample solution have been demonstrated in the literature, but the number of dehydrogenase electrodes which can detect an analyte without addition of any additional reagent to a sample solution, so called reagentless electrodes, is limited.

The most stable biosensors were produced on the basis of a carbon paste in which a “reserve pool” of the coenzyme was created, at the same time their sensitivity was high.²² Unfortunately, it is impossible to opt for carbon paste configurations to fabricate miniaturized sensors.

In the present work we report on an effort to produce reagentless NAD⁺-dehydrogenase electrodes. For this purpose we synthesized a novel NADH oxidizing polymer [Os(1,10-phenanthroline-5,6-dione)₂(PVP)₄Cl]Cl (Os-phendione-PVP), produced by complexation of poly(4-vinylpyridine) with the complex [Os(1,10-phenanthroline-5,6-dione)₂Cl₂]. We also report on the study of the electrochemical behaviour of Os-phendione-PVP adsorbed on spectrographic graphite and on the determination of the kinetics of NADH oxidation at these electrodes. We apply Os-phendione-PVP coated electrodes to the construction of reagentless glucose biosensors using glucose dehydrogenase. Furthermore, we discuss the possible limiting steps for operational stability of such sensors.

RESULTS AND DISCUSSION

Electrochemistry of Os-phendione-PVP. The water insoluble redox polymer was produced by complexation of [Os(1,10-phenanthroline-5,6-dione)₂Cl₂] with poly(4-vinylpyridine) at an 1:4 molar ratio in ethylene glycol (Figure S-1 in Supporting Information). The previous studies of electrochemistry of free 1,10-phenanthroline-5,6-dione^{13,23,24} and its complexes with metals^{13,24} have shown that in a protic solvent they behave as quasi reversible, pH dependent redox couple with two-electrons and two-protons participating in the redox process per phendione moiety. Cyclic voltammetric scans of Os-phendione-PVP adsorbed on a graphite electrode, recorded in aqueous phosphate buffer (Figure 1) have demonstrated one wave with a formal redox potential (E°) (calculated as the average of

cathodic and anodic peaks potentials) of $+38.7 \pm 0.4$ mV vs. Ag/AgCl/KCl_{sat} at the pH 6.0. For scan rate of 50 mV s^{-1} the peak-to-peak potential separation (ΔE_p) was 57.5 ± 0.4 mV, and the ratio I_{pa}/I_{pc} was $=1.1 \pm 0.1$. The voltammetric waves of Os^{II/III} are reversible, the formal standard potential for this redox couple is 407 ± 2 mV as expected for the osmium atom coordinated with two phendione ligands, one pyridine ligand of PVP, and a Cl⁻. Taking into consideration that this couple exchanges only one electron and comparing the peak areas for the phendione/catechol and Os^{II/III} it was estimated that the number of electrons exchanged in phendione is equal to 4.0 ± 0.1 at the pH lower than 6.4. At higher values of the pH the apparent number of electrons cycling decreased (Figure S-2 in Supporting Information), probably, because of the chemical irreversibility of phendione redox couple at pH > 6.4. The stability of Os-phendione-PVP modified graphite electrodes at pH 6.0 was studied by running 50 consecutive cyclic voltammograms with the scan limits from -200 to 600 mV. At the end of this experiment the phendione peak area stabilized after having decreased by 11%, without any change in the voltammogram shape. It seems therefore that a slow desorption of the polymer occurs while the chemical stability of the redox moieties is not affected at these time scales.

The cyclic voltammetry at pH 5.0, 6.0 and 7.0 demonstrated a linear dependence of the anodic (Figure S-3 in Supporting Information) and cathodic (Figure S-4 in Supporting Information) peak currents (I_{pa} and I_{pc}) on scan rate (ν) at scan rates up to 500 mV/s . The plots of I_p versus $\nu^{1/2}$ were not linear at any scan rate range, suggesting that the very thin film of Os-phendione-PVP deposited on the electrodes is strongly adsorbed and there are no electron or proton diffusion processes limiting the electrochemistry. The surface coverage of Os-phendione-PVP on the graphite electrodes was $(6.7 \pm 0.5) \times 10^{-10} \text{ mol cm}^{-2}$.

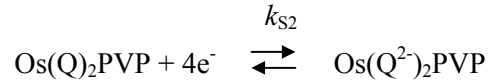
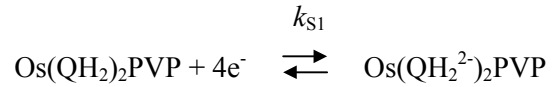
Protons take part in the redox reaction of Os-phendione-PVP according to the following scheme:



where Os(Q)₂PVP and Os(QH₂)₂PVP stand for oxidized and reduced forms of the ligand, respectively. This equation explains why the redox potential of phendione in the electroactive polymer must be pH dependent. The phendione's E^0 , dependence on the value of pH (Figure S-5 in Supporting Information)

was studied by recording cyclic voltammograms of electrodes modified with Os-phendione-PVP changing the pH from 3 to 8. The value of the lowest limit of the pH was selected as 3 because of NADH hydrolysis in acidic media²⁵ therefore the behaviour of the mediator is not of interest at pH<3 for NADH catalysis. The value of 8 for the highest pH limit was chosen due to the fact that phendione is unstable at pH values higher than 8.²³ The standard redox potential shifts in the negative direction with the increase in the solution pH (Figure S-5 in Supporting Information). Three different regression lines can be drawn for three pH intervals. Within the range of pH from 3 to 5.5 the regression line is $E^{0'}/V=0.385-0.060\text{pH}$, ($r^2=0.9991$; $n=6$), the slope is close to its theoretical value of 59 mV per pH unit, calculated for processes in which equal number of protons and electrons participate, strongly indicating that the overall reaction proceeds with the participation of equal number of electrons and protons. From pH 5.5 to 6.4 the line is $E^{0'}/V=0.348-0.052\text{pH}$, ($r^2=0.9993$; $n=9$). Knowing that the pK of pyridine in PVP is 5.5 this change of the slope can be explained in terms of deprotonation of pyridine rings. For the pH range from 6.4 to 8 the line is $E^{0'}/V=0.327-0.049\text{pH}$, ($r^2=0.9994$; $n=7$). Taking into consideration that the theoretical slope value for the redox process with the participation of four electrons and three protons is 44 mV per pH unit it can be concluded that only one of four hydroxyls in Os(QH₂)₂PVP complex is deprotonated in this pH range. This change in slope occurs at pH 6.4 suggesting that the pK_a of the reduced mediator has the same value. This data coincide with the value of the pK_a obtained in our previously reported electrochemical study of another complex of osmium with phendione [Os(4,4'-dimethyl-2,2'-bipyridine)₂(1,10-phenanthroline-5,6-dione)](PF₆)₂.¹⁴ Free 1,10-phenanthroline-5,6-dihydroquinone demonstrates the pK_a of 9.0,²³ but its complexation with divalent metals leads to the strong acid shift of the pK_a.¹³ The dependence of ΔE_p on the pH (Figure S-6 in Supporting Information) reflects the dependence of the apparent heterogeneous electron transfer rate constant (k_s , s⁻¹) on the pH. It can be seen that ΔE_p increases with the pH until the pH 6.0 with the breaking point at the pH 4.5 and next at the pH 6.5. This variation of k_s with the pH corroborates with the theory developed by Laviron for organic redox couples in which protonation reactions take place.^{26,27} Laviron's theory predicts the decrease in k_s with the pH. The quantitative variation of k_s and hence ΔE_p can be calculated if the

constants of all protonation reactions for all participating forms of the mediator together with k_{S1} and k_{S2} are known for the following reversible reactions insensitive to pH:



Where $\text{Os}(\text{QH}_2)_2\text{PVP}$ is a fully protonated oxidized form and $\text{Os}(\text{Q}^{2-})\text{PVP}$ is a fully deprotonated reduced form of the mediator. Unfortunately, these constants for this mediator can not be found due to its chemical instability at $\text{pH} > 6.5$. So only qualitative analysis of the ΔE_p vs. pH plot can be undertaken.

The variation of the cathodic and anodic peak potential (E_{pc} and E_{pa}) for the phendione couple with the scan rate was used to estimate the heterogeneous electron transfer rate constant (k_s, s^{-1}) of the redox process, taking place at the interface between the electrode surface and Os-phendione-PVP adsorbed on it, according to Laviron's approach:²⁸

$$E_{pc} - E^{0'} = (2.303RT/\alpha nF) \log[\alpha nF \nu / (RTk_s)] \quad (1)$$

$$E_{pa} - E^{0'} = (2.303RT/(1-\alpha)nF) \log[(1-\alpha)nF \nu / (RTk_s)] \quad (2)$$

where ν is the scan rate (V s^{-1}), n -the number of exchanged electrons, F is Faraday's constant 96487 C mol^{-1} , and α the transfer coefficient. If the transfer rate is fast enough in comparison with the scan rate then the peak separation is close to zero and when the scan rate is greater than the transfer rate the peak separation increases. This approach is supposed to give a lower limit estimate for the value of k_s , which in the case of Os-phendione-PVP is equal to $18 \pm 2 \text{ s}^{-1}$ at pH 6.0 (calculated as average of cathodic and anodic constants) and surface coverage $(7.5 \pm 0.2) \times 10^{-10} \text{ mol cm}^{-2}$, oxidation and reduction transfer numbers being 0.86 ± 0.05 and 0.12 ± 0.01 at pH 6.0. The estimated apparent k_s value for this polymer is higher than this for Meldola Blue (10 s^{-1}),⁹ and of the same order of magnitude as these for $[\text{Os}(4,4'\text{-dimethyl-2,2'\text{-bipyridine})}_2(1,10\text{-phenanthroline-5,6\text{-dione})](\text{PF}_6)_2$ (20.1 s^{-1}).¹⁴ The sum of the anodic and

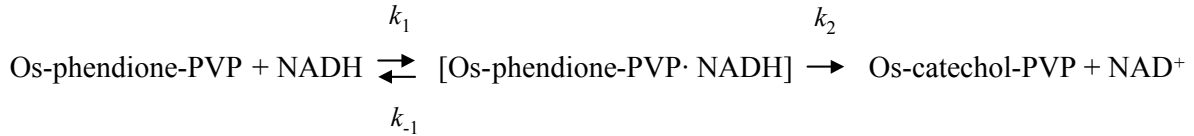
cathodic transfer coefficients is almost one, but the small asymmetry with respect to the abscissa of the anodic and cathodic linear branches of the $(E_p - E^{0'})$ vs. $\log(\nu)$ plot can be seen (Figure S-7 in Supporting Information). The exact numerical values of k_s could not be estimated exactly at the pH greater than 6.4 due to the chemical instability of Os-phendione-PVP nevertheless the dependence of ΔE_p on the pH allows to see the decrease of peak separation starting from this pH indicating increased reversibility upon protonation of resulting catechol.

According to theory the peak width at half peak height, E_{fwhm} depends on the reversibility of a redox couple. It should be equal to $90.6/n$ mV for an ideally Nernstein reversible reaction (when $n = 4$ E_{fwhm} should be 22.5 mV) and $62.5/(\alpha n)$ for the irreversible electrochemical process (when $n = 4$ and $\alpha = 0.86$, oxidation E_{fwhm} is 18.38 mV, for $\alpha = 0.12$ reduction E_{fwhm} should be 130.2 mV). In the case of Os-phendione-PVP, E_{fwhm} was pH dependent as is shown in Table I. The values of oxidation and reduction E_{fwhm} increase with pH and are greater than those predicted by theory for reversible and irreversible processes indicating repulsing interactions between adsorbed molecules. Thus it can be concluded that Os-phendione-PVP is a quasi-reversible redox couple exchanging four protons and four electrons at pH less than 6.4.

Electrocatalytic oxidation of NADH at Os-phendione-PVP modified electrodes. Cyclic voltammograms showing electrocatalytic current due to the NADH oxidation on Os-phendione-PVP modified graphite electrodes at different NADH concentrations are shown in Figure 2. In the absence of NADH (a) the response is ascribed to the oxidation/reduction of catechol/phendione couple. Upon addition of increasing concentrations of NADH (b-d) the cyclic voltammograms exhibit a dramatic enhancement of the anodic peak current with the disappearance of the cathodic peak. The peak of the NADH oxidation at bare graphite electrodes is at 332 ± 5 mV vs. Ag/AgCl/KCl_{sat}, modified electrodes show a plateau at $+112 \pm 8$ mV vs. Ag/AgCl/KCl_{sat} at pH 6.0, at scan rate of 20 mV s^{-1} with NADH concentration of 2.4 mM (curve d), which is close to the oxidation peak of adsorbed mediator itself at

the same value of pH (+53±3 mV vs. Ag/AgCl/KCl_{sat}). Therefore, a decrease in NADH electrooxidation overvoltage by about 220 mV compared to electrooxidation at bare graphite electrodes under the same conditions (Figure 3) is achieved with the redox polymer. Rotating disk electrodes (RDE) were used to assess the stability of the steady state signal and calculate the rate constants of NADH oxidation by Os-phendione-PVP adsorbed on graphite electrodes.

The estimation of rate constants for the reaction between NADH and Os-phendione-PVP was based on the hypothesis that in thin polymeric films diffusional transport of both charge and NADH can be neglected and the substrate-mediator complex is formed in this interaction according to the following mechanism:



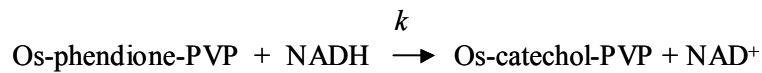
The model proposed by Gorton and coworkers^{4,9} to calculate the dependence of the catalytic current (I_{cat}) on experimental parameters on the basis of a Michaelis-Menten kinetic model was employed in this work.

$$1/I_{\text{cat}} = 1/(nFA\Gamma k c_{\text{NADH}}) + [1/(0.62nFAD^{2/3} c_{\text{NADH}} \nu^{-1/6})](1/\omega^{1/2}) \quad (3)$$

$$1/I_{\text{cat}} = 1/(nFA\Gamma k_2) + [K_M/(nFA\Gamma k_2) + 1/(0.62nFAD^{2/3} \nu^{-1/6} \omega^{1/2})](1/c_{\text{NADH}}) \quad (4)$$

$$K_M = (k_{-1} + k_2)/k_1 \quad (5)$$

where D (cm² s⁻¹) is the diffusion coefficient of NADH, ν (cm² s⁻¹) the hydrodynamic viscosity, ω (rad s⁻¹) the speed of rotation, A (cm²) the electrode surface area, Γ (mol cm⁻²) the surface coverage of the mediator, c_{NADH} (M) the concentration of NADH, and k (M⁻¹ s⁻¹) the rate coefficient of the formal overall chemical reaction:



When the data obtained from RDE measurements, were plotted as $1/I_{\text{cat}}$ against $1/\omega^{1/2}$ for different concentrations of NADH straight lines were obtained in agreement with equation 4 (Figure S-8 in Supporting Information). From the intercepts of these lines with the $1/I_{\text{cat}}$ axis the coefficients k were estimated and the graph of k^{-1} vs. c_{NADH} (Figure S-9 in Supporting Information) according to equation 6 was made.

$$1/k = K_M/k_2 + c_{\text{NADH}}/k_2 \quad (6)$$

On the basis of the resulting straight line ($y = 0.896 + 0.9495x$, $R = 0.997$ ($n = 6$)) the values of kinetic constants k_2 , K_M , and $k_{[\text{NADH}]=0}$ (rate coefficient of the overall reaction at zero NADH concentration) were found at pH 6.0 and 5.0 and are summarized in Table II.

The value of K_M for the present redox polymer is equal to that of Meldola Blue (1.2 mM),⁹ lower than that for $[\text{Os}(4,4'\text{-dimethyl-2,2'}\text{-bipyridine})_2(1,10\text{-phenanthroline-5,6-dione})](\text{PF}_6)_2$ (0.39-0.43).¹⁴ Comparing the value of k_2 with this reported for other NAD^+ oxidizing mediators it can be seen that it is of the same order of magnitude as k_2 of $[\text{Os}(4,4'\text{-dimethyl-2,2'}\text{-bipyridine})_2(1,10\text{-phenanthroline-5,6-dione})](\text{PF}_6)_2$ ($0.75\text{-}0.8 \text{ s}^{-1}$)¹⁴ and it is inferior to k_2 of Meldola Blue (31.8 s^{-1}).⁹ The rate coefficient k strongly depends on the NADH concentration, for this reason it was proposed¹⁷ to use its value extrapolated to zero NADH concentration ($k_{[\text{NADH}]=0} = k_2/K_M$), which in case of Os-phendione-PVP was lower than the corresponding value for Meldola Blue ($2.7 \times 10^4 \text{ M}^{-1} \text{ s}^{-1}$)⁹ or for poly(3,4-dihydroxybenzaldehyde) ($4.3 \times 10^3 \text{ M}^{-1} \text{ s}^{-1}$)³⁸ and practically equal to that of $[\text{Os}(4,4'\text{-dimethyl-2,2'}\text{-bipyridine})_2(1,10\text{-phenanthroline-5,6-dione})](\text{PF}_6)_2$ ($0.9 \text{ M}^{-1} \text{ s}^{-1}$).¹⁴

The construction of stable and operational NADH-based reagentless biosensors requires not only efficient electrocatalytic oxidation of NADH by the mediator but also that the electrocatalytic process yields enzymatically active NAD^+ . Recycling of NADH into enzymatically active NAD^+ was carried out by electrochemical conversion experiments as described in Supporting Information. This experiment showed that 100% of the oxidation product is enzymatically active NAD^+ .

Reagentless glucose biosensors constructed using Os-phendione-PVP. With an objective to prove the applicability of the redox polymer Os-phendione-PVP to the construction of dehydrogenase-based biosensors glucose dehydrogenase (GDH) was selected as a model enzyme to be used in a biosensor configuration based on NAD^+ recycling. The sequence of electrochemical reactions taking place in this biosensor is demonstrated in Figure 4. Os-phendione-PVP was used in conjunction with GDH and NAD^+ crosslinked with PEGDGE in the matrix based on the “binder” polymer. The electrocatalytic behavior of the modified electrode containing GDH and NAD^+ is shown in Figure 5. It can be observed that when D-glucose is added into the bulk solution a significant oxidation current appears associated with the disappearance of the reduction peak. Controlled electrodes have been prepared excluding one of the following components: a) NAD^+ ; b) Os-phendione-PVP; c) GDH; d) “binder” polymer; e) PEGDGE. None of them demonstrated any significant response to glucose. The characterization of glucose dehydrogenase from *Bacillus megaterium*, the enzyme used in this work, was reported for the first time by Pauly and Pfeleiderer.²⁹ The free enzyme follows a Bi Bi sequential ordered mechanism taking place via the formation of a ternary complex. NAD^+ adds first and the NADH formed dissociates from the enzyme last, hence the calculations of characteristics of the glucose sensors were performed using the steady-state kinetic model published elsewhere³⁰ and modified as shown in Supporting Information.

Experimental calibration curves for the glucose biosensors prepared with different loadings of GDH operating in the presence of saturating 26 mM NAD^+ in the external solution were used to find the values of the apparent Michaelis constants, the apparent maximum current densities and the fluxes from the Eadie-Hofstee plots (Figure S-25 in Supporting Information). By fitting the experimental data to equation S-22 (Supporting Information) using non-linear regression analysis the values of LV_1 , K_B , and k'_B were found (Table S-I in Supporting Information). For the meaning of LV_1 , K_B , and k'_B see Supporting Information. The Eadie-Hofstee plots were linear and the values of calculated apparent Michaelis constants were practically equal when the loading of GDH was varied, at the same time the apparent maximum current densities changed linearly with the variation in the GDH loading. Fitting the

experimental calibration data gave the values of LV_1 of K_B coinciding with those of the apparent maximum fluxes and the apparent Michaelis constants for glucose. The computed value of K_B agrees well with that of the free GDH in solution (9.7 mM) determined under the same experimental conditions. The computed values of the mass transfer constants of glucose (k'_B) were greater than 1×10^{-8} cm s^{-1} implying that in the experimental range of substrate concentrations starting from 0.047 mM the flux of the mass transfer of the substrate was not less than the maximum flux of the enzymatic reduction of NAD^+ (4.77×10^{-10} $\text{mol s}^{-1} \text{cm}^{-2}$). Hence, the response of the glucose biosensors operating in the presence of saturating NAD^+ concentration in a sample solution is limited by the enzymatic reaction of the glucose oxidation i.e. by the GDH loading.

The experimental calibration curves and the Eadie-Hofstee plots (Figure S-26 in Supporting Information) for the biosensors prepared with varied loadings of GDH operating in the reagentless mode i.e. without NAD^+ in the sample solution yielded the values of the apparent Michaelis constants, the apparent maximum current densities and fluxes obtained from the Eadie-Hofstee plots. The Eadie-Hofstee plots were linear implying that the response of the biosensors is limited neither by the rate of NADH oxidation at the electrode surface nor by the mass transfer of glucose. The values of apparent Michaelis constants were dependent on the GDH loading and the values of the apparent current densities, and fluxes did not rise linearly with the increase in the GDH loading. Fitting the experimental calibration data to the equation S-21 in Supporting Information by non-linear regression analysis using the values of LV_1 , K_B , and k'_B yielded by previous fitting allowed to assess the values of K_A , K_{AB} , and A_t (Table S-II in Supporting Information). For the meaning of K_A , K_{AB} , and A_t see Supporting Information. The values of K_A and K_{AB} were quite similar at varied NAD^+ loading but the values of the computed NAD^+ loading (A_t) decreased with the increase in GDH loading meaning that GDH competes for crosslinking by PEGDGE with the entrapment of NAD^+ in the resulting hydrogel. The decrease in maximum current densities caused by the decrease in NAD^+ concentration showed by the reagentless glucose biosensors, in comparison with the biosensors operating in the presence of NAD^+ in an external solution, proves that the response of the reagentless biosensors to glucose is limited by the enzymatic

reduction of NAD^+ i.e. by NAD^+ loading (A_t). In conclusion it should be noted that the values of K_A , and K_{AB} obtained by fitting agree well with those of free GDH in the solution under the same experimental conditions: 1.85 mM and 5.1 mM² respectively.

The effect of pH on the response of the glucose biosensors is demonstrated in Figure 6. One can see that the response of the biosensors increases with pH in agreement with pH behavior of free GDH from *Bacillus megaterium* reaching the maximum current at pH 9.0 which is the pH optimum of GDH. The effect of temperature on the response to glucose of the biosensors was studied. (Figure S-27 in Supporting Information). In the reagentless mode of operation the glucose biosensors demonstrated the maximum current at the temperature of 54°C and in the presence of 29 mM NAD^+ in the sample solution they achieved maximum response at 66°C. Free GDH has optimum temperature at 55°C and shows 80% of its maximum activity at 66°C. The lower thermal stability of the reagentless sensors can be explained by the increased rate of NAD^+ leaching at elevated temperatures, on the other hand the increased thermal stability, demonstrated by the immobilized enzyme in the sensors operating in the presence of the cofactor in the sample solution, is most probably a reflection of the stabilization of the enzyme proteins due to their chemical crosslinking with the hydrogel matrix. The activation energies calculated from the temperature vs. response plots for the reagentless and non-reagentless biosensors have the values of 54±6 kJ mol⁻¹ K⁻¹ and 61 ±6 kJ mol⁻¹ K⁻¹ respectively. They corroborate with the activation energy of free GDH (60 kJ mol⁻¹ K⁻¹) measured under the same experimental conditions in the presence of 26 mM NAD^+ , this fact means that at elevated temperatures the response of the glucose sensors is also governed by the enzymatic reaction of glucose with NAD^+ .

The operational stability studies performed at the saturating glucose concentration (220 mM) with the sensors prepared using 0.135 U per electrode of glucose dehydrogenase demonstrated that the half-life time of reagentless biosensors is 1 h (RSD 6.4 % for three electrodes) and they lost 33% (RSD=11% for n=3) of phendione activity, when at the end NAD^+ was added to obtain saturating concentration of cofactor the current density rose to 54.1 $\mu\text{A cm}^{-2}$ (60 % of the initial response in the presence of 26 mM NAD^+). Controlled biosensors operated in the absence of glucose during 1 h under the same conditions

lost 8% (RSD 10%, n=3) of the mediator. When the glucose sensors were operated in the presence of NAD^+ in the bulk solution since the beginning of experiment the operational half-life was 2.4 h (RSD=12% for n=3). Those sensors lost 56 % of phenidone activity (RSD is 15% for n=3). The enzymatic measurements of NAD^+ concentration based on the spectroscopical monitoring at A_{340} of its reduction to NADH by glucose dehydrogenase showed that NAD^+ was stable in the sample solution under the experimental conditions during the at least 2.4 h. Controlled sensors lost only 28 % (RSD 13%, n=3) of the mediator after 2.4 h in the absence of glucose. The significant difference in the loss of Os-phenidone-PVP between the glucose biosensors operating in the reagentless mode and those operating in the presence of NAD^+ (33% and 56 % respectively) upon reaching 50% of their initial response proves that the mediator loading is not the limiting factor for the response of the sensors to glucose. Otherwise, if the oxidation of NADH by the mediator is the limiting step, the loss of the response to glucose should be linearly dependent on the loss of the mediator. The most important reason for the deactivation of the reagentless glucose biosensors is leaching of NAD^+ . This is confirmed by shorter half-life time demonstrated by the reagentless biosensors.

CONCLUDING REMARKS

A new NADH oxidizing polymer was synthesized and used for the modification of graphite electrodes by adsorption on their surface. Four protons and four electrons participate in the redox process taking place at two 1,10-phenanthroline-5,6-dione ligands complexed with osmium central cation causing pH dependent electrochemical behaviour. Although the complexation increases the relative stability of the electrocatalytic ligand, still the redox active polymer was useful at $\text{pH} < 7$. Work continues on the stabilization of these types of ligand to achieve faster kinetics, chemically reversible behaviour and greater stability. The reaction of the polymer with NADH proceeds reversibly through the formation of an intermediate complex, as was shown by RDE studies at different rotation velocities and NADH concentrations, when thin polymeric monolayer was immobilized on graphite. The polymer generates

enzymatically active NAD^+ according to the conversion study. Good electrocatalytic activity of the polymer for NADH oxidation allowed to construct the reagentless glucose biosensors based on NAD^+ and glucose dehydrogenase entrapped in the hydrogel. It was confirmed that the response of the reagentless glucose biosensors is governed by the kinetics of the enzymatic reaction of glucose with NAD^+ .

ACKNOWLEDGMENTS

Financial support from the European Community under the Industrial & Materials Technologies Programme Ref.: PROMOFILM BRITE EURAM Program BE97-4511, the Spanish Ministry of Education and Culture Ref.: Acciones Especiales MAT98-1413.CE, and the Biotechnology Program Ref.: DIAMONDS BIO4-CT97-2199 financed by European community is gratefully acknowledged. V.P. acknowledges scholarship from the Department of Chemical Engineering of 'Rovira i Virgili' University. O. R. and A. N. acknowledges scholarships from the Spanish Ministry of Education and Culture and the Community of Madrid, respectively. S. S. acknowledges a summer training scholarship from the PROMOFILM project.

Supporting Information Available. Additional information as noted in text. This material is available free of charge via the Internet at <http://pubs.acs.org>

FIGURE CAPTIONS

Figure 1. Consecutive cyclic voltammograms at 50 mVs^{-1} of Os-phendione-PVP adsorbed on spectrographic graphite: a) 2nd scan; b) 50th scan. In deoxygenated. In 0.1 M phosphate buffer, pH 6.0.

Figure 2. Cyclic voltammetry of an electrode modified with Os-phendione-PVP: a) in buffer; b) in 2.4 mM of NADH; c) in 4.7 mM of NADH; d) in 6.9 mM of NADH. Experimental conditions: Os-

phendione-PVP coverage $(1.1\pm 0.2)\times 10^{-10}$ mol cm^{-2} ; scan rate 20 mV s^{-1} , 0.1 M phosphate buffer, pH 6.0.

Figure 3. Cyclic voltammetry of: a) bare electrode in buffer; b) bare electrode in 2.4 mM of NADH; c) electrode modified with Os-phendione-PVP (surface coverage $(1.1\pm 0.2)\times 10^{-10}$ mol/ cm^2) in buffer; d) electrode modified with Os-phendione-PVP (coverage $(1.1\pm 0.2)\times 10^{-10}$ mol/ cm^2) in 2.4 mM of NADH. Experimental conditions: 0.1 M phosphate buffer deaerated with argon, pH 6.0.

Figure 4. Schematic representation of the electron transfer steps for the glucose sensor based on Os-phendione-PVP polymer, NAD^+ , and glucose dehydrogenase (participating protons are not shown).

Figure 5. Cyclic voltammetry of a reagentless glucose biosensor: a) in the absence of glucose; b) in 186 mM of glucose. Experimental conditions: scan rate 2 mV s^{-1} , 0.1 M phosphate buffer deaerated with argon, pH 6.0.

Figure 6. The effect of pH on the response of glucose biosensors: (●) biosensors operating in the presence of 26 mM NAD^+ ; (◆) reagentless biosensors; (o) controlled electrodes prepared without GDH and studied in the presence of 26 mM NAD^+ ; (◇) controlled electrodes prepared with GDH, without NAD^+ and studied without NAD^+ in the sample solution; (Δ) controlled electrodes prepared without GDH and studied without NAD^+ in the sample solution. Experimental conditions: temperature 25°C, glucose concentration 220 mM.

TABLES

Table I. Effect of pH on the peak width at half peak height E_{fwhm} .

| PH | 3.0 | 4.0 | 5.0 | 6.0 |
|---|-------|-------|--------|--------|
| Oxidation E_{fwhm} (mV) | 95±8 | 110±9 | 121±10 | 134±10 |
| Reduction E_{fwhm} (mV) | 139±9 | 150±9 | 150±10 | 154±10 |

Table II. Results of data interpretation for electrocatalysis of NADH oxidation at Os-phendione-PVP modified RDE at pH 6.0 and 5.0.

| pH | $k_{[NADH]=0}$ ($M^{-1}s^{-1}$) | K_M (mM) | k_{+2} (s^{-1}) |
|-----------|-----------------------------------|------------|-----------------------|
| 6.0 | 1900±200 | 0.75±0.09 | 1.5±0.1 |
| 5.0 | 3400±300 | 0.4±0.07 | 1.3±0.1 |

REFERENCES

- (1) Chenault, H. K.; Whitesides G. M. *Appl. Biochem. Biotechnol.* **1987**, *14*, 147-197.
- (2) Clark, W. M. In *Oxidation-Reduction Potentials of Organic Systems*, The Williams and Wilkins Co.: Baltimore, MD, 1960.
- (3) Aizawa, M.; Coughlin R. W.; Charles, M. *Biochim. Biophys. Acta* **1975**, *385*, 362-370.
- (4) Gorton, L. J. *Chem. Soc., Faraday Trans.* **1986**, *82*, 1245-1258.
- (5) Katakis, I.; Domínguez E. *Mikrochim. Acta* **1997**, *126*, 11-32.
- (6) Blaedel, W. J.; Jenkins R. A. *Anal. Chem.* **1976**, *48*, 1240-1247.
- (7) Tse, D. C. S.; Kuwana, T. *Anal. Chem.* **1978**, *50*, 1315-1318.
- (8) Huck, H.; Schmidt, H.L. *Angew. Chem.* **1981**, *93*, 421-422.
- (9) Gorton L.; Torstensson A.; Jaegfeldt, H.; Johansson G. *J. Electroanal. Chem.* **1984**, *161*, 103-111.
- (10) Kitani, A.; Miller L. L. *J. Am. Chem. Soc.* **1981**, *103*, 3595-3597.
- (11) Kulys, J. J. *Enzyme Microb. Technol.* **1981**, *3*, 344-352.
- (12) Gorton, L.; Johansson, G.; Torstensson, A. *J. Electroanal. Chem.* **1985**, *196*, 81-92.
- (13) Goss C. A.; Abruña H. D. *Inorg. Chem.* **1985**, *24*, 4263-4267.
- (14) Popescu, I. C.; Domínguez, E.; Narváez, A.; Pavlov, V.; Katakis, I. *J. Electroanal. Chem.* **1999**, *464*, 208-214.
- (15) Murray, R. (Ed.), In *Molecular Design of Electrode Surfaces*, Wiley: New York, 1992.
- (16) Atta, N. F.; Galal, A.; Karagözler, A. E.; Zimmer, H.; Rubinson, J. F.; Mark, H. B. *J. Chem. Soc., Chem. Commun.* **1990**, 1347-1349.

- (17) Ohsaka, T.; Tanaka, T.; Tokuda, K. *J. Chem. Soc., Chem. Commun.* **1993**, 222-224.
- (18) Pariente, F.; Lorenzo, E.; Abruña, H. D. *Anal. Chem.* **1994**, *66*, 4337-4344.
- (19) Degrand, C.; Miller, L. L. *J. Am. Chem. Soc.* **1980**, *102*, 5728-5732.
- (20) Domínguez, E.; Lan, H. L.; Okamoto, Y.; Hale, P. D.; Skotheim, T. A.; Gorton, L. *Biosens. Bioelectron.* **1993**, *8*, 167-175.
- (21) Persson, B.; Lee, H. S.; Gorton, L.; Skotheim, T.; Bartlett, P. *Electroanalysis*, **1995**, *7*, 935-940.
- (22) Parellada, J.; Narváez, A.; Domínguez, E.; Katakis, I. *Biosens. Bioelectron.* **1997**, *12*, 267-275.
- (23) Evans, D. H.; Griffith, D. A. *J. Electroanal. Chem.* **1981**, *134*, 301-310.
- (24) Eckert, T. S.; Bruice, T. C.; Gainor, J. A.; Weinreb, S. M. *Proc. Natl. Acad. Sci. USA* **1982**, *79*, 2533-2536.
- (25) Chenault, H. K.; Whitesides, G. M. *Appl. Biochem. Biotechnol.* **1987**, *14*, 147-197.
- (26) Laviron, E. *J. Electroanal. Chem.* **1980**, *109*, 57-67.
- (27) Laviron, E. *J. Electroanal. Chem.* **1984**, *164*, 213-227.
- (28) Laviron, E. *J. Electroanal. Chem.* **1979**, *101*, 19-28.
- (29) Pauly, H. E.; Pfeleiderer, G. *Hoppe-Seyler's Z. Physiol. Chem.* **1975**, *356*, 1613-1623.
- (30) Albery, W. J.; Bartlett, P. N.; Cass, E. G. A.; Sim, K. W. *J. Electroanal. Chem.* **1987**, *218*, 127-134.

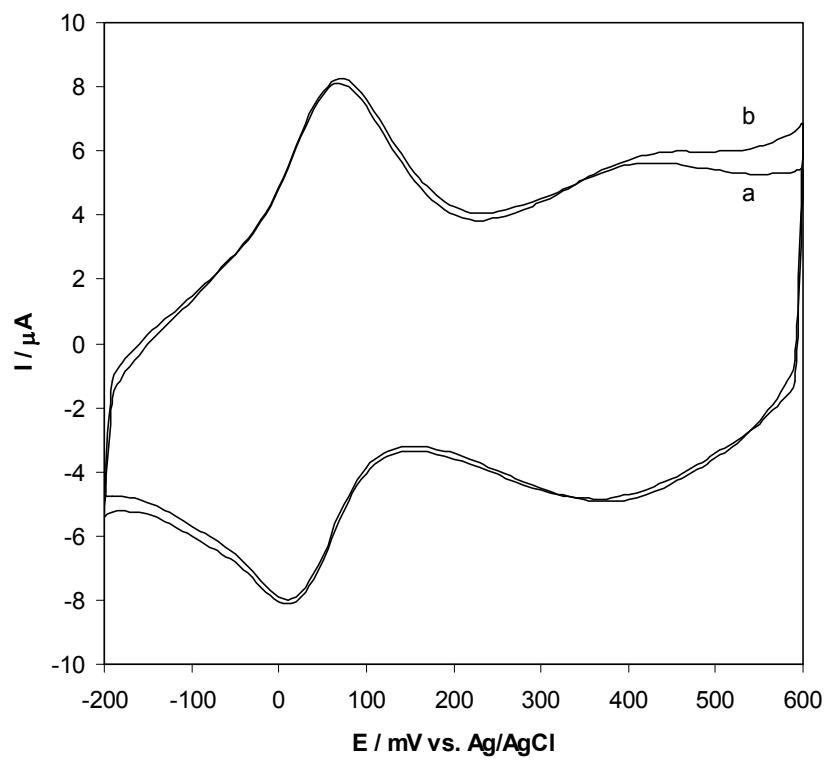


Figure 1

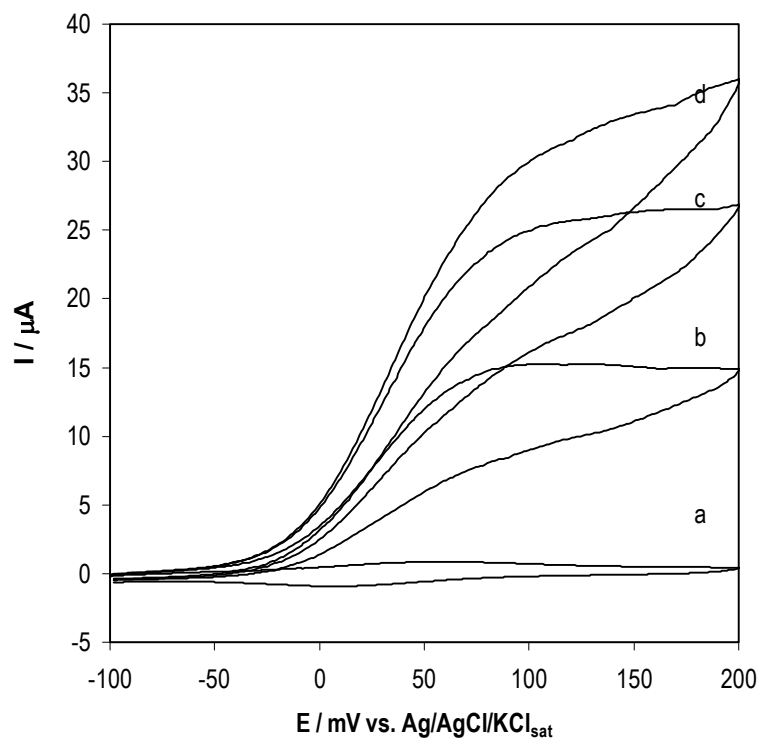


Figure 2

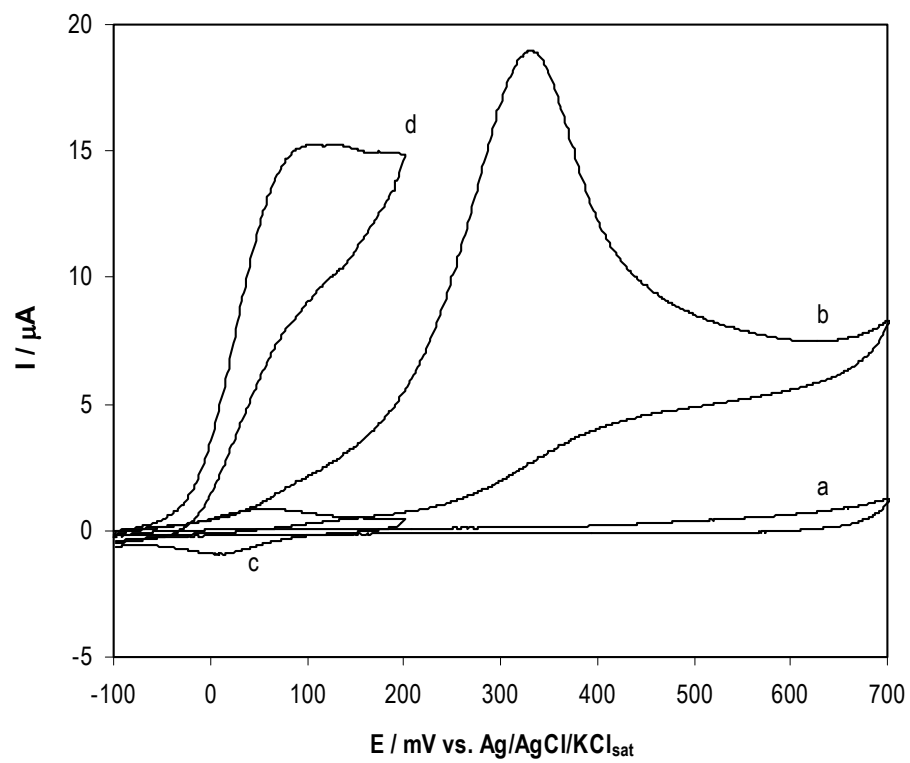


Figure 3

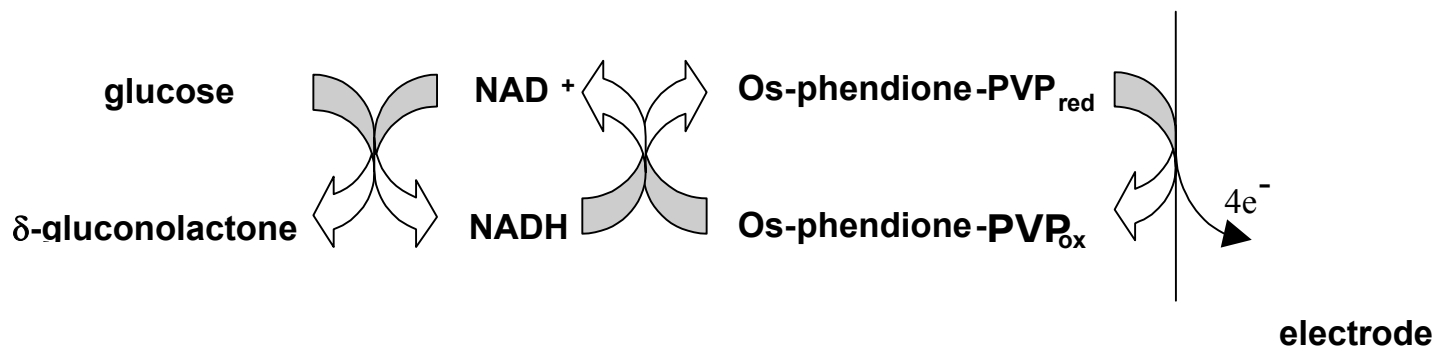


Figure 4

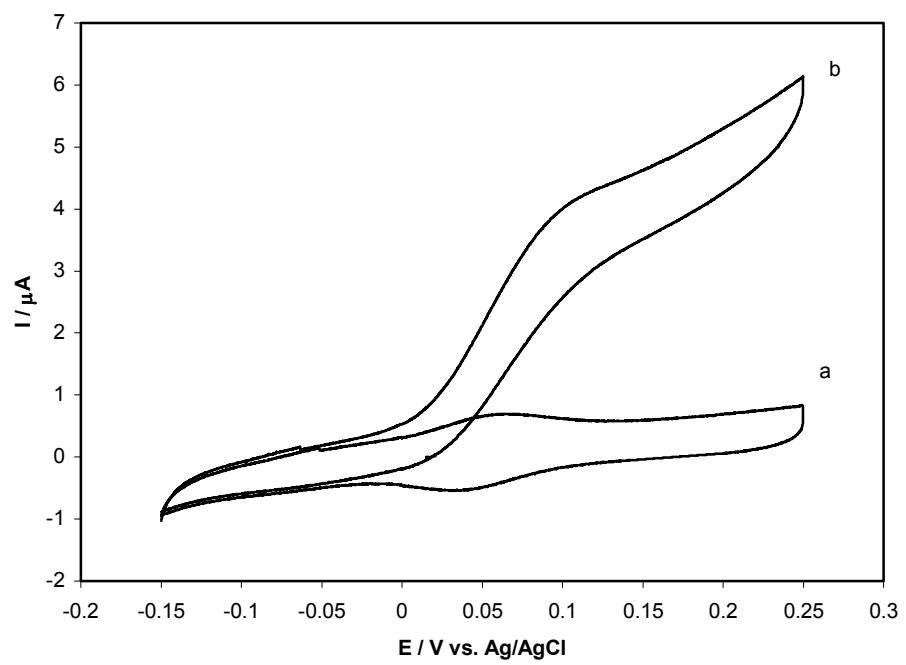


Figure 5

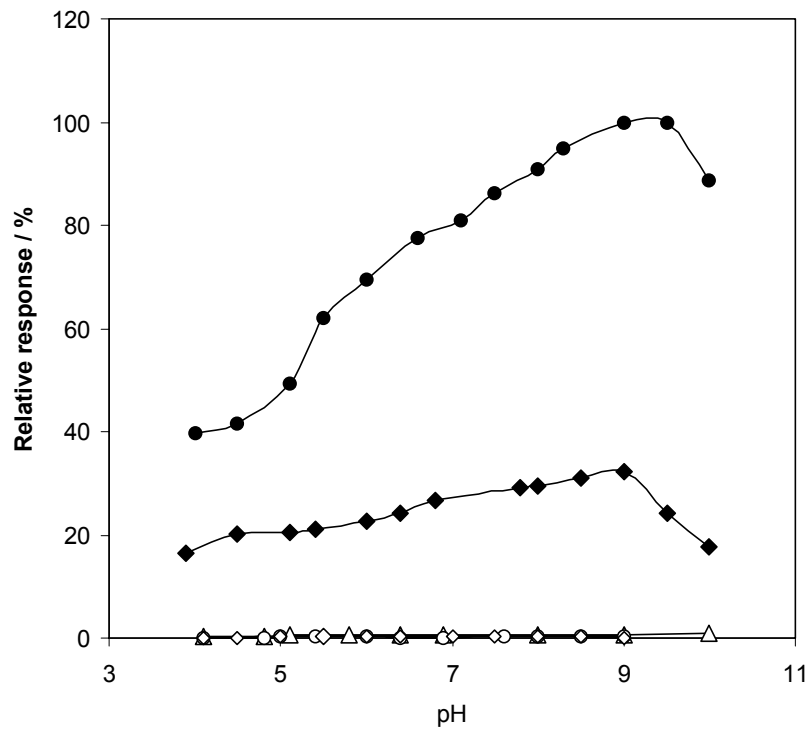


Figure 6

New Reagentless Glutamate Biosensors Based on Mesophilic and Thermophilic Glutamate Dehydrogenases

*Valeri Pavlov,¹ Serve Kengen,² Ioanis Katakis^{*1}*

Bioanalysis and Bioelectrochemistry Group, Chemical Engineering, Universitat Rovira i Virgili, E-43006, Tarragona (Catalonia), Spain, and Laboratory of Microbiology, Department of Biochemical Science, Wageningen Agricultural University, Hesselink van Suchtelenweg 4, Wageningen NL-6703 CT, Netherlands.

RECEIVED DATE

* To whom the correspondence should be addressed. E-mail: ioanis.katakis@urv.net, Tel: +34 977 55 9655, Fax: +34 977 55 9667.

¹Universitat Rovira i Virgili.

²Wageningen Agricultural University.

ABSTRACT. Two novel methods for NAD^+ and dehydrogenase immobilization on the graphite electrode surfaces have been developed and applied to the construction of reagentless biosensors for L-glutamate based on mesophilic glutamate dehydrogenase (GLDH) from bovine liver and thermophilic glutamate dehydrogenase from *Pyrococcus furiosus*. The methods rely on modification of graphite electrodes with new NADH oxidizing polymer $[\text{Os}(1,10\text{-phenanthroline-5,6\text{-phendione})}_2(\text{PVP})_4\text{Cl}]\text{Cl}$ followed by physical adsorption of dehydrogenase and alginic acid modified with NAD^+ (NAD^+ -alginate) on the surface of electrodes or on entrapment of NAD^+ and dehydrogenase in the hydrogel formed *in situ* by crosslinking of PVP bearing amino groups (“binder” polymer) with polyethyleneglycol diglycedyl ester (PEGDGE) on electrodes. Biosensors constructed with the use of bovine GLDH and NAD^+ -alginate showed detection limit equal to 0.5 mM and linear range 1.852-6.0 mM. The immobilization of bovine GLDH in the hydrogel gave sensors with the detection limit equal to 0.33 mM and the linear range 1.4-4.3 mM. The response time for both configurations was 100 s. When GLDH from *Pyrococcus furiosus* was adsorbed together with NAD^+ -alginate on the electrode surface the resulting sensors showed the detection limit equal to 4 mM and linear range 13-38.5 mM. Crosslinking of this thermophilic enzyme together with “binder” polymer yielded biosensors demonstrating detection limit equal to 6 mM and the linear range 6.6-34 mM. The response time of the last two configurations was 70 s. The 90 °C. The sensors constructed with the use of bovine GLDH demonstrated rapid loss of response at this elevated temperature. In addition, disposable glutamate sensors based on thermophilic and mesophilic glutamate biosensors based on the thermophilic enzyme showed ability to operate at elevated temperature equal to dehydrogenases mixed with stabilizers have been constructed and their shelf life time was studied to demonstrate that the use of thermophilic GLDH allows to extend the shelf stability of glutamate biosensors by 10 times.

KEYWORDS. glutamate analysis, thermophilic, glutamate dehydrogenase, reagentless biosensors, NAD⁺.

Glutamate determination is very important in the food analysis, pharmacology, and medicine because L-glutamic acid is an important neurotransmitter¹ implicated in the development of neurological diseases such as amnesia, depression, and schizophrenia.^{2,3} It also is a marker in the diagnosis of miocardic diseases and hepatitis.⁴ Different analytical methods have been developed for the detection of glutamate: gas chromatography,⁵ kinetic potentiometry based on the reaction of glutamate with dinitrofluorobenzene,⁶ high performance liquid chromatography,⁷ and capillary electrophoresis.⁸

In order to reduce analysis time bioanalytical methods based on glutamate decarboxylase, glutamate oxidase, and glutamate dehydrogenase (GLDH) coupled with optical transduction⁹⁻¹¹ have been developed. Amperometric transduction was employed in biosensors based on glutamate oxidase.¹²⁻¹⁴ The biosensors based on glutamate oxidase are dependent on oxygen. The dependence of biosensor response on oxygen can be eliminated by using NAD(P)⁺ dependent GLDH as a biorecognition element. Glutamate biosensors constructed by the immobilization of GLDH on carbon fiber microelectrodes were based on direct NADH oxidation on the carbon surface¹⁵ requiring high applied overpotential (>0.55 V vs. SCE). The overpotential can be lowered by employing enzymatic NADH oxidation via diaphorase and NADH oxidase.¹⁶⁻¹⁷ Another alternative is the use of mediators catalyzing the electrochemical oxidation of NAD(P)H.¹⁸

The above mentioned glutamate sensors require NAD⁺ in a sample solution for their operation. Reagentless biosensors based on dehydrogenases, in general, can be produced by immobilization of enzymes, NAD⁺ and mediator for the coenzyme reoxidation on the surface of an electrode. Five strategies for the coenzyme immobilization have been demonstrated in the literature: entrapment in hydrogels formed *in situ* by polymeric macromolecules,^{19,20} adsorption onto pre-prepared polymeric membranes,²¹ entrapment in electropolymerized films,²² entrapment in carbon paste,²⁴⁻²⁶ and attachment

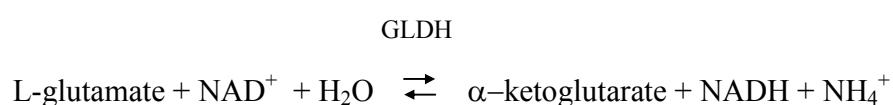
to self-assembled monolayers.²⁷ Biosensors in which NAD⁺ was entrapped in hydrogels formed *in situ* have good sensitivities because of very fast transport of analyte to the enzyme, but suffer from low stability in the reagentless mode of operation due to easy desorption of the coenzyme and the enzyme. When NAD⁺ was entrapped in electropolymerized films and pre-prepared membranes the sensitivity was low due to the slow transport of analyte. The most stable reagentless biosensors were produced on the basis of carbon paste in which a “reserve pool” of the coenzyme was created in the paste, retaining high sensitivity. Such biosensors are however difficult to miniaturize.

The use of more stable enzyme, such as thermophilic dehydrogenases can improve shelf and operational stability of biosensors if the enzymatic reaction is the rate-limiting step or stability determining. Thermophilic glutamate dehydrogenase has been purified from different microorganisms such as *Sulfolobus solfataricus*,²⁸ *Pyrococcus furiosus*,²⁹ archaeobacteria AN1,³⁰ and *Thermococcus litoralis*.³¹ The enzyme demonstrates high stability at elevated temperatures, for instance, the half life of GLDH from *Thermococcus litoralis* at 80°C is 15 h, from *Pyrococcus furiosus* at 100°C is 12 h, and from AN1 at 90°C is 12.5 h. Thermophilic enzymes can be successfully employed in the construction of biosensors, so glutamate carbon paste biosensors operating in the range 40-60°C constructed using GLDH from AN1 cells have been reported.^{32,33}

In this work we report on our efforts to solve the problems associated with NAD⁺ dehydrogenase electrodes. Namely, we use an efficient NADH oxidizing mediator and we show that it is sufficiently catalytic to permit reagentless dehydrogenase electrodes. We achieve such reagentless sensors by immobilizing NAD⁺ for continuous and disposable operation. We achieve stable and long shelf life sensors by using thermophilic enzymes.

RESULTS AND DISCUSSION

Methods for the fabrication of reagentless glutamate biosensors. The glutamate biosensors described in the present article are based on the oxidation of L-glutamate by NAD^+ through mesophilic and thermophilic glutamate dehydrogenase (GLDH) according to the reaction:



with the equilibrium constant shifted to the formation of L-glutamate, but the reoxidation of the formed NADH by the Os-phendione-PVP mediator, which is oxidized in its turn at the graphite surface of a working electrode at low positive potential of 150 mV vs. Ag/AgCl/KCl displaces the equilibrium to the formation of α -ketoglutarate. This principle of operation is shown schematically in Figure 1. The immobilization of GLDH, NAD^+ and mediators is the necessary condition for design of reagentless glutamate biosensors. The group of Lo Gorton reported reagentless glutamate biosensors based on the immobilization of thermophilic NADP^+ dependent glutamate dehydrogenase in carbon paste^{32,33} in which NADH was reoxidized electrochemically by a polyethylenimine Toluiden Blue O redox mediator at applied potential 100 mV vs. Ag/AgCl/KCl_{sat}. Unfortunately, carbon paste electrodes can not be easily miniaturized. Our purpose was to construct cheap reagentless glutamate electrodes which can be miniaturized hence we opted for thermophilic GLDH from *Pyrococcus furiosus* which can use NAD^+ as cofactor and developed in this work two new methods to produce reagentless biosensors. The methods rely on NADH oxidation by a new polymer Os-phendione-PVP.³⁹ The 1,10-phenanthroline-5,6-dione moieties in this polymer impart it the capacity for the reversible regeneration of coenzyme. This fact was confirmed by the electrochemical conversion experiment, described in the experimental

part, in which 100 % conversion of NADH by the mediator to enzymatically active NAD^+ was obtained. This conclusion was drawn by comparing spectrophotometric and coulometric data produced by bulk electrolysis of NADH with those recorded during spectrophotometric determination of the enzymatic reconversion of NAD^+ by glutamate dehydrogenase in the presence of L-glutamate, and taking into account the spontaneous hydrolysis of NADH under the experimental conditions. This result is in good agreement with the result of similar study into electrochemical conversion of NAD^+/NADH couple by the monomeric osmium complex $[\text{Os}(4,4'\text{-dimethyl-2,2'\text{-bipyridine}})_2(1,10\text{-phenanthroline-5,6-dione})](\text{PF}_6)_2$, which showed 100 % conversion too.²⁵

The first method consisted in physical adsorption of Os-phendione-PVP, GLDH, and polymeric form of NAD^+ (NAD^+ -alginate) on the surface of a graphite electrode. Nakamura and co-workers³⁸ published the procedure for modification of alginic acid with NAD^+ through carbodiimide reaction, which yields a water-soluble polymer.

The second method was more complicated because, a graphite electrode was, first, pre-modified with Os-phendione-PVP, then GLDH and the coenzyme were entrapped in the hydrogel formed *in situ* on the electrode surface. The hydrogel was created by crosslinking poly(vinyl pyridine) (PEGDGE) bearing amino groups (“binder” polymer) with active epoxide functionalities of poly(ethylene glycol) diglycidyl ether. The immobilization of oxidases in hydrogels based on PEGDGE and redox polymers bearing amino groups has been utilized in fabrication of a number of biosensors.^{40,41}

Electrocatalytic oxidation of L-glutamate. Reagentless glutamate biosensors of these two configurations demonstrated change in the cyclic voltammetry when glutamate solution was injected into the cell (Figure 2). In the presence of saturating glutamate concentration the reagentless configurations demonstrated clear electrocatalytic waves reaching almost a plateau at potentials more negative than 200 mV vs. $\text{Ag}/\text{AgCl}/\text{KCl}_{\text{sat}}$. Our previous study of Os-phendione-PVP proved that the

potential of 150 mV vs. Ag/AgCl/KCl_{sat} was sufficient for electrocatalytical oxidation of NADH³⁹ hence the same potential was used in this work.

Effect of pH on the response of glutamate biosensors. The effect of pH on the maximum response of reagentless glutamate biosensors fabricated by the two methods using mesophilic and thermophilic GLDH was studied in steady state mode using 0.1 M phosphate buffer, the pH being adjusted with aqueous solutions of 1 M NaOH or H₃PO₄. In Figures 3 and 4 it can be seen that biosensors based on NAD⁺-alginate prepared from mesophilic and thermophilic GLDH have maximum response at pH 9.0. This result is in good agreement with the pH optimum of 8.5-9.0 for glutamate oxidation by free bovine GLDH in a solution,⁴² and pH optimum of 9.0 for GLDH from *Pyrococcus furiosus*.²⁹ Meanwhile the biosensors based on the immobilization by crosslinking with the “binder” polymer constructed using mesophilic and thermophilic GLDH achieved maximum response at pH 9.5. This change in pH optimum can be explained in by the increased enzymatic stability caused by crosslinking and by the effect of local buffering due to the presence of pyridine moieties and amino groups in the “binder” polymer.

The rate of reaction between Os-phendione-PVP and NADH slows down with the increase in pH³⁹ because the formal potential of this mediator in alkaline solutions shifts more negative and it loses the capacity of NADH oxidation. Os-phendione-PVP is not stable at pH values higher than 6.5, moreover, the controlled electrodes prepared without GLDH showed increase in non-specific oxidation of glutamate starting from pH 9.0, hence the pH 7.4 was chosen for further experiments, given the fact that this is the physiologic value of pH at which the analysis *in vivo* could be carried out.

Effect of temperature on the response of glutamate biosensors. The effect of temperature on the response of the reagentless glutamate biosensors is presented in Figures 5 and 6. The thermophilic GLDH based biosensors, independently of the immobilization procedure, have shown increase in response to L-glutamate until 88°C (the maximum temperature achieved), still below the optimal

temperature of 95°C of free thermophilic GLDH. Mesophilic biosensors demonstrated maximum response at lower temperatures. Biosensors based on NAD⁺-alginate showed the lowest optimal temperature of 52°C, binder polymer biosensors had the highest optimal temperature 56°C possibly because of improvement in thermostability due to crosslinking. This data is in good agreement with the published thermostability study of bovine GLDH according to which this enzyme starts to lose activity at 52°C.⁴³ The employment of new immobilization methods allowed to avoid the desintegration of electrodes at elevated temperatures, which was reported for carbon paste biosensors based on thermophilic GLDH by the group of Lo Gorton.³² The activation energies for the glutamate biosensors were calculated from Arrhenius plots. The activation energies are listed in Table I. Activation energies of mesophilic GLDH biosensors are significantly higher than the activation energy of free bovine GLDH, 12.9 kJ/mol,⁴³ and those of thermophilic GLDH biosensors are lower than the activation energy of GLDH from *Pyrococcus furiosus* 79.3 kJ/mol.²⁹ This indicates that the response of the glutamate biosensors is not limited by the kinetics of glutamate oxidation with NAD⁺ through GLDH. The response of mesophilic biosensors to L-glutamate was studied at 30°C, while the response of thermophilic biosensors at this temperature was not reproducible hence it was decided to characterize them at 40°C.

Response curves and operational stability of the glutamate biosensors. The kinetic mechanism of oxidative deamination catalyzed by bovine GLDH has been debated in the literature. The order of binding of glutamate and NAD(P)⁺ to the apoenzyme was in the centre of this discussion. Engel and coworkers arrived to the conclusion that this reaction could proceed via an ordered mechanism, NAD⁺ being the leading substrate.⁴⁴⁻⁴⁶ A random order mechanism for of L-glutamate oxidation by NADP⁺ was offered too.⁴⁷ Then a random sequential mechanism was shown.⁴⁸ Later it was suggested that this reaction proceeds through ordered binding and NADP⁺ leads in complexation with the apoenzyme.⁴⁹ The latest kinetic study into this controversial deamination mechanism confirmed that bovine dehydrogenase has an ordered sequential mechanism of substrate binding preceded by complexation

with NAD^{+} ⁵⁰ therefore the analysis of the response of the glutamate sensors was based on the modified kinetic model⁵¹ for the conversion of substrate B to products Q and R shown in Supporting Information.

The calibration curves and the Eadie-Hofstee plots for the reagentless glutamate biosensors constructed with the use of mesophilic or thermophilic GLDH based on NAD^{+} -alginate or the “binder” polymer are shown in Figures S-10 and S-11 (Supporting Information). Their basic characteristics are represented in Table II. All reagentless glutamate biosensors have demonstrated the concave Eadie-Hofstee plots (Figures S-10(B), S-11(B)) revealing that the response currents are limited by the rate of NADH oxidation at the electrode surface through Os-phendione-PVP.

The literature value of the Michaelis constant for mesophilic bovine GLDH determined at 30°C is 2.5 mM,⁵¹ and that determined by us for thermophilic GLDH from *Pyrococcus furiosus* in the presence of 26 mM NADH at 40°C and pH 7.4 is 14 mM.

The biosensors based on mesophilic enzyme showed apparent Michaelis constants which are about 6 times greater than that of the free enzyme. The biosensors based on thermophilic enzyme demonstrated Michaelis constants greater by 3-4 times than that for free enzyme under the same conditions. Taking into account the influence of mass transport on the simulated response of biosensors (Figures S-8 and S-9 and Tables S-II and S-III in Supporting Information) one can arrive to a conclusion that the experimental data imply that the response to glutamate is limited by two factors: the rate of NADH oxidation at the electrode surface and the mass transport. The fact that thermophilic biosensors based on the “binder” polymer demonstrated higher apparent current density than those prepared with the use of mesophilic GLDH implies that the thermophilic enzyme is less deactivated than the mesophilic one by crosslinking with PEGDGE.

The biosensors based on thermophilic GLDH were operated at higher temperature, which enhanced the diffusion, and demonstrated shorter response times. The detection limits of thermophilic biosensors were considerably greater than those of the mesophilic GLDH based biosensors, because of higher

specific activity of mesophilic GLDH at low temperatures. The greater operational linear ranges of thermophilic biosensors can be explained by the greater Michaelis constant of thermophilic GLDH. The thermophilic biosensors demonstrated much shorter operational stability than the mesophilic sensors due to higher temperature of operation (40°C) whereas the operational stability of mesophilic electrodes was studied at 30°C. The loss of response in both cases was caused by leaching of NAD⁺ from the electrode surface accelerated at high temperatures. This was proven by injection of NAD⁺ at the end of operational stability study, which normally lead to the recovery of response current (shown by the sensors of the same batch in the presence on NAD⁺ in a bulk solution), hence another operational stability study was performed in the presence of 30 mM NAD⁺ in the bulk solution. This study was performed at elevated temperature of 65°C to show that the half life of thermophilic GLDH based biosensors was 16 min whereas mesophilic biosensors instantly and completely lost response at this temperature so the use of thermophilic enzyme instead of the mesophilic one allowed to increase the operational stability of glutamate biosensors at elevated temperatures. Cyclic voltammetry of thermophilic biosensors revealed that 30% of phendione activity was lost in the course of study, on the other hand calibration of biosensors with fresh glutamate solution in the presence of fresh coenzyme under the same conditions did not result in increase of response current, therefore the main reason for the lose of current was the decomposition of Os-phendione-PVP at the electrode surface, the leaching of the enzyme was a less important factor.

Shelf-life study of glutamate biosensors. In order to compare the efficiency of different ways for the improvement of operational stability of glutamate biosensors, screen printed electrodes (Figure S-3 in Supporting Information) were modified by deposition 0.5 µl of a mixture containing GLDH (thermophilic or mesophilic one), NAD⁺, stabilizing additive, and soluble mediator for the electrochemical oxidation of NADH [Os(4,4'-dimethyl-2,2'-bipyridine)₂(1,10-phenanthroline-5,6-dione)]Cl₂ as described in Supporting Information. It was found that the best procedure to measure the response (when the relative standard deviation for 3-5 electrodes was minimized to 10-15 %) was to

apply 0.5 μL of a sample solution to an electrode heated to 40°C , wait for 20 s, apply the potential of 200 mV and record the current after 30 s. Big batches of glutamate sensors were prepared and kept at 40°C to carry out the accelerated shelf-life study. The response to glutamate was measured as the difference between response currents to pure buffer and 0.6 M glutamate solution in the same buffer. In order to take into account the decrease in response originated from the instability of NAD^+ , the response to samples of 0.6 M glutamate containing 0.18 M NAD^+ was registered during this stability study. The results of this study can be found in Figure S-12 and Table S-IV in the Supporting Information.

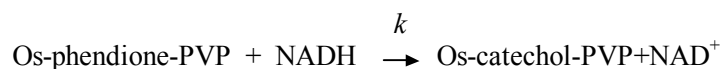
The common trend for all tested glutamate sensors based on screen printed electrodes was that the response to pure glutamate was higher by 1.5 times than the response to glutamate samples containing 0.18 M NAD^+ . The controlled electrodes prepared without enzymes showed the response to 6 mg/mL NADH equal to $0.46 \mu\text{A}$ whereas the response to NADH of the same concentration in the presence of 0.18 M NAD^+ was $0.307 \mu\text{A}$ i.e. once again the ratio was 1.5. According to the literature⁵² a charge-transfer complex between a mediator and NADH is involved in the mechanism of electrochemical oxidation of NADH:



The fact that the overall rate of NADH oxidation can be decreased by addition of NAD^+ supports the hypothesis of charge transfer complex and suggests that the parasite complex between NAD^+ and $[\text{Os}(4,4'\text{-dimethyl-2,2'}\text{-bipyridine})_2(1,10\text{-phenanthroline-5,6-dione})]\text{Cl}_2$ is formed too.

In order to obtain more experimental data about the influence of NAD^+ on the rate of electrocatalytic NADH oxidation by the mediator graphite electrodes were modified with $[\text{Os}(4,4'\text{-dimethyl-2,2'}\text{-bipyridine})_2(1,10\text{-phenanthroline-5,6-dione})](\text{PF}_6)_2$ according to.⁵⁴ Then the effect of NAD^+ concentration on the response of modified electrodes to 1.3 mM NADH was studied (Figure S-13 in Supporting Information). The effect of NAD^+ is significant starting from 10 mM. In addition the kinetic

constants k_{+2} , K_M and coefficient k of NADH oxidation in the presence of NAD^+ were measured using graphite rotating disk electrodes modified with the above mentioned mediator.⁵³ Where k is the apparent coefficient of the following overall reaction:



The determination of the kinetic constants was performed at pH 7.0 under argon by diluting the initial 1.8 mM NADH solution containing 20 mM NAD^+ with deaerated phosphate buffer containing only NAD^+ of the same concentration in order to avoid the influence of possible electrode fouling. The obtained experimental data in the form of the Koutecky-Levich plot can be seen in Figure S-14 in Supporting Information.. The experimental data were treated by the method published elsewhere⁵⁵ to yield $k_{[\text{NADH}] = 0}$ $(0.5 \pm 0.1) \times 10^3 \text{ M}^{-1} \text{ s}^{-1}$, k_{+2} $0.6 \pm 0.1 \text{ s}^{-1}$, and K_M $1.4 \pm 0.2 \text{ mM}$. According to our previous study⁵⁴ this mediator has the following constants under the same experimental conditions but in the absence of NAD^+ : $k_{[\text{NADH}] = 0}$ $0.9 \times 10^3 \text{ M}^{-1} \text{ s}^{-1}$, k_{+2} 0.8 s^{-1} , and K_M 4.3 mM . This decrease in the value of kinetic constant k_{+2} is obviously caused by the interaction of NAD^+ with the charge transfer complex between NADH and mediator. The two fold change in $k_{[\text{NADH}] = 0}$ could be explained by the competition between NADH and NAD^+ for the free mediator hence it should be admitted that the oxidized cofactor is capable to form parasite complex with the molecules of the osmium mediator.

The use of thermophilic GLDH instead of mesophilic enzyme allowed to increase the shelf half life at 40°C by 11 times (from 7 to 75 h) because of intrinsic thermostability of thermophilic GLDH. Gorton with coworkers also reported that carbon pastes based on thermophilic GLDH retain 90-100% of activity at 4°C during 2 weeks.³²

In addition a number of compounds such as the copolymer of vinyl-pyrrolidone and dimethylamino ethyl methacrylate termed as Gafquat[®] HS100, poly(ethylene imine), trehalose, and glycerol were tested by us with the respect to improvement of shelf stability (Table S-IV in the Supporting Information). Electrodes prepared with the use of glycerol proved to be very unstable and lost one half of initial

response in less than 6 h probably because of denaturing effect of glycerol which stayed on the electrode surface during the study. Poly(ethylene imine) was not active in improvement of stability of the thermophilic GLDH based sensors prepared utilizing this polymer as additive, these sensors were less stable than the sensors based on pure enzyme by 2 times, supposedly due to oxidation of imino groups. Trehalose had almost no influence on stability of neither mesophilic or thermophilic GLDH based sensors. Only copolymer of vinyl-pyrrolidone and dimethylamino ethyl methacrylate, Gafquat[®] HS100, significantly improved stability of both mesophilic and thermophilic sensors by 4.6 and 3.3 times respectively. The most important factor contributing to enzyme stability is the control of the relative water activity at the enzyme surface. We suggest that the latter polyelectrolyte, promoting electrostatic interactions, forms a protein-polyelectrolyte complex resulting in mimicking aqueous environment of enzymes.

CONCLUDING REMARKS

Two novel methods for the fabrication of reagentless biosensors based on NAD⁺ dependent dehydrogenases have been developed and reagentless glutamate biosensors operating at 150 mV vs. Ag/AgCl/KCl_{sat} have been constructed and characterized by studying response curves, operational stability, dependence of response on temperature and pH. Their response is limited by the rate of NADH oxidation at the electrode surface. Use of thermophilic glutamate dehydrogenase and the stabilizing additive Gafquat[®] HS100 helped to improve operational and shelf stability of these biosensors. The hypothesis of charge-transfer complex formed between NADH and a mediator was confirmed.

ACKNOWLEDGEMENTS

This paper was supported by the grant of European Community, Industrial & Material Technologies Programme (Brite-EuRam III), Ref.: project No. BE97-4511 and by the Spanish Ministry of Education and Culture Ref.: Acciones Especiales MAT98-1413 CE. V. P. acknowledges the Ph. D. fellowship from the Department of Chemical Engineering of the University Rovira i Virgili.

Supporting Information Available. Additional information as noted in text. This material is available free of charge via the Internet at <http://pubs.acs.org>

FIGURE CAPTIONS

Figure 1. Schematic diagram of the electron transfer steps for the mediated glutamate biosensors.

Figure 2. Cyclic voltammograms of reagentless glutamate biosensors fabricated with the use of mesophilic bovine GLDH based on NAD⁺-alginate (**A**) and the “binder” polymer (**B**). Experimental conditions: scan rate 0.4 mV s⁻¹, 0.1 M phosphate buffer (pH 7.4), 0.35 M glutamate, temperature 30°C

Figure 3. Effect of pH on maximum response of reagentless glutamate biosensors based on NAD-alginate fabricated with the use mesophilic (**A**) and thermophilic GLDH (**B**). Experimental conditions: E_{app} 150 mV vs. Ag/AgCl/KCl_{sat}, 0.1 M phosphate buffer of varied pH, temperature 30°C for mesophilic biosensors and 40°C for thermophilic ones, glutamate concentration was 0.3 M.

Figure 4. Effect of pH on maximum response of reagentless glutamate biosensors based on binder polymer fabricated with the use of mesophilic (**A**) and thermophilic GLDH (**B**). Experimental conditions: E_{app} 150 mV vs. Ag/AgCl/KCl_{sat} 0.1 M phosphate buffer of varied pH, 0.35 M glutamate, temperature 30°C for mesophilic biosensors and 40°C for thermophilic ones.

Figure 5. Effect of temperature on maximum response of reagentless glutamate biosensors based on NAD⁺-alginate fabricated with the use of mesophilic (A) and thermophilic GLDH (B). Experimental conditions: E_{app} 150 mV vs. Ag/AgCl/KCl_{sat}, 0.1 M phosphate buffer (pH 7.4), 0.35 M glutamate.

Figure 6. Effect of temperature on maximum response of reagentless glutamate biosensors based on binder polymer fabricated with the use of mesophilic (A) and thermophilic GLDH (B). Experimental conditions are the same as in Figure 5.

Table I. Activation energies of the reagentless glutamate biosensors calculated from Arrhenius plots.

| Methods of NAD⁺ immobilization | E_a for mesophilic GLDH / kJ mol⁻¹ | E_a for thermophilic GLDH / kJ mol⁻¹ |
|--|--|--|
| NAD ⁺ -alginate | 53.9 | 58.24 |
| “binder” polymer | 56.9 | 62.2 |

Table II. Basic characteristics of reagentless glutamate biosensors calculated from Eadie-Hofstee plots. Detection limit is defined as the analyte concentration at which the response is three times higher than the background.

| Methods of NAD ⁺ immobilization | Mesophilic GLDH | | | | | | | |
|--|---|-----------|---------------------|---------------------------|------------------------------|---------------------|--|----------------------------------|
| | J _{max} , μA cm ⁻² | RSD, % | Response time, s | K _B app, mM | Limit of detection, mM | Linear range, mM | Sensitivity, μA mM ⁻¹ cm ⁻² | Operational half-life time, h |
| NAD ⁺ -alginate | 14.26 | 21 | 100 | 14.3 | 0.5 | 1.852-6.0 | 0.496 | 1.5 |
| Binder polymer | 7.8 | 5.0 | 100 | 10.1 | 0.3366 | 1.4-4.3 | 0.3366 | 12 |

| Methods of NAD ⁺ immobilization | Thermophilic GLDH | | | | | | | |
|--|---|-----------|---------------------|---------------------------|------------------------------|---------------------|--|----------------------------------|
| | J _{max} , μA cm ⁻² | RSD, % | Response time, s | K _B app, mM | Limit of detection, mM | Linear range, mM | Sensitivity, μA mM ⁻¹ cm ⁻² | Operational half-life time, h |
| NAD ⁺ -alginate | 13.0 | 14 | 70 | 39 | 4.0 | 13-38.5 | 0.0633 | 0.4 |
| Binder polymer | 19.1 | 20 | 70 | 55 | 6.0 | 6.6-34.0 | 0.214 | 0.73 |

REFERENCES

- (1) Niwa, O.; Torimitsu, K.; Osborne, P.; Yamamoto, K. *Anal. Chem.* 1996, *68*, 1865-1870.
- (2) Engelsen, B. *J. Neurochem.* 1986, *74*, 1634-1641.
- (3) Greenamyre, J. T. *Arch. Neurol.* 1986, *43*, 1058-1063.
- (4) Rietz, B.; Guilbault, G. G. *Anal. Chim. Acta* 1975, *74*, 191-198.
- (5) Fortier, G.; Tenaschuk, D.; Mackenzie, S. L. *J. Chromatogr.* 1986, *361*, 253-261.
- (6) Athanasiou-Malakai, E.; Koupparis, M. M. *Analyst* 1987, *112*, 757-761.
- (7) Mora, R.; Berndt, K. D.; Tsai, H.; Meredith, S. C. *Anal. Biochem.* 1988, *172*, 368-376.
- (8) O'Shea, T. J.; Weber, P. L.; Bammel, B. P.; Lunte, C. E.; Smyth, M. R. *J. Chromatogr.* 1992, *608*, 189-195.
- (9) Kiba, N.; Moriya, T.; Furasawa, M. *Anal. Chim. Acta* 1992, *256*, 221-224.
- (10) Dremel, B. A. A.; Schmidt, R. D.; Wolfbeis, O. S. *Anal. Chim. Acta* 1991, *248*, 351-359.
- (11) Cosford, R. J.; Kuhr, W. G. *Anal. Chem.* 1996, *68*, 2164-2169.
- (12) Yao, T.; Kobayashi, N.; Wasa, T. *Anal. Chim. Acta* 1990, *231*, 121-124.
- (13) Berners, M. O. M.; Boutelle, M. G.; Filinz, M. *Anal. Chem.* 1994, *66*, 2017-2021.
- (14) Hale, P. D.; Lee, H. S.; Okamoto, Y.; Skotheim, T. A. *Anal. Lett.* 1991, *24*, 345-356.
- (15) Pantano, P.; Kuhr, W. *Anal. Chem.* 1993, *65*, 623-630.
- (16) Davies, P.; Mosbach, K. *Biochim. Biophys. Acta* 1974, *370*, 329-338.

- (17) Smith, M. D.; Olson, C. L. *Anal. Chem.* 1975, 47, 1074-1077.
- (18) Amine, A.; Kauffmann, J. -M.; Palleschi, G. *Anal. Chim. Acta* 1993, 273, 213-218.
- (19) Laurinavicius, V.; Kurtinaitiene, B.; Gureviciene, V.; Boguslavsky, L.; Geng, L.; Scotheim, T. *Anal. Chim. Acta* 1996, 330, 159-166.
- (20) Leca, B.; Marty, J. L. *Biosens. Bioelectron.* 1997, 12, 1083-1088.
- (21) Maines, A.; Prodromidis, M. I.; Tzouwara, S. M.; Karayannis, M. I.; Ashworth, D.; Vadgama, P. *Anal. Chim. Acta* 2000, 408, 217-224.
- (22) Ikariyama, Y.; Ishizuka, T.; Sinohara, H.; Aizawa, M. *Denki Kagaku* 1990, 58, 1097-1102.
- (24) Yoon, H. C.; Kim, H. S. *Anal. Chim. Acta* 1996, 336, 57-65.
- (25) Hedemno, M.; Narváez, A.; Dominguez, E.; Katakis, I. *Analyst* 1996, 121, 1891-1895.
- (26) Alvarez, S. L.; Lobo, M. J.; Miranda, A. J.; Tuñon, P. *Biosens. Bioelectron.* 1997, 12, 739-747.
- (27) Katz, E.; Heleg, V.; Bardea, A.; Willner, I.; Rau, H. K.; Haehnel, W. *Biosens. Bioelectron.* 1998, 13, 741-756.
- (28) Consalvi, V.; Chiaraluce, R.; Politi, L.; Gambacorta, A.; DeRosa, M.; Scandurra, R. *Eur. J. Biochem.* 1991, 196, 459-467.
- (29) Consalvi, V.; Chiaraluce, R.; Politi, L.; Vaccaro, R.; DeRosa, M.; Scandurra, R. *Eur. J. Biochem.* 1991, 202, 1189-1196.
- (30) Hudson, R. C.; Ruttersmith, L.D.; Daniel, R. M. *Biochim. Biophys. Acta* 1993, 1202, 244-250.
- (31) Ma, K.; Robb, F. T.; Adams, M. W. W. *Appl. Environ. Microbiol.* 1994, 60, 562-568.
- (32) Jeffries, C.; Pasco, N.; Baronian, K.; Gorton, L. *Biosens. Bioelectron.* 1997, 12, 225-232.

- (33) Pasco, N.; Jeffries, C.; Davies, Q.; Downard, A. J.; Roddick-Lanzilotta, A. D.; Gorton, L. *Biosens. Bioelectron.* 1999, *14*, 171-178.
- (34) Amouyal, E.; Homsí, A.; Chambron, J.-C.; Sauvage, J.-P. *J. Chem. Soc., Dalton Trans.* 1990, 1841-1845.
- (35) Parellada, J.; Narvaez, A.; Dominguez, E.; Katakis, I. *Biosens. Bioelectron.* 1997, *14*, 267-275.
- (36) Lay, P. A.; Sargeson, A. M.; Taube, H. In *Inorganic Synthesis*; Shreeve J. M., Ed.; John Wiley: New York, 1986; Vol 24; pp. 293-295.
- (37) Goss, C. A.; Abruña, H. D. *Inorg. Chem.* 1985, *24*, 4263-4267.
- (38) Nakamura, Y.; Suye, S.; Kira, J.; Tera, H.; Tabata, I.; Senda, M. *Biochim. Biophys. Acta* 1996, *1289*, 221-225.
- (39) Pavlov, V.; Rincón, O.; Solé, S.; Narváez, A.; Domínguez, E.; Katakis, I. Submitted to *Anal. Chem.*
- (40) Degani, Y.; Heller, A. *J. Am. Chem. Soc.* 1989, *111*, 2357-2358.
- (41) Gregg, B. A.; Heller, A. *J. Phys. Chem.* 1991, *95*, 5976-5980.
- (42) Smith, E. L.; Austen, B. M.; Blumenthal, M. K.; Nyc, J. F. In *The Enzymes*; Boyer, P. D., Ed.; Academic Press: New York, 1975, volume XI, pp. 359-360.
- (43) Yamamura, A.; Sakaguchi, T.; Murakami, Y.; Yokoyama, K.; Tamiya, E. *J. Biochem.* 1999, *125*, 760-769.
- (44) Engel, P. C.; Dalziel, K. *Biochem. J.* 1969, *115*, 621-631.
- (45) Engel, P. C.; Dalziel, K. *Biochem. J.* 1970, *118*, 409-419.
- (46) Engel, P. C.; Chen, S. S. *Biochem. J.* 1975, *151*, 305-318.

- (47) Colen, A. H.; Prough, R. A.; Fisher, H. F. *J. Biol. Chem.* 1972, *247*, 7905-7909.
- (48) Silverstein, E.; Sulebele, G. *Biochemistry* 1973, *12*, 2164-2172.
- (49) Rife, J. C.; Cleland, W. W. *Biochemistry* 1980, *19*, 2321-2328.
- (50) O'Flaherty, M.; McMahon, M.; Forde, J.; Mulcahy, P. *Prot. Express. Purif.* 1999, *16*, 276-297.
- (51) Albery, W. J.; Bartlett, P. N.; Cass, A. E. G.; Sim, K. W. *J. Electroanal. Chem.* 1987, *218*, 127-134.
- (52) Gorton, L. *J. Chem. Soc., Faraday Trans.* 1986, *82*, 1245-1258.
- (53) Fahien, L. A.; Strmecki, M. *Arch. Biochem. Biophys.* 1969, *130*, 468-477.
- (54) Popescu, I. C.; Domínguez, E.; Narváez, A.; Pavlov, V.; Katakis, I. *J. Electroanal. Chem.* 1999, *464*, 208-214.
- (55) Gorton, L.; Torstensson, A.; Jaegfeldt, H.; Johansson, G. *J. Electroanal. Chem.* 1984, *161*, 103-120.

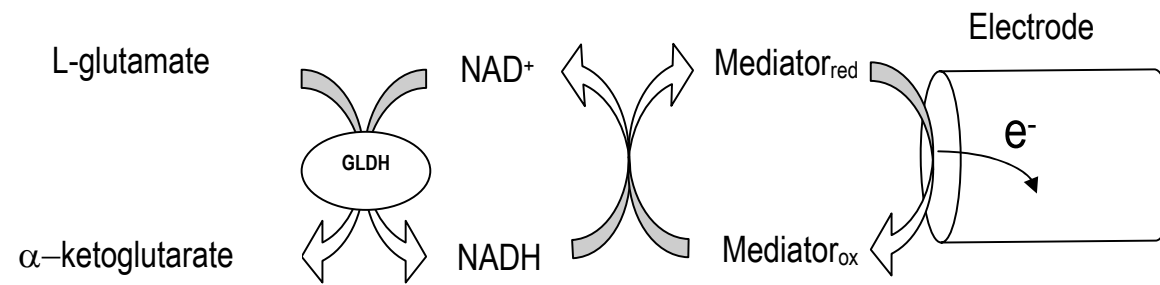
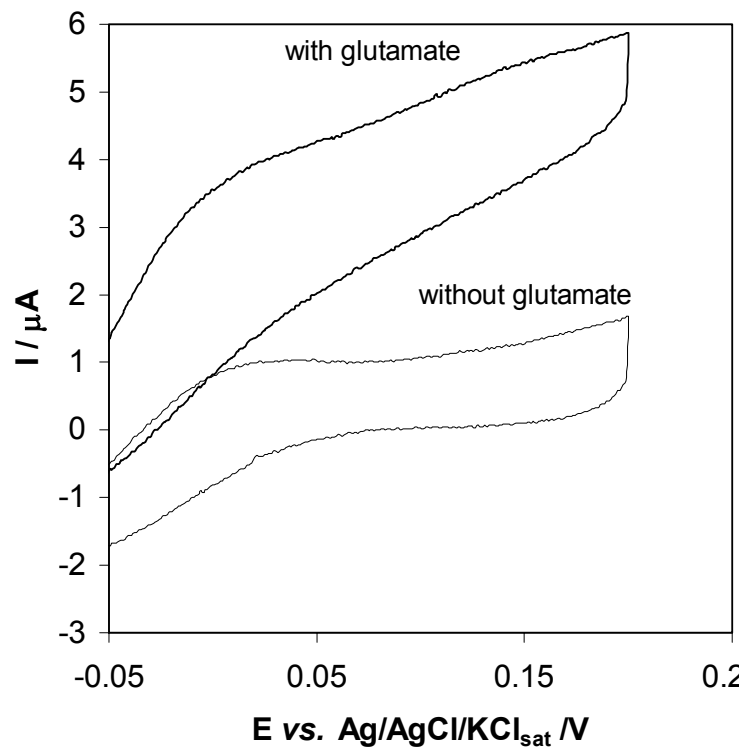
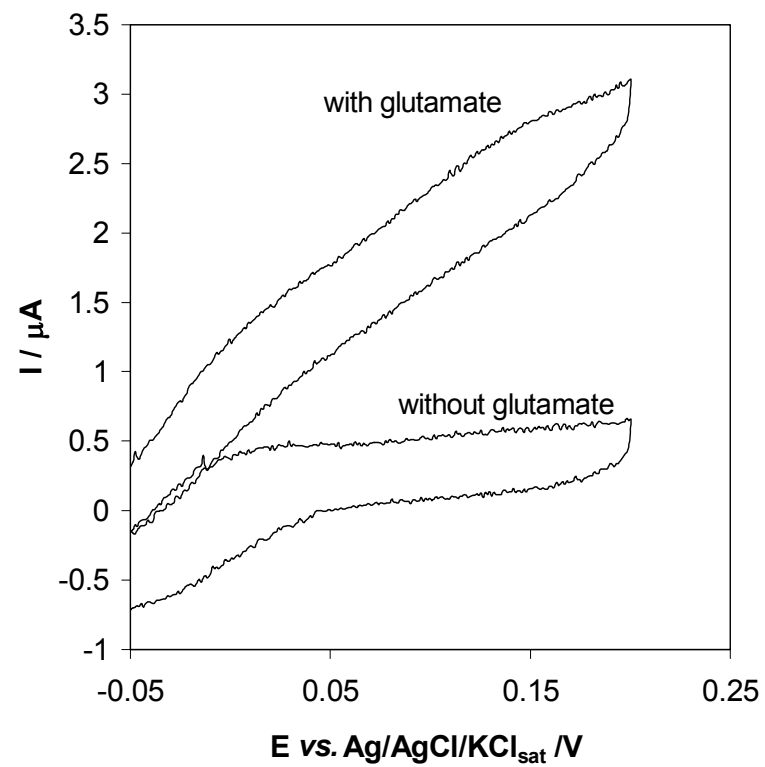


Figure 1

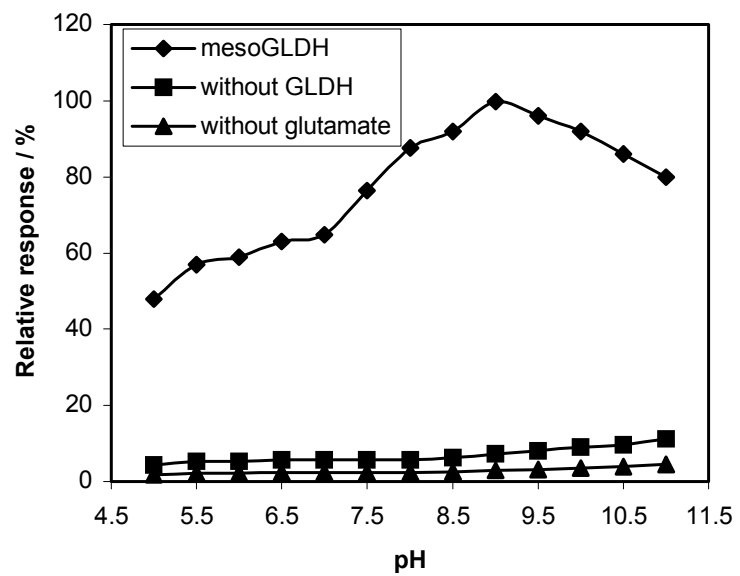


(A)

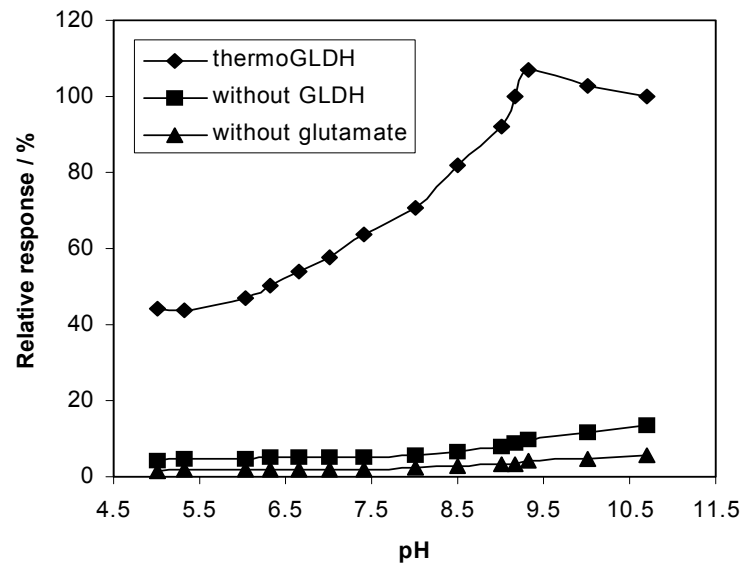


(B)

Figure 2

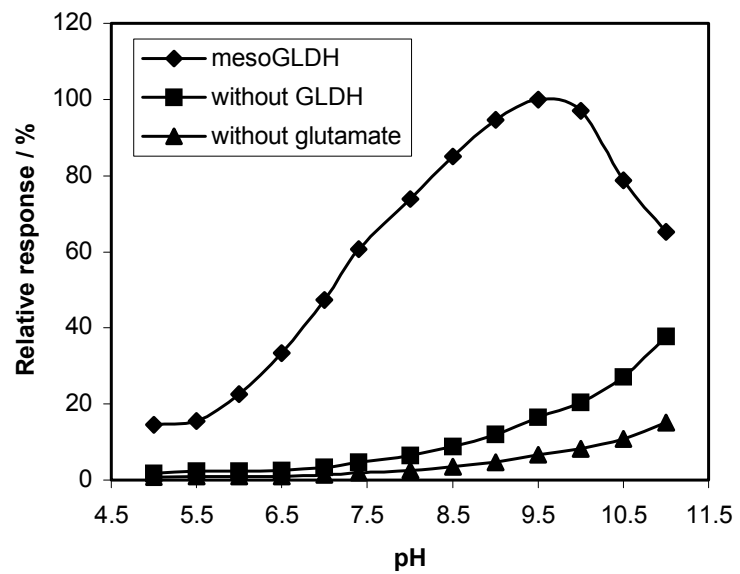


(A)

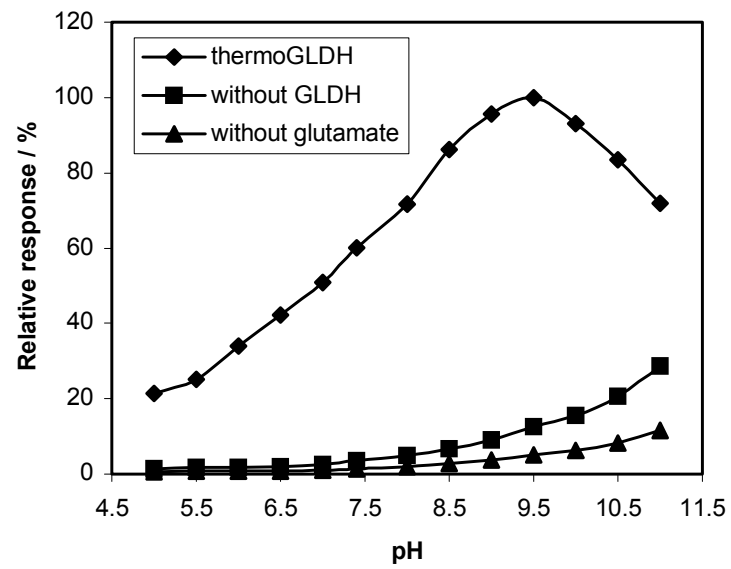


(B)

Figure 3

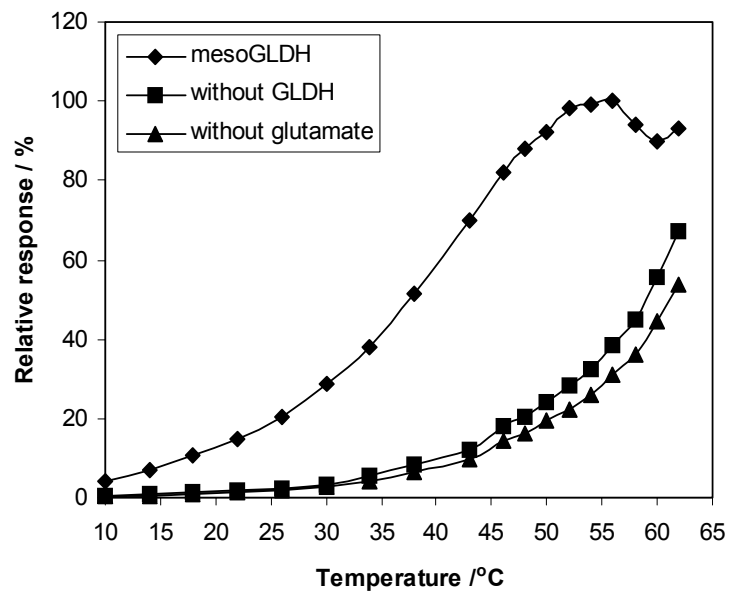


(A)

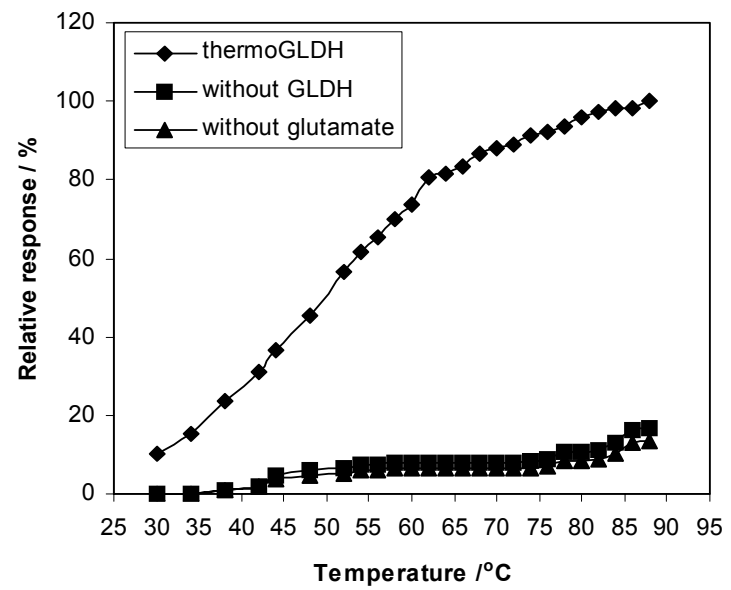


(B)

Figure 4

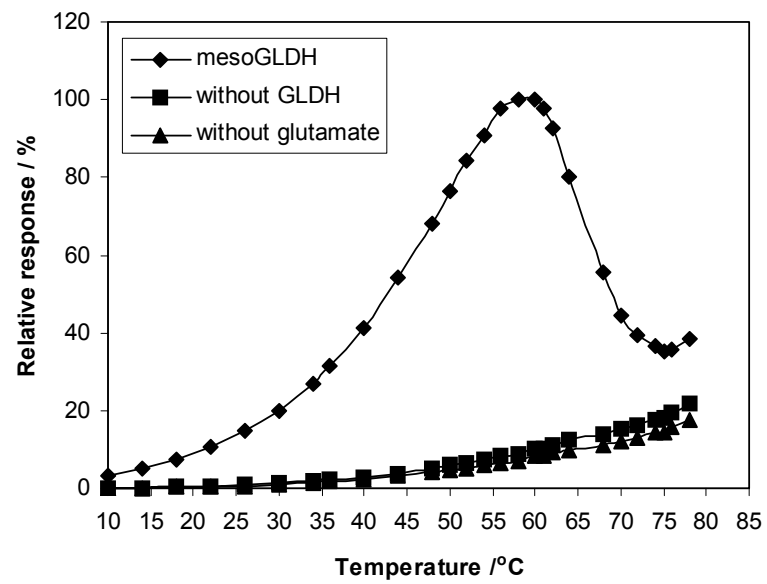


(A)

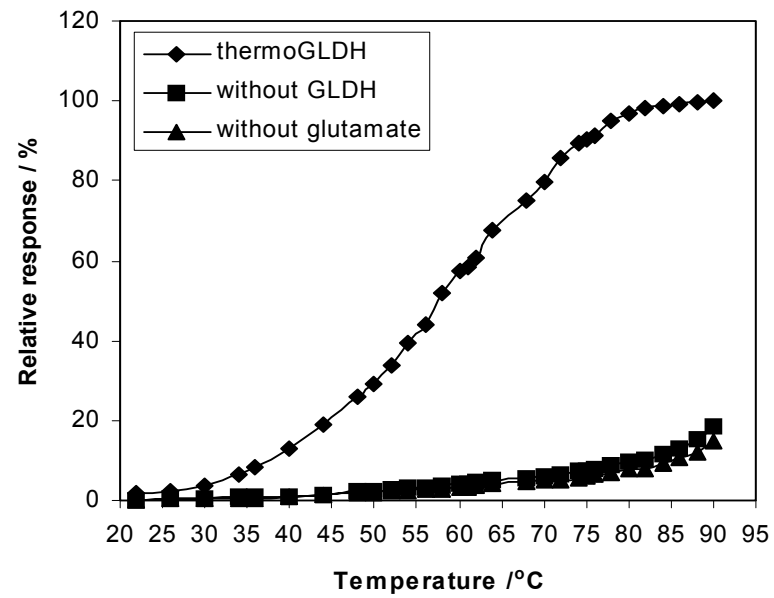


(B)

Figure 5



(A)



(B)

Figure 6

Supporting Information

A Novel [Os(1,10-phenanthroline-5,6-dione)₂(PVP)₄Cl]Cl Redox Polymer for Electrocatalytic Oxidation of NADH and its Application to the Construction of Reagentless β -D-glucose Biosensors

Valeri Pavlov¹, Óscar Rincón², Sonia Solé¹, Arantzazu Narváez², Elena Domínguez², Ioanis Katakis^{1*}

¹Bioanalysis and Bioelectrochemistry Group, Chemical Engineering, Universitat Rovira i Virgili, E-43006, Tarragona (Catalonia), Spain. ²Departamento de Química Analítica, Universidad de Alcalá, E-28871 Alcalá de Henares (Madrid), Spain.

EXPERIMENTAL SECTION

Materials. β -Dihyronicotinamide adenine dinucleotide (NADH), β -nicotinamide adenine dinucleotide (NAD⁺), were purchased from Sigma (Madrid, Spain). Glucose dehydrogenase (GDH) (EC 1.1.1.47) from *Bacillus megaterium* (220 U/mg protein) was obtained from Merck (Darmstadt, Germany). Sodium phosphate salts, sodium chloride and dimethylformamide were from Aldrich (Madrid, Spain). Ethylene glycol and β -D-glucose were purchased from Panreac (Madrid, Spain). Poly(ethylene glycol) diglycidyl ether (PEGDGE) and poly(4-vinyl pyridine) (PVP) were obtained from Polysciences Inc. (Warrington, PA, USA). Spectrographic graphite rods were acquired from Carbone of America Corp. Ultra Carbon Division (Bay City, MI, USA). Fine emery paper was from Buehler Ltd. (Lake Bluff, IL, USA). All other reagents were of analytical grade. Water was produced in a Mili-QTM system (Millipore Corp., Bedford, MA, USA). [Os(1,10-phenanthroline-5,6-dione)₂Cl₂] was synthesized according to an earlier published modified method.^{28,31} The ¹H NMR investigation performed in (CD₃)₂SO with a tetramethylsilane standard demonstrated following shifts δ_{H} : 8.1 ppm (2H dd), 7.53 ppm (2H dd), and 7.15 ppm (2H dd). Poly(4-vinyl pyridine) was derivatized with bromoethylamine as reported elsewhere⁶² to yield the “binder” polymer.

Synthesis of Os-phendione-PVP. 80 mg of [Os(1,10-phenanthroline-5,6-dione)₂Cl₂] and 50 mg of poly(4-vinylpyridine) were mixed in 3 mL ethylene glycol. The mixture was deaerated with argon during 10 min and refluxed under argon in darkness during 1 h, the temperature of the oil bath being maintained below 220°C, next the reaction mixture was cooled to room temperature and added dropwise to

100 mL of aqueous 1 M sodium chloride solution during 15 min. The resulting mixture was left to stay overnight at 4°C, the precipitate was filtered off, washed with water and air-dried. The synthesis route and the suggested structure of the resulting redox polymer is shown in Figure 1. [Anal. Calcd. For n=4: C, 61.52%; H, 1.76%; N, 10.99%. Found: C, 61.71%; H, 1.70%; N, 10.7%.

Preparation of electrodes modified with Os-phendione-PVP. Spectrographic graphite rods of 3 mm diameter were fixed inside heat shrunk PVC tubes. Before use they were wet polished on fine (grit 400 and 600) emery paper to produce graphite electrodes having a flat circular surface.

Modification of the surface of electrodes was carried out by spreading of 1 μL on an electrode of 1.8 mg/mL Os-phendione-PVP solution in ethylene glycol. The polymer solution was left on the electrode surface for 3 min, the surface was washed with 2-3 drops of ethylene glycol and deionised water. The surface coverage was determined at pH 5.0 from the areas under the peak of cyclic voltammograms of phendione ligands at 10 mV s^{-1} assuming that four electrons were exchanged.

Preparation of β -D-glucose biosensors. A mixture containing 8.5 mg/mL “binder” polymer, 34 mg/mL NAD^+ , 1 mg/mL PEGDGE, and 28 U/mL glucose dehydrogenase in 0.04 M sodium phosphate buffer (pH 7.6) was composed. Next 5 μL of the resulting mixture were placed on an Os-phendione-PVP modified electrode and dried under vacuum during 12 h.

Electrochemical measurements. For both amperometry and cyclic voltammetry a three-electrode conventional thermostabilised cell (3 mL) equipped with a $\text{Ag}/\text{AgCl}/\text{KCl}_{\text{sat}}$ reference electrode, and a platinum auxiliary electrode was used, a graphite electrode, modified according to one of the above mentioned procedures, being the working electrode. The buffer, pH 6.0 (0.1 M sodium phosphate and 0.15 M sodium chloride) served as supporting electrolyte. The pH was adjusted using concentrated NaOH or H_3PO_4 . A computer-controlled BAS CV-50W voltammetric analyser (Bioanalytical Systems Inc., West Lafayette, IN, USA) was employed in cyclic voltammetry and steady state rotating electrode measurements. The rotating disk electrode, having the same spectrographic graphite as disk material, was operated by a modulated speed rotator AMSFRX (Pine Instruments Co., Grove City, PA, USA). The response to successive additions of stock β -D-glucose was registered as the steady state current with a computer controlled three-electrode potentiostat AUTOLAB PGSTAT 10 (Eco Chemie BV, The Netherlands). The working potential was 150 mV vs. $\text{Ag}/\text{AgCl}/\text{KCl}_{\text{sat}}$ and the temperature of the thoroughly stirred solution was 25°C unless indicated otherwise.

Electrochemical Conversion Experiments. Electrodes were prepared by fixing spectrographic graphite rods having diameter of 6 mm inside a heat shrunk PVC. They were wet polished on fine (grit 400 and 600) emery paper, cleaned by sonication, air-dried and modified with 4 μL of 1.8 mg/mL Os-phendione-PVP solution according to the above mentioned procedure. Next they were immersed into 2 mL of 18 μM NADH solution in 0.1 M phosphate buffer (pH 6.0) deaerated with argon, and poised at 150 mV vs. $\text{Ag}/\text{AgCl}/\text{KCl}_{\text{sat}}$ with stirring in a three-electrode electrochemical cell at 25 °C. Spectrophotometrical measurements of absorbance at 340 nm (A_{340}) were used to determine the depletion of the NADH concentration during 1 hour (A_{340} changed from 0.1117 in the beginning to 0.0540 at the end of experiment, RSD 5%). Then, 1 mL of the resulting solution was mixed with 30 μL of a mixture

containing glucose dehydrogenase and 50 fold excess of glucose and the recovery of NADH concentration was monitored spectrophotometrically until reaching the end point (A_{340} equal to 0.0867). These values were corrected for the ΔA_{340} (from 0.1117 to 0.0902, RSD 6%) of a controlled solution of NADH during 1 hour which was not subjected to electrolysis in order to quantify the spontaneous decomposition of NADH. The area under the chronoamperometric plots was assessed to find the charge passed through the circuit during the electrocatalytic NADH oxidation which was equal to (2.3 ± 0.3) mC.

STEADY-STATE KINETIC MODEL OF BIOSENSORS

Figure 8S illustrates the kinetic scheme for the operation of reagentless biosensors based on a dehydrogenase enzyme (E) catalyzing the reaction of NAD^+ (A) with a substrate (B) to give NADH (P) and a product (Q). Then a mediator (M), which has reduced (M_{red}) and oxidized (M_{ox}) forms, immobilized on the electrode surface, catalyzes the electrochemical conversion of P back to A. A_{im} and P_{im} are the concentrations of immobilized A and P. B_0 and Q_0 are the concentrations of the substrate and the product inside of the hydrogel. B_∞ and Q_∞ are the concentrations of the substrate and the product in the external medium. k'_B and k'_Q are mass transfer constants of the substrate and the product (cm s^{-1}), respectively. L is the thickness of the hydrogel layer. The following expressions for the flux of P to the electrode surface (j_{el}), which determines the current density of a biosensor (j) through the expression $j = nFj_{\text{el}}$, where n is the number of exchanged electrons and F is the Faraday's constant, can be obtained:

$$j_{\text{el}} = k'_B(B_\infty - B_0) \quad (1\text{S})$$

$$j_{\text{el}} = L(k_3 A_{\text{im}}[E] - k_{-3}[E \cdot A]) \quad (2\text{S})$$

$$j_{\text{el}} = L(k_4 B_0[E \cdot A] - k_{-4}[E \cdot A \cdot B]) \quad (3\text{S})$$

$$j_{\text{el}} = L(k_5[E \cdot A \cdot B] - k_{-5}[E \cdot P \cdot Q]) \quad (4\text{S})$$

$$j_{\text{el}} = L(k_6[E \cdot P \cdot Q] - k_{-6}[E \cdot P]Q_0) \quad (5\text{S})$$

$$j_{\text{el}} = L(k_7[E \cdot P] - k_{-7}[E]P_{\text{im}}) \quad (6\text{S})$$

$$j_{\text{el}} = k'_Q Q_0 \quad (7\text{S})$$

$$j_{\text{el}} = k_1 P_{\text{im}} \Gamma_{\text{Mox}} - k_{-1} \Gamma_{\text{M} \cdot \text{P}} \quad (8\text{S})$$

$$j_{\text{el}} = k_2 \Gamma_{\text{M} \cdot \text{P}} \quad (9\text{S})$$

$$j_{\text{el}} = k_3 \Gamma_{\text{Mred}} \quad (10\text{S})$$

$$E_t = [E] + [E \cdot A] + [E \cdot A \cdot B] + [E \cdot P \cdot Q] + [E \cdot P] \quad (11\text{S})$$

$$\Gamma = \Gamma_{\text{M} \cdot \text{P}} + \Gamma_{\text{Mox}} + \Gamma_{\text{Mred}} \quad (12\text{S})$$

$$A_t = A_{\text{im}} + P_{\text{im}} \quad (13\text{S})$$

Where Γ_{Mox} and Γ_{Mred} are surface coverages of the mediator in oxidized and reduced forms, respectively. Γ is the total mediator surface coverage. $\Gamma_{\text{M} \cdot \text{P}}$ is the surface coverage of the intermediate complex between the mediator and NADH. A_t and E_t are the total concentrations of the cofactor and the enzyme immobilized in the hydrogel, respectively. A_{im} and P_{im} are the concentrations of NAD^+ and NADH in the hydrogel respectively. The equations(2S-6S, 11S) yield the equation (14S) describing the enzyme kinetics.

$$j_{el} = \frac{E_t L(k_3 k_4 k_5 k_6 k_7 A_{im} B_o - k_{-3} k_{-4} k_{-5} k_{-6} k_{-7} P_{im} Q_o)}{K_6 k_7 k_{-3} k_{-4} + k_{-3} k_5 k_6 k_7 + k_7 k_{-3} k_{-4} k_{-5} + (k_3 k_6 k_7 k_{-4} + k_3 k_5 k_6 k_7 + k_3 k_7 k_{-4} k_{-5}) A_{im} + k_4 k_5 k_6 k_7 B_o + (k_3 k_4 k_6 k_7 + k_3 k_4 k_7 k_{-5} + k_3 k_4 k_5 k_7 + k_3 k_4 k_5 k_6) A_{im} B_o + (k_6 k_{-3} k_{-4} k_{-7} + k_5 k_6 k_{-3} k_{-7} + k_{-3} k_{-4} k_{-5} k_{-7}) P_{im} + k_{-3} k_{-4} k_{-5} k_{-6} Q_o + (k_{-4} k_{-5} k_{-6} k_{-7} + k_{-3} k_{-5} k_{-6} k_{-7} + k_{-3} k_{-4} k_{-6} k_{-7} + k_5 k_{-3} k_{-6} k_{-7}) P_{im} Q_o + k_3 k_{-4} k_{-5} k_{-6} A_{im} Q_o + (k_4 k_{-5} k_{-6} k_{-7} + k_4 k_5 k_{-6} k_{-7}) B_o P_{im} Q_o + (k_3 k_4 k_{-5} k_{-6} + k_3 k_4 k_5 k_{-6}) A_{im} B_o Q_o + k_4 k_5 k_6 k_{-7} B_o P_{im}} \quad (14S)$$

When numerator and denominator of this rate equation are multiplied by the factor $(k_{-3} k_{-4} k_{-5} k_{-6} k_{-7}) / ((k_3 k_4 k_6 k_7 + k_3 k_4 k_7 k_{-5} + k_3 k_4 k_5 k_7 + k_3 k_4 k_5 k_6)(k_{-4} k_{-5} k_{-6} k_{-7} + k_{-3} k_{-5} k_{-6} k_{-7} + k_{-3} k_{-4} k_{-6} k_{-7} + k_5 k_{-3} k_{-6} k_{-7}))$ the following equation can be obtained:

$$j_{el} = \frac{L(V_1 V_2 A_{im} B_o - (V_1 V_2 P_{im} Q_o) / K_{eq})}{K_{AB} V_2 + K_B V_2 A_{im} + K_A V_2 B_o + V_2 A_{im} B_o + K_Q V_1 P_{im} / K_{eq} + K_P V_1 Q_o / K_{eq} + V_1 P_{im} Q_o / K_{eq} + K_P V_1 A_{im} Q_o / (K_{iA} K_{eq}) + K_A V_2 B_o P_{im} Q_o / (K_{iP} K_{iQ}) + K_P V_1 A_{im} B_o Q_o / (K_{iA} K_{iB} K_{eq}) + K_A V_2 B_o P_{im} / K_{iP}} \quad (15S)$$

Where $V_1 = E_t(k_4 k_5 k_6 k_7) / (k_4 k_6 k_7 + k_4 k_7 k_{-5} + k_4 k_5 k_7 + k_4 k_5 k_6)$ and $V_2 = E_t(k_{-3} k_{-4} k_{-5} k_{-6}) / (k_{-4} k_{-5} k_{-6} + k_{-3} k_{-5} k_{-6} + k_{-3} k_{-4} k_{-6} + k_5 k_{-3} k_{-6})$ are the maximum velocities in forward and reverse directions, the equilibrium constant $K_{eq} = (k_3 k_4 k_5 k_6 k_7) / (k_{-3} k_{-4} k_{-5} k_{-6} k_{-7})$, Michaelis constants for A, B, P, Q are $K_A = (k_5 k_6 k_7) / (k_3 k_6 k_7 + k_3 k_7 k_{-5} + k_3 k_5 k_7 + k_3 k_5 k_6)$, $K_B = (k_6 k_7 k_{-4} + k_5 k_6 k_7 + k_7 k_{-4} k_{-5}) / (k_4 k_6 k_7 + k_4 k_7 k_{-5} + k_4 k_5 k_7 + k_4 k_5 k_6)$, $K_P = (k_{-3} k_{-4} k_{-5}) / (k_{-4} k_{-5} k_{-7} + k_{-3} k_{-5} k_{-7} + k_{-3} k_{-4} k_{-7} + k_5 k_{-3} k_{-7})$, $K_Q = (k_6 k_{-3} k_{-4} + k_5 k_6 k_{-3} + k_{-3} k_{-4} k_{-5}) / (k_{-4} k_{-5} k_{-6} + k_{-3} k_{-5} k_{-6} + k_{-3} k_{-4} k_{-6} + k_5 k_{-3} k_{-6})$, the inhibition constants for A, B, P, Q are $K_{iA} = k_{-3} / k_3$, $K_{iB} = (k_{-4} k_{-5} k_{-6} + k_{-3} k_{-5} k_{-6} + k_{-3} k_{-4} k_{-6} + k_5 k_{-3} k_{-6}) / (k_4 k_{-5} k_{-6} + k_4 k_5 k_{-6})$, $K_{iP} = k_7 / k_{-7}$, $K_{iQ} = (k_5 k_6) / (k_{-5} k_{-6} + k_5 k_{-6})$ and $K_{AB} = (k_6 k_7 k_{-3} k_{-4} + k_{-3} k_5 k_6 k_7 + k_7 k_{-3} k_{-4} k_{-5}) / (k_3 k_4 k_6 k_7 + k_3 k_4 k_7 k_{-5} + k_3 k_4 k_5 k_7 + k_3 k_4 k_5 k_6) = K_B K_{iA}$, $K_{PQ} = (k_6 k_7 k_{-3} k_{-4} + k_{-3} k_5 k_6 k_7 + k_7 k_{-3} k_{-4} k_{-5}) / (k_{-4} k_{-5} k_{-6} k_{-7} + k_{-3} k_{-5} k_{-6} k_{-7} + k_{-3} k_{-4} k_{-6} k_{-7} + k_5 k_{-3} k_{-6} k_{-7}) = K_Q K_{iP}$

Dividing numerator and denominator of (15S) by V_2 and taking into account that $V_1 / (V_2 K_{eq}) = (K_B K_{iA}) / (K_Q K_{iP})$ one can derive the equation (16S):

$$j_{el} = \frac{L(V_1 A_{im} B_o - (V_1 P_{im} Q_o) / K_{eq})}{K_{AB} + K_B A_{im} + K_A B_o + A_{im} B_o + K_B K_{iA} P_{im} / K_{iP} + K_P K_B K_{iA} Q_o / (K_Q K_{iP}) + K_B K_{iA} P_{im} Q_o / (K_Q K_{iP}) + K_P K_B K_{iA} A_{im} Q_o / (K_Q K_{iA} K_{iP}) + K_A B_o P_{im} Q_o / (K_{iP} K_{iQ}) + K_B K_P A_{im} B_o Q_o / (K_Q K_{iB} K_{iP}) + K_A B_o P_{im} / K_{iP}} \quad (16S)$$

The equations (8S-10S, 12S) give the equation (17S) which governs the kinetics of NADH oxidation at the electrode surface modified with the mediator

$$j_{el} = \frac{\Gamma k_1 k_2 k_S P_{im}}{k_2 k_S + k_{-1} k_S + (k_1 k_2 + k_1 k_S) P_{im}} = \frac{\Gamma P_{im} k_1 k_2 k_S / (k_1 k_2 + k_1 k_S)}{(k_2 k_S + k_{-1} k_S) / (k_1 k_2 + k_1 k_S) + P_{im}} = \frac{k_{cat} \Gamma P_{im}}{K_M + P_{im}} \quad (17S)$$

where the Michaelis constant for the mediator M is $K_M = (k_2 k_S + k_{-1} k_S) / (k_1 k_2 + k_1 k_S)$ and $k_{cat} = k_2 k_S / (k_2 + k_S)$. Using the equations (13S) and (17S) the concentrations of NAD^+ and $NADH$ (A_{im} and P_{im}) as well as B_o and Q_o from (1S) and (7S) can be found: $P_{im} = j_{el} K_M / (k_{cat} \Gamma - j_{el})$, $A_{im} = A_t - P_{im} = A_t - j_{el} K_M / (k_{cat} \Gamma - j_{el})$, $B_o = B_\infty - j_{el} / k'_B$, $Q_o = j_{el} / k'_Q$. Substitution of A_{im} , B_o , P_{im} , Q_o in equation (16S) by their expressions gives following equation:

$$j_{el} = \frac{L(V_1(A_t - j_{el} K_M / (k_{cat} \Gamma - j_{el})) (B_\infty - j_{el} / k'_B) - (V_1(j_{el} K_M / (k_{cat} \Gamma - j_{el})) (j_{el} / k'_Q)) / K_{eq})}{K_{AB} + K_B(A_t - j_{el} K_M / (k_{cat} \Gamma - j_{el})) + K_A(B_\infty - j_{el} / k'_B) + (A_t - j_{el} K_M / (k_{cat} \Gamma - j_{el})) (B_\infty - j_{el} / k'_B) + K_B K_{iA} (j_{el} K_M / (k_{cat} \Gamma - j_{el})) / K_{iP} + K_P K_B K_{iA} (j_{el} / k'_Q) / (K_Q K_{iP}) + K_B K_{iA} (j_{el} K_M / (k_{cat} \Gamma - j_{el})) (j_{el} / k'_Q) / (K_Q K_{iP}) + K_P K_B K_{iA} (A_t - j_{el} K_M / (k_{cat} \Gamma - j_{el})) (j_{el} / k'_Q) / (K_Q K_{iA} K_{iP}) + K_A (B_\infty - j_{el} / k'_B) (j_{el} K_M / (k_{cat} \Gamma - j_{el})) (j_{el} / k'_Q) / (K_{iP} K_{iQ}) + K_B K_P (A_t - j_{el} K_M / (k_{cat} \Gamma - j_{el})) (B_\infty - j_{el} / k'_B) (j_{el} / k'_Q) / (K_Q K_{iB} K_{iP}) + K_A (B_\infty - j_{el} / k'_B) (j_{el} K_M / (k_{cat} \Gamma - j_{el})) / K_{iP}} \quad (18S)$$

The latter is transformed into the equation of the fourth order:

$$LV_1 \Gamma k_{cat} A_t B_\infty = j_{el} [K_{AB} \Gamma k_{cat} + K_A \Gamma k_{cat} B_\infty + \Gamma k_{cat} A_t B_\infty + K_B \Gamma k_{cat} A_t + LV_1 ((A_t + K_M) k'_B B_\infty + \Gamma k_{cat} A_t) / k'_B] + j_{el}^2 [V_1 L K_M / (K_{eq} k'_Q) + K_B K_{iA} K_M / K_{iP} + K_P K_B K_{iA} \Gamma k_{cat} / (K_Q K_{iP} k'_Q) + K_P K_B K_{iA} \Gamma k_{cat} A_t / (K_Q K_{iA} K_{iP} k'_Q) + \Gamma k_{cat} A_t B_\infty k'_B K_B K_P / (K_Q K_{iB} K_{iP} k'_B k'_Q) + K_M K_A B_\infty / K_{iP} - LV_1 (A_t + K_M) / k'_B - K_{AB} - K_B (A_t + K_M) - (k'_B B_\infty + \Gamma k_{cat}) K_A / k'_B - (A_t + K_M) B_\infty - \Gamma k_{cat} A_t / k'_B] + j_{el}^3 [K_A / k'_B + (A_t + K_M) / k'_B + K_M K_B K_{iA} / (K_Q K_{iP} k'_Q) + K_M K_A B_\infty / (K_{iP} K_{iQ} k'_Q) - K_P K_B K_{iA} / (K_Q K_{iP} k'_Q) - (A_t + K_M) K_P K_B K_{iA} / (K_Q K_{iA} K_{iP} k'_Q) - K_M K_A / (K_{iP} k'_B) - (\Gamma k_{cat} A_t) K_B K_P / (K_Q K_{iB} K_{iP} k'_B k'_Q) - (A_t + K_M) B_\infty K_B K_P / (K_Q K_{iB} K_{iP} k'_Q)] + j_{el}^4 [(A_t + K_M) K_B K_P / (K_Q K_{iB} K_{iP} k'_B k'_Q) - K_M K_A / (K_{iP} K_{iQ} k'_B k'_Q)] \quad (19S)$$

In some enzymatic reactions, including the reaction catalyzed by GDH, the equilibrium is greatly shifted towards the formation of the reaction products and their concentrations P_o and Q_o exert negligible influence on the reaction rate. In this case the equation (16S) can be rewritten as follows:

$$j_{el} = \frac{LV_1 A_{im} B}{K_{AB} + K_B A_{im} + K_A B_o + A_{im} B_o} = \frac{LV_1 (A_t - j_{el} K_M / (k_{cat} \Gamma - j_{el})) (B_\infty - j_{el} / k'_B)}{K_{AB} + K_B (A_t - j_{el} K_M / (k_{cat} \Gamma - j_{el})) + K_A (B_\infty - j_{el} / k'_B) + (A_t - j_{el} K_M / (k_{cat} \Gamma - j_{el})) (B_\infty - j_{el} / k'_B)} \quad (20S)$$

or

$$LV_1 \Gamma k_{cat} k'_B A_t B_\infty = j_{el} [K_{AB} k'_B \Gamma k_{cat} + K_B k'_B \Gamma k_{cat} A_t + K_A k'_B \Gamma k_{cat} B_\infty + \Gamma k_{cat} k'_B A_t B_\infty + LV_1 \Gamma k_{cat} A_t + LV_1 k'_B (A_t + K_M) B_\infty] - j_{el}^2 [K_{AB} k'_B + K_B k'_B (A_t + K_M) + K_A k'_B B_\infty + K_A \Gamma k_{cat} + \Gamma k_{cat} A_t + k'_B (A_t + K_M) B_\infty + LV_1 (A_t + K_M)] + j_{el}^3 [K_A + A_t + K_M] \quad (21S)$$

If the concentration of the immobilized cofactor A_t is so high that it is not a limiting factor of the enzymatic reaction the equation 21S can be simplified to give:

$$LV_1\Gamma k_{\text{cat}}k'_B B_\infty = j_{\text{el}}[K_B k'_B \Gamma k_{\text{cat}} + \Gamma k_{\text{cat}}k'_B B_\infty + LV_1\Gamma k_{\text{cat}} + LV_1k'_B B_\infty] - j_{\text{el}}^2[K_B k'_B + \Gamma k_{\text{cat}} + k'_B B_\infty + LV_1] + j_{\text{el}}^3 \quad (22S)$$

When the concentration of the substrate B_∞ is infinitely high the latter equation can be rewritten as:

$$LV_1\Gamma k_{\text{cat}}k'_B = j_{\text{el max}}[\Gamma k_{\text{cat}}k'_B + LV_1k'_B] - j_{\text{el max}}^2 k'_B \quad (23S)$$

$$j_{\text{el max}}^2 - j_{\text{el max}}[\Gamma k_{\text{cat}} + LV_1] + LV_1\Gamma k_{\text{cat}} = 0 \quad (24S)$$

$$\text{The roots of this square equation are } j_{\text{el max 1}} = \Gamma k_{\text{cat}} \quad (25S)$$

and

$$j_{\text{el max 2}} = LV_1 \quad (26S)$$

It follows from the equation (24S) that the maximum flux in reagentless biosensors in the presence of saturating concentration of NAD^+ is equal to LV_1 (the maximum response is limited by the enzymatic reaction) or Γk_{cat} (the maximum response is limited by the reaction of the mediated oxidation of NADH at the electrode surface). The value of the maximum flux of the electrochemical NADH oxidation (Γk_{cat}) was found from calibration curves of the graphite electrodes modified with Os-phendione-PVP according to the Eadie-Hofstee plots. Calibration of these electrodes with NADH was performed to demonstrate the maximum current density of $492 \mu\text{A cm}^{-2}$ which corresponds to Γk_{cat} equal to $2.55 \times 10^{-9} \text{ mol s}^{-1} \text{ cm}^{-2}$.

Cubic equation (21S), having exact analytical solution, was used to simulate the response of reagentless glucose biosensors. The typical calibration curves and the Eadie-Hofstee plots for glucose biosensors computed at varied loading of NAD^+ (A_t), the infinitely rapid mass transport of glucose ($k'_B \rightarrow \infty$), and the maximum flux of the enzymatic reduction of NAD^+ (LV_1) less than the maximum flux of the electrochemical oxidation of NADH (Γk_{cat}) are represented in the Figure 9S. The straight lines of the Eadie-Hofstee plots indicate that under these conditions the response of the biosensors is determined only by the rate of the enzymatic reduction of NAD^+ . The slope of the Eadie-Hofstee plots which is equal to $-1/K_{B \text{ app}}$, where $K_{B \text{ app}}$ is the apparent Michaelis constant for the substrate B, depends on the loading of NAD^+ . The intercept of the Eadie-Hofstee plots with the axis of j which is the apparent maximum current density ($j_{\text{max app}}$) is determined by A_t too. So, an increase in the loading of NAD^+ results in a rise in the apparent Michaelis constant and the maximum current density. Only when the NAD^+ loading reaches a saturating level ($A_t \rightarrow \infty$) the values of the apparent maximum current density ($j_{\text{max app}}$) and the apparent Michaelis constant ($K_{B \text{ app}}$) coincide with those of the product $LV_1 nF$ and the Michaelis constant (K_B) respectively.

The Figure 10S demonstrates the effect of the mass transfer constant of the substrate (k'_B) on the calibration curves and the Eadie-Hofstee plots simulated with the saturating loading of NAD^+ ($A_t \rightarrow \infty$) and the maximum flux of the enzymatic reduction of NAD^+ (LV_1) less than the maximum flux of the electrochemical oxidation of NADH (Γk_{cat}). In this case the smaller is the mass transfer constant of the

substrate the greater is the deviation from the straight line in the Eadie-Hofstee plots which is characteristic of the process governed by the enzymatic reaction of the NAD^+ reduction. The values of the apparent current densities and apparent Michaelis constants obtained by the Eadie-Hofstee plots coincide with the values of LV_1nF and K_B , respectively, only if very high concentrations of the substrate (B_∞) are used to build the plots

The Figures 11S-18S show the influence of the maximum flux of the electrochemical NADH oxidation (Γk_{cat}), maximum flux of the enzymatic reduction of NAD^+ (LV_1), and the NAD^+ loading on calibration curves and the Eadie-Hofstee plots simulated with the infinitively rapid mass transport of glucose ($k'_B \rightarrow \infty$). Clearly, the maximum current density is determined by the maximum flux of the enzymatic reduction of NAD^+ (LV_1) when the latter is less than the maximum flux of the electrochemical NADH oxidation (Γk_{cat}). The maximum flux of the electrochemical NADH oxidation (Γk_{cat}) limits the maximum current density if Γk_{cat} is less than the flux of the enzymatic reduction of NAD^+ at given NAD^+ loading (A_t). The sharp breaks followed by the horizontal lines in the Figures 11S, 12S, 15S, 16S are due to NAD^+ depletion caused by rapid enzymatic reaction at the saturating NAD^+ loading in the steady state model. The decrease in the NAD^+ loading results in the decrease in the flux of the enzymatic reduction of NAD^+ (Figures 13S, 17S) making that less or equal to the flux of the electrochemical NADH oxidation at a given value of A_t . That's why, at low NAD^+ loading the response of the biosensors is limited by the enzymatic reduction of NAD^+ even if Γk_{cat} is less than LV_1 (Figures 14S, 18S). The Eadie-Hofstee plots show linear parts in the range of low substrate concentrations (B_∞) in the Figures 11S, 12S, 13S, 15S, 16S, 17S and none linear parts in the range of high substrate concentrations. Therefore they can yield correct values of Michaelis constants (K_B) and the maximum flux of the enzymatic reduction of NAD^+ (LV_1) in the range of low substrate concentrations even if the maximum response of the biosensors is limited by the rate of NADH oxidation at the electrode surface. That is true only if the transport of substrate is not a limiting factor. Certainly, the intercepts of none linear parts of Eadie-Hofstee plots with the axis of j give the correct values of the maximum response to glucose.

The Figures 19S-22S illustrate the influence of the maximum flux of the enzymatic reduction of NAD^+ (LV_1), the NAD^+ loading (A_t), and the mass transfer constant of the substrate (k'_B) on response of biosensors. The smaller are the NAD^+ loading and the maximum fluxes of the enzymatic reduction of NAD^+ in comparison with the maximum flux of the electrochemical NADH oxidation, the straighter are the Eadie-Hofstee plots. At lower concentrations of the substrate (B_∞) the slopes of the Eadie-Hofstee plots and hence the apparent Michaelis constants depend very much on k'_B . The effect of this factor on the apparent Michaelis constant is less pronounced at high values of B_∞ .

GLOSSARY

| | |
|-----------------|--|
| j_{el} | flux of reactants ($\text{mol cm}^{-2} \text{s}^{-1}$) |
| j | current density (A cm^{-2}) |

| | |
|--|--|
| k_3, k_4, k_5, k_6, k_7 | rate constants of the elemental enzymatic reactions in forward direction ($M^{-1} s^{-1}, M^{-1} s^{-1}, s^{-1}, s^{-1}, s^{-1}$, respectively) |
| $k_{-3}, k_{-4}, k_{-5}, k_{-6}, k_{-7}$ | rate constants of the elemental enzymatic reactions in backward direction ($s^{-1}, s^{-1}, s^{-1}, M^{-1} s^{-1},$ and $M^{-1} s^{-1}$, respectively) |
| $k_B^?$ | mass transfer rate coefficient for the substrate ($cm s^{-1}$) |
| $k_Q^?$ | mass transfer rate coefficient for the product ($cm s^{-1}$) |
| L | thickness of a hydrogel layer (cm) |
| P_{im} | concentration of NADH immobilized in the hydrogel (M) |
| V_1 | maximum velocity of the enzymatic reaction in forward direction (s^{-1}) |
| V_2 | maximum velocity of the enzymatic reaction in reverse direction (s^{-1}) |

Greek letters

| | |
|----------------------|---|
| Γ | total surface coverage of Os-phendione-PVP ($mol\ cm^{-2}$) |
| Γ_{Mox} | surface coverage of the mediator in the oxidized form ($mol\ cm^{-2}$) |
| Γ_{Mred} | surface coverage of the mediator in the reduced form ($mol\ cm^{-2}$) |
| $\Gamma_{M \cdot P}$ | surface coverage of the intermediate complex between Os-phendione-PVP and NADH ($mol\ cm^{-2}$) |

FIGURES AND FIGURE LEGENDS

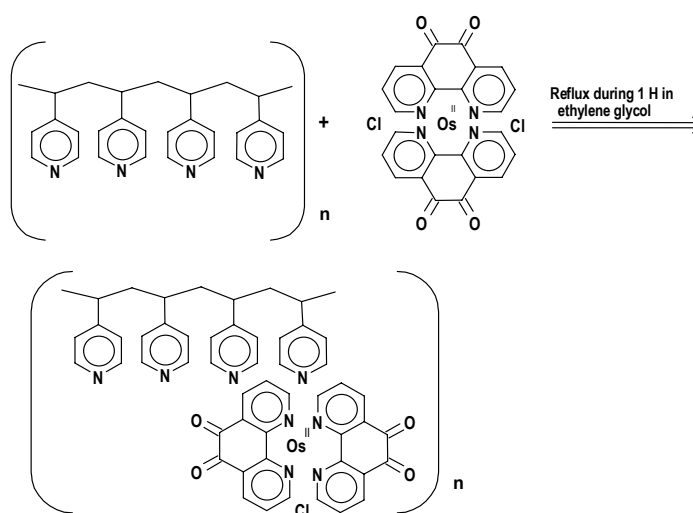


Figure 1S. The synthetic route to Os-phendione-PVP.

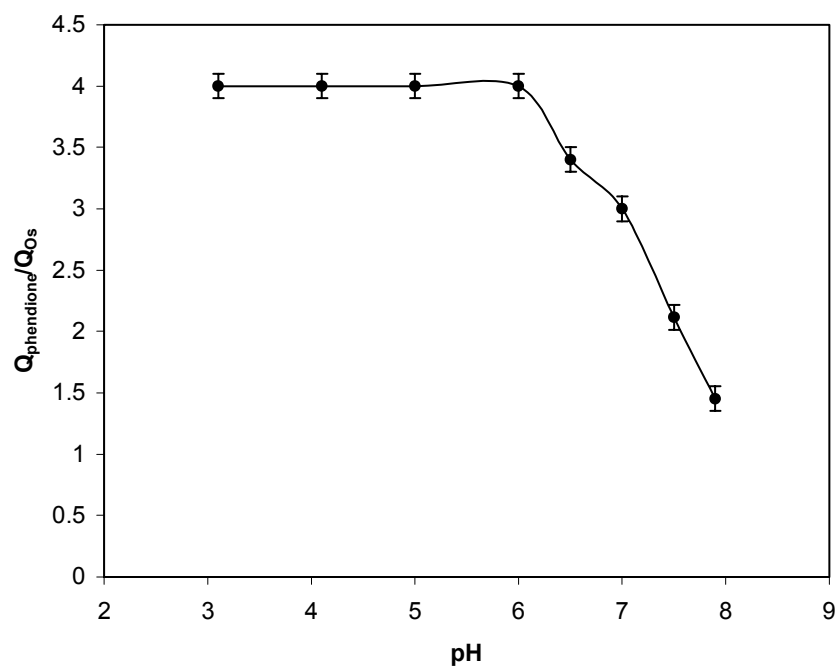


Figure 2S. The effect of pH on the ratio of phendione peak area to that of osmium atom in cyclic voltammetry.

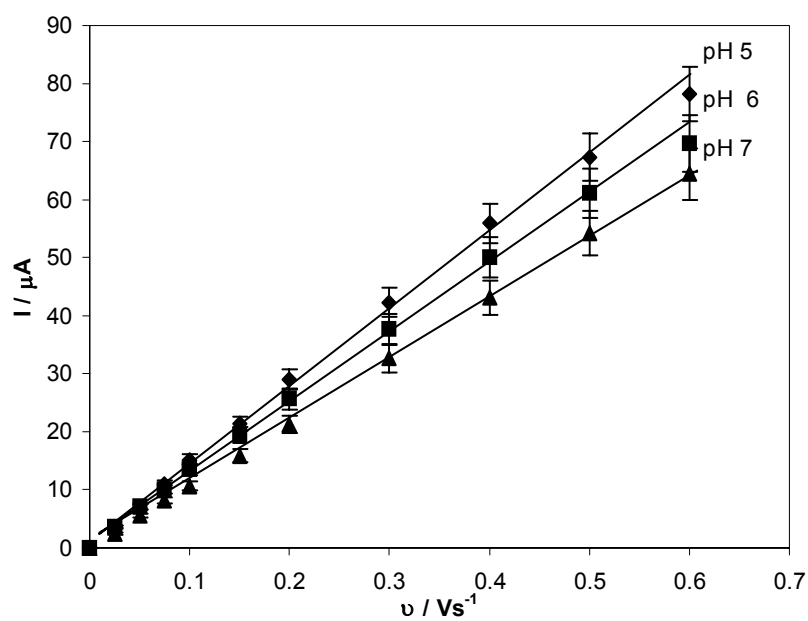


Figure 3S. The effect of scan rate on the anodic peak current of phendione. Experimental conditions: Os-phendione-PVP coverage $(6.7 \pm 0.5) \times 10^{-10} \text{ mol cm}^{-2}$, 0.1 M phosphate buffer.

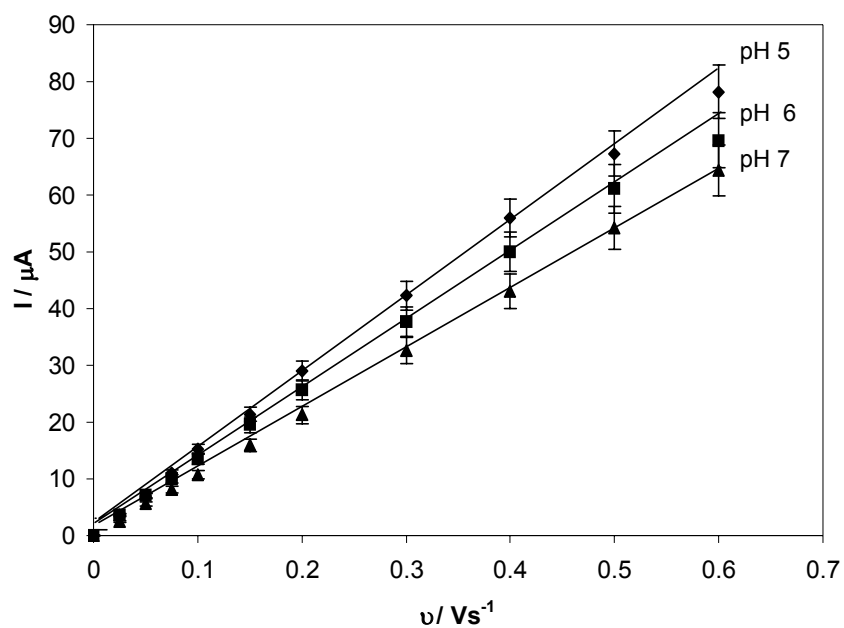


Figure 4S. The effect of scan rate on the cathodic peak current of phendione. Experimental conditions are the same as in Figure 3S.

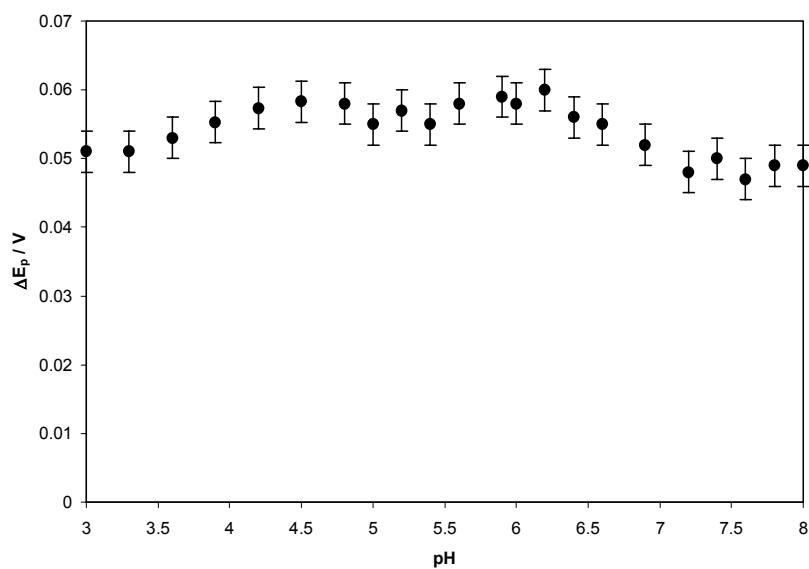


Figure 5S. Variation of ΔE_p as a function of pH. Experimental conditions are the same as in Figure 2.

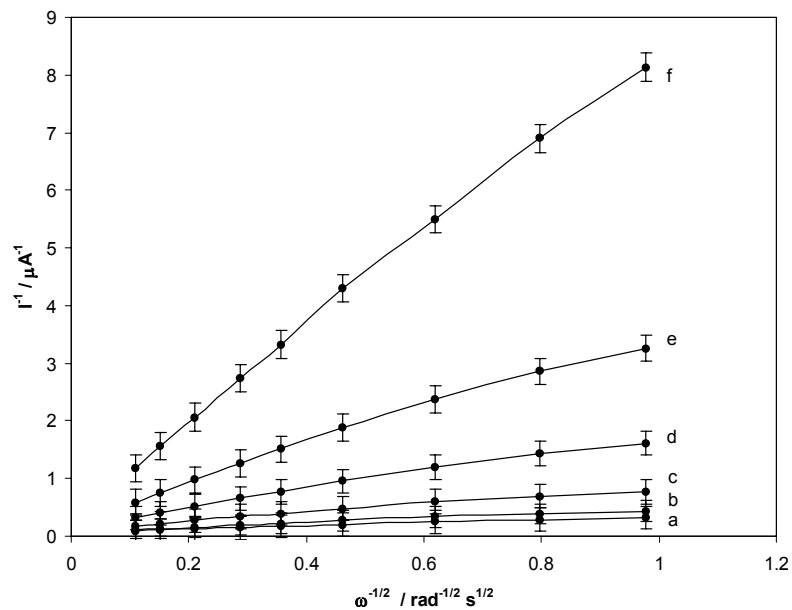


Figure 6S. Koutecky-Levich plot of steady state electrocatalytic response for an Os-phendione-PVP modified graphite RDE at different NADH concentrations: a) 0.05 mM; b) 0.1 mM; c) 0.2 mM; d) 0.4 mM; e) 0.8 mM; f) 1.2 mM. Experimental conditions: Os-phendione-PVP coverage $(7.3 \pm 0.3) \times 10^{-10} \text{ mol cm}^{-2}$; applied potential 200 mV vs. Ag/AgCl/KCl_{sat}, 0.1 M phosphate buffer, pH 5.0, deaerated with argon.

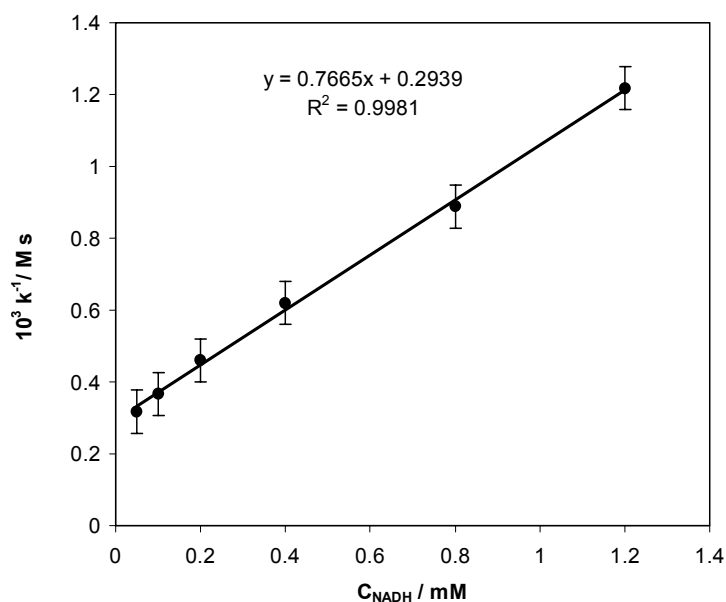


Figure 7S. Plot of k^{-1} vs. concentration of NADH for the electrooxidation of NADH at Os-phendione-PVP modified electrodes. Experimental conditions are the same as in Figure 6S.

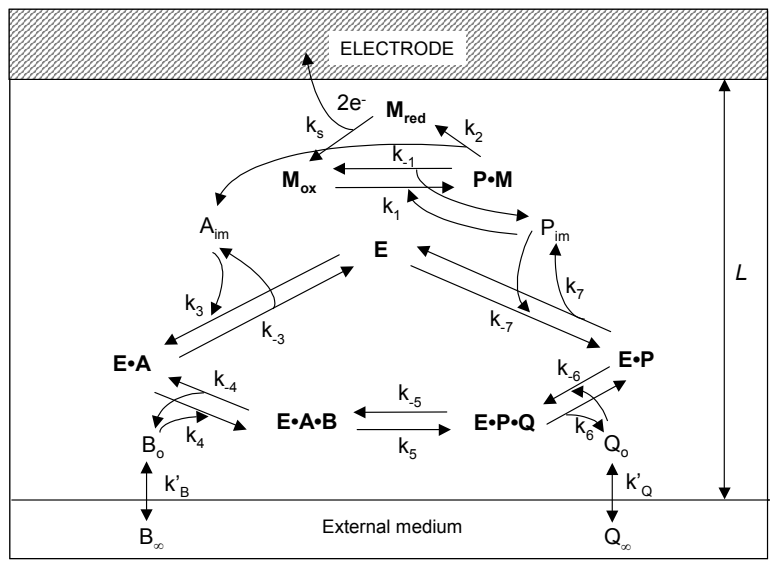
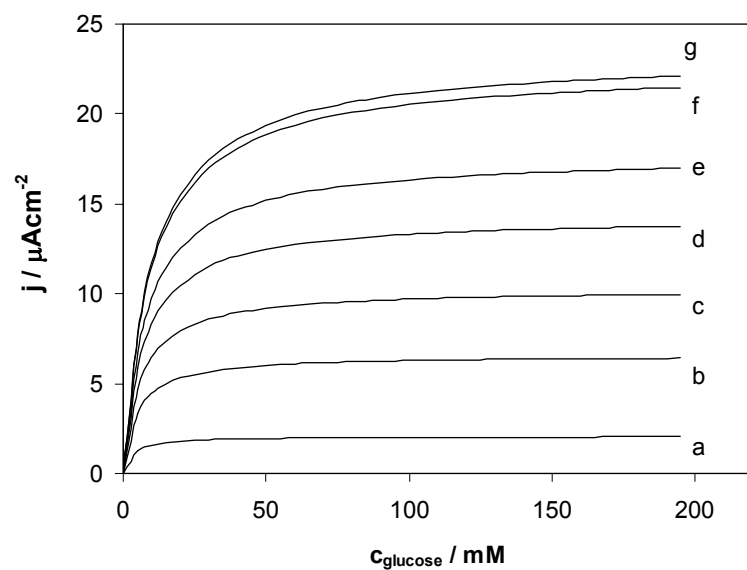
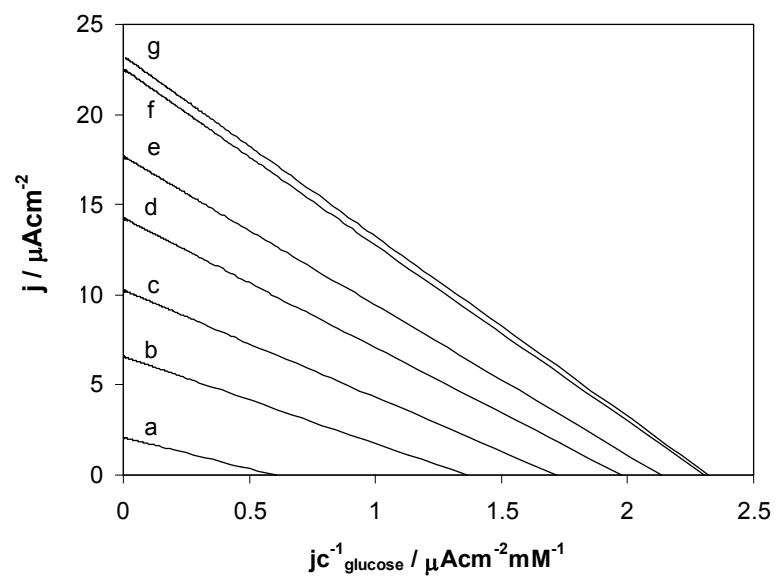


Figure 8S. Reaction scheme for a reagentless glucose biosensor.

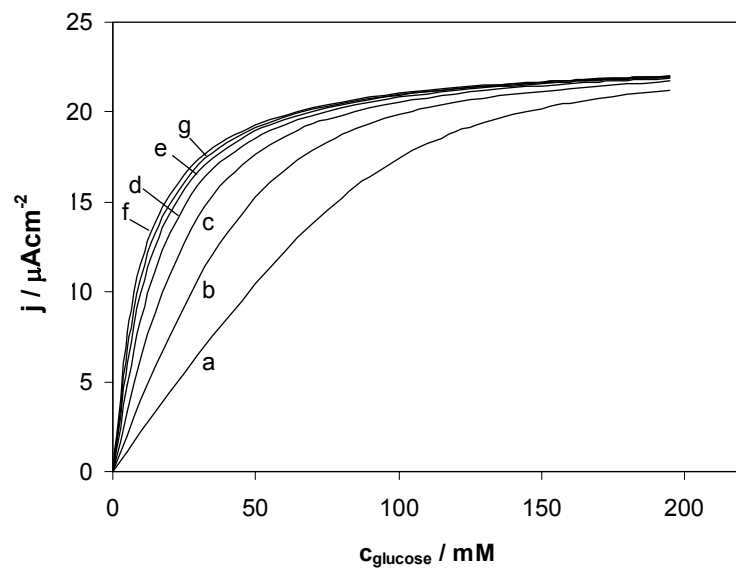


(A)

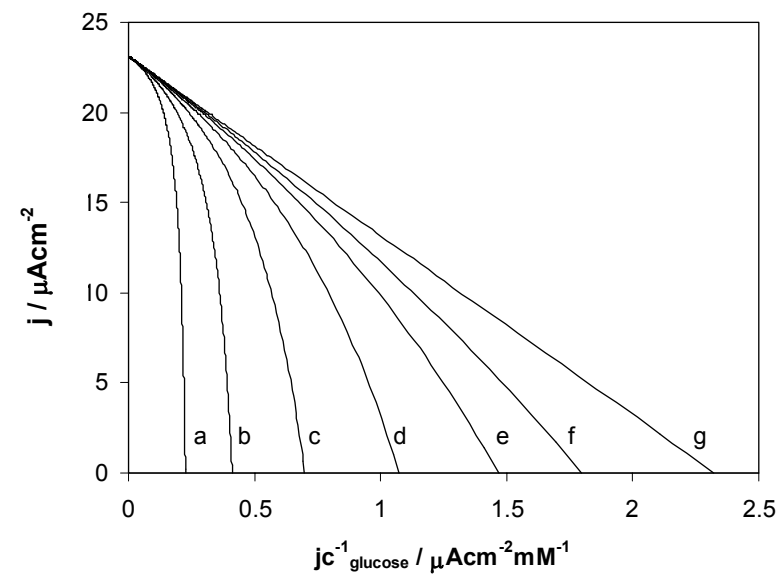


(B)

Figure 9S. Simulation of calibration curves (A) and Eadie-Hofstee plots (B) for the reagentless glucose biosensors with varying loading of NAD^+ in the hydrogel (A_i): a) 0.2 mM; b) 0.8 mM; c) 1.6 mM; d) 3.2 mM; e) 6.4 mM; f) 64 mM; g) ∞ . The values of other parameters are: $\Gamma k_{\text{cat}} = 2.55 \times 10^{-9} \text{ mol s}^{-1} \text{ cm}^{-2}$; $LV_1 = 1.2046 \times 10^{-10} \text{ mol s}^{-1} \text{ cm}^{-2}$; $k'_{\text{B} \rightarrow} \rightarrow \infty$; $K_A = 2 \text{ mM}$; $K_B = 10 \text{ mM}$; $K_{AB} = 5.6 \text{ mM}^2$; $K_M = 0.8 \text{ mM}$.

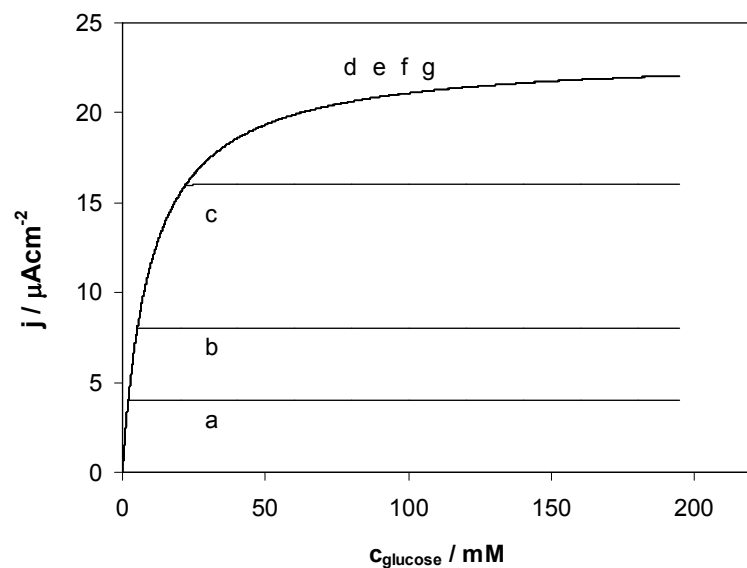


(A)

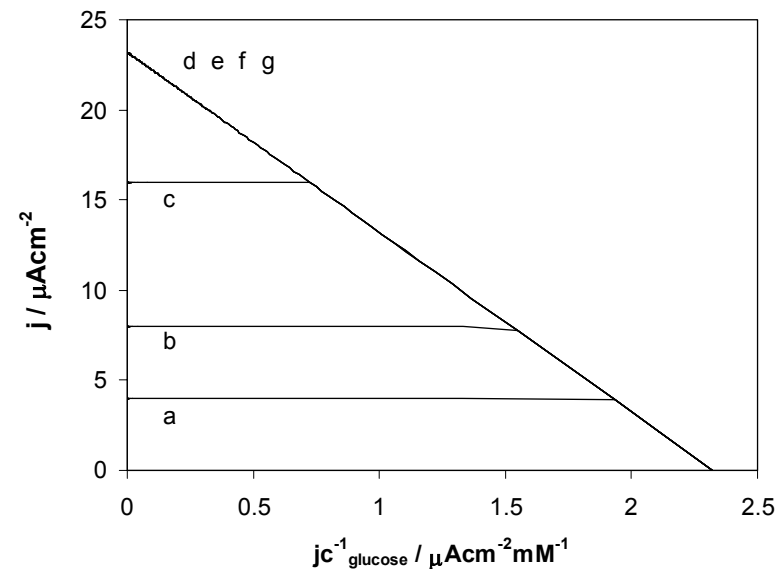


(B)

Figure 10S. Simulation of calibration curves **(A)** and Eadie-Hofstee plots **(B)** for the reagentless glucose biosensors with varying mass transfer coefficient (k'_B): a) $1.3 \times 10^{-12} \text{ cm s}^{-1}$; b) $2.6 \times 10^{-12} \text{ cm s}^{-1}$; c) $5.18 \times 10^{-12} \text{ cm s}^{-1}$; d) $1.04 \times 10^{-11} \text{ cm s}^{-1}$; e) $2.07 \times 10^{-11} \text{ cm s}^{-1}$; f) $4.15 \times 10^{-11} \text{ cm s}^{-1}$; g) ∞ . The values of other parameters are: $A_t \rightarrow \infty$; $\Gamma k_{\text{cat}} = 2.55 \times 10^{-9} \text{ mol s}^{-1} \text{ cm}^{-2}$; $LV_1 = 1.2046 \times 10^{-10} \text{ mol s}^{-1} \text{ cm}^{-2}$; $K_A = 2 \text{ mM}$; $K_B = 10 \text{ mM}$; $K_{AB} = 5.6 \text{ mM}^2$; $K_M = 0.8 \text{ mM}$.

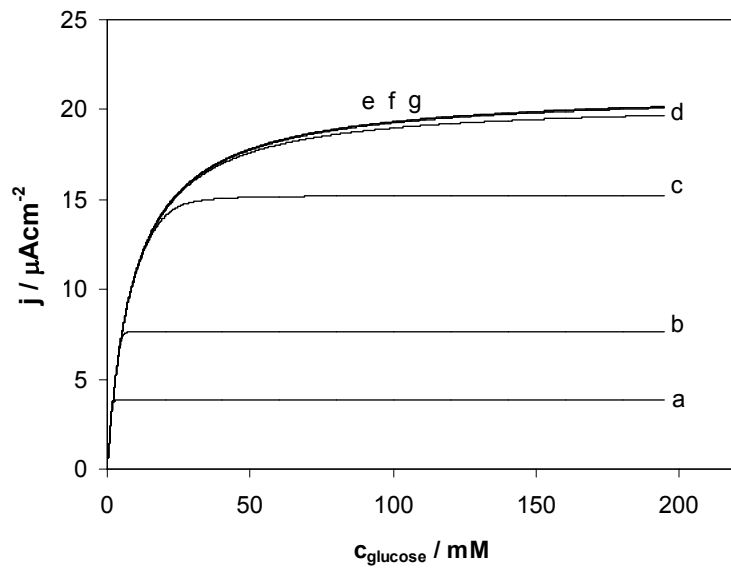


(A)

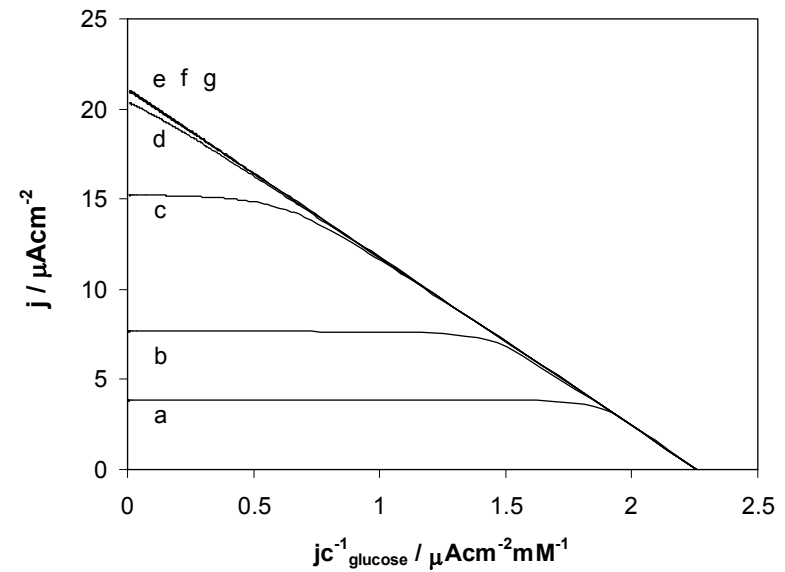


(B)

Figure 11S. Simulation of calibration curves **(A)** and Eadie-Hofstee plots **(B)** for the reagentless glucose biosensors at $A_t \rightarrow \infty$ with varying maximum fluxes of the electrochemical NADH oxidation (Γk_{cat}): a) $2.073 \times 10^{-11} \text{ mol s}^{-1} \text{ cm}^{-2}$; b) $4.145 \times 10^{-11} \text{ mol s}^{-1} \text{ cm}^{-2}$; c) $8.291 \times 10^{-11} \text{ mol s}^{-1} \text{ cm}^{-2}$; d) $1.204 \times 10^{-10} \text{ mol s}^{-1} \text{ cm}^{-2}$; e) $2.073 \times 10^{-10} \text{ mol s}^{-1} \text{ cm}^{-2}$; f) $4.145 \times 10^{-10} \text{ mol s}^{-1} \text{ cm}^{-2}$; g) ∞ . The values of other parameters are: $k_{\text{B}}^{\rightarrow} \rightarrow \infty$; $LV_1 = 1.204 \times 10^{-10} \text{ mol s}^{-1} \text{ cm}^{-2}$; $K_{\text{A}} = 2 \text{ mM}$; $K_{\text{B}} = 10 \text{ mM}$; $K_{\text{AB}} = 5.6 \text{ mM}^2$; $K_{\text{M}} = 0.8 \text{ mM}$.

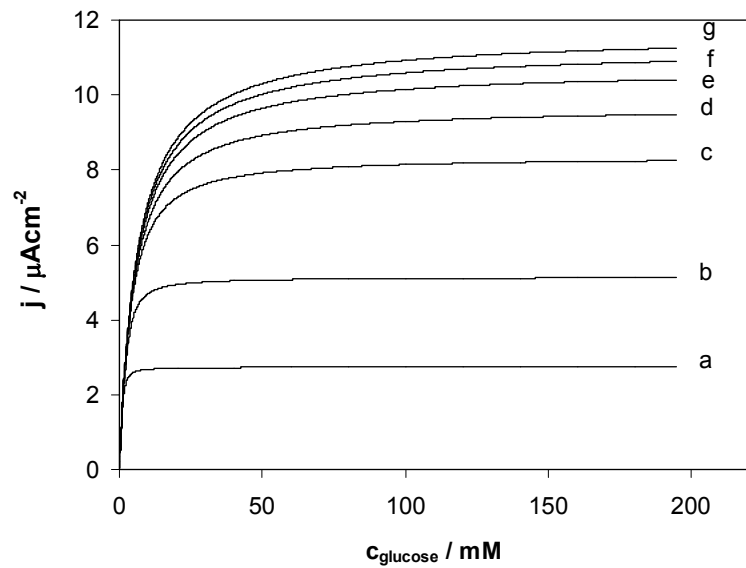


(A)

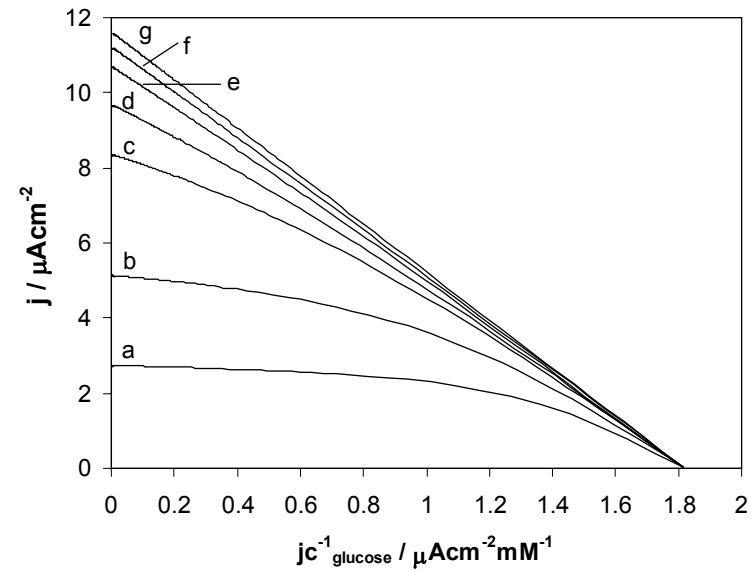


(B)

Figure 12S. Simulation of calibration curves **(A)** and Eadie-Hofstee plots **(B)** for the reagentless glucose biosensors at A_t equal to 20 mM with varying maximum fluxes of the electrochemical NADH oxidation (Γk_{cat}): a) $2.073 \times 10^{-11} \text{ mol s}^{-1} \text{ cm}^{-2}$; b) $4.145 \times 10^{-11} \text{ mol s}^{-1} \text{ cm}^{-2}$; c) $8.291 \times 10^{-11} \text{ mol s}^{-1} \text{ cm}^{-2}$; d) $1.204 \times 10^{-10} \text{ mol s}^{-1} \text{ cm}^{-2}$; e) $2.073 \times 10^{-10} \text{ mol s}^{-1} \text{ cm}^{-2}$; f) $4.145 \times 10^{-10} \text{ mol s}^{-1} \text{ cm}^{-2}$; g) ∞ . The values of other parameters are: $k'_B \rightarrow \infty$; $LV_1 = 1.204 \times 10^{-10} \text{ mol s}^{-1} \text{ cm}^{-2}$; $K_A = 2 \text{ mM}$; $K_B = 10 \text{ mM}$; $K_{AB} = 5.6 \text{ mM}^2$; $K_M = 0.8 \text{ mM}$.



(A)



(B)

Figure 13S. Simulation of calibration curves (A) and Eadie-Hofstee plots (B) for the reagentless glucose biosensors at A_t equal to 2 mM with varying maximum fluxes of the electrochemical NADH oxidation (Γk_{cat}): a) $2.073 \times 10^{-11} \text{ mol s}^{-1} \text{ cm}^{-2}$; b) $4.145 \times 10^{-11} \text{ mol s}^{-1} \text{ cm}^{-2}$; c) $8.291 \times 10^{-11} \text{ mol s}^{-1} \text{ cm}^{-2}$; d) $1.204 \times 10^{-10} \text{ mol s}^{-1} \text{ cm}^{-2}$; e) $2.073 \times 10^{-10} \text{ mol s}^{-1} \text{ cm}^{-2}$; f) $4.145 \times 10^{-10} \text{ mol s}^{-1} \text{ cm}^{-2}$; g) ∞ . The values of other parameters are: $k'_{\text{B}} \rightarrow \infty$; $LV_1 = 1.204 \times 10^{-10} \text{ mol s}^{-1} \text{ cm}^{-2}$; $K_A = 2 \text{ mM}$; $K_B = 10 \text{ mM}$; $K_{AB} = 5.6 \text{ mM}^2$; $K_M = 0.8 \text{ mM}$.

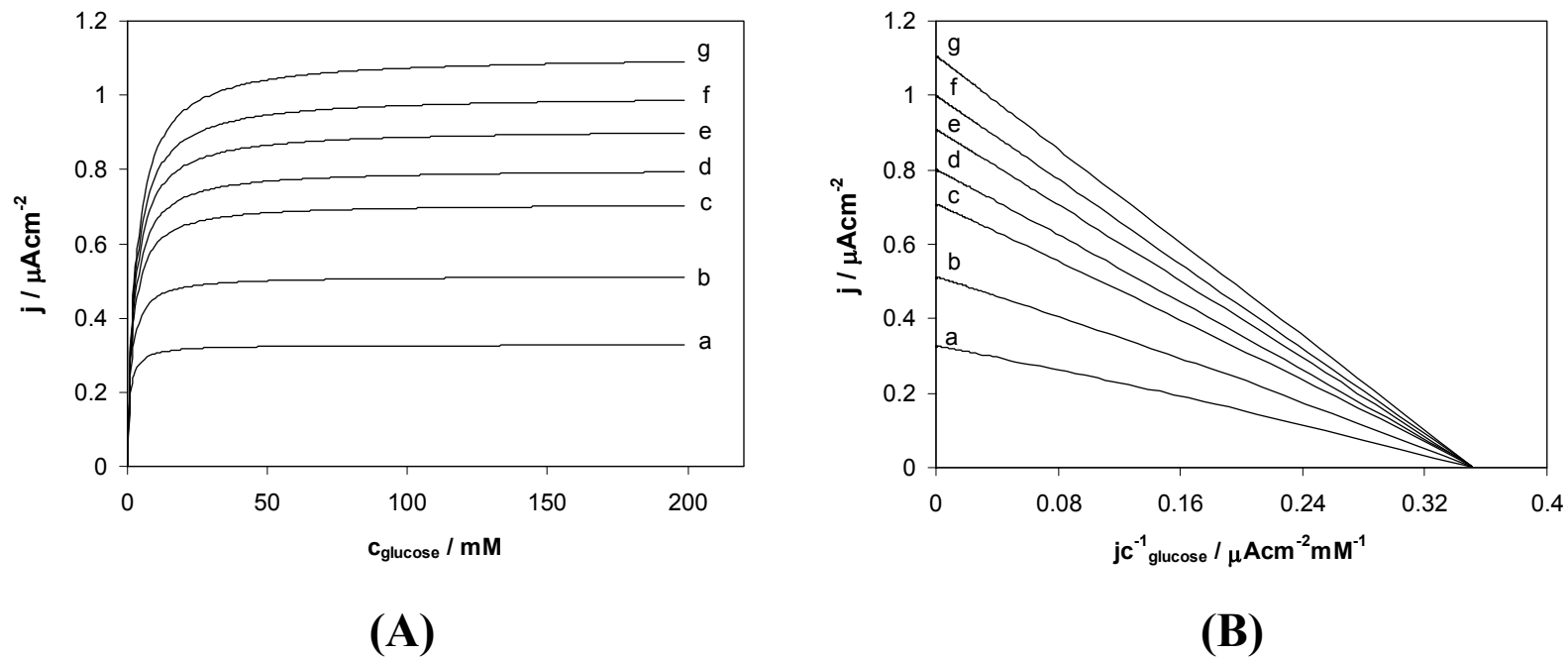
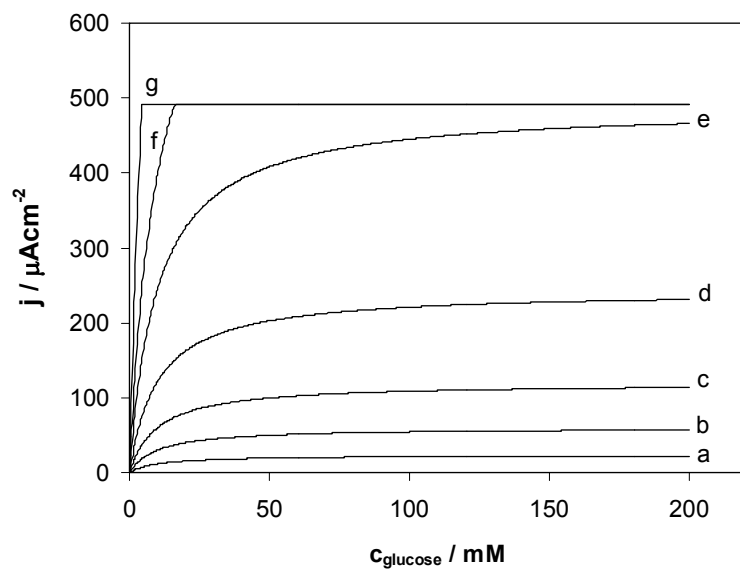
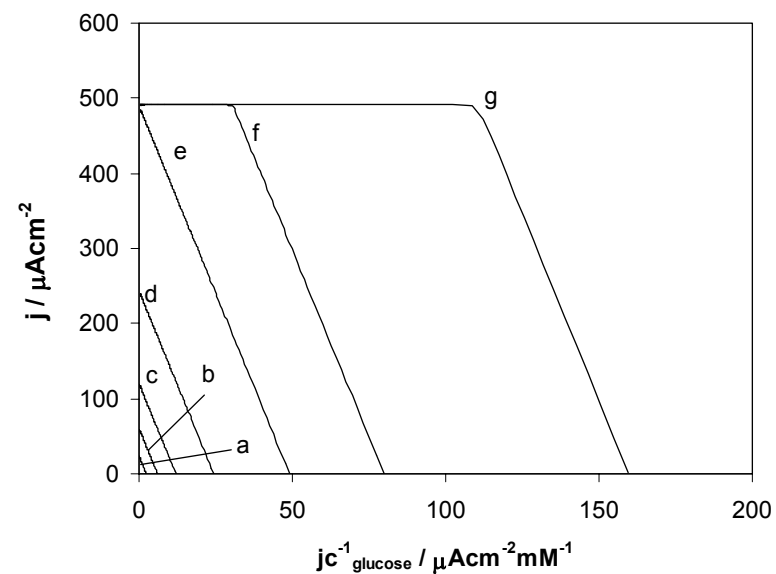


Figure 14S. Simulation of calibration curves **(A)** and Eadie-Hofstee plots **(B)** for the reagentless glucose biosensors at A_i equal to 0.1 mM with varying maximum fluxes of the electrochemical NADH oxidation (Γk_{cat}): a) $2.073 \times 10^{-11} \text{ mol s}^{-1} \text{ cm}^{-2}$; b) $4.145 \times 10^{-11} \text{ mol s}^{-1} \text{ cm}^{-2}$; c) $8.291 \times 10^{-11} \text{ mol s}^{-1} \text{ cm}^{-2}$; d) $1.204 \times 10^{-10} \text{ mol s}^{-1} \text{ cm}^{-2}$; e) $2.073 \times 10^{-10} \text{ mol s}^{-1} \text{ cm}^{-2}$; f) $4.145 \times 10^{-10} \text{ mol s}^{-1} \text{ cm}^{-2}$; g) ∞ . The values of other parameters are: $k'_{\text{B}} \rightarrow \infty$; $LV_1 = 1.204 \times 10^{-10} \text{ mol s}^{-1} \text{ cm}^{-2}$; $K_{\text{A}} = 2 \text{ mM}$; $K_{\text{B}} = 10 \text{ mM}$; $K_{\text{AB}} = 5.6 \text{ mM}^2$; $K_{\text{M}} = 0.8 \text{ mM}$.

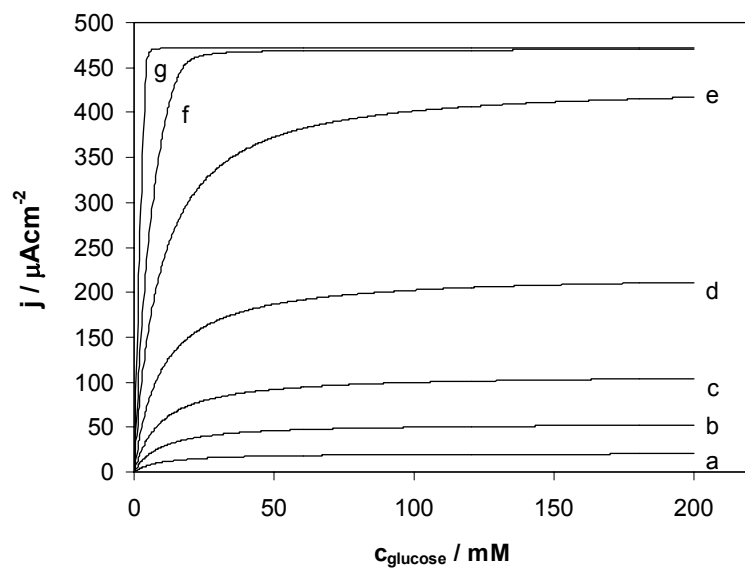


(A)

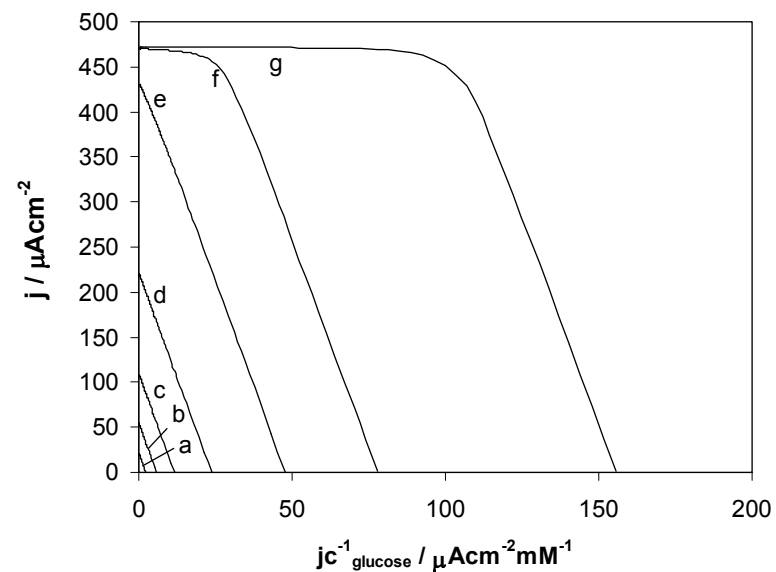


(B)

Figure 15S. Simulation of calibration curves (A) and Eadie-Hofstee plots (B) for the reagentless glucose biosensors at $A_t \rightarrow \infty$ with varying maximum fluxes of the enzymatic reduction of NAD^+ (LV_1): a) $1.204 \times 10^{-10} \text{ mol s}^{-1} \text{ cm}^{-2}$; b) $3.109 \times 10^{-10} \text{ mol s}^{-1} \text{ cm}^{-2}$; c) $6.218 \times 10^{-10} \text{ mol s}^{-1} \text{ cm}^{-2}$; d) $1.264 \times 10^{-9} \text{ mol s}^{-1} \text{ cm}^{-2}$; e) $2.549 \times 10^{-9} \text{ mol s}^{-1} \text{ cm}^{-2}$; f) $4.146 \times 10^{-9} \text{ mol s}^{-1} \text{ cm}^{-2}$; g) $8.281 \times 10^{-9} \text{ mol s}^{-1} \text{ cm}^{-2}$. The values of other parameters are: $k'_{B \rightarrow \infty}$; $\Gamma k_{\text{cat}} = 2.549 \times 10^{-9} \text{ mol s}^{-1} \text{ cm}^{-2}$; $K_A = 2 \text{ mM}$; $K_B = 10 \text{ mM}$; $K_{AB} = 5.6 \text{ mM}^2$; $K_M = 0.8 \text{ mM}$

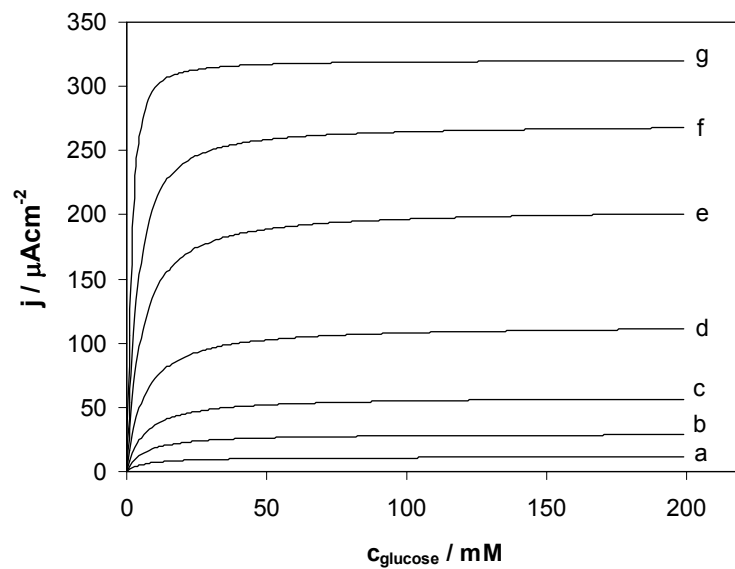


(A)

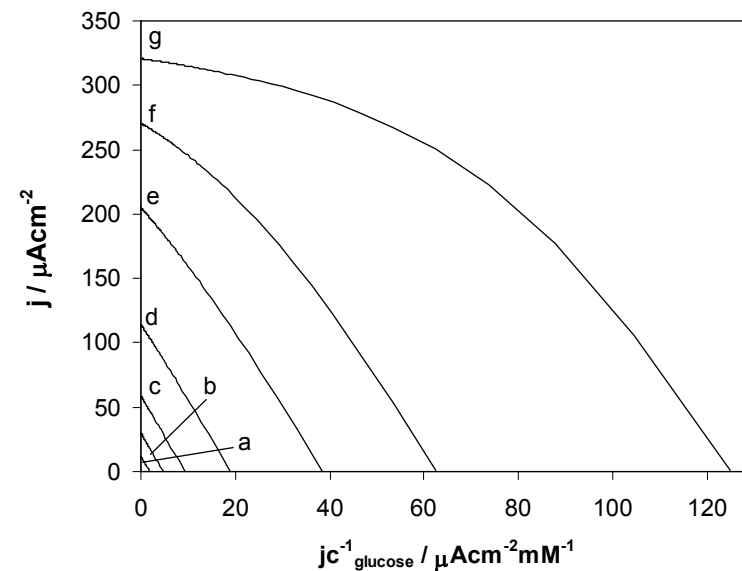


(B)

Figure 16S. Simulation of calibration curves (A) and Eadie-Hofstee plots (B) for the reagentless glucose biosensors at A_i equal to 20 mM with varying maximum fluxes of the enzymatic reduction of NAD^+ (LV_1): a) $1.204 \times 10^{-10} \text{ mol s}^{-1} \text{ cm}^{-2}$; b) $3.109 \times 10^{-10} \text{ mol s}^{-1} \text{ cm}^{-2}$; c) $6.218 \times 10^{-10} \text{ mol s}^{-1} \text{ cm}^{-2}$; d) $1.264 \times 10^{-9} \text{ mol s}^{-1} \text{ cm}^{-2}$; e) $2.549 \times 10^{-9} \text{ mol s}^{-1} \text{ cm}^{-2}$; f) $4.146 \times 10^{-9} \text{ mol s}^{-1} \text{ cm}^{-2}$; g) $8.281 \times 10^{-9} \text{ mol s}^{-1} \text{ cm}^{-2}$. The values of other parameters are: $k_{B \rightarrow \infty}^2$; $\Gamma k_{\text{cat}} = 2.549 \times 10^{-9} \text{ mol s}^{-1} \text{ cm}^{-2}$; $K_A = 2 \text{ mM}$; $K_B = 10 \text{ mM}$; $K_{AB} = 5.6 \text{ mM}^2$; $K_M = 0.8 \text{ mM}$.

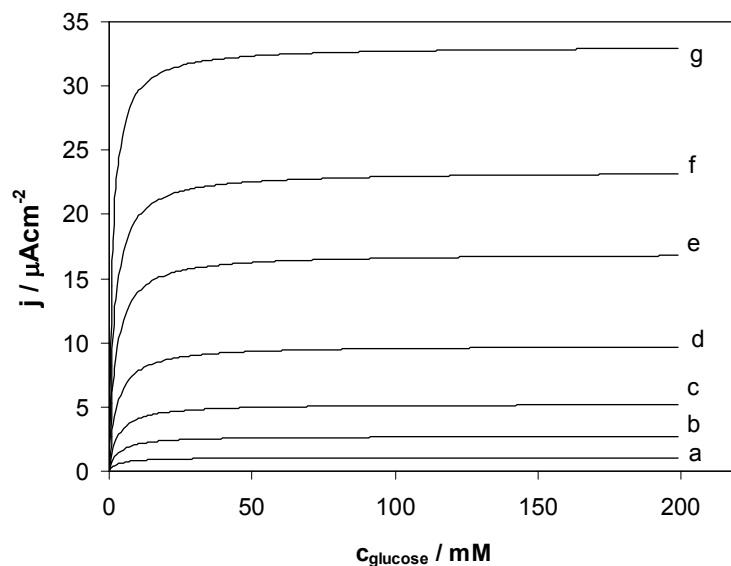


(A)

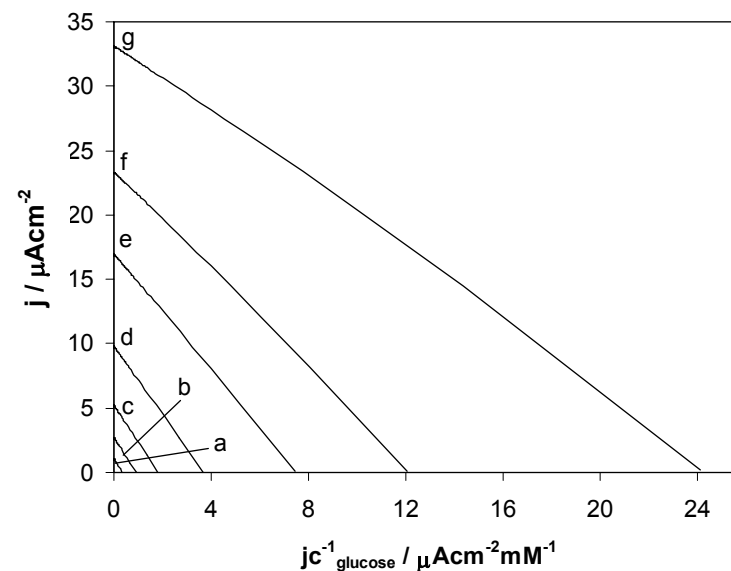


(B)

Figure 17S. Simulation of calibration curves (A) and Eadie-Hofstee plots (B) for the reagentless glucose biosensors at A_t equal to 2.0 mM with varying maximum fluxes of the enzymatic reduction of NAD^+ (LV_1): a) $1.204 \times 10^{-10} \text{ mol s}^{-1} \text{ cm}^{-2}$; b) $3.109 \times 10^{-10} \text{ mol s}^{-1} \text{ cm}^{-2}$; c) $6.218 \times 10^{-10} \text{ mol s}^{-1} \text{ cm}^{-2}$; d) $1.264 \times 10^{-9} \text{ mol s}^{-1} \text{ cm}^{-2}$; e) $2.549 \times 10^{-9} \text{ mol s}^{-1} \text{ cm}^{-2}$; f) $4.146 \times 10^{-9} \text{ mol s}^{-1} \text{ cm}^{-2}$; g) $8.281 \times 10^{-9} \text{ mol s}^{-1} \text{ cm}^{-2}$. The values of other parameters are: $k_{B \rightarrow \infty}^2$; $\Gamma k_{\text{cat}} = 2.549 \times 10^{-9} \text{ mol s}^{-1} \text{ cm}^{-2}$; $K_A = 2 \text{ mM}$; $K_B = 10 \text{ mM}$; $K_{AB} = 5.6 \text{ mM}^2$; $K_M = 0.8 \text{ mM}$

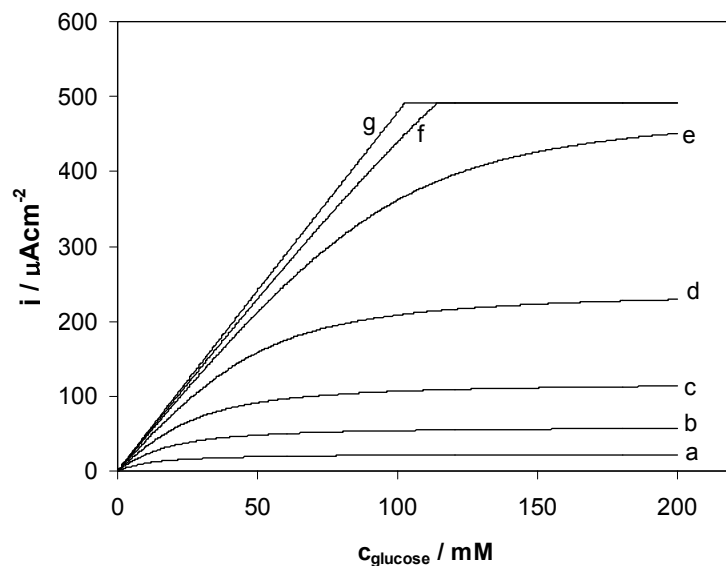


(A)

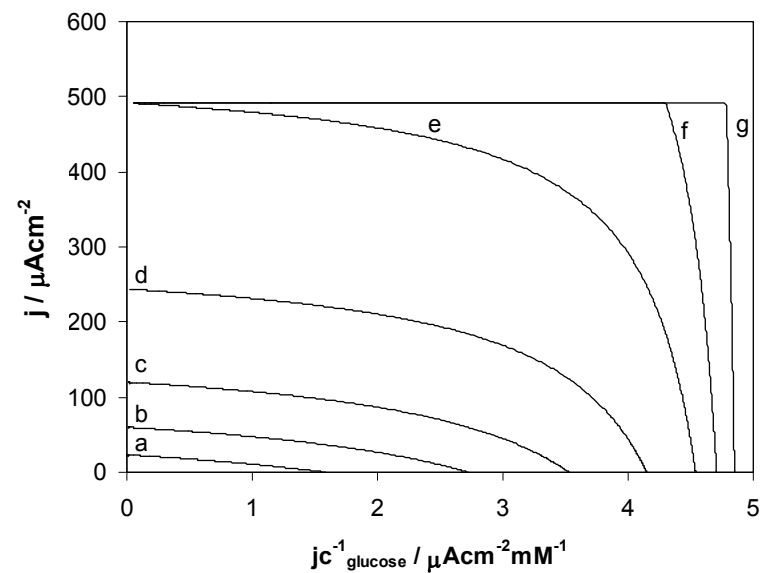


(B)

Figure 18S. Simulation of calibration curves (A) and Eadie-Hofstee plots (B) for the reagentless glucose biosensors at A_t equal to 0.1 mM with varying maximum fluxes of the enzymatic reduction of NAD^+ (LV_1): a) $1.204 \times 10^{-10} \text{ mol s}^{-1} \text{ cm}^{-2}$; b) $3.109 \times 10^{-10} \text{ mol s}^{-1} \text{ cm}^{-2}$; c) $6.218 \times 10^{-10} \text{ mol s}^{-1} \text{ cm}^{-2}$; d) $1.264 \times 10^{-9} \text{ mol s}^{-1} \text{ cm}^{-2}$; e) $2.549 \times 10^{-9} \text{ mol s}^{-1} \text{ cm}^{-2}$; f) $4.146 \times 10^{-9} \text{ mol s}^{-1} \text{ cm}^{-2}$; g) $8.281 \times 10^{-9} \text{ mol s}^{-1} \text{ cm}^{-2}$. The values of other parameters are: $k_B^2 \rightarrow \infty$; $\Gamma k_{\text{cat}} = 2.549 \times 10^{-9} \text{ mol s}^{-1} \text{ cm}^{-2}$; $K_A = 2 \text{ mM}$; $K_B = 10 \text{ mM}$; $K_{AB} = 5.6 \text{ mM}^2$; $K_M = 0.8 \text{ mM}$.

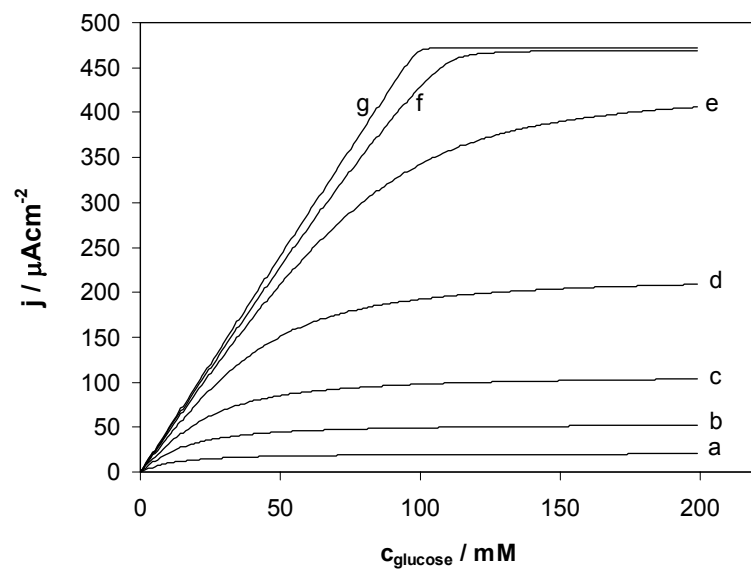


(A)

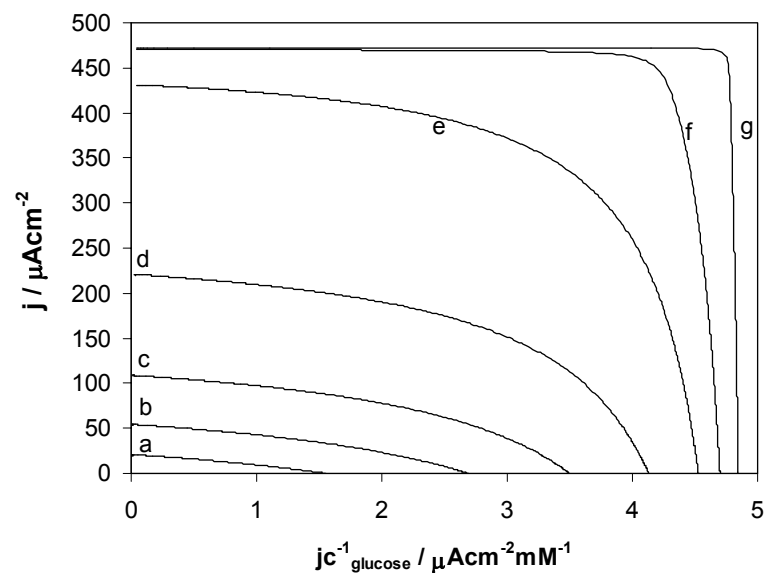


(B)

Figure 19S. Simulation of calibration curves **(A)** and Eadie-Hofstee plots **(B)** for the reagentless glucose biosensors at k_B^2 equal to $2.591 \times 10^{-11} \text{ cm s}^{-1}$ and $A_t \rightarrow \infty$ with varying maximum fluxes of the enzymatic reduction of NAD^+ (LV_1): a) $1.204 \times 10^{-10} \text{ mol s}^{-1} \text{ cm}^{-2}$; b) $3.109 \times 10^{-10} \text{ mol s}^{-1} \text{ cm}^{-2}$; c) $6.218 \times 10^{-10} \text{ mol s}^{-1} \text{ cm}^{-2}$; d) $1.264 \times 10^{-9} \text{ mol s}^{-1} \text{ cm}^{-2}$; e) $2.549 \times 10^{-9} \text{ mol s}^{-1} \text{ cm}^{-2}$; f) $4.146 \times 10^{-9} \text{ mol s}^{-1} \text{ cm}^{-2}$; g) $8.281 \times 10^{-9} \text{ mol s}^{-1} \text{ cm}^{-2}$. The values of other parameters are: $\Gamma k_{\text{cat}} = 2.549 \times 10^{-9} \text{ mol s}^{-1} \text{ cm}^{-2}$; $K_A = 2 \text{ mM}$; $K_B = 10 \text{ mM}$; $K_{AB} = 5.6 \text{ mM}^2$; $K_M = 0.8 \text{ mM}$.

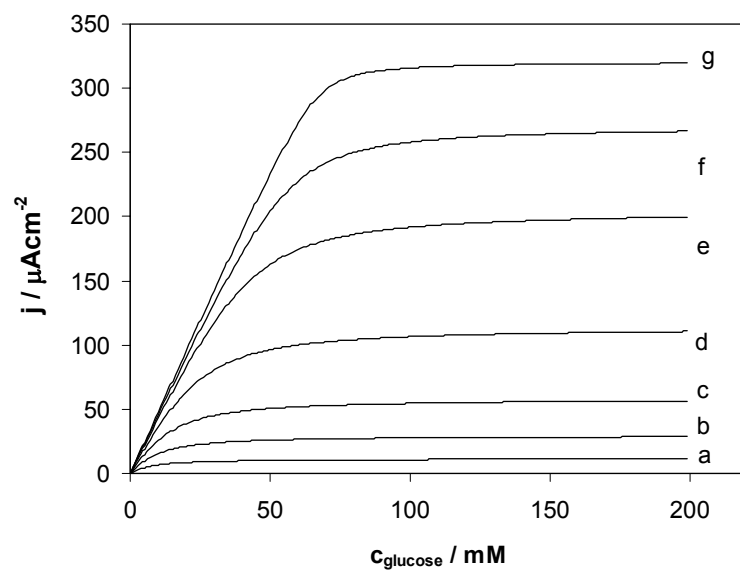


(A)

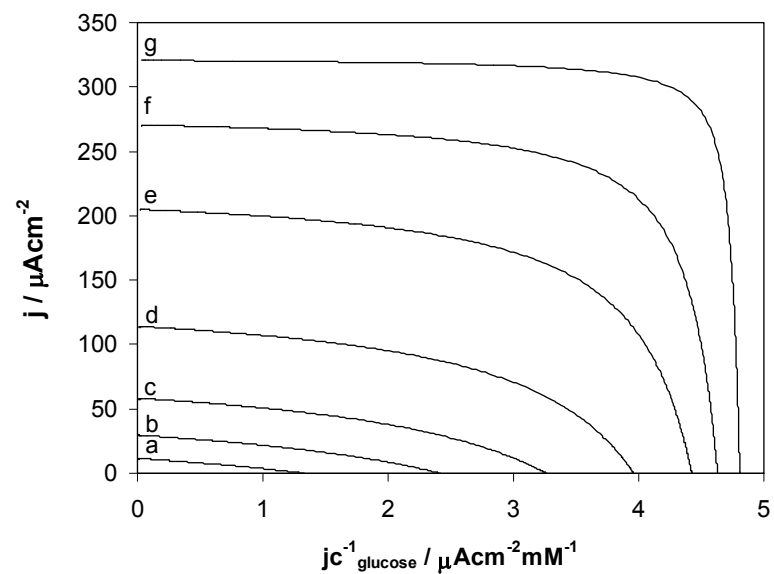


(B)

Figure 20S. Simulation of calibration curves (A) and Eadie-Hofstee plots (B) for the reagentless glucose biosensors at k'_B equal to $2.591 \times 10^{-11} \text{ cm s}^{-1}$ and A_i equal to 20 mM with varying maximum fluxes of the enzymatic reduction of NAD^+ (LV_1): a) $1.204 \times 10^{-10} \text{ mol s}^{-1} \text{ cm}^{-2}$; b) $3.109 \times 10^{-10} \text{ mol s}^{-1} \text{ cm}^{-2}$; c) $6.218 \times 10^{-10} \text{ mol s}^{-1} \text{ cm}^{-2}$; d) $1.264 \times 10^{-9} \text{ mol s}^{-1} \text{ cm}^{-2}$; e) $2.549 \times 10^{-9} \text{ mol s}^{-1} \text{ cm}^{-2}$; f) $4.146 \times 10^{-9} \text{ mol s}^{-1} \text{ cm}^{-2}$; g) $8.281 \times 10^{-9} \text{ mol s}^{-1} \text{ cm}^{-2}$. The values of other parameters are: $\Gamma k_{\text{cat}} = 2.549 \times 10^{-9} \text{ mol s}^{-1} \text{ cm}^{-2}$; $K_A = 2 \text{ mM}$; $K_B = 10 \text{ mM}$; $K_{AB} = 5.6 \text{ mM}^2$; $K_M = 0.8 \text{ mM}$.

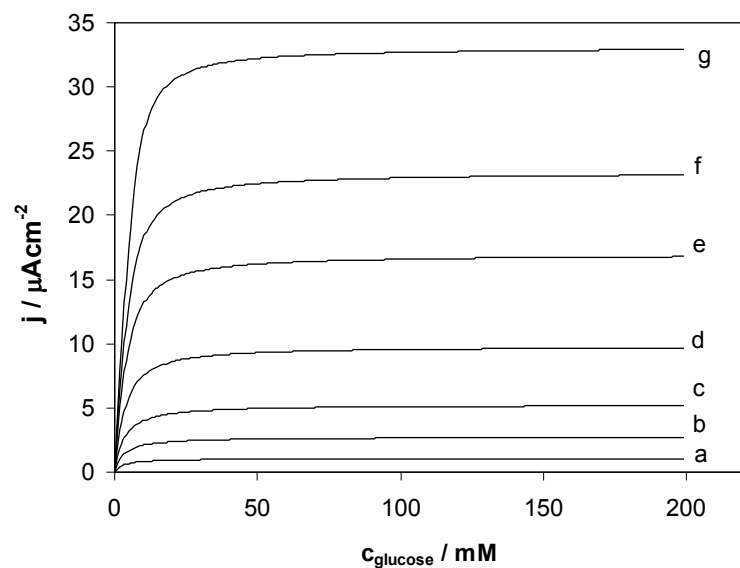


(A)

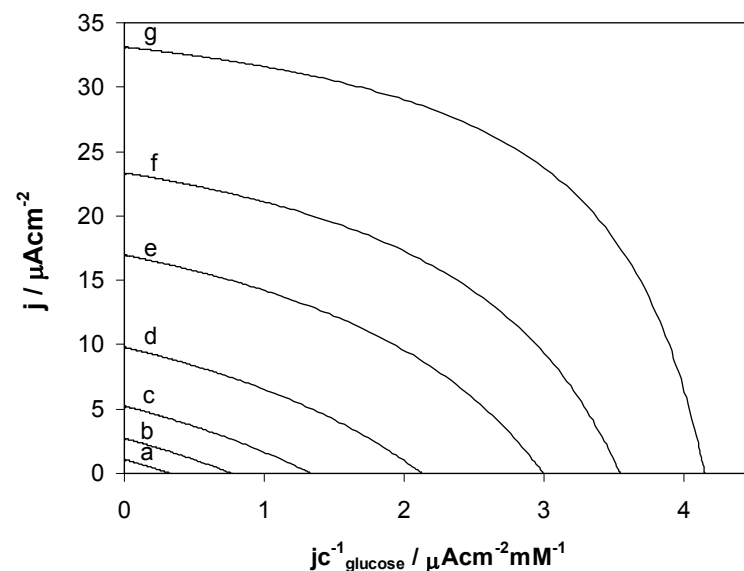


(B)

Figure 21S. Simulation of calibration curves **(A)** and Eadie-Hofstee plots **(B)** for the reagentless glucose biosensors at k'_B equal to $2.591 \times 10^{-11} \text{ cm s}^{-1}$ and A_i equal to 2.0 mM with varying maximum fluxes of the enzymatic reduction of NAD^+ (LV_1): a) $1.204 \times 10^{-10} \text{ mol s}^{-1} \text{ cm}^{-2}$; b) $3.109 \times 10^{-10} \text{ mol s}^{-1} \text{ cm}^{-2}$; c) $6.218 \times 10^{-10} \text{ mol s}^{-1} \text{ cm}^{-2}$; d) $1.264 \times 10^{-9} \text{ mol s}^{-1} \text{ cm}^{-2}$; e) $2.549 \times 10^{-9} \text{ mol s}^{-1} \text{ cm}^{-2}$; f) $4.146 \times 10^{-9} \text{ mol s}^{-1} \text{ cm}^{-2}$; g) $8.281 \times 10^{-9} \text{ mol s}^{-1} \text{ cm}^{-2}$. The values of other parameters are: $\Gamma k_{\text{cat}} = 2.549 \times 10^{-9} \text{ mol s}^{-1} \text{ cm}^{-2}$; $K_A = 2 \text{ mM}$; $K_B = 10 \text{ mM}$; $K_{AB} = 5.6 \text{ mM}^2$; $K_M = 0.8 \text{ mM}$.

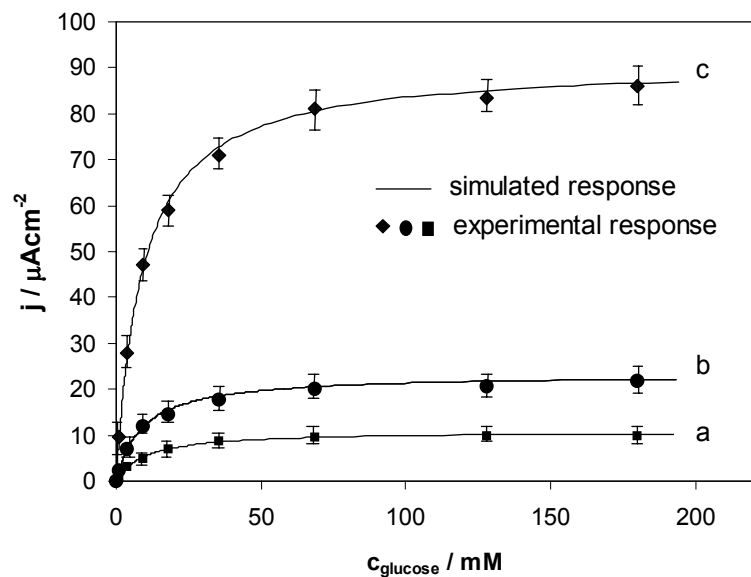


(A)

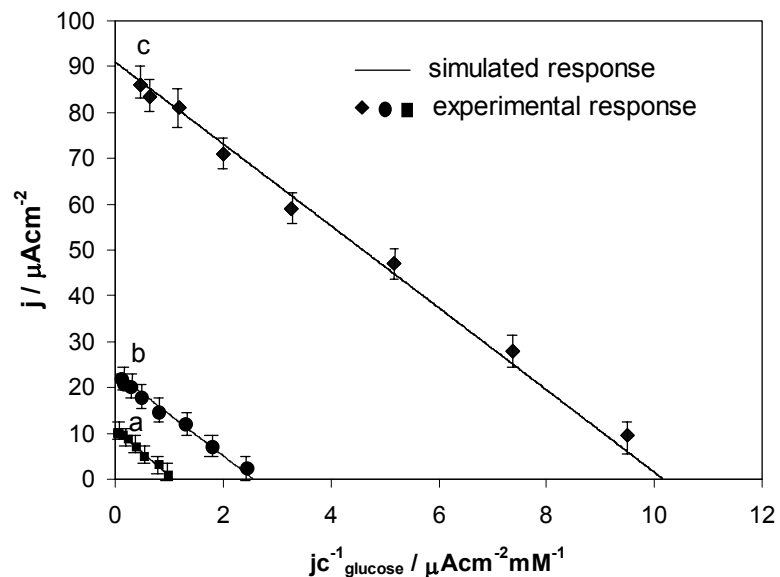


(B)

Figure 22S. Simulation of calibration curves (A) and Eadie-Hofstee plots (B) for the reagentless glucose biosensors at k_B^* equal to $2.591 \times 10^{-11} \text{ cm s}^{-1}$ and A_t equal to 0.1 mM with varying maximum fluxes of the enzymatic reduction of NAD^+ (LV_1): a) $1.204 \times 10^{-10} \text{ mol s}^{-1} \text{ cm}^{-2}$; b) $3.109 \times 10^{-10} \text{ mol s}^{-1} \text{ cm}^{-2}$; c) $6.218 \times 10^{-10} \text{ mol s}^{-1} \text{ cm}^{-2}$; d) $1.264 \times 10^{-9} \text{ mol s}^{-1} \text{ cm}^{-2}$; e) $2.549 \times 10^{-9} \text{ mol s}^{-1} \text{ cm}^{-2}$; f) $4.146 \times 10^{-9} \text{ mol s}^{-1} \text{ cm}^{-2}$; g) $8.281 \times 10^{-9} \text{ mol s}^{-1} \text{ cm}^{-2}$. The values of other parameters are: $\Gamma k_{\text{cat}} = 2.549 \times 10^{-9} \text{ mol s}^{-1} \text{ cm}^{-2}$; $K_A = 2 \text{ mM}$; $K_B = 10 \text{ mM}$; $K_{AB} = 5.6 \text{ mM}^2$; $K_M = 0.8 \text{ mM}$.

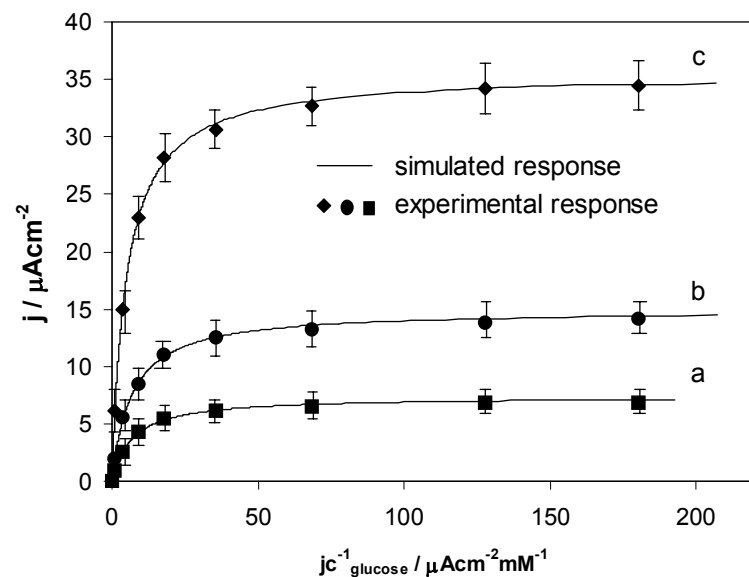


(A)

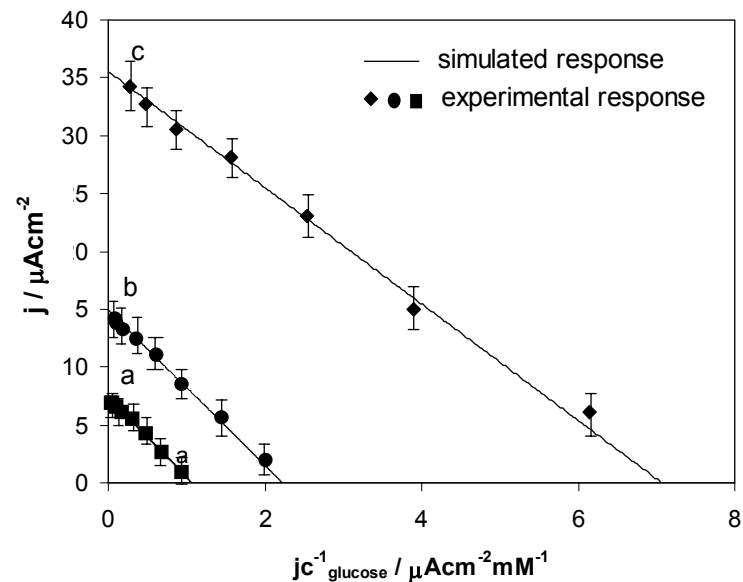


(B)

Figure 23S. Simulated and experimental calibration curves (A) and Eadie-Hofstee plots (B) for the biosensors prepared using varied loading of GDH per electrode: a) 0.135 U; b) 0.027 U; c) 0.0135 U. Experimental conditions: temperature 25°C, applied potential 150 mV vs. Ag/AgCl/KCl_{sat}, 0.1 M phosphate buffer, pH 7.0, containing 26 mM NAD⁺. The value of Γk_{cat} employed for fitting and simulation was $2.549 \times 10^{-9} \text{ mol s}^{-1} \text{ cm}^{-2}$. The values of K_B , LV_1 , and k_B' found by fitting and employed for simulation are listed in Table III.



(A)



(B)

Figure 24S. Simulated and experimental calibration curves (A) and Eadie-Hofstee plots (B) for the biosensors operating in the reagentless mode prepared using varied loading of GDH per electrode: a) 0.135 U; b) 0.027; c) 0.0135 U. Experimental conditions: temperature 25°C, applied potential 150 mV vs. Ag/AgCl/KCl_{sat}, 0.1 M phosphate buffer, pH 7.0. The values of Γk_{cat} and K_M employed for fitting and simulation were $2.549 \times 10^{-9} \text{ mol s}^{-1} \text{ cm}^{-2}$ and 0.8 mM respectively. The values of k'_B , K_A , K_{AB} , K_B , LV_1 , and A_i found by fitting and employed for simulation are listed in Tables III and IV.

The Use of the Lamellar Phase for the Construction of Reagentless Biosensors Based on NAD⁺ Dependent Glutamate Dehydrogenase.

Valeri Pavlov¹, Britta Lindholm-Sethson², Goran Lindblom², Ioanis. Katakis^{1}*

¹Bioanalysis and Bioelectrochemistry Group, Chemical Engineering, Universitat Rovira i Virgili, E-43006, Tarragona (Catalonia), Spain. ²Department of Chemistry, Umeå University, Umeå, SE-901 87, Sweden. Tel: +34 977 55 9655. Fax: +34 977 55 9667. E-mail: ioanis.katakis@urv.net

A new NADH oxidizing redox surfactant [Os(1,10-phenanthroline-5,6-dione)₂(4,4'-[CH₃(CH₂)₁₇NHCO]₂bpy)](PF₆)₂ (Os-phendione-surfactant) has been synthesized. The study of its tensoactive behaviour in a Langmuir-Blodgett trough demonstrated high stability of the resulting monolayer on the water-air interface and mean molecular area from 170 to 230 Å. The lamellar phase suspension based on the lipid 1,2-dioleoyl-sn-glycero-3-phosphatidylcholine containing Os-phendione-surfactant, NAD⁺ and bovine glutamate dehydrogenase was prepared and immobilized on graphite electrodes to yield reagentless biosensors operating at low applied potential of 150 mV vs. Ag/AgCl/KCl_{sat}. Their response curves and dependence of the response current on temperature and pH have been studied in order to determine the rate limiting factor. The operational half-life time of these sensors was 0.5 h.

Keywords: glutamate analysis, glutamate dehydrogenase, reagentless biosensors, NAD⁺, amphiphilic mediator

* To whom the correspondence should be addressed

Amphiphilic compounds or surfactants form micelles, liposomes, vesicles and lamellar phase in liquids and monolayers in gas-liquid interface, which can be transferred to solid substrates by Langmuir-Blodgett (LB) techniques. The development of inorganometallic surfactants serving as electron transfer reagents has been mentioned in the literature. Tenoactive bipyridine complexes of ruthenium were synthesised and their LB films were transferred on glass substrates for the photo-generation of hydrogen from water.^{1,2} These redox active amphiphilic complexes can be utilized in electrochemical biosensors for the mediation of enzymes. For example, surfactants derived from bipyridine complexes of osmium and ruthenium,^{3,4} and ferrocene^{5,6} demonstrated capacity for the exchange of electrons with the active centre of glucose oxidase.

Another class of amphiphilic molecules are lipids, which form cell membranes, also can be used in biosensors for immobilization of proteins on solid substrates. There are two basic ways for the membrane creation: the transfer a monolayer from the liquid-gas interface using the Langmuir –Blodgett technique and vesicle spreading.⁷ In both methods the inner monolayer can be deposited by the LB method or attached to the substrate surface by self-assembly from a solution through forming covalent bonds of alkyl mercaptanes on gold and alkyl silanes on silicon surfaces^{8,9} or through ion bridges.¹⁰ The advantages of the LB techniques are easy automation of the process and easy optical following by imaging ellipsometry or microfluorescence.^{11,12} In addition, by choosing different lipid mixtures and thermodynamic conditions one can deposit alternating layers with different microstructures. Vesicle spreading is based on the electrostatical or covalent linking of vesicles under high tension to the substrate surface followed by their spreading and collapse.¹³ Vesicle spreading proceeds through two mechanisms: the advancement of single bilayers, resulting in incomplete coverage, or viscous fingerlike spreading of giant vesicles leading to closed bilayers by self-healing. The resulting solid-supported lipid bilayers are model systems for biological membranes⁷ but they can incorporate membrane proteins only if the lipid bilayers are separated from the solid support by polymer spacer groups such as poly(oxyethylene).¹⁴ Membrane proteins can be incorporated in lipid bilayers by the transfer of a mixed monolayer containing proteins and lipids on a solid support us LB techniques but the serious drawback of this method is the requirement to dissolve lipids and a protein in organic solvent before spreading on the water-air interface, which may denature proteins. Hence the alternative method based on the fusion of liposomes and vesicles containing membrane proteins in lipid bilayers have been developed. It was successfully used in case of cytochrome c oxidase,^{15,16,17} and H⁺-ATPase,¹⁸ acetylcholine receptor.¹⁹ The majority of commercially available enzymes and coenzymes is hydrophilic so they can be incorporated only between hydrophilic sides of lipid bilayers. For example, vesicles containing encapsulated glucose oxidase were immobilized under a dialysis membrane on hydrogen peroxide electrodes to fabricate glucose biosensors with the increased linear range.^{20,21} To our knowledge the fabrication of “reagentless” biosensors based on the immobilization of NAD⁺ dependent dehydrogenases together with the cofactor in the lipid lamellar phase has never been reported. In this work we present “reagentless” biosensors based on bovine glutamate dehydrogenase (GLDH). Glutamate is a well known neurotransmitter, which plays important role in the development of neurological diseases such as amnesia, depression, and schizophrenia.^{22,23} It is also a marker in the diagnosis of miocardic diseases and hepatitis.²⁴ In order to develop sensors based on NAD⁺ dependent dehydrogenase we synthesized the new NADH oxidizing

amphiphilic complex of osmium with 1,10-phenanthroline-5,6-dione which allows to recycle NAD^+ at applied potential as low as 150 mV vs. Ag/AgCl/KCl_{sat}.

EXPERIMENTAL SECTION

Materials. GLDH (E.C. 1.4.1.3) from bovine liver, as suspension in saturated ammonium was purchased from Biozyme (UK), nicotinamide adenine nucleotide (NAD^+), L-glutamic acid monosodium salt, dimethylformamid (DMF), $n\text{-C}_{18}\text{H}_{37}\text{NH}_2$, sodium dihydrogen phosphate, sodium hydroxide, *ortho*-phosphoric acid, sodium chloride, thionyl chloride, NH_4PF_6 , 2,2'-bipyridine-4,4'-dicarboxylic acid, absolute 1,4-dioxane were obtained from Sigma-Aldrich (USA), K_2OsCl_6 was from Alfa (Spain), ethylene glycol and sodium dithionite were obtained from Pancreac (Madrid, Spain), 1,2-dioleoyl-sn-glycero-3-phosphatidylcholine from Larodan Fine Chemicals (Sweden), 1,10-phenanthroline-5,6-dione was prepared by the published procedure.²⁵

$[\text{Os}(1,10\text{-phenanthroline-5,6-dione})_2\text{Cl}_2]$ was synthesized according to the adapted method.²⁶ Generally the synthesis procedure involved refluxing of K_2OsCl_6 with 1,10-phenanthroline-5,6-dione in DMF under argon in the dark for 1 hr, followed by reduction with aqueous sodium dithionite solution.

Synthesis of 4,4'-[CH₃(CH₂)₁₇NHCO]₂bpy (I)

0.82 mmol of 2,2'-bipyridine-4,4'-dicarboxylic acid were refluxed during 24 h in 4 ml of thionyl chloride (Aldrich, USA), next thionyl chloride was evaporated under vacuum during 4 h. The reaction product was dissolved in 40 ml of absolute 1,4-dioxane. This solution was added dropwise to a solution 1.8 mmol of $n\text{-C}_{18}\text{H}_{37}\text{NH}_2$ in 200 ml of absolute 1,4-dioxane during 20 min, the reaction mixture was left to stay overnight. The next day the solid was filtered off, washed with 1,4-dioxane and airdried to give compound I.

Synthesis of [Os(1,10-phenanthroline-5,6-dione)₂(4,4'-[CH₃(CH₂)₁₇NHCO]₂bpy)](PF₆)₂ (II) (Os-phendione-surfactant)

0.1468 mmol of $[\text{Os}(1,10\text{-phenanthroline-5,6-dione})_2\text{Cl}_2]$ and 0.1762 mmol of compound I were refluxed during 1 h in 5 ml of deaerated ethylene glycol under argon in the dark. Next the product was precipitated by mixing with a solution of 1 g of NH_4PF_6 in 100 ml of water. The solid was filtered off and washed with water, extracted with acetone and air dried to yield compound II. The synthesis route is presented in Figure 2. ¹H NMR performed in CDCl_3 with a tetramethylsilane standard confirmed the presence of long alkane chains: 1.29 p. p. m. (m) 1.26 (m), 0.88 (t).

Preparation of bovine GLDH solution

In order to purify mesophilic bovine GLDH 4 ml of meso GLDH suspension in saturated ammonium sulphate solution were centrifuged during 10 min at 14000 RPM at 5°C. The precipitated enzyme was isolated from the ammonium sulfate solution and dissolved in 3 ml of 0.1 M sodium phosphate buffer (pH 7.4) containing 0.15 M

sodium chloride, next the resulting enzyme solution was extensively dialyzed at 5°C against 200 ml of the same buffer during 24 h, the buffer solution being changed every two hours.

Preparation of graphite electrodes. Spectrographic graphite rods of 3 mm in diameter (Carbone of America, USA) were cut into pieces of 2 cm in longitude, introduced into heat-shrinkable PVC plastic tubes, shrunk by heating, wet polished on fine (grit 400 and 600) emery paper (Buehler, USA) and sonicated in water.

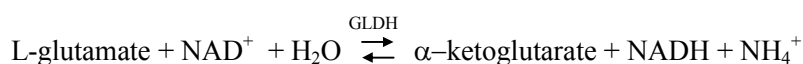
Preparation of reagentless glutamate biosensors based on immobilization between lipid bilayers. 1.5 mg of Os-phendione-surfactant and 10 mg of 1,2-dioleoyl-sn-glycero-3-phosphatylcholine were dissolved in 0.5 mL of chloroform. Then this solution was evaporated under vacuum in a pear shaped flask to form the solid thin layer on the bottom. Next 1 mL of a solution containing 5.8 mg mL⁻¹ (38 U mL⁻¹ at 30°C) of bovine glutamate dehydrogenase and 40 mg of NAD⁺ in 0.1 M phosphate buffer pH 7.6 were stirred during 2 h to form the lamellar phase. The suspension was washed 6 times with 1 mL of 0.1 M phosphate buffer (pH 7.6), using centrifugation at 4000 rpm during 10 min every time. Next the volume of this suspension was adjusted to 1 mL and 5 µL of it was deposited per graphite electrode and air-dried during 1 h.

Electrochemical measurements. A three-electrode conventional thermostabilised cell (3 mL) equipped with an Ag/AgCl/KCl_{sat} reference electrode, a platinum auxiliary electrode, and a graphite electrode modified according to one of the above mentioned methods as working electrode. The buffer, pH 7.4 (0.1 M sodium phosphate containing 0.15 M sodium chloride) served as supporting electrolyte. The response to successive additions of stock glutamate solution was registered as steady state current on a three-electrode potentiostat Autolab PGSTAT 10 (Eco chemie, Holland) controlled by a computer. The working potential was 150 mV vs. Ag/AgCl/KCl_{sat} and the temperature of a thoroughly stirred solution was 30°C.

GLDH assay method. The activity of GLDH was tested spectrophotometrically by following the increase in absorbance at 340 nm 30°C. The assay solution contained 5 mM NAD⁺ and 10 mM in 0.1 M sodium phosphate buffer (pH 7.4). The ΔA_{340} (Au/min) was obtained using the maximum linear rate for both the test and blank (without the enzyme) mixtures. The activity was calculated using $\epsilon_{\text{NADH}}=6.22 \text{ mM}^{-1}\text{cm}^{-1}$ extinction coefficient of β -NADH. One unit of GLDH oxidizes 1 µmol of L-glutamate per minute at pH 7.4 at 30°C. Protein concentration was determined spectrophotometrically at A_{280} using an absorbance coefficient of 0.973 cm² mg⁻¹.

RESULTS AND DISCUSSION

Methods for the fabrication of reagentless glutamate biosensors. The glutamate biosensors presented hereby are based on the oxidation of L-glutamate by NAD⁺ through mesophilic and thermophilic glutamate dehydrogenase (GLDH) according to the reaction:



with the equilibrium constant shifted to the formation of L-glutamate, nevertheless the reoxidation of NADH by Os-phendione-surfactant mediator, which is oxidized in its turn at the graphite surface of the electrode at low positive potential of 150 mV vs. Ag/AgCl/KCl_{sat}, displaces the equilibrium to the production of NADH. The sequence of chemical reactions in the glutamate biosensor is shown schematically in Figure 1. The immobilization of GLDH, NAD⁺ and mediator is the necessary condition for design of reagentless glutamate biosensors. It was achieved by the formation of the lamellar phase suspension containing new NADH oxidizing surfactant (Os-phendione-surfactant), 1,2-dioleoyl-sn-glycero-3-phosphatidylcholine, NAD⁺, and GLDH. The synthetic root to Os-phendione-surfactant can be seen in Figure 2. It was shown in the literature that complexes of transition metals with 1,10-phenanthroline-5,6-dione are stable mediators for the electrochemical oxidation of NADH,^{27,28,29} therefore we converted [Os(1,10-phenanthroline-5,6-dione)₂Cl₂] complex into a surfactant by complexation with amphiphilic bipyridine (I). This compound has demonstrated tensoactivity and forms stable Langmuir monolayer on water-air interface in a Langmuir's trough. The surface pressure/area isotherm of this mediator is shown in Figure 3. The results obtained from this isotherm point out to mean molecular area from 170 to 230 Å². This high value can be explained by the presence of bulky phenanthroline ligands. Some reorganization of a monolayer takes place starting from surface pressure value of 40 mN m⁻¹. The lamellar phase suspension was formed by mixing biosensor components with the lipid in an aqueous solution, next they were separated by centrifuge, adsorbed on the graphite electrode surface, and air-dried. ³¹P NMR investigation was utilized to confirm the structures of the lamellar phase suspension in water and on the graphite surface. In both cases the NMR spectra showed the broad peak from -7 to -15 ppm, which is the strong indication to the presence of lamellar phase.

Electrocatalytical oxidation of L-glutamate. The reagentless glutamate biosensor demonstrated change in the CV behaviour when glutamate solution was injected into the cell (Figure 4). In the presence of glutamate clear electrocatalytic waves achieving almost a plateau at potentials more negative than 200 mV vs. Ag/AgCl/KCl_{sat} have been seen. Our previous study of the complex of [Os(1,10-phenanthroline-5,6-dione)₂Cl₂] with poly(4-vinylpyridine)³⁰ proved that the potential of 150 mV vs. Ag/AgCl/KCl_{sat} was sufficient for electrocatalytic oxidation of NADH hence the same potential was used in continuation of the work.

Effect of pH on the response of glutamate biosensors. The effect of the pH on the maximum response current of glutamate biosensors was studied in steady state mode using 0.1 M phosphate buffer, pH was adjusted

with aqueous solutions of 1 M NaOH or H₃PO₄. In Figure 5 it can be seen that the biosensors have maximum response at pH 9.0. This result is in good agreement with the pH optimum of 8.5-9.0 for glutamate oxidation by free bovine GLDH in the solution.³¹ The complexes of osmium are unstable at the pH values higher than 8.0, at the same time, the controlled electrodes prepared without GLDH showed increase in non-specific oxidation of glutamate starting from pH 9.0, hence the pH of 7.4 was chosen for further experiments, because this is the physiologic value of the pH at which the analysis *in vivo* could be carried out.

Effect of temperature on the response of glutamate biosensors. The effect of temperature on the response of glutamate biosensors is presented in Figures 6. Vesicles based sensors demonstrated optimal temperature of 54°C. This data is in good agreement with the published thermostability study of bovine GLDH according to which this enzyme loses activity starting from the temperature of 52°C.³² The activation energies for the glutamate biosensors were calculated from Arrhenius plot obtained by plotting the logarithm of the relative response current against the reciprocal of the absolute temperature. The activation energy is 56.3 kJ mol⁻¹. Activation energies of the GLDH biosensors are significantly higher than the activation energy of free bovine GLDH, 12.9 kJ mol⁻¹.³² This fact indicates that the response of the glutamate biosensors was not limited by the kinetics of glutamate oxidation with NAD⁺ through GLDH.

Response curves and operational stability of the glutamate biosensors. The latest kinetic study into the mechanism of enzymatic deamination confirmed that bovine dehydrogenase has an ordered sequential mechanism of substrate binding preceded by complexation with NAD⁺³³ therefore the calculations of characteristics of the glucose sensors were based on the following modified kinetic model for the conversion of substrate B to product Q.³⁴ Figure 7 illustrates the kinetic scheme for the operation of reagentless biosensors based on the enzyme glutamate dehydrogenase (E) catalyzing the reaction of immobilized NAD⁺ (A) with a L-glutamate (B) to give immobilized NADH (P), α-ketoglutarate (Q), and NH₄⁺ (R). Then a mediator (M), which can stay in reduced (M_{red}) and oxidized (M_{ox}) forms, immobilized on the electrode surface catalyzes the electrochemical conversion of P back to A. A_{im} and P_{im} are the concentrations of immobilized A and P. B_o , Q_o , R_o are the concentrations of the substrate and the products in the lamellar phase B_∞ , Q_∞ and R_∞ are the concentrations of the substrate and the products in the external medium. k'_B , k'_Q and k'_R are mass transfer coefficients of the substrate and the products (cm s⁻¹), respectively. L is the thickness of the hydrogel layer. The following expressions for the flux of B to the electrode surface (j_{el}), which determines the current density of a biosensor (j) through the equation $j = nFj_{el}$, where n is the number of exchanged electrons and F is the Faraday's constant, can be obtained.

$$j_{el} = k'_B(B_\infty - B_o) \quad (1)$$

$$j_{el} = L(k_1 A_{im} [E] - k_{-1} [E \cdot A]) \quad (2)$$

$$j_{el} = L(k_2 B_o [E \cdot A] - k_{-2} [E \cdot A \cdot B]) \quad (3)$$

$$j_{el} = L(k_3 [E \cdot A \cdot B] - k_{-3} [E \cdot P \cdot Q \cdot R]) \quad (4)$$

$$j_{el} = L(k_4 [E \cdot P \cdot Q \cdot R] - k_{-4} [E \cdot P \cdot Q] Q_o) \quad (5)$$

$$j_{el} = L(k_5 [E \cdot P \cdot Q] - k_{-5} [E \cdot P] Q_o) \quad (6)$$

$$j_{el} = L(k_6 [E \cdot P] - k_{-6} [E] P_{im}) \quad (7)$$

$$j_{el} = k'_Q Q_o \quad (8)$$

$$\begin{aligned}
j_{el} &= k'_R R_0 & (9) \\
j_{el} &= k_7 P_0 \Gamma_{Mox} - k_7 \Gamma_{M \cdot P} & (10) \\
j_{el} &= k_8 \Gamma_{M \cdot P} & (11) \\
j_{el} &= k_9 \Gamma_{Mred} & (12) \\
E_t &= [E] + [E \cdot A] + [E \cdot A \cdot B] + [E \cdot P \cdot Q \cdot R] + [E \cdot P \cdot Q] + [E \cdot P] & (13) \\
\Gamma_M &= \Gamma_{M \cdot P} + \Gamma_{Mox} + \Gamma_{Mred} & (14) \\
A_t &= A_{im} + P_{im} & (15)
\end{aligned}$$

Where Γ_{Mox} and Γ_{Mred} are the surface coverages of the mediator in oxidized and reduced forms, respectively. Γ_M is the total mediator surface coverage. $\Gamma_{M \cdot P}$ is the surface coverage of the intermediate complex between the mediator and NADH. A_t and E_t are the total concentrations of NAD⁺ and the enzyme immobilized in the lamellar phase, respectively. The equations (1-15) yield the equation (16):

$$\begin{aligned}
LV_1 \Gamma_M k_{cat} E_t A_t B_\infty &= j_{el} [K_{AB} \Gamma_M k_{cat} + K_B \Gamma_M k_{cat} A_t + K_A \Gamma_M k_{cat} B_\infty + A_t \Gamma_M k_{cat} B_\infty + LV_1 (A_t + K_M) B_\infty + \\
&(LV_1 A_t \Gamma_M k_{cat}) / k'_B] + j_{el}^2 [(K_{PQ} K_B A_t \Gamma_M k_{cat}) / (K_{iP} K_{iQ} K_R k'_R) - LV_1 (A_t + K_M) / k'_B - K_{AB} - K_B (A_t + K_M) - K_A B_\infty + \\
&K_M K_{QR} K_{iA} K_B / (K_{iP} K_{iQ} K_R) - (A_t + K_M) B_\infty - A_t \Gamma_M k_{cat} / k'_B + \Gamma_M k_{cat} K_{PQ} K_{iA} K_B R_0 / (K_{iP} K_{iQ} K_R k'_R) + K_A K_M B_\infty / K_{iP} + \\
&K_{iR} K_P K_B A_t B_\infty \Gamma_M k_{cat} / (K_{iB} K_{iP} K_{iQ} K_R k'_Q) + K_{PQ} K_B A_t B_\infty \Gamma_M k_{cat} / (K_{iB} K_{iP} K_{iQ} k'_R)] + j_{el}^3 [LV_1 K_M / (K_{eq} k'_Q k'_R) + K_A / k'_B + (A_t \\
&+ K_M) / k'_B - K_{PQ} K_{iA} K_B / (K_{iP} K_{iQ} K_R k'_R) + \Gamma_M k_{cat} K_P K_{iA} K_B / (K_{iP} K_{iQ} K_R k'_Q k'_R) + K_M K_R K_{iA} K_B / (K_{iP} K_{iQ} K_R k'_Q) + \\
&K_M K_P K_{iA} K_B / (K_{iP} K_{iQ} K_R k'_R) - K_A K_M / (K_{iP} k'_B) + K_A K_M B_\infty / (K_{iQ} K_{iP} k'_Q) - K_{iR} K_P K_B (A_t + K_M) B_\infty / (K_{iB} K_{iP} K_{iQ} K_R k'_Q) - \\
&K_{iR} K_P K_B A_t \Gamma_M k_{cat} / (K_{iB} K_{iP} K_{iQ} K_R k'_Q k'_R) + K_P K_B A_t \Gamma_M k_{cat} / (K_{iP} K_{iQ} K_R k'_Q k'_R) - K_{PQ} K_B (A_t + K_M) / (K_{iP} K_{iQ} K_R k'_R) + \\
&K_P K_B A_t B_\infty \Gamma_M k_{cat} / (K_{iB} K_{iP} K_{iQ} K_R k'_Q k'_R) - K_{PQ} K_B B_\infty (A_t + K_M) / (K_{iB} K_{iP} K_{iQ} K_R k'_R) - A_t \Gamma_M k_{cat} K_{PQ} K_B / (K_{iB} K_{iP} K_{iQ} K_R k'_Q k'_R) \\
&+ j_{el}^4 [K_{iA} K_B K_M / (K_{iP} K_{iQ} K_R k'_Q k'_R) - K_P K_{iA} K_B / (K_{iP} K_{iQ} K_R k'_Q k'_R) - K_A K_M / (K_{iQ} K_{iP} k'_B k'_Q) + K_{iR} K_P K_B (A_t \\
&+ K_M) / (K_{iB} K_{iP} K_{iQ} K_R k'_Q k'_R) - K_P K_B (A_t + K_M) / (K_{iP} K_{iQ} K_R k'_Q k'_R) - \\
&K_P K_B B_\infty / (K_{iB} K_{iP} K_{iQ} K_R k'_Q k'_R) - K_P K_B A_t \Gamma_M k_{cat} / (K_{iB} K_{iP} K_{iQ} K_R k'_Q k'_R) + K_A B_\infty K_M / (K_{iR} K_{iP} K_{iQ} k'_Q k'_R) + \\
&K_{PQ} K_B (A_t + K_M) / (K_{iB} K_{iP} K_{iQ} K_R k'_Q k'_R)] + j_{el}^5 [K_P K_B (A_t + K_M) / (K_{iB} K_{iP} K_{iQ} K_R k'_Q k'_R) - K_A K_M / (K_{iR} K_{iP} K_{iQ} k'_Q k'_R)] & (16)
\end{aligned}$$

Where $V_1 = E_t (k_1 k_2 k_3 k_4 k_5 k_6) / (k_1 k_2 k_5 k_6 k_3 + k_1 k_2 k_4 k_5 k_6 + k_1 k_2 k_3 k_5 k_6 + k_1 k_2 k_3 k_4 k_6 + k_1 k_2 k_3 k_4 k_5)$ and $V_2 = E_t (k_{-1} k_{-2} k_{-3} k_{-4} k_{-5} k_{-6}) / (k_{-2} k_{-3} k_{-4} k_{-5} k_{-6} + k_{-1} k_{-3} k_{-4} k_{-5} k_{-6} + k_{-1} k_{-2} k_{-4} k_{-5} k_{-6} + k_3 k_{-1} k_{-4} k_{-5} k_{-6})$ are the maximum velocities in forward and reverse directions, the Michaelis constants for A, B, P, Q, R are $K_A = (k_2 k_3 k_4 k_5 k_6) / (k_1 k_2 k_5 k_6 k_3 + k_1 k_2 k_4 k_5 k_6 + k_1 k_2 k_3 k_5 k_6 + k_1 k_2 k_3 k_4 k_6 + k_1 k_2 k_3 k_4 k_5)$, $K_B = (k_1 k_5 k_6 k_2 k_3 + k_1 k_4 k_5 k_6 k_2 + k_1 k_3 k_4 k_5 k_6) / (k_1 k_2 k_5 k_6 k_3 + k_1 k_2 k_4 k_5 k_6 + k_1 k_2 k_3 k_5 k_6 + k_1 k_2 k_3 k_4 k_6 + k_1 k_2 k_3 k_4 k_5)$, $K_{AB} = (k_5 k_6 k_{-1} k_{-2} k_{-3} + k_4 k_5 k_6 k_{-1} k_{-2} + k_{-1} k_3 k_4 k_5 k_6) / (k_1 k_2 k_5 k_6 k_3 + k_1 k_2 k_4 k_5 k_6 + k_1 k_2 k_3 k_5 k_6 + k_1 k_2 k_3 k_4 k_6 + k_1 k_2 k_3 k_4 k_5)$, $K_P = k_{-1} k_{-2} k_{-3} k_{-4} k_{-5} / (k_{-2} k_{-3} k_{-4} k_{-5} k_{-6} + k_{-1} k_{-3} k_{-4} k_{-5} k_{-6} + k_{-1} k_{-2} k_{-4} k_{-5} k_{-6} + k_3 k_{-1} k_{-4} k_{-5} k_{-6})$, $K_Q = k_{-1} k_{-2} k_{-3} k_{-4} k_{-6} / (k_{-2} k_{-3} k_{-4} k_{-5} k_{-6} + k_{-1} k_{-3} k_{-4} k_{-5} k_{-6} + k_{-1} k_{-2} k_{-4} k_{-5} k_{-6} + k_3 k_{-1} k_{-4} k_{-5} k_{-6})$, $K_R = (k_{-1} k_{-2} k_{-3} k_{-5} k_{-6} + k_4 k_{-1} k_{-2} k_{-5} k_{-6} + k_3 k_4 k_{-1} k_{-5} k_{-6}) / (k_{-2} k_{-3} k_{-4} k_{-5} k_{-6} + k_{-1} k_{-3} k_{-4} k_{-5} k_{-6} + k_{-1} k_{-2} k_{-4} k_{-5} k_{-6} + k_3 k_{-1} k_{-4} k_{-5} k_{-6})$, $K_{QR} = (k_5 k_{-1} k_{-2} k_{-3} k_{-6} + k_4 k_5 k_{-1} k_{-2} k_{-6} + k_3 k_4 k_5 k_{-1} k_{-6}) / (k_{-2} k_{-3} k_{-4} k_{-5} k_{-6} + k_{-1} k_{-3} k_{-4} k_{-5} k_{-6} + k_{-1} k_{-2} k_{-4} k_{-5} k_{-6} + k_3 k_{-1} k_{-4} k_{-5} k_{-6})$, $K_{PQ} = k_6 k_{-1} k_{-2} k_{-3} k_{-4} / (k_{-2} k_{-3} k_{-4} k_{-5} k_{-6} + k_{-1} k_{-3} k_{-4} k_{-5} k_{-6} + k_{-1} k_{-2} k_{-4} k_{-5} k_{-6} + k_3 k_{-1} k_{-4} k_{-5} k_{-6})$, $K_{PQR} = (k_5 k_6 k_{-1} k_{-2} k_{-3} + k_4 k_5 k_6 k_{-1} k_{-2} + k_{-1} k_3 k_4 k_5 k_6) / (k_{-2} k_{-3} k_{-4} k_{-5} k_{-6} + k_{-1} k_{-3} k_{-4} k_{-5} k_{-6} + k_{-1} k_{-2} k_{-4} k_{-5} k_{-6} + k_3 k_{-1} k_{-4} k_{-5} k_{-6})$. The inhibition constants for A, B, P, Q, R are $K_{iA} = k_{-1} / k_1$, $K_{iB} = (k_2 k_{-3}) / (k_2 (k_{-3} + k_3))$, $K_{iP} = k_6 / k_{-6}$, $K_{iQ} = k_5 / k_{-5}$, $K_{iR} = (k_3 k_4) / (k_4 (k_3 + k_{-3}))$. Use of the inhibition constants allows to redefine: $K_{PQ} = K_{iP} K_Q$ and $K_{QR} = K_{iQ} K_R$.

The equation 16 was employed to simulate the response curves and Eadie-Hofstee plots for the reagentless glutamate biosensors using the values of the Michaelis and inhibition constants found in the literature.³⁵

Figure 8 demonstrates the effect of the value of maximum flux of the electrochemical oxidation of NADH (Γk_{cat}) on the simulated response of the reagentless glutamate biosensors (at $A_t = 1$ mM). The Eadie-

Hofstee plots yield the straight line characteristic for the process limited by the enzymatic reduction of NAD^+ only when Γk_{cat} is infinitively high. The decrease in the value of Γk_{cat} leads to the decrease in the values of intercepts of the Eadie-Hofstee plots with the axis of j and their negative slopes i.e. the apparent maximum current densities and apparent Michaelis constants, respectively, become lower due to the limitation set by the flux of the electrochemical oxidation of NADH. The decrease in the value of Γk_{cat} also effects the shape of Eadie-Hofstee plots making them more concave. Hence the concavity of Eadie-Hofstee plots is diagnostic for reagentless glutamate biosensors limited by the rate of electrochemical NADH oxidation at the electrode surface.

Figure 9 represents the effect of mass transport rate on the response of biosensors limited by the rate of the electrochemical NADH oxidation. The decrease in the mass transfer coefficients leads to the drastic increase in the slope of Eadie-Hofstee plots, making the apparent Michaelis constants (measured using high concentrations of glutamate) higher than K_B of free GLDH. It can be concluded that the concave Eadie-Hofstee plots, giving the values of apparent Michaelis constant higher than the value of K_M of the free enzyme, are diagnostic for the reagentless glutamate biosensors limited by the rate of electrochemical NADH oxidation at the electrode surface and by the rate of mass transport.

The effect of the maximum flux of the enzymatic reduction of NAD^+ (LV_1) rate on the response of biosensors limited by the rate of the electrochemical NADH oxidation and mass transport is illustrated in Figure 10. The increase in LV_1 leads to the drastic increase in apparent current densities and the concavity of the Eadie-Hofstee plots, making the apparent Michaelis constants higher than K_B of free GLDH.

The response curve of the glutamate biosensors is shown in Figures 11 and their basic characteristics obtained from the Eadie-Hofstee plots are represented in Table II. The Eadie-Hofstee plots (Figure 10(B)) show concavity characteristic for the process limited by the rate of NADH oxidation at the electrode surface. The value of the apparent Michaelis constant (47 mM) is significantly higher than the literature value of that for mesophilic bovine GLDH (2.5 mM)³⁵ implying that the response of these glutamate sensors is limited by the rate of electrochemical NADH oxidation and the mass transfer between the lamellar phase and the external solution.

The glutamate biosensors prepared using immobilization in the lamellar phase layers have very short operational half-life time (30 min) and long response time 7-8 min. The loss of the response was caused by leaching of NAD^+ from the electrode surface. This was proven by the injection of NAD^+ at the end of operational stability study (when one half of the initial response to glutamate and 20% of Os-phendione-PVP were lost according to the data obtained by cyclic voltammetry. The injection of NAD^+ lead to the recovery of c.a. 80 % of the initial response current demonstrated by the biosensors operated in the presence of NAD^+ .

CONCLUSIONS

The new NADH oxidizing surfactant can be synthesized by complexation of $[\text{Os}(1,10\text{-phenanthroline-5,6-dione})_2\text{Cl}_2]$ with hydrophobic ligand and can be used for the formation of the aqueous lamellar phase which entraps NAD^+ dependent glutamate dehydrogenase and NAD^+ . The resulting lamellar phase suspension can be

immobilized by adsorption on graphite electrodes to yield reagentless glutamate biosensors operating at 150 mV vs. Ag/AgCl/KCl_{sat}. Their response is limited by the rate of electrochemical NADH oxidation and the mass transfer between the lamellar phase and the external solution. Their low operational stability is determined by leaching of NAD⁺.

ACKNOWLEDGEMENTS

This paper was supported by the grants of European Community, Industrial & Material Technologies Programme (Brite-EuRam III), project No. BE97-4511, the Spanish Ministry of Education and Culture Ref.: Acciones Especiales MAT98-1413.CE. V.P. acknowledges Ph. D. fellowship and the special grant Ref.:M3C99-80 from the Department of chemical engineering, University Rovira I Virgili.

LEGEND TO TABLE

Table I. Basic characteristics of the reagentless glutamate biosensors calculated from the Eadie-Hofstee plot.

LEGENDS TO FIGURES

Figure 1. Schematic diagram of the electron transfer steps for the mediated glutamate biosensors.

Figure 2. Synthetic route to the NADH oxidising tensoactive mediator Os-phendione-surfactant.

Figure 3. Surface pressure/area isotherm for Os-phendione-surfactant.

Figure 4. Cyclic voltammograms of reagentless glutamate biosensors based on the lamella phase layers and GLDH in the absence of glutamate and the presence 0.35 M glutamate. Scan rate 0.3 mV s⁻¹. Experimental conditions: E_{app} 150 mV vs. Ag/AgCl/KCl_{sat}, 0.1 M phosphate buffer (pH 7.4), temperature 30°C.

Figure 5. Effect of pH on maximum response of reagentless glutamate biosensors based on the lamellar phase. Experimental conditions: E_{app} 150 mV vs. Ag/AgCl/KCl_{sat}, 0.1 M phosphate buffer, temperature 30°C.

Figure 6. Effect of temperature on maximum response of reagentless glutamate biosensors based on the lamellar phase. Experimental conditions: E_{app} 150 mV vs. Ag/AgCl/KCl_{sat}, 0.1 M phosphate buffer (pH 7.4).

Figure 7. Reaction scheme for a reagentless glutamate biosensor.

Figure 8. Simulation of the Eadie-Hofstee plots for the reagentless glutamate biosensors with varying maximum fluxes of the electrochemical NADH oxidation (Γk_{cat}): a) 2.6×10^{-11} mol s⁻¹ cm⁻²; b) 1.04×10^{-10} mol s⁻¹ cm⁻²;

c) $4.15 \times 10^{-10} \text{ mol s}^{-1} \text{ cm}^{-2}$; d) $8.3 \times 10^{-10} \text{ mol s}^{-1} \text{ cm}^{-2}$; e) $1.7 \times 10^{-9} \text{ mol s}^{-1} \text{ cm}^{-2}$; f) $1.3 \times 10^{-8} \text{ mol s}^{-1} \text{ cm}^{-2}$; g) $5.178 \times 10^{-8} \text{ mol s}^{-1} \text{ cm}^{-2}$; h) ∞ . The values of other parameters are: $A_t=1 \text{ mM}$; $k'_B \rightarrow \infty$; $k'_Q \rightarrow \infty$; $k'_R \rightarrow \infty$; $LV_1=3.63 \times 10^{-10} \text{ mol s}^{-1} \text{ cm}^{-2}$; $K_M = 0.8 \text{ mM}$; $K_A = 0.23 \text{ mM}$; $K_B = 2.5 \text{ mM}$; $K_{AB} = 0.3 \text{ mM}^2$; $K_{iA} = 10 \text{ mM}$; $K_{iB} = 11 \text{ mM}$; $K_R = 20 \text{ mM}$; $K_Q = 0.25 \text{ mM}$; $K_P = 0.04 \text{ mM}$; $K_{iR} = 9 \text{ mM}$; $K_{iQ} = 1.6 \text{ mM}$; $K_{iP} = 0.03 \text{ mM}$.

Figure 9. Simulation of the Eadie-Hofstee plots for the reagentless glutamate biosensors with varying mass transfer coefficients (k'_B , k'_Q , k'_R): a) $5.18 \times 10^{-12} \text{ cm s}^{-1}$; b) $2.6 \times 10^{-11} \text{ cm s}^{-1}$; c) $5.18 \times 10^{-11} \text{ cm s}^{-1}$; d) $1.03 \times 10^{-10} \text{ cm s}^{-1}$; e) $2.6 \times 10^{-10} \text{ cm s}^{-1}$; f) ∞ . The values of other parameters are: $A_t=1 \text{ mM}$; $LV_1 = 3.63 \times 10^{-10} \text{ mol s}^{-1} \text{ cm}^{-2}$; $\Gamma k_{\text{cat}} = 8.3 \times 10^{-10} \text{ mol s}^{-1} \text{ cm}^{-2}$; $K_M = 0.8 \text{ mM}$; $K_A = 0.23 \text{ mM}$; $K_B = 2.5 \text{ mM}$; $K_{AB} = 0.3 \text{ mM}^2$; $K_{iA} = 10 \text{ mM}$; $K_{iB} = 11 \text{ mM}$; $K_R = 20 \text{ mM}$; $K_Q = 0.25 \text{ mM}$; $K_P = 0.04 \text{ mM}$; $K_{iR} = 9 \text{ mM}$; $K_{iQ} = 1.6 \text{ mM}$; $K_{iP} = 0.03 \text{ mM}$.

Figure 10. Simulation of the Eadie-Hofstee plots for the reagentless glutamate biosensors with varying maximum flux of enzymatic reduction of NAD^+ (LV_1): a) $1.55 \times 10^{-10} \text{ mol s}^{-1} \text{ cm}^{-2}$; b) $3.63 \times 10^{-10} \text{ mol s}^{-1} \text{ cm}^{-2}$; c) $6.22 \times 10^{-10} \text{ mol s}^{-1} \text{ cm}^{-2}$; d) $1.24 \times 10^{-9} \text{ mol s}^{-1} \text{ cm}^{-2}$; e) $2.49 \times 10^{-9} \text{ mol s}^{-1} \text{ cm}^{-2}$. The values of other parameters are: $k'_B = 2.6 \times 10^{-11} \text{ cm s}^{-1}$; $k'_Q = 2.6 \times 10^{-11} \text{ cm s}^{-1}$; $k'_R = 2.6 \times 10^{-11} \text{ cm s}^{-1}$; $A_t=1 \text{ mM}$; $\Gamma k_{\text{cat}} = 8.3 \times 10^{-10} \text{ mol s}^{-1} \text{ cm}^{-2}$; $K_M = 0.8 \text{ mM}$; $K_A = 0.23 \text{ mM}$; $K_B = 2.5 \text{ mM}$; $K_{AB} = 0.3 \text{ mM}^2$; $K_{iA} = 10 \text{ mM}$; $K_{iB} = 11 \text{ mM}$; $K_R = 20 \text{ mM}$; $K_Q = 0.25 \text{ mM}$; $K_P = 0.04 \text{ mM}$; $K_{iR} = 9 \text{ mM}$; $K_{iQ} = 1.6 \text{ mM}$; $K_{iP} = 0.03 \text{ mM}$.

Figure 11. Dependence of the steady apparent current density on L-glutamate concentration (**A**) and the Eadie-Hofstee plots (**B**) for reagentless biosensors based on the lamellar phase. Experimental conditions: $E_{\text{app}} 150 \text{ mV}$ vs. $\text{Ag/AgCl/KCl}_{\text{sat}}$, 0.1 M phosphate buffer (pH 7.4), temperature 30°C .

REFERENCES

- (1) Sprintschik, G.; Sprintschik, H. W.; Kirsch, P. P.; Whitten, D. G. *J. Am. Chem. Soc.* **1976**, *98*, 2337-2338.
- (2) Gaines, G. L.; Behnken, P. E.; Valenty, S. J. *J. Am. Chem. Soc.* **1978**, *100*, 6549-6559.
- (3) Saudan, P.; Zakeeruddin, S. M.; Malavallon, M. A.; Grätzel, M.; Fraser, D. M. *Biotechnol. Bioengin.* **1994**, *44*, 407-418.
- (4) Zakeeruddin, S. M.; Grätzel, M.; Fraser, D. M. *Biosens. Bioelectron.* **1996**, *11*, 305-315.
- (5) Fraser, D. M.; Zakeeruddin, S. M.; Grätzel, M. *Biochim. Biophys. Acta* **1992**, *1099*, 91-101.
- (6) Ryabov, A. D.; Amon, A.; Gorbatova, R. K.; Ryabova, E. S.; Gnedenko, B. B. *J. Phys. Chem.* **1995**, *99*, 14072-14077.
- (7) Sackmann, E. *Science*, **1996**, *271*, 43-48.
- (8) Miller, C.; Cuendet, P.; Grätzel, M. *J. Electroanal. Chem.* **1990**, *278*, 175-192.
- (9) Florin E. L.; Gaub, H. E. *Biophys. J.* **1993**, *64*, 375-383.
- (10) Kuhn, H.; Möbius H. D.; Bücher, H. In *Physical Methods of Chemistry*, Part IIIB, Weissenberger, A.; Rossiter, B. M. Eds.; Wiley: New York, 1972; pp. 577-578.
- (11) Egger, M.; Heyn, S. P.; Gaub, H. E. *Biophys. J.* **1990**, *57*, 669-673.

- (12) Kalb, E.; Frey, S.; Tamm, L. K. *Biochim. Biophys Acta* **1992**, *1103*, 307-316.
- (13) Bayerl, Th. M.; Bloom, M. *Biophys. J.* **1990**, *58*, 357-362.
- (14) Duschl, C.; Liley, M.; Lang, H.; Ghandi, A.; Zakeeruddin, S. M.; Stahlberg, H.; Dubochet, J.; Nemetz, A.; Knoll, W.; Vogel, H. *Mater. Sci. Eng. C* **1996**, *4*, 7-18.
- (15) Salamon, Z.; Hazzard, J. T.; Tollin, G. *Proc. Natl. Acad. U.S.A.* **1993**, *90*, 6420-6423.
- (16) Lindholm-Sethson, B.; Gonzalez, J. C.; Puu, G. *Langmuir* **1998**, *14*, 6705-6708.
- (17) Naumann, R.; Schmidt, E. K.; Jonczyk, A.; Fendler, K.; Kadenbach, B.; Liebermann, T.; Offenhäusser, A.; Knoll, W. *Biosens. Bioelectron.* **1999**, *14*, 651-662.
- (18) Bunjes, N.; Schmidt, E. K.; Jonczyk, A.; Rippmann, F.; Beyer, D.; Ringsdorf, H.; Gräber, P.; Knoll, Naumann, W.; R. *Langmuir*, **1997**, *13*, 6188-6194.
- (19) Schmidt, E. K.; Liebermann, T.; Kreiter, M.; Jonczyk, A.; Naumann, R.; Offenhäuser, A.; Neumann, E.; Kukol, A.; Maelicke, A.; Knoll, W. *Biosens. Bioelectron.* **1998**, *13*, 585-591.
- (20) Taylor, M. A.; Jones, M. N.; Vadgama, P.; Higson, S. P. J. *Biosens. Bioelectron.* **1995**, *10*, 251-260.
- (21) Taylor, M. A.; Jones, M. N.; Vadgama, P.; Higson, S. P. J. *Biosens. Bioelectron.* **1997**, *12*, 467-477.
- (22) Engelsen, B. *J. Neurochem.* **1986**, *47*, 1634-1641.
- (23) Greenamyre, J. T. *Arch. Neurol.* **1986**, *43*, 1058-1063.
- (24) Rietz, B.; Guilbault, G. G. *Anal. Chim. Acta* **1975**, *77*, 191-198.
- (25) Amouyal, E.; Homsy, A.; Chambron, J.-C.; Sauvage, J.-P. *J. Chem. Soc., Dalton Trans.* **1990**, 1841-1845.
- (26) Lay, P. A.; Sargeson, A. M.; Taube, H. In *Inorganic Synthesis*; Shreeve J. M., Ed.; John Wiley: New York, 1986; Vol 24; pp. 293-295.
- (27) Wu, Q.; Maskus, M.; Pariente, F.; Tobalina, F.; Fernandez, V. M.; Lorenzo, E.; Abruña, H. D. *Anal. Chem.* **1996**, *68*, 3688-3696.
- (28) Goss, C. A.; Abruña, H. D. *Inorg. Chem.* **1985**, *24*, 4263-4267.
- (29) Popescu, I. C.; Dominguez, E.; Narvaez, A.; Pavlov, V.; Katakis, I. *J. Electroanal. Chem.* **1999**, *464*, 208-214.
- (30) Pavlov, V.; Rincón, O.; Solé, S.; Narváez, A.; Domínguez, E.; Katakis I. Submitted to *Anal. Chem.*
- (31) Smith, E. L.; Austen, B. M.; Blumenthal, M. K.; Nyc, J. F. In *The Enzymes*; Boyer, P. D., Ed.; Academic Press: New York, 1975, volume XI, pp. 359-360.
- (32) Yamamura, A.; Sakaguchi, T.; Murakami, Y.; Yokoyama, K.; Tamiya, E. *Biochem. J.* **1999**, *125*, 760-769.
- (33) O'Flaherty, M.; McMahon, M.; Forde, J.; Mulcahy, P. *Prot. Express. Purif.* **1999**, *16*, 276-297.
- (34) Albery, W. J.; Bartlett, P. N.; Cass, A. E. G.; Sim, K. W. *J. Electroanal. Chem.* **1987**, *218*, 127-134.
- (35) Fahien, L. A.; Strmecki, M. *Arch. Biochem. Biophys.* **1969**, *130*, 468-477.

Table I

| J_{\max}, $\mu\text{A cm}^{-2}$ | RSD, % | Response time, s | K_M, mM | Operational half-life time, h |
|--|---------------|-------------------------|-----------------------------|--------------------------------------|
| 3.5 | 25.0 | 220 | 47 | 0.5 |

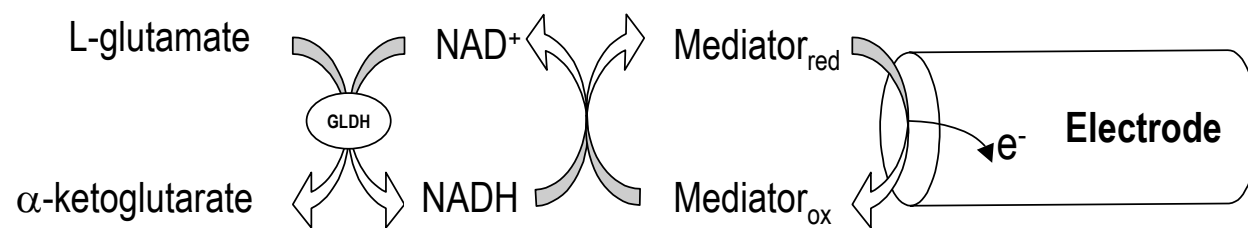


Figure 1

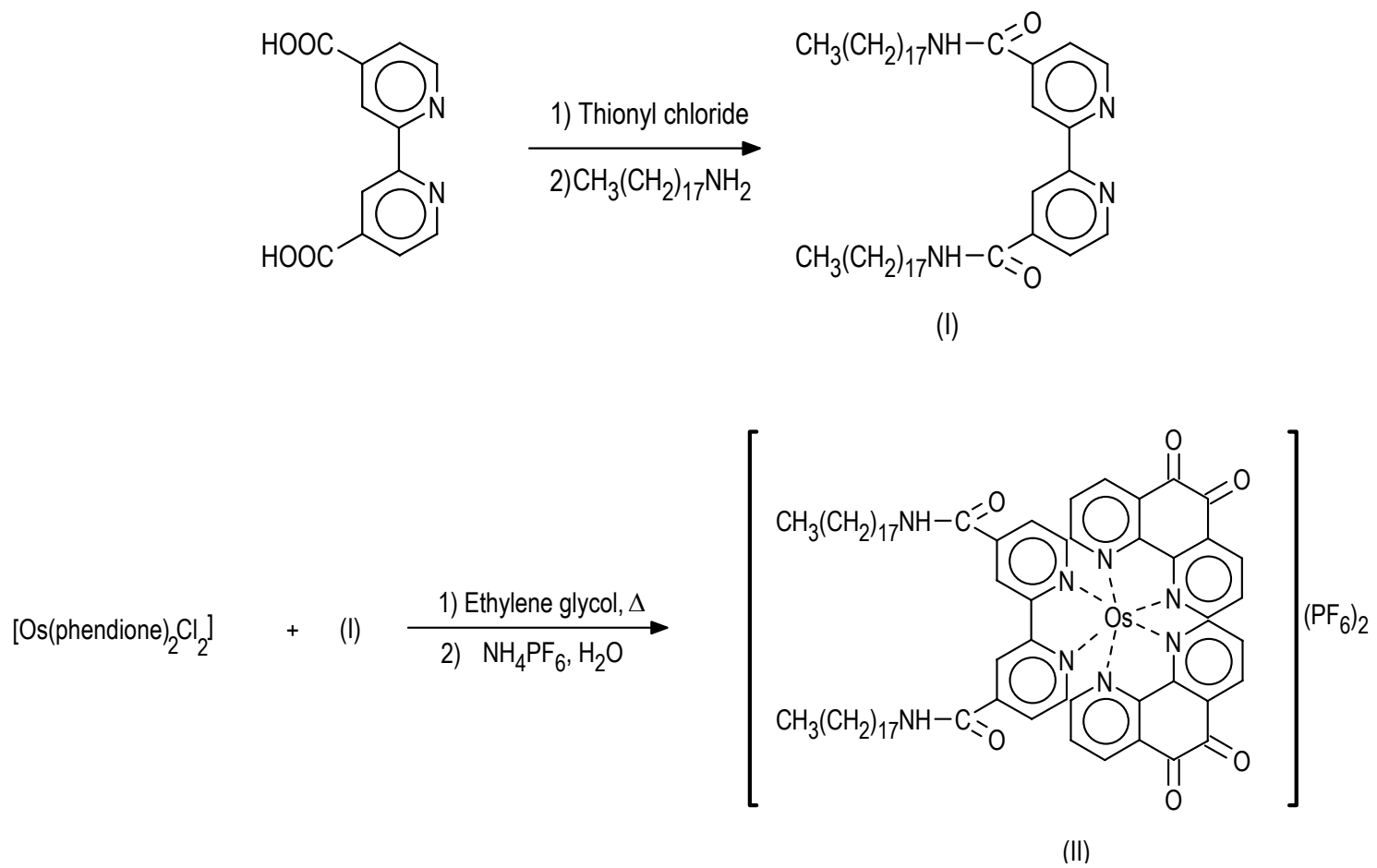


Figure 2

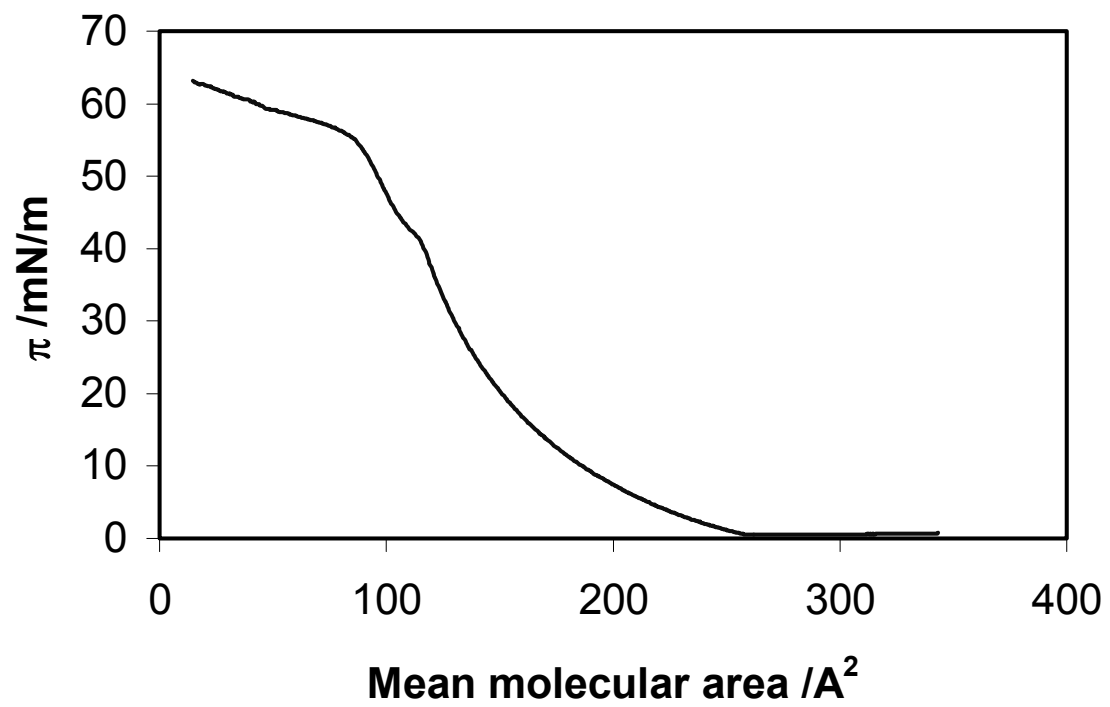


Figure 3

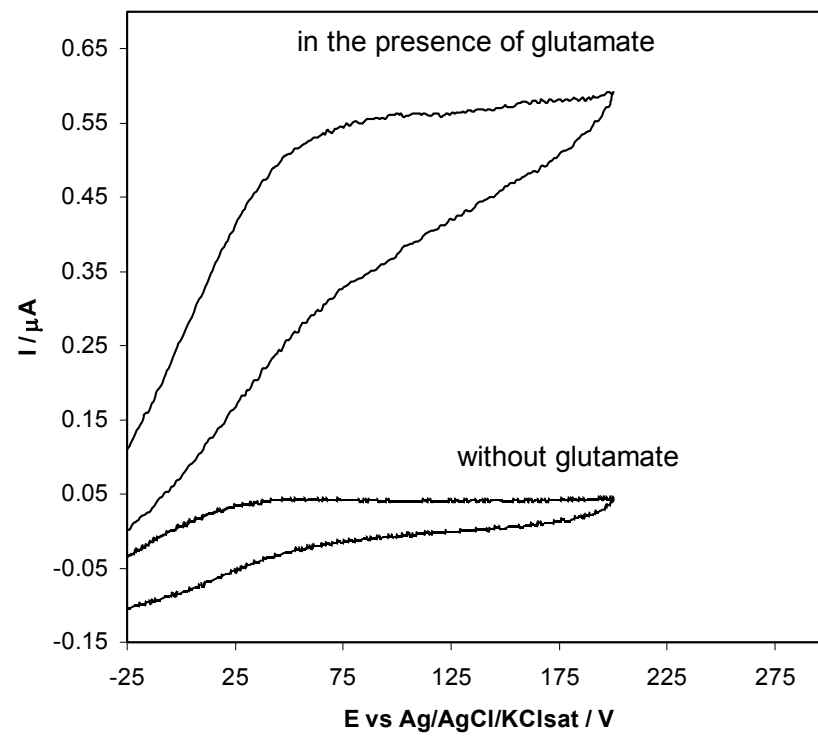


Figure 4

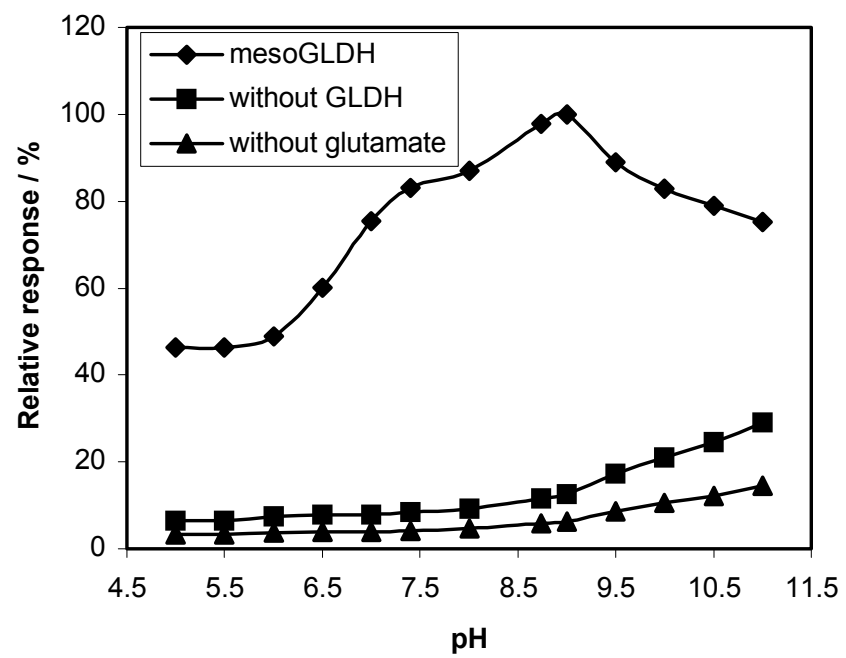


Figure 5

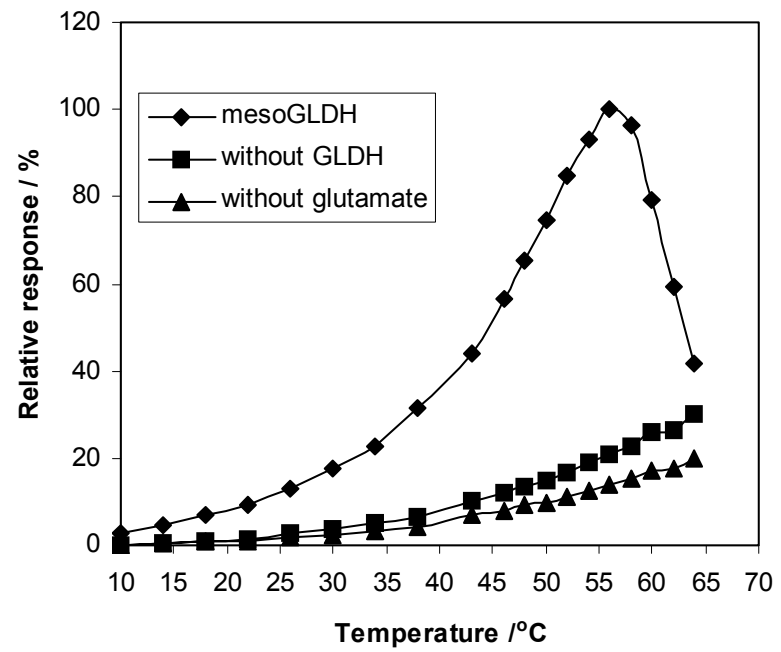


Figure 6

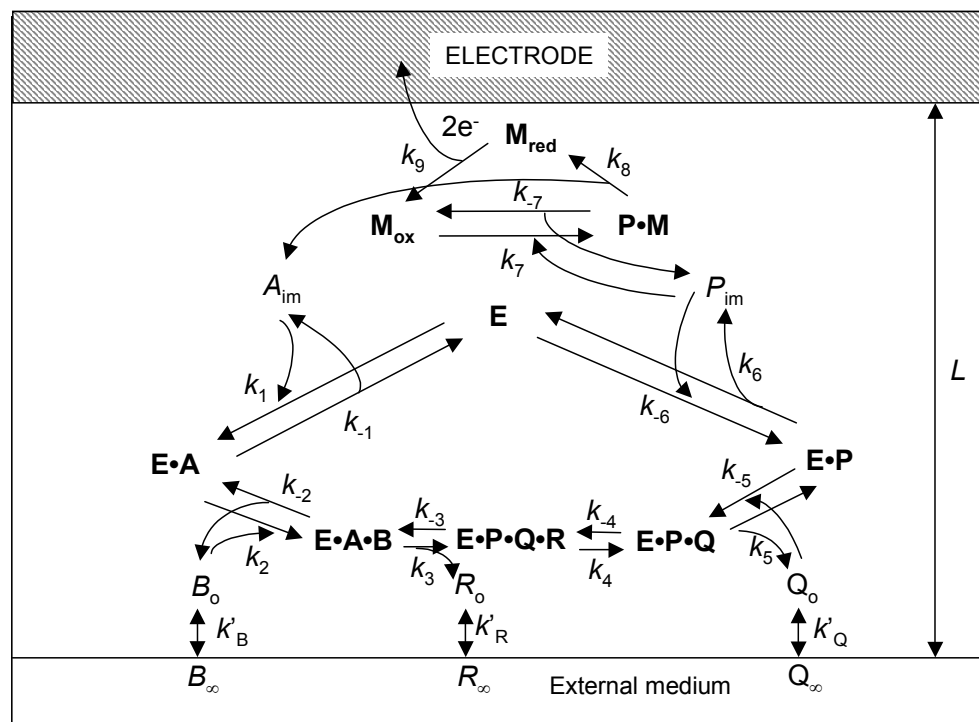


Figure 7

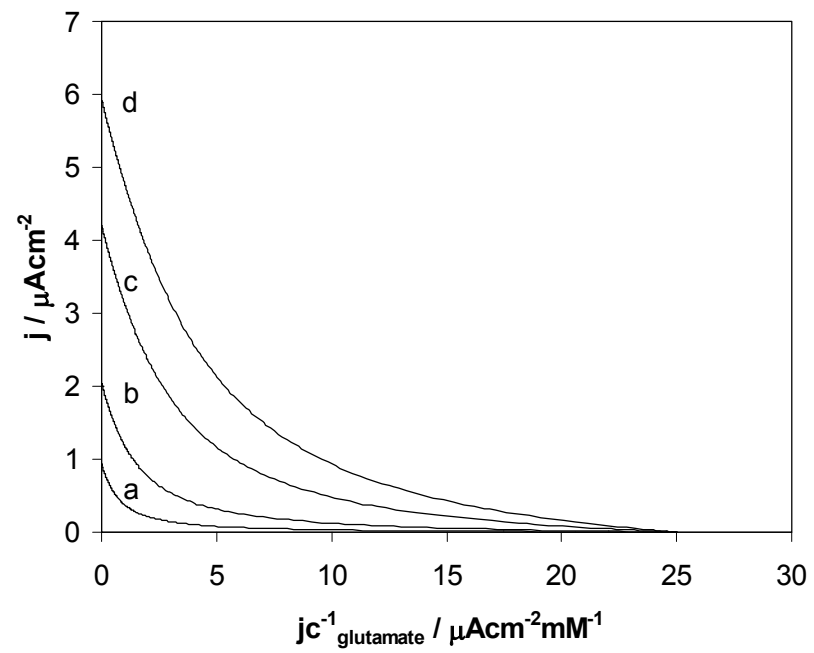
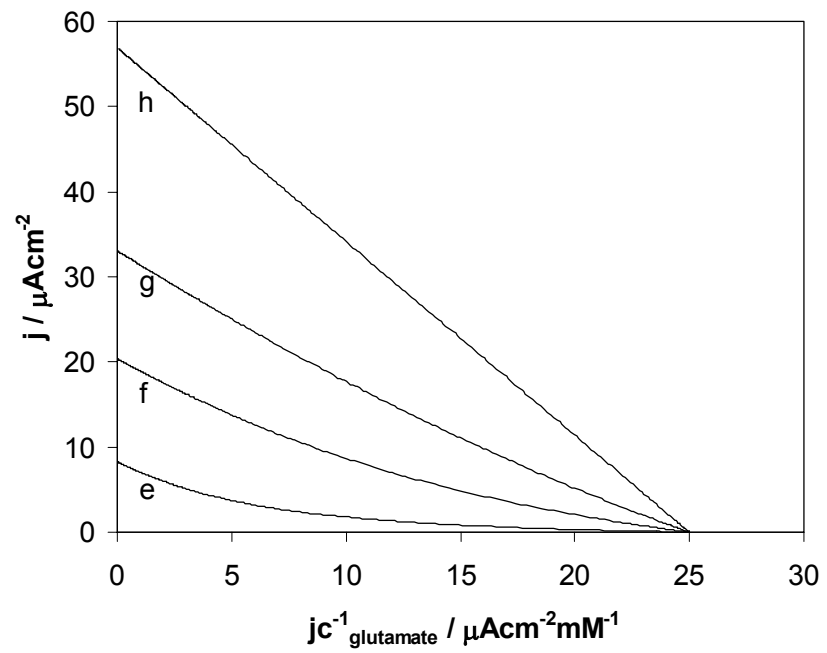


Figure 8

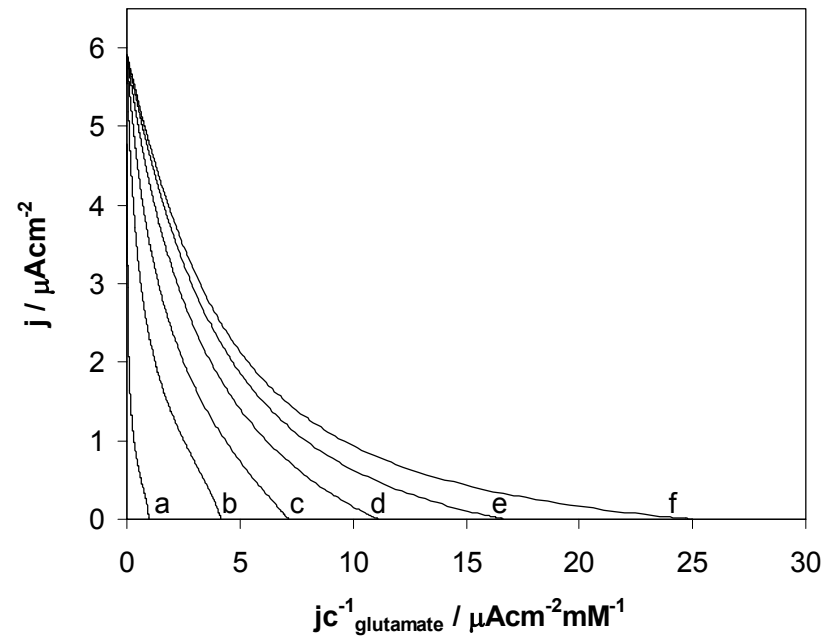


Figure 9

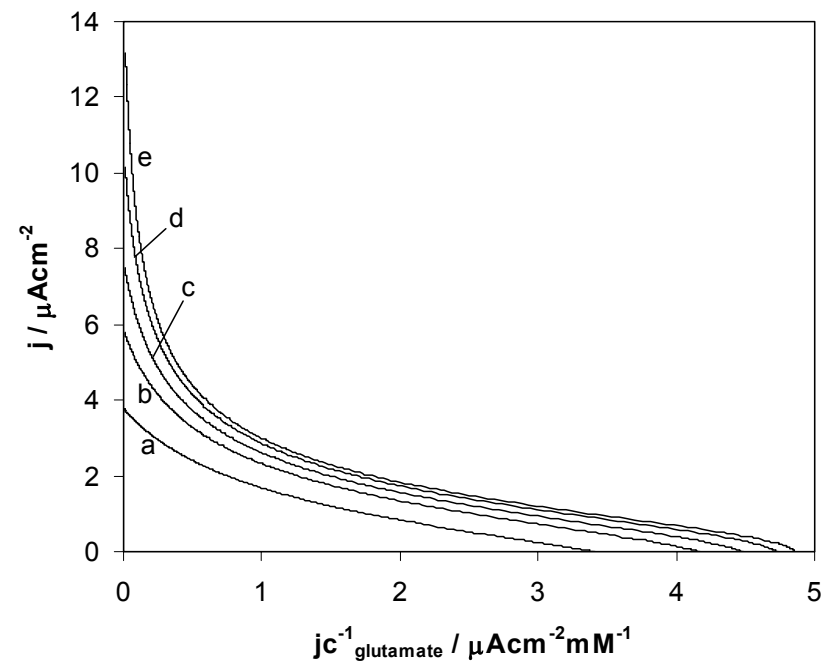
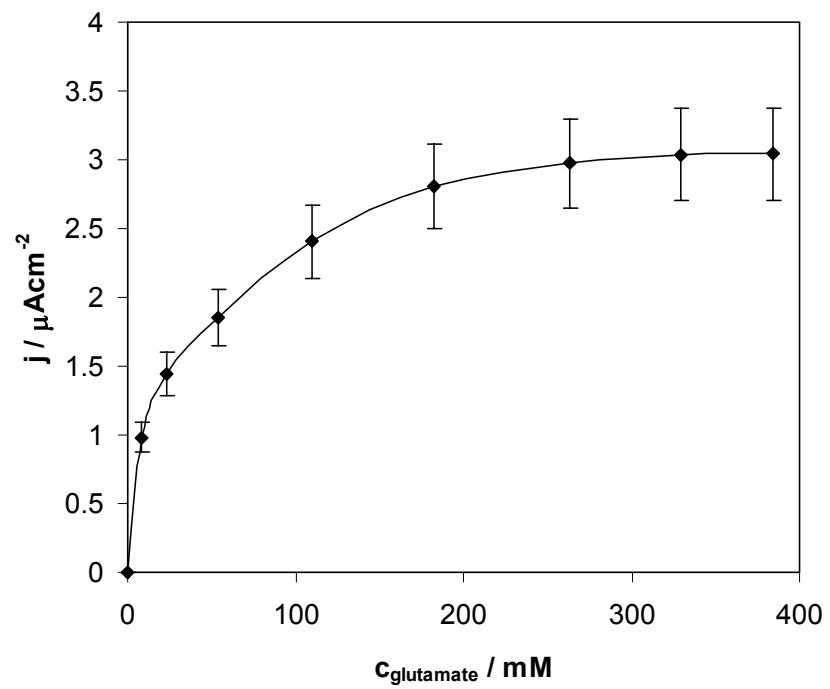
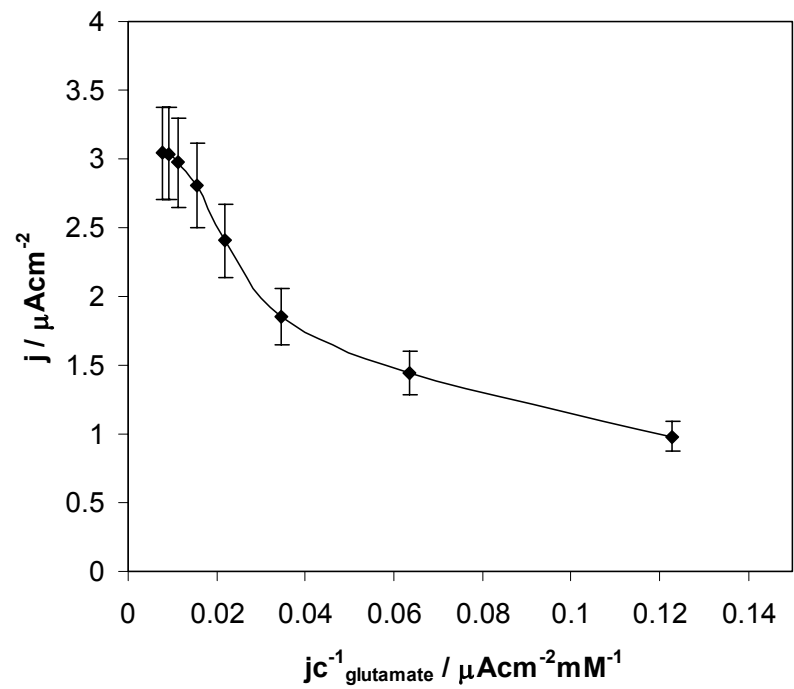


Figure 10



(A)



(B)

Figure 11

Supporting Information

New Reagentless Glutamate Biosensors Based on Mesophilic and Thermophilic Glutamate Dehydrogenases

Valeri Pavlov,¹ Serve Kengen,² Ioanis Katakis^{*1}

¹Bioanalysis and Bioelectrochemistry Group, Chemical Engineering, Universitat Rovira i Virgili, E-43006, Tarragona (Catalonia), Spain. ²Laboratory of Microbiology, Department of Biochemical Science, Wageningen Agricultural University, Hesselink van Suchtelenweg 4, Wageningen NL-6703 CT, Netherlands.

* E-mail: ioanis.katakis@urv.net. Tel: +34 977 55 9655, Fax: +34 977 55 9667.

EXPERIMENTAL SECTION

Materials. Mesophilic GLDH (E.C. 1.4.1.3) from bovine liver, as suspension in saturated ammonium sulfate was purchased from Biozyme (UK), thermophilic GLDH was purified from *Pyrococcus furiosus* as reported elsewhere.²⁹ Nicotinamide adenine nucleotide (NAD⁺), 1,4-dihyronicotinamide adenine dinucleotide (NADH, disodium salt), alginic acid sodium salt, L-glutamic acid monosodium salt were purchased from Sigma (USA). Bromoethylamine hydrobromide, 4,4'-dimethyl-2,2'-bipyridine, sodium dihydrogen phosphate, sodium hydroxide, *ortho*-phosphoric acid, sodium chloride, thionyl chloride, NH₄PF₆, N-(3-dimethylaminopropyl)-N-ethylcarbodiimide hydrochloride were obtained from Aldrich (USA), K₂OsCl₆ - from Alfa (Spain), poly(4-vinylpyridine) (PVP) and poly(ethylene glycol) diglycedyl ether (PEGDGE) were purchased from Polysciences Inc. (USA), chloride form ion exchange beads AG 1-X8 – from BioRad Laboratories (USA). Ethylene glycol and sodium dithionite were obtained from Pancreac (Spain), Gafquat[®] HS100-from ISP Europe, 1,10-phenanthroline-5,6-dione was prepared by the published procedure.³⁴ PVP modified with amino groups was synthesized according to the procedure described elsewhere.³⁵

[Os(4,4'-dimethyl-2,2'-bipyridine)₂Cl₂] and [Os(1,10-phenanthroline-5,6-dione)₂Cl₂] were synthesized according to the adapted method.³⁶ Generally the synthesis procedure involved refluxing of K₂OsCl₆ with 4,4'-dimethyl-2,2'-bipyridine or 1,10-phenanthroline-5,6-dione in DMF under argon in the dark for 1 hr, followed by reduction with aqueous sodium dithionite solution.

Synthesis of [Os(4,4'-dimethyl-2,2'-bipyridine)₂(1,10-phenanthroline-5,6-dione)]Cl₂. The complex [Os(4,4'-dimethyl-2,2'-bipyridine)₂(1,10-phenanthroline-5,6-dione)] was synthesized according to the published procedure,³⁷ precipitated from a NH₄PF₆ saturated aqueous solution, ion exchanged with chloride form ion exchange beads, filtered and dried under vacuum to yield the solid product.

Synthesis of complex of Os(1,10-phenanthroline-5,6-dione)₂ with PVP (Os-phendione-PVP). PVP was dissolved in methanol and recrystallized twice from ether. Next 80 mg of [Os(1,10-phenanthroline-5,6-

dione)₂Cl₂] and 50 mg of PVP were mixed in 3 mL ethylene glycol. The mixture was deaerated with argon during 10 min and refluxed under argon in the dark during 1 h, the temperature of the oil bath being maintained below 220°C, next the reaction mixture was cooled to room temperature and added dropwise to 100 mL of aqueous 1 M sodium chloride solution during 15 min. The resulting mixture was left to stand over night at 4°C, the precipitate was filtered off, washed with water, and air-dried. The synthesis procedure and the structure of resulting Os-phendione-PVP are represented in Figure S-1.

Synthesis of NAD⁺-alginate. Modification of alginic acid with NAD⁺ was performed according to the published method.³⁸ 13.8 mg of sodium alginate and 70 μmol of N-(3-dimethylaminopropyl)-N-ethylcarbodiimide hydrochloride were dissolved in 15 mL of water. The pH was adjusted with aqueous HCl to 4.7 and the solution was stirred for 40 min at room temperature. Next 70 μmol of β-NAD⁺ was added. After readjustment of pH to 4.7 the resulting solution was stirred for 12 h at room temperature. Then the reaction mixture was dialyzed against 1 L of 10 mM Tris buffer (pH 7.0) for 12 h at 4°C and then dialyzed against 1 L of water at 4°C. The dialyate was lyophilized to yield solid NAD⁺-alginate, the structure of which can be seen in Figure S-2.

Preparation of bovine GLDH solution. In order to purify mesophilic bovine GLDH 4 mL of meso GLDH suspension in saturated ammonium sulfate solution were centrifuged during 10 min at 14000 RPM at 5°C. The precipitated enzyme was isolated from the ammonium sulfate solution and dissolved in 3 mL of 0.1 M sodium phosphate buffer (pH 7.4) containing 0.15 M sodium chloride, next the resulting enzyme solution was extensively dialyzed at 5°C against 200 ml of the same buffer during 24 h. The buffer solution was changed every two hours.

Preparation of graphite electrodes. Spectrographic graphite rods of 3 mm in diameter (Carbone of America, USA) were cut into 2 cm pieces, introduced into heat-shrinkable PVC plastic tubes, shrunk by heating, wet polished on fine (grit 400 and 600) emery paper (Buehler, USA) and sonicated in water.

Preparation of reagentless glutamate biosensors based on NAD⁺-alginate. 1 μL of 1.8 mg/mL Os-phendione-PVP solution in ethylene glycol was deposited on a graphite electrode and left to stand for 3 min. The electrodes were washed with ethylene glycol and with water and air-dried.

a. Biosensors based on mesophilic or thermophilic GLDH. A solution containing 24 mg/mL (24 U/mL at 30°C) bovine GLDH or 1.8 mg/mL (0.7 U/mL at 40°C) GLDH from *Pyrococcus furiosus* and 28.6 mg/mL NAD⁺-alginate in 0.1 M sodium phosphate buffer (pH 7.4) was prepared and 4 μL of the resulting mixture was placed on a Os-phendione-PVP modified electrode and dried during 1 h.

Preparation of reagentless glutamate biosensors based on crosslinked hydrogel.

a. Biosensors based on mesophilic GLDH. A solution containing 5.28 mg/mL (36 U/mL at 30°C) bovine GLDH, and 34 mg/mL NAD⁺, 8.6 mg/mL “binder” polymer, and 1 mg/mL PEGDGE in 0.1 M sodium phosphate buffer (pH 7.4) was prepared and 4 μL of the resulting mixture was placed on a Os-phendione-PVP modified electrode and dried under vacuum during 24 h.

b. Biosensors based on thermophilic GLDH. A solution containing 3.24 mg/mL (1.2 U/mL at 40°C) bovine GLDH, and 34 mg/mL NAD⁺, 8.6 mg/mL “binder” polymer, and 1 mg/mL PEGDGE in 0.1 M sodium phosphate buffer (pH 7.4) was prepared and 4 μL of the resulting mixture was placed on a Os-phendione-PVP modified electrode and dried under vacuum during 24 h.

Preparation of glutamate biosensors for the shelf-life stability study. Disposable screen printed electrodes, shown in Figure S-3, with a working electrode area of 1 mm² (KREJCI Engineering, Tisnov, Czech Republic) were employed in the shelf life study in which a number of glutamate sensors was constructed in the following way. A solution containing 5.5 U/mL thermophilic or mesophilic GLDH, 5 mM [Os(dimethylbipyridine)₂(phendione)]Cl₂, and 127 mg/mL NAD⁺ in 0.1 M Tris buffer (pH 7.4) was prepared and 0.5 μL of the mixture were deposited on a screen printed electrode and air-dried during 5 min.

Study of glutamate biosensors in a bulk solution. A three-electrode conventional thermostabilised cell (3 mL) equipped with an Ag/AgCl/KCl_{sat} reference electrode, a platinum auxiliary electrode, and a graphite electrode modified according to one of the above-mentioned methods as a working electrode. The buffer, pH 7.4 (0.1 M sodium phosphate containing 0.15 M sodium chloride) served as supporting electrolyte. The response to successive additions of stock glutamate solution was registered as steady state current on a three-electrode potentiostat Autolab PGSTAT 10 (Eco chemie, Holland) controlled by a computer. The working potential was 150 mV vs. Ag/AgCl/KCl_{sat} and the temperature of the thoroughly stirred solution was 30° or 40°C.

Shelf-life study of glutamate biosensors. Disposable glutamate biosensors were connected to the potentiostat Autolab PGSTAT 10 in the following way: the carbon electrode was connected to the working lead and Ag/AgCl reference electrode to the reference and auxiliary leads, next the biosensor was fixed during 5 min on a glass heat exchanger thermostabilized at 40°C. In order to determine the response of the sensor 0.5 μL of a sample solution was deposited and after 20 s a potential of 200 mV vs. Ag/AgCl electrode was applied to the working electrode. The current after 30 s (starting from the moment of applying the potential) was recorded for every electrode. Between three and five sensors were used for measurements at every point. All sensors were assayed by depositing three different samples: 0.1 M Tris buffer, pH 7.4 (containing 0.15 M NaCl), or 0.6 M glutamate solution in this buffer, or 0.6 M glutamate solution with 0.18 M NAD⁺ in the buffer.

GLDH assay method. Both mesophilic and thermophilic GLDH were tested spectrophotometrically by following the increase in absorbance at 340 nm at 30°C or 40°C. The assay solution contained 5 mM NAD⁺ and 10 mM in 0.1 M sodium phosphate buffer (pH 7.4). The ΔA₃₄₀ (Au/min) was obtained using the maximum linear rate for both the test and blank (without enzyme) mixtures. The activity was calculated using ε_{NADH} = 6.22 mM⁻¹cm⁻¹ extinction coefficient of β-NADH. One unit of GLDH oxidizes 1 μmol of L-glutamate per minute at pH 7.4 at 30 or 40°C. Protein concentration was determined spectrophotometrically at A₂₈₀ using an absorbance coefficient of 0.973 cm²/mg.

Electrochemical conversion experiment. To determine the amount of enzymatically active NAD⁺ produced, during the bulk electrolysis, by the oxidation of NADH at the surface of graphite electrode modified with NADH oxidizing polymer Os-phendione-PVP the electrochemical conversion experiment has been carried out in argon-saturated solution as follows. A graphite electrode (6 mm in diameter) was produced by the above-mentioned method and 4 μl of 1.8 mg/ml Os-phendione-PVP solution in ethylene glycol were deposited on its surface and left for 3 min. The electrode was washed with ethylene glycol and water. Then it was inserted into 2 ml of 18.97 μM NADH solution in 0.1 M phosphate buffer containing 0.15 M sodium chloride (pH 7.4) and poised at 150 mV vs. Ag/AgCl/KCl_{sat} in a three electrode electrochemical cell at room temperature. NADH absorbance at 340

nm was followed during 7 h until it had declined to 10% of the initial value to give the resulting solution, which was used as a coenzyme for glutamate dehydrogenase. The rate of NADH reduction was monitored by change in A_{340} till the constant value. The values of A_{340} were compared with those for controlled NADH solution which had been saturated with argon without electrolysis during the time of the conversion experiment to take into account the spontaneous hydrolysis of NADH.

STEADY-STATE KINETIC MODEL OF BIOSENSORS

Figure S-4 illustrates the kinetic scheme for the operation of reagentless biosensors based on glutamate dehydrogenase enzyme (E) catalyzing the reaction of immobilized NAD^+ (A) with a L-glutamate (B) to give immobilized NADH (P), α -ketoglutarate (Q), and NH_4^+ (R). The mediator (M), which can stay in reduced (M_{red}) and oxidized (M_{ox}) forms, immobilized on the electrode surface catalyzes the electrochemical conversion of P back to A. A_{im} and P_{im} are the concentrations of immobilized A and P. B_0 , Q_0 , R_0 are the concentrations of the substrate and the products in the hydrogel. B_∞ , Q_∞ and R_∞ are the concentrations of the substrate and the products in the external medium. k'_B , k'_Q and k'_R are mass transfer constants of the substrate and the products (cm s^{-1}), respectively. L is the thickness of the hydrogel layer. The following expressions for the flux of P_{im} to the electrode surface (j_{el}), which determines the current density of a biosensor (j) through the equation $j = nFj_{\text{el}}$, where n is the number of exchanged electrons and F is the Faraday's constant (96487 C/mol), can be obtained.

$$j_{\text{el}} = k'_B(B_\infty - B_0) \quad (\text{S-1})$$

$$j_{\text{el}} = L(k_1 A_{\text{im}}[E] - k_{-1}[E \cdot A]) \quad (\text{S-2})$$

$$j_{\text{el}} = L(k_2 B_0[E \cdot A] - k_{-2}[E \cdot A \cdot B]) \quad (\text{S-3})$$

$$j_{\text{el}} = L(k_3[E \cdot A \cdot B] - k_{-3}[E \cdot P \cdot Q \cdot R]) \quad (\text{S-4})$$

$$j_{\text{el}} = L(k_4[E \cdot P \cdot Q \cdot R] - k_{-4}[E \cdot P \cdot Q]Q_0) \quad (\text{S-5})$$

$$j_{\text{el}} = L(k_5[E \cdot P \cdot Q] - k_{-5}[E \cdot P]Q_0) \quad (\text{S-6})$$

$$j_{\text{el}} = L(k_6[E \cdot P] - k_{-6}[E]P_{\text{im}}) \quad (\text{S-7})$$

$$j_{\text{el}} = k'_Q Q_0 \quad (\text{S-8})$$

$$j_{\text{el}} = k'_R R_0 \quad (\text{S-9})$$

$$j_{\text{el}} = k_7 P_0 \Gamma_{\text{Mox}} - k_{-7} \Gamma_{\text{M-P}} \quad (\text{S-10})$$

$$j_{\text{el}} = k_8 \Gamma_{\text{M-P}} \quad (\text{S-11})$$

$$j_{\text{el}} = k_5 \Gamma_{\text{Mred}} \quad (\text{S-12})$$

$$E_t = [E] + [E \cdot A] + [E \cdot A \cdot B] + [E \cdot P \cdot Q \cdot R] + [E \cdot P \cdot Q] + [E \cdot P] \quad (\text{S-13})$$

$$\Gamma = \Gamma_{\text{M-P}} + \Gamma_{\text{Mox}} + \Gamma_{\text{Mred}} \quad (\text{S-14})$$

$$A_t = A_{\text{im}} + P_{\text{im}} \quad (\text{S-15})$$

Where Γ_{Mox} and Γ_{Mred} are surface coverages of the mediator in oxidized and reduced forms, respectively. Γ is the total mediator surface coverage. $\Gamma_{\text{M-P}}$ is the surface coverage of the intermediate complex between the mediator and NADH. A_t and E_t are the total concentrations of NAD^+ and the enzyme immobilized in the hydrogel, respectively. k_1, k_2, \dots, k_6 are the rate constants of the elemental enzymatic reactions in forward direction. $k_{-1}, k_{-2}, \dots, k_{-6}$ are the rate constants of the elemental enzymatic reactions in backward direction. k_7 is the rate constant of the reaction between NADH oxidizing mediator and NADH, k_{-7} is the rate constant of the decomposition of the mediator-NADH complex into NADH and the oxidized mediator, k_8 is the rate constant of

the decomposition of mediator-NADH complex into the reduced mediator and NAD⁺. k_s the the heterogeneous electron transfer rate constant. The equations (S-2 - S7, S-13) yield the equation (S-16) describing the enzyme kinetics

$$j_{el} = \frac{E_1 L(k_1 k_2 k_3 k_4 k_5 k_6 A_{im} B_0 - k_{-1} k_{-2} k_{-3} k_{-4} k_{-5} k_{-6} P_{im} Q_0 R_0)}{k_5 k_6 k_{-1} k_{-2} k_{-3} + k_4 k_5 k_6 k_{-1} k_{-2} + k_{-1} k_3 k_4 k_5 k_6 + (k_1 k_5 k_6 k_{-2} k_{-3} + k_1 k_4 k_5 k_6 k_{-2} + k_1 k_3 k_4 k_5 k_6) A_{im} + k_2 k_3 k_4 k_5 k_6 B_0 + (k_1 k_2 k_5 k_6 k_{-3} + k_1 k_2 k_4 k_5 k_6 + k_1 k_2 k_3 k_5 k_6 + k_1 k_2 k_3 k_4 k_6 + k_1 k_2 k_3 k_4 k_5) A_{im} B_0 + (k_5 k_{-1} k_{-2} k_{-3} k_{-6} + k_4 k_5 k_{-1} k_{-2} k_{-6} + k_3 k_4 k_5 k_{-1} k_{-6}) P_{im} + k_6 k_{-1} k_{-2} k_{-3} k_{-4} R_0 + k_{-1} k_{-2} k_{-3} k_{-4} k_{-5} R_0 Q_0 + (k_{-1} k_{-2} k_{-3} k_{-5} k_{-6} + k_4 k_{-1} k_{-2} k_{-5} k_{-6} + k_3 k_4 k_{-1} k_{-5} k_{-6}) P_{im} Q_0 + (k_{-2} k_{-3} k_{-4} k_{-5} k_{-6} + k_{-1} k_{-3} k_{-4} k_{-5} k_{-6} + k_{-1} k_{-2} k_{-4} k_{-5} k_{-6} + k_3 k_{-1} k_{-4} k_{-5} k_{-6}) P_{im} Q_0 R_0 + k_{-1} k_{-2} k_{-3} k_{-4} k_{-6} P_{im} R_0 + k_2 k_3 k_4 k_5 k_{-6} B_0 P_{im} + k_2 k_3 k_4 k_{-5} k_{-6} B_0 P_{im} Q_0 + k_1 k_2 k_3 k_4 k_{-5} A_{im} B_0 Q_0 + k_1 k_{-2} k_{-3} k_{-4} k_{-5} A_{im} R_0 Q_0 + k_1 k_6 k_{-2} k_{-3} k_{-4} A_{im} R_0 + (k_1 k_2 k_{-3} k_{-4} k_{-5} + k_1 k_2 k_3 k_{-4} k_{-5}) A_{im} B_0 R_0 Q_0 + (k_2 k_{-3} k_{-4} k_{-5} k_{-6} + k_2 k_3 k_{-4} k_{-5} k_{-6}) B_0 R_0 P_{im} Q_0 + (k_1 k_2 k_6 k_{-3} k_{-4} + k_1 k_2 k_3 k_6 k_{-4}) A_{im} B_0 R_0$$

(S-16)

When numerator and denominator of this rate equation are multiplied by the factor $(k_{-1} k_{-2} k_{-3} k_{-4} k_{-5} k_{-6}) / ((k_1 k_2 k_3 k_4 k_5 k_6 k_{-3} + k_1 k_2 k_4 k_5 k_6 + k_1 k_2 k_3 k_5 k_6 + k_1 k_2 k_3 k_4 k_6 + k_1 k_2 k_3 k_4 k_5)(k_{-2} k_{-3} k_{-4} k_{-5} k_{-6} + k_{-1} k_{-3} k_{-4} k_{-5} k_{-6} + k_{-1} k_{-2} k_{-4} k_{-5} k_{-6} + k_3 k_{-1} k_{-4} k_{-5} k_{-6}))$ the equation S-17 can be obtained:

$$j_{el} = \frac{L(V_1 V_2 A_{im} B_0 - (V_1 V_2 P_{im} Q_0 R_0) / K_{eq})}{K_{AB} V_2 + K_B V_2 A_{im} + K_A V_2 B_0 + V_2 A_{im} B_0 + K_{QR} V_1 P_{im} / K_{eq} + K_{PQ} V_1 R_0 / K_{eq} + K_P V_1 Q_0 R_0 / K_{eq} + K_R V_1 P_{im} Q_0 / K_{eq} + V_1 P_{im} Q_0 R_0 / K_{eq} + K_Q V_1 R_0 P_{im} / K_{eq} + K_A V_2 B_0 P_{im} / K_{iP} + K_A V_2 B_0 P_{im} Q_0 / (K_{iQ} K_{iP}) + K_{iR} K_P V_1 A_{im} B_0 Q_0 / (K_{iA} K_{iB} K_{eq}) + K_P V_1 A_{im} R_0 Q_0 / (K_{iA} K_{eq}) + K_{PQ} V_1 A_{im} R_0 / (K_{iA} K_{eq}) + K_P V_1 A_{im} B_0 Q_0 R_0 / (K_{iA} K_{iB} K_{eq}) + K_A V_2 B_0 R_0 P_{im} Q_0 / (K_{iR} K_{iP} K_{iQ}) + K_{PQ} V_1 A_{im} B_0 R_0 / (K_{iA} K_{iB} K_{eq})}$$

(S-17)

Where $V_1 = E_1(k_1 k_2 k_3 k_4 k_5 k_6) / (k_1 k_2 k_3 k_4 k_5 k_6 k_{-3} + k_1 k_2 k_4 k_5 k_6 + k_1 k_2 k_3 k_5 k_6 + k_1 k_2 k_3 k_4 k_6 + k_1 k_2 k_3 k_4 k_5)$ and $V_2 = E_1(k_{-1} k_{-2} k_{-3} k_{-4} k_{-5} k_{-6}) / (k_{-2} k_{-3} k_{-4} k_{-5} k_{-6} + k_{-1} k_{-3} k_{-4} k_{-5} k_{-6} + k_{-1} k_{-2} k_{-4} k_{-5} k_{-6} + k_3 k_{-1} k_{-4} k_{-5} k_{-6})$ are the maximum velocities in forward and reverse directions, the equilibrium constant $K_{eq} = k_1 k_2 k_3 k_4 k_5 k_6 / (k_{-1} k_{-2} k_{-3} k_{-4} k_{-5} k_{-6})$, the Michaelis constants for A, B, P, Q, R are $K_A = (k_2 k_3 k_4 k_5 k_6) / (k_1 k_2 k_5 k_6 k_{-3} + k_1 k_2 k_4 k_5 k_6 + k_1 k_2 k_3 k_5 k_6 + k_1 k_2 k_3 k_4 k_6 + k_1 k_2 k_3 k_4 k_5)$, $K_B = (k_1 k_5 k_6 k_{-2} k_{-3} + k_1 k_4 k_5 k_6 k_{-2} + k_1 k_3 k_4 k_5 k_6) / (k_1 k_2 k_5 k_6 k_{-3} + k_1 k_2 k_4 k_5 k_6 + k_1 k_2 k_3 k_5 k_6 + k_1 k_2 k_3 k_4 k_6 + k_1 k_2 k_3 k_4 k_5)$, $K_{AB} = (k_5 k_6 k_{-1} k_{-2} k_{-3} + k_4 k_5 k_6 k_{-1} k_{-2} + k_{-1} k_3 k_4 k_5 k_6) / (k_1 k_2 k_5 k_6 k_{-3} + k_1 k_2 k_4 k_5 k_6 + k_1 k_2 k_3 k_5 k_6 + k_1 k_2 k_3 k_4 k_6 + k_1 k_2 k_3 k_4 k_5)$, $K_P = k_{-1} k_{-2} k_{-3} k_{-4} k_{-5} / (k_{-2} k_{-3} k_{-4} k_{-5} k_{-6} + k_{-1} k_{-3} k_{-4} k_{-5} k_{-6} + k_{-1} k_{-2} k_{-4} k_{-5} k_{-6} + k_3 k_{-1} k_{-4} k_{-5} k_{-6})$, $K_Q = k_{-1} k_{-2} k_{-3} k_{-4} k_{-6} / (k_{-2} k_{-3} k_{-4} k_{-5} k_{-6} + k_{-1} k_{-3} k_{-4} k_{-5} k_{-6} + k_{-1} k_{-2} k_{-4} k_{-5} k_{-6} + k_3 k_{-1} k_{-4} k_{-5} k_{-6})$, $K_R = (k_{-1} k_{-2} k_{-3} k_{-5} k_{-6} + k_4 k_{-1} k_{-2} k_{-5} k_{-6} + k_3 k_4 k_{-1} k_{-5} k_{-6}) / (k_{-2} k_{-3} k_{-4} k_{-5} k_{-6} + k_{-1} k_{-3} k_{-4} k_{-5} k_{-6} + k_{-1} k_{-2} k_{-4} k_{-5} k_{-6} + k_3 k_{-1} k_{-4} k_{-5} k_{-6})$, $K_{QR} = (k_5 k_{-1} k_{-2} k_{-3} k_{-6} + k_4 k_5 k_{-1} k_{-2} k_{-6} + k_3 k_4 k_5 k_{-1} k_{-6}) / (k_{-2} k_{-3} k_{-4} k_{-5} k_{-6} + k_{-1} k_{-3} k_{-4} k_{-5} k_{-6} + k_{-1} k_{-2} k_{-4} k_{-5} k_{-6} + k_3 k_{-1} k_{-4} k_{-5} k_{-6})$, $K_{PQ} = k_6 k_{-1} k_{-2} k_{-3} k_{-4} / (k_{-2} k_{-3} k_{-4} k_{-5} k_{-6} + k_{-1} k_{-3} k_{-4} k_{-5} k_{-6} + k_{-1} k_{-2} k_{-4} k_{-5} k_{-6} + k_3 k_{-1} k_{-4} k_{-5} k_{-6})$.

The inhibition constants for A, B, P, Q, R are $K_{iA} = k_{-1} / k_1$, $K_{iB} = (k_2 k_3) / (k_2 (k_3 + k_3))$, $K_{iP} = k_6 / k_{-6}$, $K_{iQ} = k_5 / k_{-5}$, $K_{iR} = (k_3 k_4) / (k_4 (k_3 + k_3))$. Using the inhibition constants allows to redefine: $K_{PQ} = K_{iP} K_Q$ and $K_{QR} = K_{iQ} K_R$.

After division of the numerator and the denominator in the equation S-17 by V_2 and substitution of $V_1/(V_2K_{eq})$ with $(K_B K_{iA})/(K_{iQ} K_{iP} K_R)$ one can obtain the equation:

$$j_{el} = \frac{L(V_1 A_{im} B_o - (V_1 P_{im} Q_o R_o)/K_{eq})}{K_{AB} + K_B A_{im} + K_A B_o + A_{im} B_o + K_{QR} K_{iA} K_B P_{im}/(K_{iP} K_{iQ} K_R) + K_{PQ} K_{iA} K_B R_o/(K_{iP} K_{iQ} K_R) + K_P K_{iA} K_B Q_o R_o/(K_{iP} K_{iQ} K_R) + K_R K_{iA} K_B P_{im} Q_o/(K_{iP} K_{iQ} K_R) + K_{iA} K_B P_{im} Q_o R_o/(K_{iP} K_{iQ} K_R) + K_P K_{iA} K_B R_o P_{im}/(K_{iP} K_{iQ} K_R) + K_A B_o P_{im}/K_{iP} + K_A B_o P_{im} Q_o/(K_{iQ} K_{iP}) + K_{iR} K_P K_B A_{im} B_o Q_o/(K_{iB} K_{iP} K_{iQ} K_R) + K_P K_B A_{im} R_o Q_o/(K_{iP} K_{iQ} K_R) + K_{PQ} K_B A_{im} R_o/(K_{iP} K_{iQ} K_R) + K_P K_B A_{im} B_o Q_o R_o/(K_{iB} K_{iP} K_{iQ} K_R) + K_A B_o R_o P_{im} Q_o/(K_{iR} K_{iP} K_{iQ}) + K_{PQ} K_B A_{im} B_o R_o/(K_{iB} K_{iP} K_{iQ} K_R)}$$

(S-18)

The equations (S-10 – S-12, S-14) give the equation (S-19) which governs the kinetics of NADH oxidation at the electrode surface modified with a mediator

$$j_{el} = \frac{\Gamma k_7 k_8 k_S P_o}{k_8 k_S + k_7 k_S + (k_7 k_8 + k_7 k_S) P_{im}} = \frac{\Gamma P_{im} k_7 k_8 k_S / (k_7 k_8 + k_7 k_S)}{(k_8 k_S + k_7 k_S) / (k_7 k_8 + k_7 k_S) + P_{im}} = \frac{k_{cat} \Gamma P_{im}}{k_M + P_{im}}$$

(S-19)

where the Michaelis constant for the mediator M is $k_M = (k_8 k_S + k_7 k_S) / (k_7 k_8 + k_7 k_S)$ and $k_{cat} = k_8 k_S / (k_8 + k_S)$. Using the equations (S-15) and (S-19) the concentrations of NAD^+ and NADH (A_{im} and P_{im}) as well as B_o , Q_o and R_o from (S-1), (S-8) and (S-9) can be found: $P_{im} = j_{el} K_M / (k_{cat} \Gamma_M - j_{el})$, $A_{im} = A_t - P_{im} = A_t - j_{el} K_M / (k_{cat} \Gamma_M - j_{el})$, $B_o = B_\infty - j_{el} / k'_B$, $Q_o = j_{el} / k'_Q$, $R_o = j_{el} / k'_R$. Substitution of A_{im} , B_o , P_{im} , Q_o , R_o into the equation (S-18) with their expressions gives the following equation of the fourth order:

$$LV_1 \Gamma k_{cat} E A_t B_\infty = j_{el} [K_{AB} \Gamma k_{cat} + K_B \Gamma k_{cat} A_t + K_A \Gamma k_{cat} B_\infty + A_t \Gamma k_{cat} B_\infty + LV_1 (A_t + K_M) B_\infty + (LV_1 A_t \Gamma k_{cat}) / k'_B] + j_{el}^2 [(K_{PQ} K_B A_t \Gamma k_{cat}) / (K_{iP} K_{iQ} K_R k'_R) - LV_1 (A_t + K_M) / k'_B - K_{AB} - K_B (A_t + K_M) - K_A B_\infty + K_M K_{QR} K_{iA} K_B / (K_{iP} K_{iQ} K_R) - (A_t + K_M) B_\infty - A_t \Gamma k_{cat} / k'_B + \Gamma k_{cat} K_{PQ} K_{iA} K_B R_o / (K_{iP} K_{iQ} K_R k'_R) + K_A K_M B_\infty / K_{iP} + K_{iR} K_P K_B A_t B_\infty \Gamma k_{cat} / (K_{iB} K_{iP} K_{iQ} K_R k'_Q) + K_{PQ} K_B A_t B_\infty \Gamma k_{cat} / (K_{iB} K_{iP} K_{iQ} k'_R)] + j_{el}^3 [LV_1 K_M / (K_{eq} k'_Q k'_R) + K_A / k'_B + (A_t + K_M) / k'_B - K_{PQ} K_{iA} K_B / (K_{iP} K_{iQ} K_R k'_R) + \Gamma k_{cat} K_P K_{iA} K_B / (K_{iP} K_{iQ} K_R k'_Q k'_R) + K_M K_R K_{iA} K_B / (K_{iP} K_{iQ} K_R k'_Q) + K_M K_P K_{iA} K_B / (K_{iP} K_{iQ} K_R k'_R) - K_A K_M / (K_{iP} k'_B) + K_A K_M B_\infty / (K_{iQ} K_{iP} k'_Q) - K_{iR} K_P K_B (A_t + K_M) B_\infty / (K_{iB} K_{iP} K_{iQ} K_R k'_Q) - K_{iR} K_P K_B A_t \Gamma k_{cat} / (K_{iB} K_{iP} K_{iQ} K_R k'_B k'_Q) + K_P K_B A_t \Gamma k_{cat} / (K_{iP} K_{iQ} K_R k'_Q k'_R) - K_{PQ} K_B (A_t + K_M) / (K_{iP} K_{iQ} K_R k'_R) + K_P K_B A_t B_\infty \Gamma k_{cat} / (K_{iB} K_{iP} K_{iQ} K_R k'_Q k'_R) - K_{PQ} K_B B_\infty (A_t + K_M) / (K_{iB} K_{iP} K_{iQ} K_R k'_R) - A_t \Gamma k_{cat} K_{PQ} K_B / (K_{iB} K_{iP} K_{iQ} K_R k'_B k'_R)] + j_{el}^4 [K_{iA} K_B K_M / (K_{iP} K_{iQ} K_R k'_Q k'_R) - K_P K_{iA} K_B / (K_{iP} K_{iQ} K_R k'_Q k'_R) - K_A K_M / (K_{iQ} K_{iP} k'_B k'_Q) + K_{iR} K_P K_B (A_t + K_M) / (K_{iB} K_{iP} K_{iQ} K_R k'_B k'_Q) - K_P K_B (A_t + K_M) / (K_{iP} K_{iQ} K_R k'_Q k'_R) - K_P K_B B_\infty / (K_{iB} K_{iP} K_{iQ} K_R k'_Q k'_R) - K_P K_B A_t \Gamma k_{cat} / (K_{iB} K_{iP} K_{iQ} K_R k'_B k'_Q k'_R) + K_A B_\infty K_M / (K_{iR} K_{iP} K_{iQ} k'_Q k'_R) + K_{PQ} K_B (A_t + K_M) / (K_{iB} K_{iP} K_{iQ} K_R k'_B k'_R)] + j_{el}^5 [K_P K_B (A_t + K_M) / (K_{iB} K_{iP} K_{iQ} K_R k'_B k'_Q k'_R) - K_A K_M / (K_{iR} K_{iP} K_{iQ} k'_B k'_Q k'_R)]$$

(S-20)

The equation S-20 was employed to simulate the response curves and Eadie-Hofstee plots for the reagentless glutamate biosensors using the values of the Michaelis constants and inhibition constants from the literature.⁵³ Figure S-5 shows the effect of NAD^+ loading on the response to glutamate of biosensors which are not limited neither by Os-phendione-PVP loading nor by the mass transport. The Eadie-Hofstee plots show straight lines which are characteristic for the process of enzymatic oxidation of glutamate limited only the concentration of NAD^+ . At saturating NAD^+ loading the values of the apparent maximum current density and the apparent

Michaelis constant coincide with those of the product LV_1nF and the Michaelis constant (K_B) respectively. The decrease in the NAD^+ loading results in the decrease in the values of slopes and intercepts of Eadie-Hofstee plots with the axis of j , which are the apparent Michaelis constants for the substrate B and the maximum current densities respectively.

Figure S-6 demonstrates the effect of the rate of mass transport of the substrate and reaction products on the response of glutamate electrodes. The simulation of the response to glutamate was performed using saturating loading of NAD^+ ($A_t \rightarrow \infty$) and the infinitively high maximum flux of the electrochemical oxidation of NADH ($\Gamma k_{\text{cat}} \rightarrow \infty$). The decrease in the mass transfer constants results in more convex shape of the Eadie-Hofstee plots leading to the decrease in the values of intercepts of the Eadie-Hofstee plots with the axis of j i.e. the apparent maximum current densities become lower due to the accumulation of the reaction products Q and R in the hydrogel leading to the inhibition of the reaction of glutamate oxidation. The values of apparent maximum current densities coincide with the value of LV_1nF only when the rate of mass transport is infinitively high resulting in infinitively low steady state concentrations of reaction products Q and R in the hydrogel. This means that the convex Eadie-Hofstee plots are diagnostic for the glutamate electrodes limited by rate of mass transfer.

The effect of the value of the maximum flux of the electrochemical oxidation of NADH (Γk_{cat}) on the simulated response of reagentless glutamate biosensors (at $A_t = 1$ mM) is demonstrated in Figure S-7. The Eadie-Hofstee plots give the straight line characteristic for the process limited by the enzymatic reduction of NAD^+ only when Γk_{cat} is infinitively high. The decrease in the value of Γk_{cat} leads to the decrease in the values of intercepts of the Eadie-Hofstee plots with the axis of j and their slopes i.e. the apparent maximum current densities and apparent Michaelis constants become lower due to the limitation set by the flux of the electrochemical oxidation of NADH (Table S-I). The decrease in the value of Γk_{cat} also affects the shape of the Eadie-Hofstee plots making them more concave. Hence, the concavity of Eadie-Hofstee plots is diagnostic for reagentless glutamate biosensors limited by the rate of electrochemical NADH oxidation at the electrode surface.

Figure S-8 represents the effect of mass transport rate on the response of biosensors limited by the rate of the electrochemical NADH oxidation. The decrease in the mass transfer constants leads to the drastic increase in the slope of the Eadie-Hofstee plots, making the apparent Michaelis constants (measured using high concentrations of glutamate) even higher than K_B of free GLDH (Table S-II). It can be concluded that the concave Eadie-Hofstee plots, giving the values of the apparent Michaelis constant higher than the value of K_M of the free enzyme, are diagnostic for reagentless glutamate biosensors limited by the rate of electrochemical NADH oxidation at the electrode surface and by the rate of mass transport.

The effect of the maximum flux of the enzymatic reduction of NAD^+ (LV_1) rate on the response of biosensors limited by the rate of the electrochemical NADH oxidation and mass transport is demonstrated in Figure S-9. The increase in LV_1 leads to the drastic increase in apparent current densities and the concavity of Eadie-Hofstee plots, making the apparent Michaelis constants higher than K_B of free GLDH (Table S-III).

GLOSSARY

| | |
|--|---|
| A_t | total cofactor concentration in the hydrogel (M) |
| A_{im} | concentration of NAD^+ immobilized in the hydrogel (M) |
| B_o | substrate concentration in the hydrogel (M) |
| B_∞ | substrate concentration in the external medium (M) |
| E_t | total enzyme concentration (M) |
| F | Faraday's constant (96487 C mol^{-1}) |
| GLDH | glutamate dehydrogenase |
| j_{el} | flux of reactants ($\text{mol cm}^{-2} \text{ s}^{-1}$) |
| j | current density (A cm^{-2}) |
| k | rate coefficient of the formal overall chemical reaction of NADH oxidation by the mediator ($\text{M}^{-1} \text{ s}^{-1}$) |
| $k_{[NADH]=0}$ | rate coefficient of the formal overall chemical reaction of NADH oxidation by the mediator extrapolated to zero concentration of NADH ($\text{M}^{-1} \text{ s}^{-1}$) |
| k_s | heterogeneous electron transfer rate constant (s^{-1}) |
| k_7 | rate constant of the reaction between the NADH oxidizing mediator and NADH ($\text{M}^{-1} \text{ s}^{-1}$) |
| k_{-7} | rate constant of the decomposition of the mediator-NADH complex into NADH and the oxidized mediator (s^{-1}) |
| k_8 | the rate constant of the decomposition of mediator-NADH complex into the reduced mediator and NAD^+ (s^{-1}) |
| $k_1, k_2, k_3, k_4, k_5, k_6$ | rate constants of the elemental enzymatic reactions in forward direction ($\text{M}^{-1} \text{ s}^{-1}, \text{M}^{-1} \text{ s}^{-1}, \text{s}^{-1}, \text{s}^{-1}, \text{s}^{-1}, \text{s}^{-1}$ respectively) |
| $k_{-1}, k_{-2}, k_{-3}, k_{-4}, k_{-5}, k_{-6}$ | rate constants of the elemental enzymatic reactions in reverse direction ($\text{s}^{-1}, \text{s}^{-1}, \text{s}^{-1}, \text{s}^{-1}, \text{M}^{-1} \text{ s}^{-1}, \text{M}^{-1} \text{ s}^{-1}$ respectively) |
| k'_B | mass transfer rate coefficient for the substrate B (cm s^{-1}) |
| k'_Q | mass transfer rate coefficient for the product Q (cm s^{-1}) |
| k'_R | mass transfer rate coefficient for the product R (cm s^{-1}) |
| K_M | Michaelis constant of Os-phendione-PVP (M) |
| L | thickness of the hydrogel layer (cm) |
| n | number of exchanged electrons |
| P_{im} | concentration of NADH immobilized in the hydrogel (M) |
| PVP | poly(4-vinyl pyridine) |
| phendione | 1,10-phenanthroline-5,6-dione |
| R_∞ | concentration of product R in the external medium (M) |

| | |
|------------|--|
| R_0 | concentration of product R in the hydrogel (M) |
| V_1 | maximum velocity of the enzymatic reaction in forward direction (s^{-1}) |
| V_2 | maximum velocity of the enzymatic reaction in reverse direction (s^{-1}) |
| Q_∞ | concentration of product Q in the external medium (M) |
| Q_0 | concentration of product Q in the hydrogel (M) |

Greek letters

| | |
|----------------------------------|---|
| Γ | total surface coverage of Os-phendione-PVP (mol cm^{-2}) |
| Γ_{Mox} | surface coverage of the mediator in the oxidized form (mol cm^{-2}) |
| Γ_{Mred} | surface coverage of the mediator in the reduced form (mol cm^{-2}) |
| $\Gamma_{\text{M}\cdot\text{P}}$ | surface coverage of the intermediate complex between Os-phendione-PVP and NADH (mol cm^{-2}) |
| ω | rotation speed (rad s^{-1}) |

TABLES AND TABLE LEGENDS

Table S-I. Effect of maximum flux of the electrochemical NADH oxidation on apparent Michaelis constants and maximum current densities given by simulated Eadie-Hofstee plots in the range of high glutamate concentrations. The values of parameters used in the simulation are the same as in Figure S-7.

| | | | | | | | | |
|--|-----------------------|------------------------|------------------------|-----------------------|----------------------|----------------------|-----------------------|----------|
| $\Gamma k_{\text{cat}},$ $\text{mol s}^{-1} \text{cm}^{-2}$ | 2.6×10^{-11} | 1.04×10^{-10} | 4.15×10^{-10} | 8.3×10^{-10} | 1.7×10^{-9} | 1.3×10^{-8} | 5.18×10^{-8} | ∞ |
| $j_{\text{max app}},$ $\mu\text{A cm}^{-2}$ | 0.927 | 2.055 | 4.195 | 5.923 | 8.270 | 20.37 | 33.06 | 56.91 |
| $K_{\text{B app}},$ mM | 0.89 | 1.18 | 1.2 | 1.23 | 1.28 | 1.43 | 1.67 | 2.25 |

Table S-II. Effect of mass transfer constants on the apparent Michaelis constants and maximum current densities given by simulated Eadie-Hofstee plots in the range of high glutamate concentrations. The values of parameters used in the simulation are the same as in Figure S-8.

| | | | | | | |
|--|------------------------|------------------------|------------------------|------------------------|-----------------------|----------|
| $k'_{\text{B}}, k'_{\text{Q}}, k'_{\text{R}},$ cm s^{-1} | 5.18×10^{-12} | 2.60×10^{-11} | 5.18×10^{-11} | 1.03×10^{-10} | 2.6×10^{-10} | ∞ |
| $j_{\text{max app}},$ $\mu\text{A cm}^{-2}$ | 5.260 | 5.422 | 5.881 | 5.893 | 5.921 | 5.923 |
| $K_{\text{B app}},$ mM | 99.4 | 8.80 | 3.60 | 1.99 | 1.42 | 1.24 |

Table S-III. Effect of the maximum flux of the enzymatic reduction of NAD^+ (LV_1) on apparent Michaelis constants and maximum current densities given by simulated Eadie-Hofstee plots in the range of high glutamate concentrations. The values of parameters used in the simulation are the same as in Figure S-9.

| | | | | | |
|--|------------------------|------------------------|------------------------|-----------------------|-----------------------|
| $LV_1,$ $\text{Mol s}^{-1} \text{cm}^{-2}$ | 1.55×10^{-10} | 3.63×10^{-10} | 6.22×10^{-10} | 1.24×10^{-9} | 2.49×10^{-9} |
| $j_{\text{max app}},$ $\mu\text{A cm}^{-2}$ | 3.772 | 5.837 | 7.631 | 10.64 | 14.39 |
| $K_{\text{B app}},$ mM | 3.87 | 9.11 | 18.6 | 45.5 | 92.8 |

Table S-IV. Results of shelf life study of glutamate biosensors.

| Composition of enzyme solution used for modification of screen printed electrodes | Half shelf life, h |
|--|--------------------|
| Mesophilic GLDH (11 U/mL) | 7 |
| Thermophilic GLDH (11 U/mL) | 75 |
| Mesophilic GLDH (11 U/mL) with Gafquat [®] HS100 (0.0482 % w/v) | 32 |
| Thermophilic GLDH (11 U/mL) and poly(ethylene imine) (0.24% w/v) | 38 |
| Mesophilic GLDH (11 U/mL) with glycerol (20 % w/v) | 6< |
| Thermophilic GLDH (11 U/mL) with glycerol (20 % w/v) | 6< |
| Mesophilic GLDH (11 U/mL) with Gafquat [®] HS100 (0.0482 % w/v) and glycerol (20 % w/v) | 6< |
| Thermophilic GLDH (11 U/mL) with poly(ethylene imine) (0.24% w/v) and glycerol (20 % w/v) | 6< |
| Thermophilic GLDH (11 U/mL) with Gafquat [®] HS100 (0.946 % w/v) | 246 |
| Thermophilic GLDH (11 U/mL) with trehalose (14 % w/v) | 80 |
| Mesophilic GLDH (11 U/mL) with trehalose (0.85 % w/v) | 8 |

FIGURES AND FIGURE LEGENDS

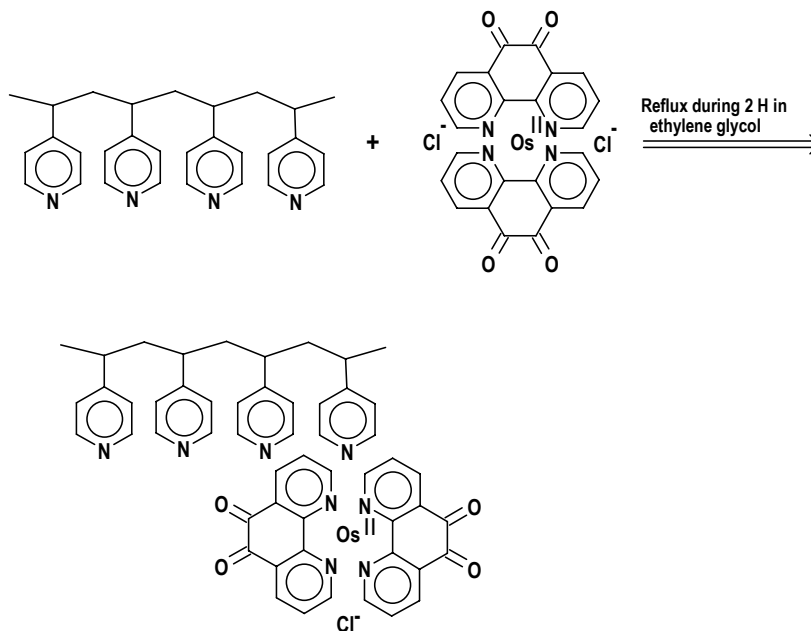


Figure S-1. Synthetic route to NADH oxidizing polymer Os-phendione-PVP.

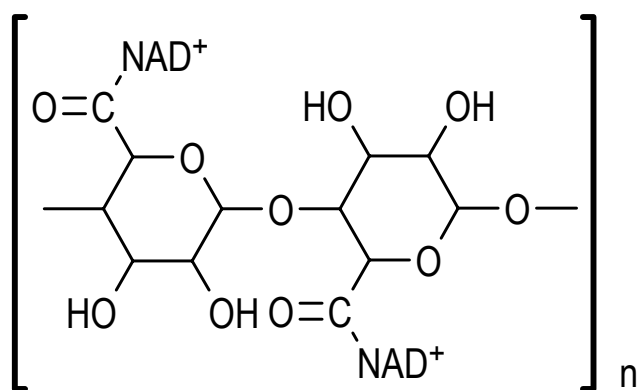


Figure S-2. Structure of NAD⁺-alginate.

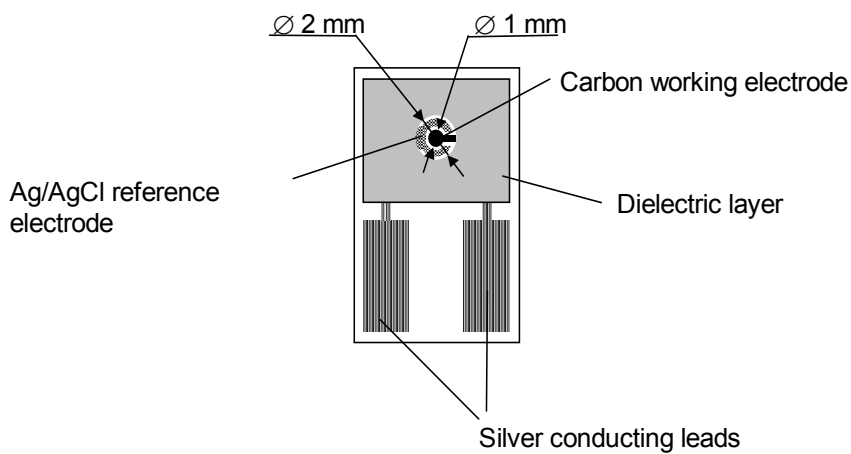


Figure S-3. Sketch of a screen printed disposable electrode utilized in the shelf stability study of glutamate biosensors.

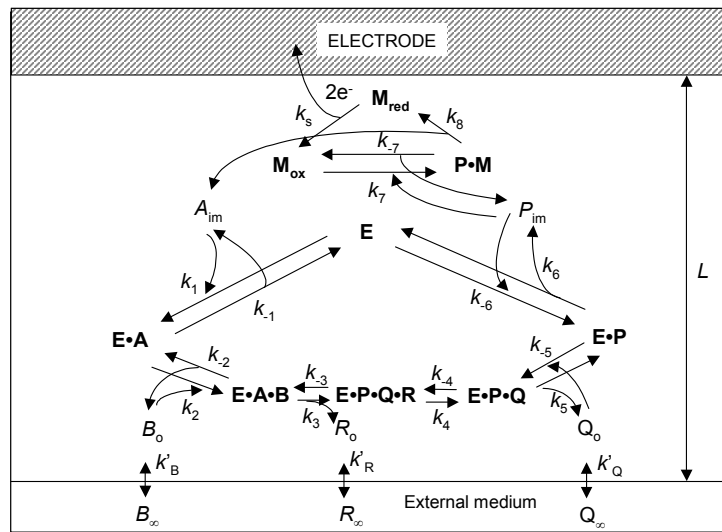
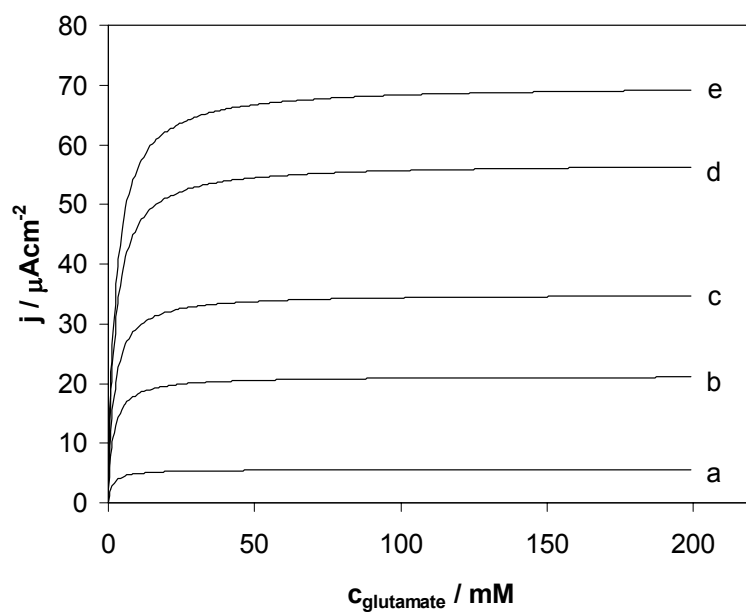
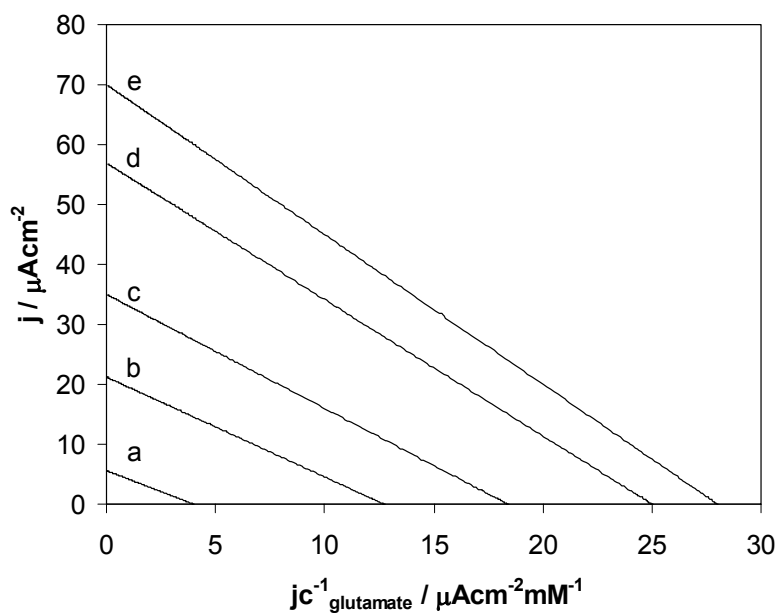


Figure S-4. Reaction scheme for a reagentless glutamate biosensor.

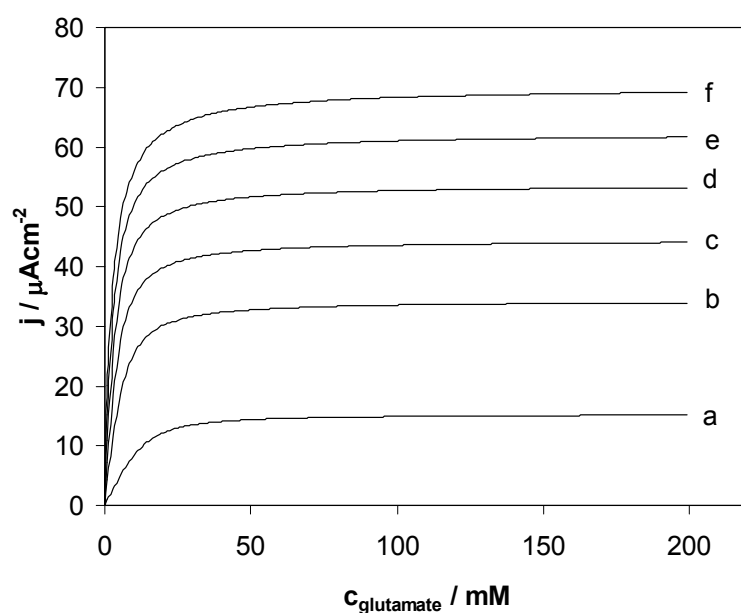


(A)

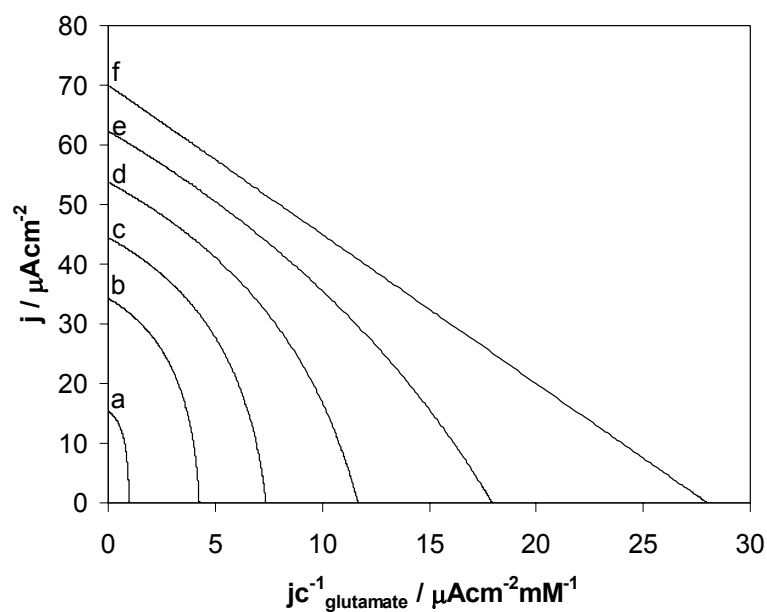


(B)

Figure S-5. Simulation of calibration curves (A) and Eadie-Hofstee plots (B) for the reagentless glutamate biosensors with varying loading of NAD^+ in the hydrogel (A_1): a) 0.02 mM ; b) 0.1 mM; c) 0.23 mM; d) 1 mM; e) ∞ . The values of other parameters are: $\Gamma k_{\text{cat}} \rightarrow \infty$; $k'_{\text{B}} \rightarrow \infty$; $k'_{\text{Q}} \rightarrow \infty$; $k'_{\text{R}} \rightarrow \infty$; $LV_1 = 3.63 \times 10^{-10} \text{ mol s}^{-1} \text{ cm}^{-2}$; $K_{\text{M}} = 0.8 \text{ mM}$; $K_{\text{A}} = 0.23 \text{ mM}$; $K_{\text{B}} = 2.5 \text{ mM}$; $K_{\text{AB}} = 0.3 \text{ mM}^2$; $K_{\text{IA}} = 10 \text{ mM}$; $K_{\text{IB}} = 11 \text{ mM}$; $K_{\text{R}} = 20 \text{ mM}$; $K_{\text{Q}} = 0.25 \text{ mM}$; $K_{\text{P}} = 0.04 \text{ mM}$; $K_{\text{IR}} = 9 \text{ mM}$; $K_{\text{IQ}} = 1.6 \text{ mM}$; $K_{\text{IP}} = 0.03 \text{ mM}$.

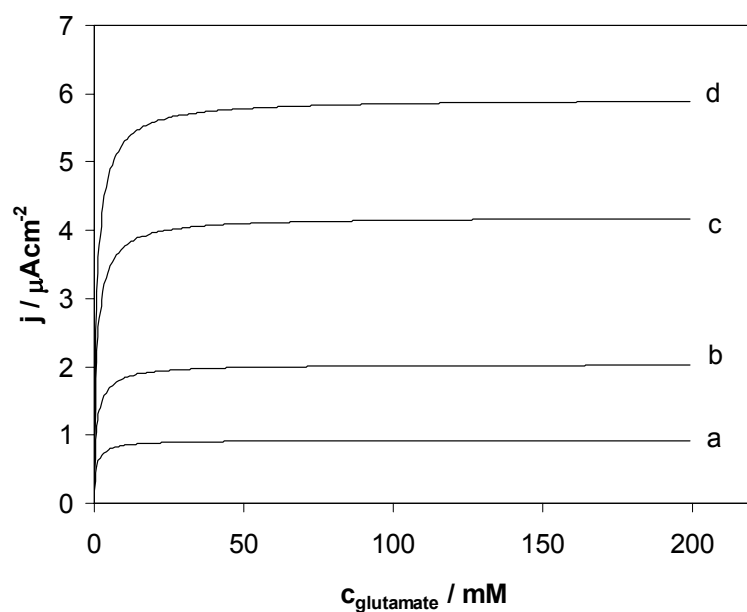


(A)

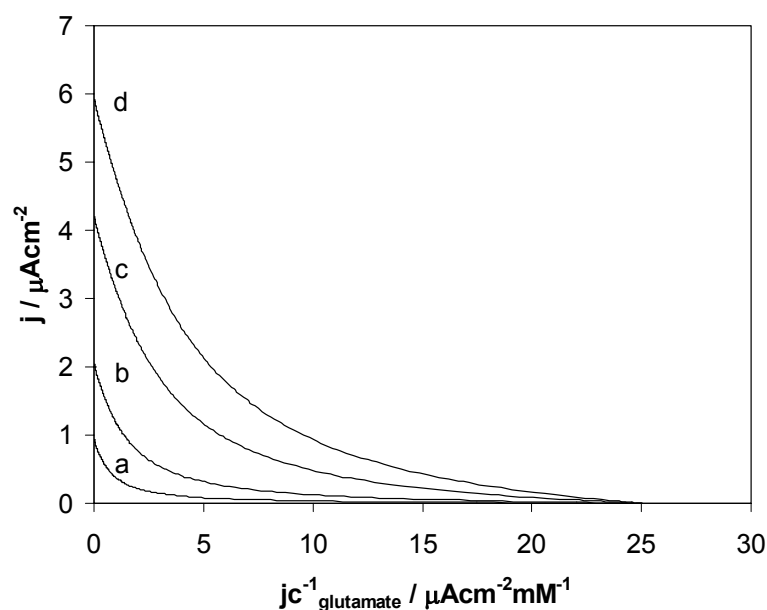


(B)

Figure S-6. Simulation of calibration curves (A) and Eadie-Hofstee plots (B) for the reagentless glutamate biosensors at $\Gamma k_{\text{cat}} \rightarrow \infty$ with varying mass transfer coefficients (k'_B, k'_Q, k'_R): a) $5.18 \times 10^{-12} \text{ cm s}^{-1}$; b) $2.6 \times 10^{-11} \text{ cm s}^{-1}$; c) $5.18 \times 10^{-11} \text{ cm s}^{-1}$; d) $1.03 \times 10^{-10} \text{ cm s}^{-1}$; e) $2.6 \times 10^{-10} \text{ cm s}^{-1}$; f) ∞ . The values of other parameters are: $A_t \rightarrow \infty$; $LV_1 = 3.63 \times 10^{-10} \text{ mol s}^{-1} \text{ cm}^{-2}$; $K_M = 0.8 \text{ mM}$; $K_A = 0.23 \text{ mM}$; $K_B = 2.5 \text{ mM}$; $K_{AB} = 0.3 \text{ mM}^2$; $K_{iA} = 10 \text{ mM}$; $K_{iB} = 11 \text{ mM}$; $K_R = 20 \text{ mM}$; $K_Q = 0.25 \text{ mM}$; $K_P = 0.04 \text{ mM}$; $K_{iR} = 9 \text{ mM}$; $K_{iQ} = 1.6 \text{ mM}$; $K_{iP} = 0.03 \text{ mM}$.

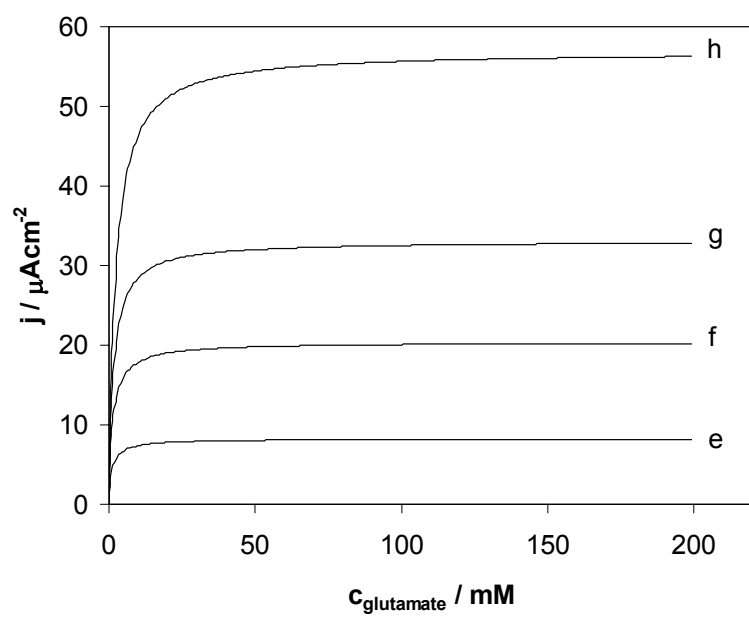


(A)

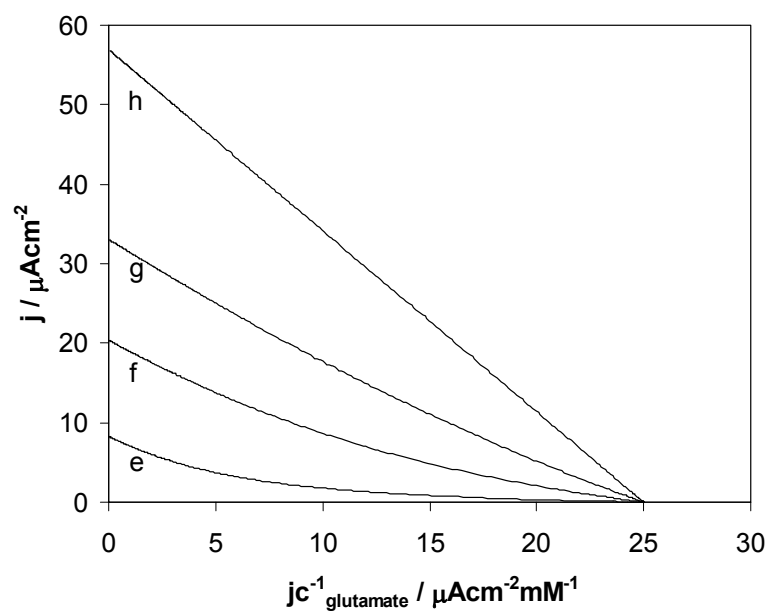


(B)

Figure S-7. Simulation of calibration curves (A) and Eadie-Hofstee plots (B) for the reagentless glutamate biosensors with varying maximum fluxes of the electrochemical NADH oxidation (Γk_{cat}): a) $2.6 \times 10^{-11} \text{ mol s}^{-1} \text{ cm}^{-2}$; b) $1.04 \times 10^{-10} \text{ mol s}^{-1} \text{ cm}^{-2}$; c) $4.15 \times 10^{-10} \text{ mol s}^{-1} \text{ cm}^{-2}$; d) $8.3 \times 10^{-10} \text{ mol s}^{-1} \text{ cm}^{-2}$; e) $1.7 \times 10^{-9} \text{ mol s}^{-1} \text{ cm}^{-2}$; f) $1.3 \times 10^{-8} \text{ mol s}^{-1} \text{ cm}^{-2}$; g) $5.178 \times 10^{-8} \text{ mol s}^{-1} \text{ cm}^{-2}$; h) ∞ . The values of other parameters are: $A_t = 1 \text{ mM}$; $k'_B \rightarrow \infty$; $k'_Q \rightarrow \infty$; $k'_R \rightarrow \infty$; $LV_1 = 3.63 \times 10^{-10} \text{ mol s}^{-1} \text{ cm}^{-2}$; $K_M = 0.8 \text{ mM}$; $K_A = 0.23 \text{ mM}$; $K_B = 2.5 \text{ mM}$; $K_{AB} = 0.3 \text{ mM}^2$; $K_{iA} = 10 \text{ mM}$; $K_{iB} = 11 \text{ mM}$; $K_R = 20 \text{ mM}$; $K_Q = 0.25 \text{ mM}$; $K_P = 0.04 \text{ mM}$; $K_{iR} = 9 \text{ mM}$; $K_{iQ} = 1.6 \text{ mM}$; $K_{iP} = 0.03 \text{ mM}$.

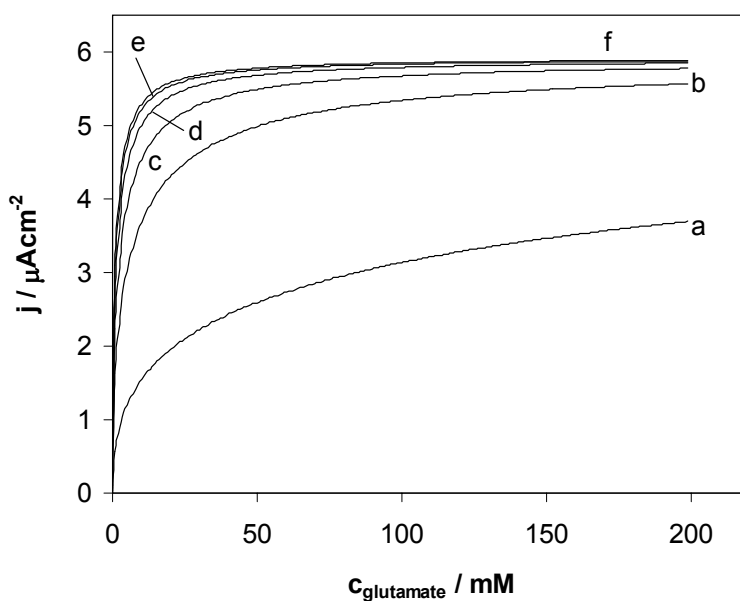


(A)

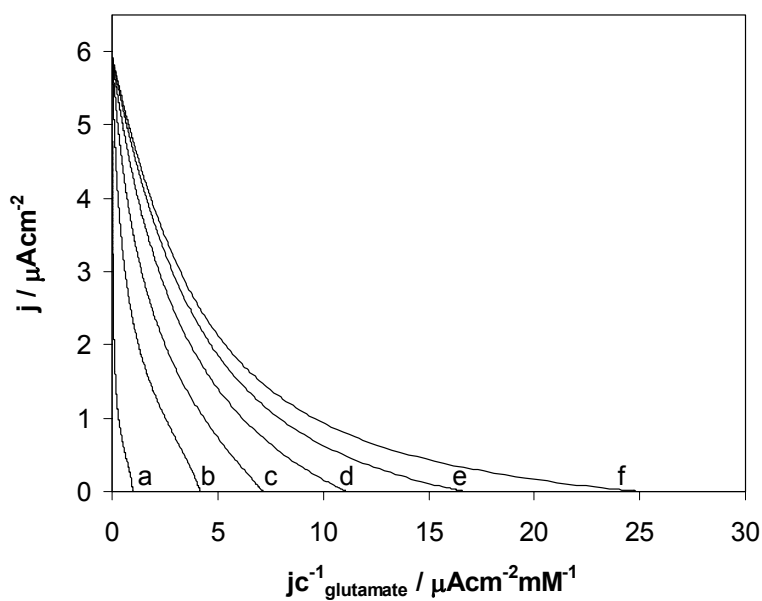


(B)

Figure S-7. (continued)

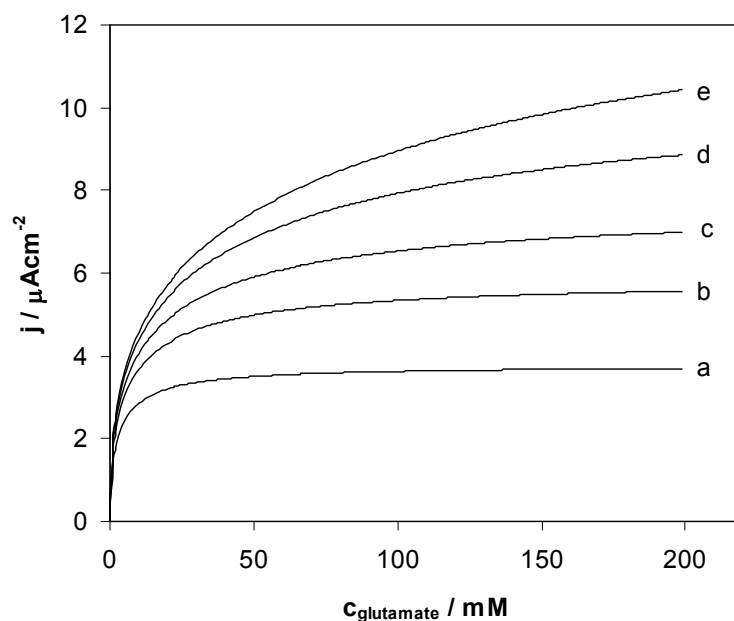


(A)

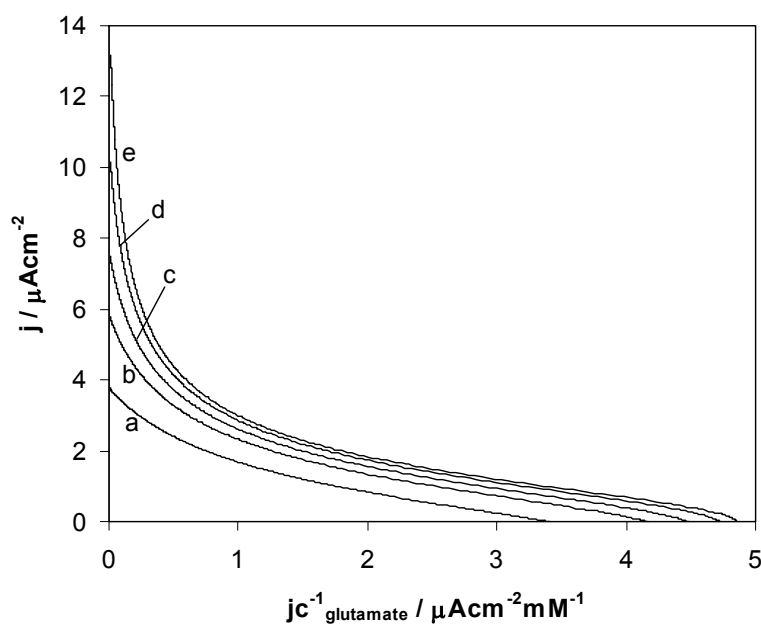


(B)

Figure S-8. Simulation of calibration curves (A) and Eadie-Hofstee plots (B) for the reagentless glutamate biosensors at Γk_{cat} equal to $8.3 \times 10^{-10} \text{ mol s}^{-1} \text{ cm}^{-2}$ with varying mass transfer coefficients (k'_{B} , k'_{Q} , k'_{R}): a) $5.18 \times 10^{-12} \text{ cm s}^{-1}$; b) $2.6 \times 10^{-11} \text{ cm s}^{-1}$; c) $5.18 \times 10^{-11} \text{ cm s}^{-1}$; d) $1.03 \times 10^{-10} \text{ cm s}^{-1}$; e) $2.6 \times 10^{-10} \text{ cm s}^{-1}$; f) ∞ . The values of other parameters are: $A_{\text{t}} = 1 \text{ mM}$; $LV_1 = 3.63 \times 10^{-10} \text{ mol s}^{-1} \text{ cm}^{-2}$; $K_{\text{M}} = 0.8 \text{ mM}$; $K_{\text{A}} = 0.23 \text{ mM}$; $K_{\text{B}} = 2.5 \text{ mM}$; $K_{\text{AB}} = 0.3 \text{ mM}^2$; $K_{\text{iA}} = 10 \text{ mM}$; $K_{\text{iB}} = 11 \text{ mM}$; $K_{\text{R}} = 20 \text{ mM}$; $K_{\text{Q}} = 0.25 \text{ mM}$; $K_{\text{P}} = 0.04 \text{ mM}$; $K_{\text{iR}} = 9 \text{ mM}$; $K_{\text{iQ}} = 1.6 \text{ mM}$; $K_{\text{iP}} = 0.03 \text{ mM}$.

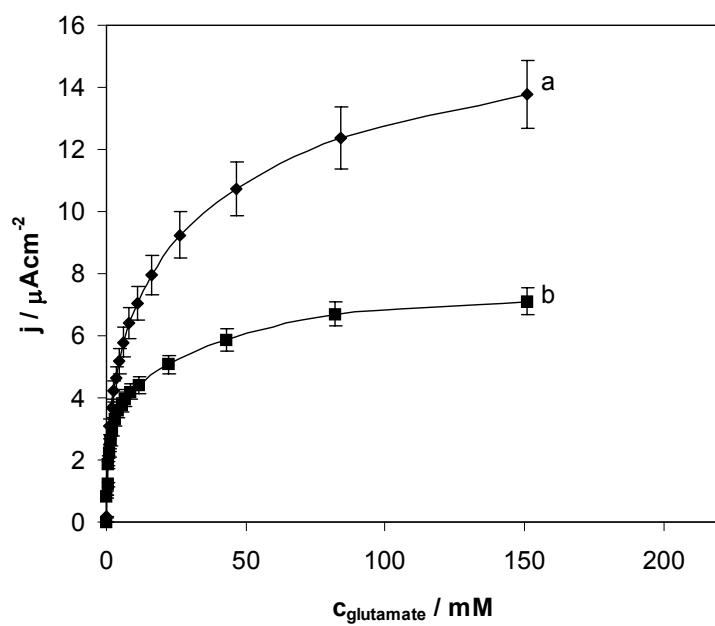


(A)

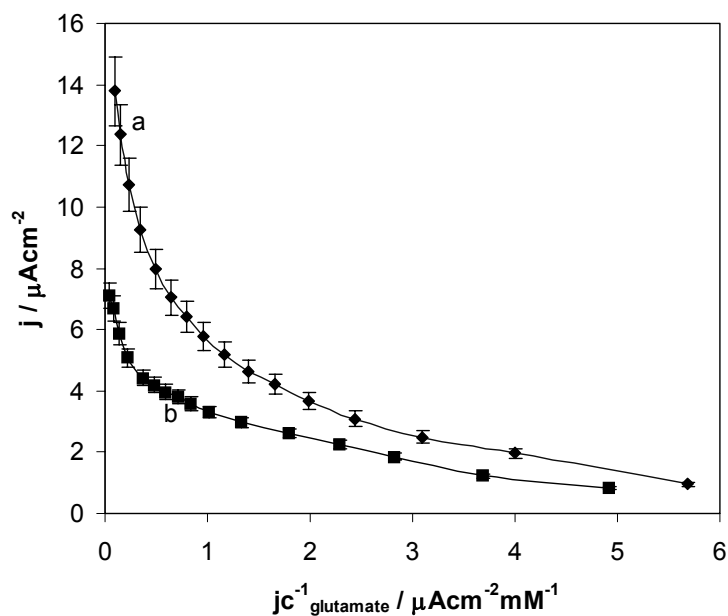


(B)

Figure S-9. Simulation of calibration curves (A) and Eadie-Hofstee plots (B) for the reagentless glutamate biosensors with varying maximum flux of enzymatic reduction of NAD^+ (LV_1): a) $1.55 \times 10^{-10} \text{ mol s}^{-1} \text{ cm}^{-2}$; b) $3.63 \times 10^{-10} \text{ mol s}^{-1} \text{ cm}^{-2}$; c) $6.22 \times 10^{-10} \text{ mol s}^{-1} \text{ cm}^{-2}$; d) $1.24 \times 10^{-9} \text{ mol s}^{-1} \text{ cm}^{-2}$; e) $2.49 \times 10^{-9} \text{ mol s}^{-1} \text{ cm}^{-2}$. The values of other parameters are: $k'_B = 2.6 \times 10^{-11} \text{ cm s}^{-1}$; $k'_Q = 2.6 \times 10^{-11} \text{ cm s}^{-1}$; $k'_R = 2.6 \times 10^{-11} \text{ cm s}^{-1}$; $A_t = 1 \text{ mM}$; $\Gamma k_{\text{cat}} = 8.3 \times 10^{-10} \text{ mol s}^{-1} \text{ cm}^{-2}$; $K_M = 0.8 \text{ mM}$; $K_A = 0.23 \text{ mM}$; $K_B = 2.5 \text{ mM}$; $K_{AB} = 0.3 \text{ mM}^2$; $K_{iA} = 10 \text{ mM}$; $K_{iB} = 11 \text{ mM}$; $K_R = 20 \text{ mM}$; $K_Q = 0.25 \text{ mM}$; $K_P = 0.04 \text{ mM}$; $K_{iR} = 9 \text{ mM}$; $K_{iQ} = 1.6 \text{ mM}$; $K_{iP} = 0.03 \text{ mM}$.

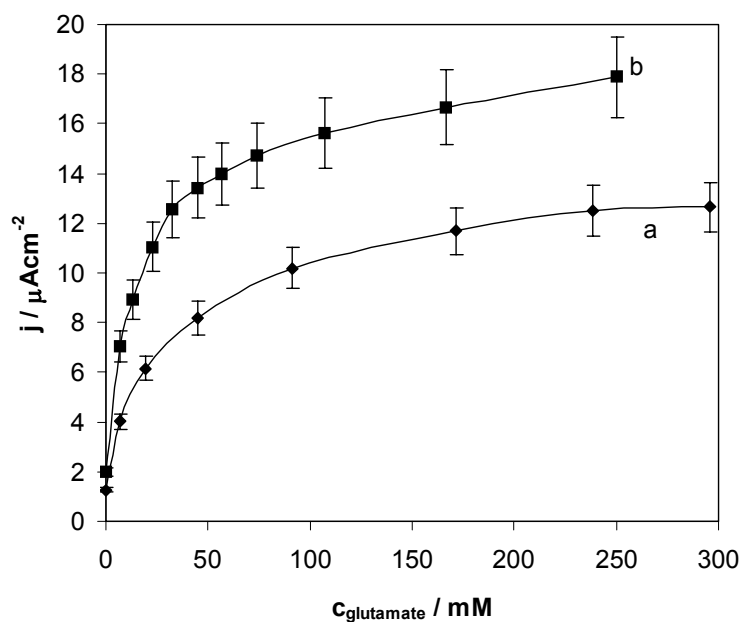


(A)

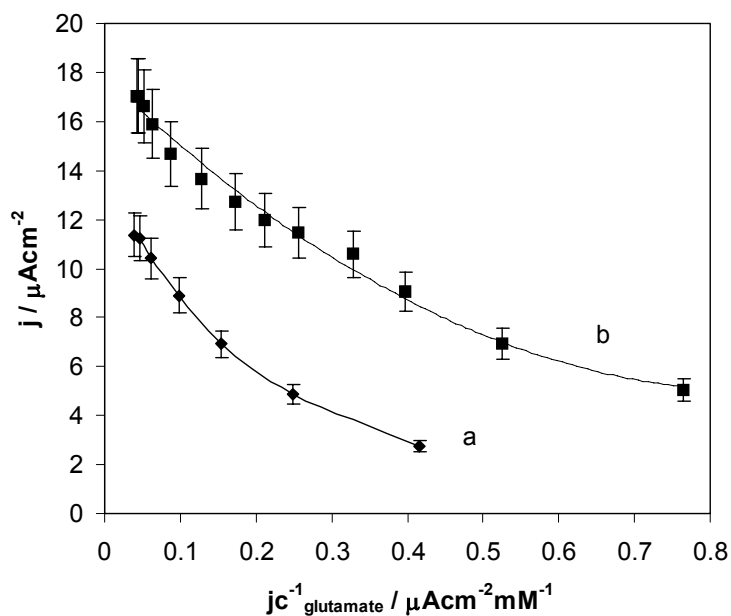


(B)

Figure S-10. Dependence of the apparent current density on L-glutamate concentration **(A)** and Eadie-Hofstee plots **(B)** for reagentless biosensors fabricated with the use of mesophilic GLDH based on: a) NAD^+ -alginate; b) binder polymer. Experimental conditions: E_{app} 150 mV vs. $\text{Ag}/\text{AgCl}/\text{KCl}_{\text{sat}}$, 0.1 M phosphate buffer (pH 7.4), temperature 30°C .

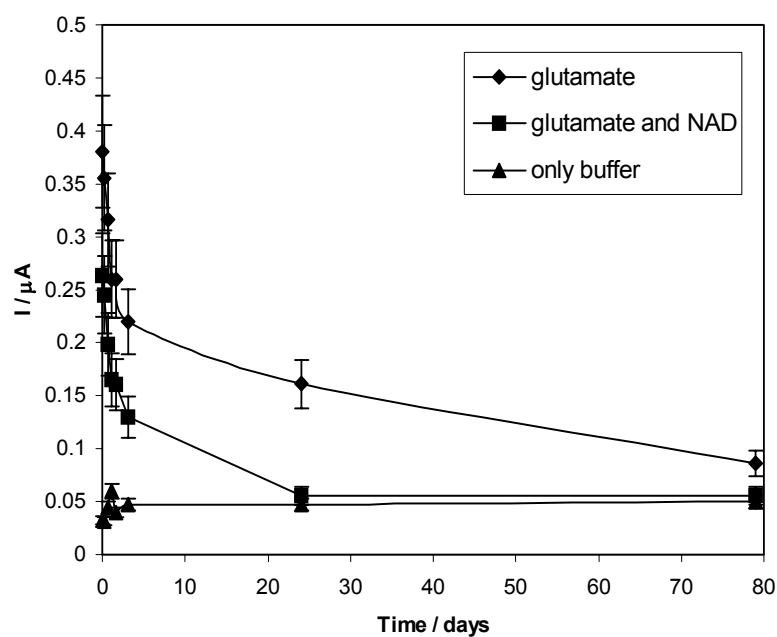


(A)

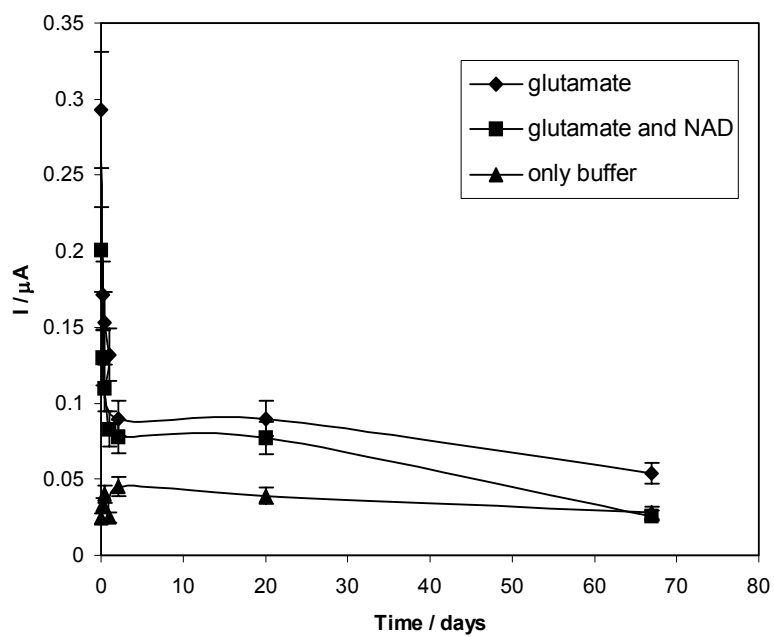


(B)

Figure S-11. Dependence of the apparent current density on L-glutamate concentration (A) and Eadie-Hofstee plots (B) for reagentless biosensors fabricated with the use of thermophilic GLDH based on: a) NAD^+ -alginate; b) binder polymer. Experimental conditions: E_{app} 150 mV vs. $\text{Ag}/\text{AgCl}/\text{KCl}_{\text{sat}}$, 0.1 M phosphate buffer (pH 7.4), temperature 40°C .



(A)



(B)

Figure S-12. Dependence of response current to 0.6 M glutamate, 0.6 M glutamate containing 0.18 M of NAD^+ , and buffer on time obtained in shelf life study for the biosensors based on thermophilic (A) and mesophilic (B) GLDH

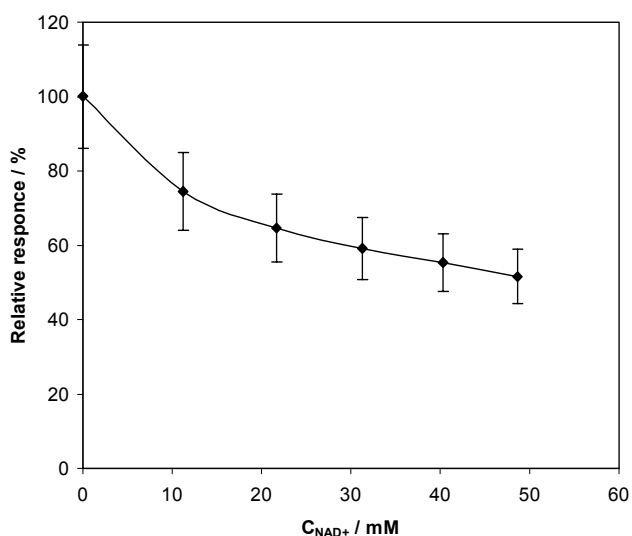


Figure S-13. Effect of NAD^+ on the response of graphite electrode in steady-state modified with osmium complex $[\text{Os}(4,4'\text{-dimethyl-2,2'}\text{-bipyridine})_2(1,10\text{-phenanthroline-5,6-dione})](\text{PF}_6)_2$. Experimental conditions: surface coverage $(2.3 \pm 0.2) \times 10^{-10} \text{ mol/cm}^2$, stirred 1.3 mM NADH solution in 0.1 M phosphate buffer deaerated with argon, pH 7.0, applied potential 150 mV vs. $\text{Ag}/\text{AgCl}/\text{KCl}_{\text{sat}}$.

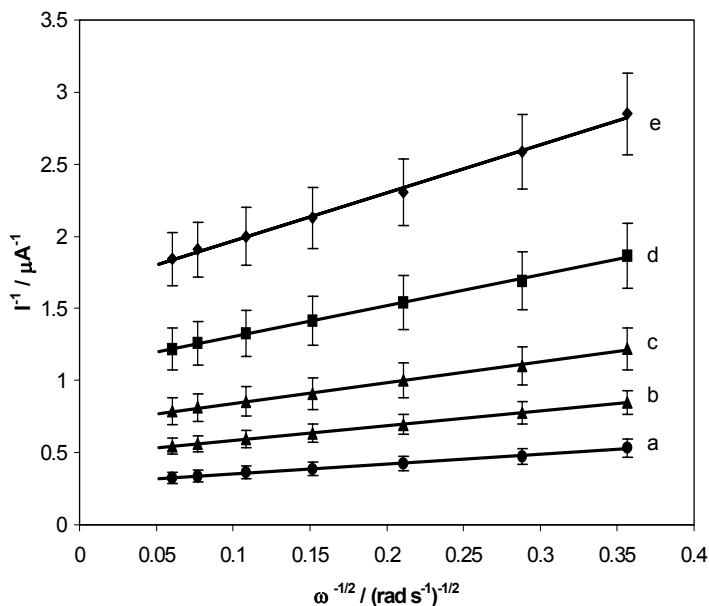


Figure S-14. Koutecky-Levich plot of steady-state electrocatalytic response for graphite RDE modified with $[\text{Os}(4,4'\text{-dimethyl-2,2'}\text{-bipyridine})_2(1,10\text{-phenanthroline-5,6-dione})](\text{PF}_6)_2$ in the presence of 20 mM NAD^+ at different NADH concentrations: (a) 1.8 mM; (b) 1.2 mM; (c) 0.8 mM; (d) 0.533 mM; (e) 0.355 mM. Experimental conditions: surface coverage $(2.8 \pm 0.3) \times 10^{-10} \text{ mol/cm}^2$, applied potential 200 mV vs. $\text{Ag}/\text{AgCl}/\text{KCl}_{\text{sat}}$, 0.1 M phosphate buffer deaerated with argon, pH 7.0.

The Use of the Lamellar Phase for the Construction of Reagentless Biosensors Based on NAD⁺ Dependent Glutamate Dehydrogenase.

Valeri Pavlov¹, Britta Lindholm-Sethson², Goran Lindblom², Ioanis Katakis^{1*}

¹Bioanalysis and Bioelectrochemistry Group, Chemical Engineering, Universitat Rovira i Virgili, E-43006, Tarragona (Catalonia), Spain. ²Department of Chemistry, Umeå University, Umeå, SE-901 87, Sweden.
Tel: +34 977 55 9655. Fax: +34 977 55 9667. E-mail: ioanis.katakis@urv.net

A new NADH oxidizing redox surfactant [Os(1,10-phenanthroline-5,6-dione)₂(4,4'-[CH₃(CH₂)₁₇NHCO]₂bpy)](PF₆)₂ (Os-phendione-surfactant) has been synthesized. The study of its tensoactive behaviour in a Langmuir-Blodgett trough demonstrated high stability of the resulting monolayer on the water-air interface and mean molecular area from 170 to 230 Å. The lamellar phase suspension based on the lipid 1,2-dioleoyl-sn-glycero-3-phosphatidylcholine containing Os-phendione-surfactant, NAD⁺ and bovine glutamate dehydrogenase was prepared and immobilized on graphite electrodes to yield reagentless biosensors operating at low applied potential of 150 mV vs. Ag/AgCl/KCl_{sat}. Their response curves and dependence of the response current on temperature and pH have been studied in order to determine the rate limiting factor. The operational half-life time of these sensors was 0.5 h.

Keywords: glutamate analysis, glutamate dehydrogenase, reagentless biosensors, NAD⁺, amphiphilic mediator

* To whom the correspondence should be addressed

Amphiphilic compounds or surfactants form micelles, liposomes, vesicles and lamellar phase in liquids and monolayers in gas-liquid interface, which can be transferred to solid substrates by Langmuir-Blodgett (LB) techniques. The development of inorganometallic surfactants serving as electron transfer reagents has been mentioned in the literature. Tenoactive bipyridine complexes of ruthenium were synthesised and their LB films were transferred on glass substrates for the photo-generation of hydrogen from water.^{1,2} These redox active amphiphilic complexes can be utilized in electrochemical biosensors for the mediation of enzymes. For example, surfactants derived from bipyridine complexes of osmium and ruthenium,^{3,4} and ferrocene^{5,6} demonstrated capacity for the exchange of electrons with the active centre of glucose oxidase.

Another class of amphiphilic molecules are lipids, which form cell membranes, also can be used in biosensors for immobilization of proteins on solid substrates. There are two basic ways for the membrane creation: the transfer a monolayer from the liquid-gas interface using the Langmuir –Blodgett technique and vesicle spreading.⁷ In both methods the inner monolayer can be deposited by the LB method or attached to the substrate surface by self-assembly from a solution through forming covalent bonds of alkyl mercaptanes on gold and alkyl silanes on silicon surfaces^{8,9} or through ion bridges.¹⁰ The advantages of the LB techniques are easy automation of the process and easy optical following by imaging ellipsometry or microfluorescence.^{11,12} In addition, by choosing different lipid mixtures and thermodynamic conditions one can deposit alternating layers with different microstructures. Vesicle spreading is based on the electrostatical or covalent linking of vesicles under high tension to the substrate surface followed by their spreading and collapse.¹³ Vesicle spreading proceeds through two mechanisms: the advancement of single bilayers, resulting in incomplete coverage, or viscous fingerlike spreading of giant vesicles leading to closed bilayers by self-healing. The resulting solid-supported lipid bilayers are model systems for biological membranes⁷ but they can incorporate membrane proteins only if the lipid bilayers are separated from the solid support by polymer spacer groups such as poly(oxyethylene).¹⁴ Membrane proteins can be incorporated in lipid bilayers by the transfer of a mixed monolayer containing proteins and lipids on a solid support us LB techniques but the serious drawback of this method is the requirement to dissolve lipids and a protein in organic solvent before spreading on the water-air interface, which may denature proteins. Hence the alternative method based on the fusion of liposomes and vesicles containing membrane proteins in lipid bilayers have been developed. It was successfully used in case of cytochrome c oxidase,^{15,16,17} and H⁺-ATPase,¹⁸ acetylcholine receptor.¹⁹ The majority of commercially available enzymes and coenzymes is hydrophilic so they can be incorporated only between hydrophilic sides of lipid bilayers. For example, vesicles containing encapsulated glucose oxidase were immobilized under a dialysis membrane on hydrogen peroxide electrodes to fabricate glucose biosensors with the increased linear range.^{20,21} To our knowledge the fabrication of “reagentless” biosensors based on the immobilization of NAD⁺ dependent dehydrogenases together with the cofactor in the lipid lamellar phase has never been reported. In this work we present “reagentless” biosensors based on bovine glutamate dehydrogenase (GLDH). Glutamate is a well known neurotransmitter, which plays important role in the development of neurological diseases such as amnesia, depression, and schizophrenia.^{22,23} It is also a marker in the diagnosis of miocardic diseases and hepatitis.²⁴ In order to develop sensors based on NAD⁺ dependent dehydrogenase we synthesized the new NADH oxidizing

amphiphilic complex of osmium with 1,10-phenanthroline-5,6-dione which allows to recycle NAD^+ at applied potential as low as 150 mV vs. Ag/AgCl/KCl_{sat}.

EXPERIMENTAL SECTION

Materials. GLDH (E.C. 1.4.1.3) from bovine liver, as suspension in saturated ammonium was purchased from Biozyme (UK), nicotinamide adenine nucleotide (NAD^+), L-glutamic acid monosodium salt, dimethylformamid (DMF), $n\text{-C}_{18}\text{H}_{37}\text{NH}_2$, sodium dihydrogen phosphate, sodium hydroxide, *ortho*-phosphoric acid, sodium chloride, thionyl chloride, NH_4PF_6 , 2,2'-bipyridine-4,4'-dicarboxylic acid, absolute 1,4-dioxane were obtained from Sigma-Aldrich (USA), K_2OsCl_6 was from Alfa (Spain), ethylene glycol and sodium dithionite were obtained from Pancreac (Madrid, Spain), 1,2-dioleoyl-sn-glycero-3-phosphatidylcholine from Larodan Fine Chemicals (Sweden), 1,10-phenanthroline-5,6-dione was prepared by the published procedure.²⁵

$[\text{Os}(1,10\text{-phenanthroline-5,6-dione})_2\text{Cl}_2]$ was synthesized according to the adapted method.²⁶ Generally the synthesis procedure involved refluxing of K_2OsCl_6 with 1,10-phenanthroline-5,6-dione in DMF under argon in the dark for 1 hr, followed by reduction with aqueous sodium dithionite solution.

Synthesis of 4,4'-[CH₃(CH₂)₁₇NHCO]₂bpy (I)

0.82 mmol of 2,2'-bipyridine-4,4'-dicarboxylic acid were refluxed during 24 h in 4 ml of thionyl chloride (Aldrich, USA), next thionyl chloride was evaporated under vacuum during 4 h. The reaction product was dissolved in 40 ml of absolute 1,4-dioxane. This solution was added dropwise to a solution 1.8 mmol of $n\text{-C}_{18}\text{H}_{37}\text{NH}_2$ in 200 ml of absolute 1,4-dioxane during 20 min, the reaction mixture was left to stay overnight. The next day the solid was filtered off, washed with 1,4-dioxane and airdried to give compound I.

Synthesis of [Os(1,10-phenanthroline-5,6-dione)₂(4,4'-[CH₃(CH₂)₁₇NHCO]₂bpy)](PF₆)₂ (II) (Os-phendione-surfactant)

0.1468 mmol of $[\text{Os}(1,10\text{-phenanthroline-5,6-dione})_2\text{Cl}_2]$ and 0.1762 mmol of compound I were refluxed during 1 h in 5 ml of deaerated ethylene glycol under argon in the dark. Next the product was precipitated by mixing with a solution of 1 g of NH_4PF_6 in 100 ml of water. The solid was filtered off and washed with water, extracted with acetone and air dried to yield compound II. The synthesis route is presented in Figure 2. ¹H NMR performed in CDCl_3 with a tetramethylsilane standard confirmed the presence of long alkane chains: 1.29 p. p. m. (m) 1.26 (m), 0.88 (t).

Preparation of bovine GLDH solution

In order to purify mesophilic bovine GLDH 4 ml of meso GLDH suspension in saturated ammonium sulphate solution were centrifuged during 10 min at 14000 RPM at 5°C. The precipitated enzyme was isolated from the ammonium sulfate solution and dissolved in 3 ml of 0.1 M sodium phosphate buffer (pH 7.4) containing 0.15 M

sodium chloride, next the resulting enzyme solution was extensively dialyzed at 5°C against 200 ml of the same buffer during 24 h, the buffer solution being changed every two hours.

Preparation of graphite electrodes. Spectrographic graphite rods of 3 mm in diameter (Carbone of America, USA) were cut into pieces of 2 cm in longitude, introduced into heat-shrinkable PVC plastic tubes, shrunk by heating, wet polished on fine (grit 400 and 600) emery paper (Buehler, USA) and sonicated in water.

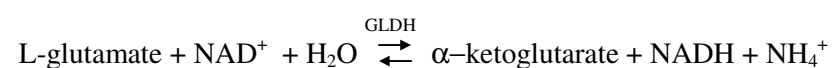
Preparation of reagentless glutamate biosensors based on immobilization between lipid bilayers. 1.5 mg of Os-phendione-surfactant and 10 mg of 1,2-dioleoyl-sn-glycero-3-phosphatidylcholine were dissolved in 0.5 mL of chloroform. Then this solution was evaporated under vacuum in a pear shaped flask to form the solid thin layer on the bottom. Next 1 mL of a solution containing 5.8 mg mL⁻¹ (38 U mL⁻¹ at 30°C) of bovine glutamate dehydrogenase and 40 mg of NAD⁺ in 0.1 M phosphate buffer pH 7.6 were stirred during 2 h to form the lamellar phase. The suspension was washed 6 times with 1 mL of 0.1 M phosphate buffer (pH 7.6), using centrifugation at 4000 rpm during 10 min every time. Next the volume of this suspension was adjusted to 1 mL and 5 µL of it was deposited per graphite electrode and air-dried during 1 h.

Electrochemical measurements. A three-electrode conventional thermostabilised cell (3 mL) equipped with an Ag/AgCl/KCl_{sat} reference electrode, a platinum auxiliary electrode, and a graphite electrode modified according to one of the above mentioned methods as working electrode. The buffer, pH 7.4 (0.1 M sodium phosphate containing 0.15 M sodium chloride) served as supporting electrolyte. The response to successive additions of stock glutamate solution was registered as steady state current on a three-electrode potentiostat Autolab PGSTAT 10 (Eco chemie, Holland) controlled by a computer. The working potential was 150 mV vs. Ag/AgCl/KCl_{sat} and the temperature of a thoroughly stirred solution was 30°C.

GLDH assay method. The activity of GLDH was tested spectrophotometrically by following the increase in absorbance at 340 nm 30°C. The assay solution contained 5 mM NAD⁺ and 10 mM in 0.1 M sodium phosphate buffer (pH 7.4). The ΔA_{340} (Au/min) was obtained using the maximum linear rate for both the test and blank (without the enzyme) mixtures. The activity was calculated using $\epsilon_{\text{NADH}}=6.22 \text{ mM}^{-1}\text{cm}^{-1}$ extinction coefficient of β -NADH. One unit of GLDH oxidizes 1 µmol of L-glutamate per minute at pH 7.4 at 30°C. Protein concentration was determined spectrophotometrically at A_{280} using an absorbance coefficient of 0.973 cm² mg⁻¹.

RESULTS AND DISCUSSION

Methods for the fabrication of reagentless glutamate biosensors. The glutamate biosensors presented hereby are based on the oxidation of L-glutamate by NAD⁺ through mesophilic and thermophilic glutamate dehydrogenase (GLDH) according to the reaction:



with the equilibrium constant shifted to the formation of L-glutamate, nevertheless the reoxidation of NADH by Os-phendione-surfactant mediator, which is oxidized in its turn at the graphite surface of the electrode at low positive potential of 150 mV *vs.* Ag/AgCl/KCl_{sat}, displaces the equilibrium to the production of NADH. The sequence of chemical reactions in the glutamate biosensor is shown schematically in Figure 1. The immobilization of GLDH, NAD⁺ and mediator is the necessary condition for design of reagentless glutamate biosensors. It was achieved by the formation of the lamellar phase suspension containing new NADH oxidizing surfactant (Os-phendione-surfactant), 1,2-dioleoyl-sn-glycero-3-phosphatylcholine, NAD⁺, and GLDH. The synthetic route to Os-phendione-surfactant can be seen in Figure 2. It was shown in the literature that complexes of transition metals with 1,10-phenanthroline-5,6-dione are stable mediators for the electrochemical oxidation of NADH,^{27,28,29} therefore we converted [Os(1,10-phenanthroline-5,6-dione)₂Cl₂] complex into a surfactant by complexation with amphiphilic bipyridine (I). This compound has demonstrated tensoactivity and forms stable Langmuir monolayer on water-air interface in a Langmuir's trough. The surface pressure/area isotherm of this mediator is shown in Figure 3. The results obtained from this isotherm point out to mean molecular area from 170 to 230 Å². This high value can be explained by the presence of bulky phenanthroline ligands. Some reorganization of a monolayer takes place starting from surface pressure value of 40 mN m⁻¹. The lamellar phase suspension was formed by mixing biosensor components with the lipid in an aqueous solution, next they were separated by centrifuge, adsorbed on the graphite electrode surface, and air-dried. ³¹P NMR investigation was utilized to confirm the structures of the lamellar phase suspension in water and on the graphite surface. In both cases the NMR spectra showed the broad peak from -7 to -15 ppm, which is the strong indication to the presence of lamellar phase.

Electrocatalytical oxidation of L-glutamate. The reagentless glutamate biosensor demonstrated change in the CV behaviour when glutamate solution was injected into the cell (Figure 4). In the presence of glutamate clear electrocatalytic waves achieving almost a plateau at potentials more negative than 200 mV *vs.* Ag/AgCl/KCl_{sat} have been seen. Our previous study of the complex of [Os(1,10-phenanthroline-5,6-dione)₂Cl₂] with poly(4-vinylpyridine)³⁰ proved that the potential of 150 mV *vs.* Ag/AgCl/KCl_{sat} was sufficient for electrocatalytic oxidation of NADH hence the same potential was used in continuation of the work.

Effect of pH on the response of glutamate biosensors. The effect of the pH on the maximum response current of glutamate biosensors was studied in steady state mode using 0.1 M phosphate buffer, pH was adjusted

with aqueous solutions of 1 M NaOH or H₃PO₄. In Figure 5 it can be seen that the biosensors have maximum response at pH 9.0. This result is in good agreement with the pH optimum of 8.5-9.0 for glutamate oxidation by free bovine GLDH in the solution.³¹ The complexes of osmium are unstable at the pH values higher than 8.0, at the same time, the controlled electrodes prepared without GLDH showed increase in non-specific oxidation of glutamate starting from pH 9.0, hence the pH of 7.4 was chosen for further experiments, because this is the physiologic value of the pH at which the analysis *in vivo* could be carried out.

Effect of temperature on the response of glutamate biosensors. The effect of temperature on the response of glutamate biosensors is presented in Figures 6. Vesicles based sensors demonstrated optimal temperature of 54°C. This data is in good agreement with the published thermostability study of bovine GLDH according to which this enzyme loses activity starting from the temperature of 52°C.³² The activation energies for the glutamate biosensors were calculated from Arrhenius plot obtained by plotting the logarithm of the relative response current against the reciprocal of the absolute temperature. The activation energy is 56.3 kJ mol⁻¹. Activation energies of the GLDH biosensors are significantly higher than the activation energy of free bovine GLDH, 12.9 kJ mol⁻¹.³² This fact indicates that the response of the glutamate biosensors was not limited by the kinetics of glutamate oxidation with NAD⁺ through GLDH.

Response curves and operational stability of the glutamate biosensors. The latest kinetic study into the mechanism of enzymatic deamination confirmed that bovine dehydrogenase has an ordered sequential mechanism of substrate binding preceded by complexation with NAD⁺³³ therefore the calculations of characteristics of the glucose sensors were based on the following modified kinetic model for the conversion of substrate B to product Q.³⁴ Figure 7 illustrates the kinetic scheme for the operation of reagentless biosensors based on the enzyme glutamate dehydrogenase (E) catalyzing the reaction of immobilized NAD⁺ (A) with a L-glutamate (B) to give immobilized NADH (P), α-ketoglutarate (Q), and NH₄⁺ (R). Then a mediator (M), which can stay in reduced (M_{red}) and oxidized (M_{ox}) forms, immobilized on the electrode surface catalyzes the electrochemical conversion of P back to A. A_{im} and P_{im} are the concentrations of immobilized A and P. B_o, Q_o, R_o are the concentrations of the substrate and the products in the lamellar phase B_∞, Q_∞ and R_∞ are the concentrations of the substrate and the products in the external medium. k'_B, k'_Q and k'_R are mass transfer coefficients of the substrate and the products (cm s⁻¹), respectively. L is the thickness of the hydrogel layer. The following expressions for the flux of B to the electrode surface (j_{el}), which determines the current density of a biosensor (j) through the equation j = nFj_{el}, where n is the number of exchanged electrons and F is the Faraday's constant, can be obtained.

$$j_{el} = k'_B(B_{\infty} - B_o) \quad (1)$$

$$j_{el} = L(k_1 A_{im} [E] - k_{-1} [E \cdot A]) \quad (2)$$

$$j_{el} = L(k_2 B_o [E \cdot A] - k_{-2} [E \cdot A \cdot B]) \quad (3)$$

$$j_{el} = L(k_3 [E \cdot A \cdot B] - k_{-3} [E \cdot P \cdot Q \cdot R]) \quad (4)$$

$$j_{el} = L(k_4 [E \cdot P \cdot Q \cdot R] - k_{-4} [E \cdot P \cdot Q] Q_o) \quad (5)$$

$$j_{el} = L(k_5 [E \cdot P \cdot Q] - k_{-5} [E \cdot P] Q_o) \quad (6)$$

$$j_{el} = L(k_6 [E \cdot P] - k_{-6} [E] P_{im}) \quad (7)$$

$$j_{el} = k'_Q Q_o \quad (8)$$

$$\begin{aligned}
j_{el} &= k'_R R_o & (9) \\
j_{el} &= k_7 P_o \Gamma_{Mox} - k_{-7} \Gamma_{M \cdot P} & (10) \\
j_{el} &= k_8 \Gamma_{M \cdot P} & (11) \\
j_{el} &= k_9 \Gamma_{Mred} & (12) \\
E_t &= [E] + [E \cdot A] + [E \cdot A \cdot B] + [E \cdot P \cdot Q \cdot R] + [E \cdot P \cdot Q] + [E \cdot P] & (13) \\
\Gamma_M &= \Gamma_{M \cdot P} + \Gamma_{Mox} + \Gamma_{Mred} & (14) \\
A_t &= A_{im} + P_{im} & (15)
\end{aligned}$$

Where Γ_{Mox} and Γ_{Mred} are the surface coverages of the mediator in oxidized and reduced forms, respectively. Γ_M is the total mediator surface coverage. $\Gamma_{M \cdot P}$ is the surface coverage of the intermediate complex between the mediator and NADH. A_t and E_t are the total concentrations of NAD⁺ and the enzyme immobilized in the lamellar phase, respectively. The equations (1-15) yield the equation (16):

$$\begin{aligned}
LV_1 \Gamma_M k_{cat} E_t A_t B_\infty &= j_{el} [K_{AB} \Gamma_M k_{cat} + K_B \Gamma_M k_{cat} A_t + K_A \Gamma_M k_{cat} B_\infty + A_t \Gamma_M k_{cat} B_\infty + LV_1 (A_t + K_M) B_\infty + \\
&(LV_1 A_t \Gamma_M k_{cat}) / k'_B] + j_{el}^2 [(K_{PQ} K_B A_t \Gamma_M k_{cat}) / (K_{iP} K_{iQ} K_R k'_R) - LV_1 (A_t + K_M) / k'_B - K_{AB} - K_B (A_t + K_M) - K_A B_\infty + \\
&K_M K_{QR} K_{iA} K_B / (K_{iP} K_{iQ} K_R) - (A_t + K_M) B_\infty - A_t \Gamma_M k_{cat} / k'_B + \Gamma_M k_{cat} K_{PQ} K_{iA} K_B R_o / (K_{iP} K_{iQ} K_R k'_R) + K_A K_M B_\infty / K_{iP} + \\
&K_{iR} K_P K_B A_t B_\infty \Gamma_M k_{cat} / (K_{iB} K_{iP} K_{iQ} K_R k'_Q) + K_{PQ} K_B A_t B_\infty \Gamma_M k_{cat} / (K_{iB} K_{iP} K_{iQ} k'_R)] + j_{el}^3 [LV_1 K_M / (K_{eq} k'_Q k'_R) + K_A / k'_B + (A_t \\
&+ K_M) / k'_B - K_{PQ} K_{iA} K_B / (K_{iP} K_{iQ} K_R k'_R) + \Gamma_M k_{cat} K_P K_{iA} K_B / (K_{iP} K_{iQ} K_R k'_Q k'_R) + K_M K_R K_{iA} K_B / (K_{iP} K_{iQ} K_R k'_Q) + \\
&K_M K_P K_{iA} K_B / (K_{iP} K_{iQ} K_R k'_R) - K_A K_M / (K_{iP} k'_B) + K_A K_M B_\infty / (K_{iQ} K_{iP} k'_Q) - K_{iR} K_P K_B (A_t + K_M) B_\infty / (K_{iB} K_{iP} K_{iQ} K_R k'_Q) - \\
&K_{iR} K_P K_B A_t \Gamma_M k_{cat} / (K_{iB} K_{iP} K_{iQ} K_R k'_B k'_Q) + K_P K_B A_t \Gamma_M k_{cat} / (K_{iP} K_{iQ} K_R k'_Q k'_R) - K_{PQ} K_B (A_t + K_M) / (K_{iP} K_{iQ} K_R k'_R) + \\
&K_P K_B A_t B_\infty \Gamma_M k_{cat} / (K_{iB} K_{iP} K_{iQ} K_R k'_Q k'_R) - K_{PQ} K_B B_\infty (A_t + K_M) / (K_{iB} K_{iP} K_{iQ} K_R k'_R) - A_t \Gamma_M k_{cat} K_{PQ} K_B / (K_{iB} K_{iP} K_{iQ} K_R k'_B k'_R)] \\
&+ j_{el}^4 [K_{iA} K_B K_M / (K_{iP} K_{iQ} K_R k'_Q k'_R) - K_P K_{iA} K_B / (K_{iP} K_{iQ} K_R k'_Q k'_R) - K_A K_M / (K_{iQ} K_{iP} k'_Q) + K_{iR} K_P K_B (A_t \\
&+ K_M) / (K_{iB} K_{iP} K_{iQ} K_R k'_B k'_Q) - K_P K_B (A_t + K_M) / (K_{iP} K_{iQ} K_R k'_Q k'_R) - \\
&K_P K_B B_\infty / (K_{iB} K_{iP} K_{iQ} K_R k'_Q k'_R) - K_P K_B A_t \Gamma_M k_{cat} / (K_{iB} K_{iP} K_{iQ} K_R k'_B k'_Q k'_R) + K_A B_\infty K_M / (K_{iR} K_{iP} K_{iQ} k'_Q k'_R) + \\
&K_{PQ} K_B (A_t + K_M) / (K_{iB} K_{iP} K_{iQ} K_R k'_B k'_Q k'_R)] + j_{el}^5 [K_P K_B (A_t + K_M) / (K_{iB} K_{iP} K_{iQ} K_R k'_B k'_Q k'_R) - K_A K_M / (K_{iR} K_{iP} K_{iQ} k'_B k'_Q k'_R)] \\
& (16)
\end{aligned}$$

Where $V_1 = E_t (k_1 k_2 k_3 k_4 k_5 k_6) / (k_1 k_2 k_5 k_6 k_3 + k_1 k_2 k_4 k_5 k_6 + k_1 k_2 k_3 k_5 k_6 + k_1 k_2 k_3 k_4 k_6 + k_1 k_2 k_3 k_4 k_5)$ and $V_2 = E_t (k_1 k_2 k_3 k_4 k_5 k_6) / (k_2 k_3 k_4 k_5 k_6 + k_1 k_3 k_4 k_5 k_6 + k_1 k_2 k_4 k_5 k_6 + k_3 k_1 k_4 k_5 k_6)$ are the maximum velocities in forward and reverse directions, the Michaelis constants for A, B, P, Q, R are $K_A = (k_2 k_3 k_4 k_5 k_6) / (k_1 k_2 k_5 k_6 k_3 + k_1 k_2 k_4 k_5 k_6 + k_1 k_2 k_3 k_5 k_6 + k_1 k_2 k_3 k_4 k_6 + k_1 k_2 k_3 k_4 k_5)$, $K_B = (k_1 k_5 k_6 k_2 k_3 + k_1 k_4 k_5 k_6 k_2 + k_1 k_3 k_4 k_5 k_6) / (k_1 k_2 k_5 k_6 k_3 + k_1 k_2 k_4 k_5 k_6 + k_1 k_2 k_3 k_5 k_6 + k_1 k_2 k_3 k_4 k_6 + k_1 k_2 k_3 k_4 k_5)$, $K_{AB} = (k_5 k_6 k_1 k_2 k_3 + k_4 k_5 k_6 k_1 k_2 + k_1 k_3 k_4 k_5 k_6) / (k_1 k_2 k_5 k_6 k_3 + k_1 k_2 k_4 k_5 k_6 + k_1 k_2 k_3 k_5 k_6 + k_1 k_2 k_3 k_4 k_6 + k_1 k_2 k_3 k_4 k_5)$, $K_P = k_1 k_2 k_3 k_4 k_5 / (k_2 k_3 k_4 k_5 k_6 + k_1 k_3 k_4 k_5 k_6 + k_1 k_2 k_4 k_5 k_6 + k_3 k_1 k_4 k_5 k_6)$, $K_Q = k_1 k_2 k_3 k_4 k_6 / (k_2 k_3 k_4 k_5 k_6 + k_1 k_3 k_4 k_5 k_6 + k_1 k_2 k_4 k_5 k_6 + k_3 k_1 k_4 k_5 k_6)$, $K_R = (k_1 k_2 k_3 k_5 k_6 + k_4 k_1 k_2 k_5 k_6 + k_3 k_4 k_1 k_5 k_6) / (k_2 k_3 k_4 k_5 k_6 + k_1 k_3 k_4 k_5 k_6 + k_1 k_2 k_4 k_5 k_6 + k_3 k_1 k_4 k_5 k_6)$, $K_{QR} = (k_5 k_1 k_2 k_3 k_6 + k_4 k_5 k_1 k_2 k_6 + k_3 k_4 k_5 k_1 k_6) / (k_2 k_3 k_4 k_5 k_6 + k_1 k_3 k_4 k_5 k_6 + k_1 k_2 k_4 k_5 k_6 + k_3 k_1 k_4 k_5 k_6)$, $K_{PQ} = k_6 k_1 k_2 k_3 k_4 / (k_2 k_3 k_4 k_5 k_6 + k_1 k_3 k_4 k_5 k_6 + k_1 k_2 k_4 k_5 k_6 + k_3 k_1 k_4 k_5 k_6)$, $K_{PQR} = (k_5 k_6 k_1 k_2 k_3 + k_4 k_5 k_6 k_1 k_2 + k_1 k_3 k_4 k_5 k_6) / (k_2 k_3 k_4 k_5 k_6 + k_1 k_3 k_4 k_5 k_6 + k_1 k_2 k_4 k_5 k_6 + k_3 k_1 k_4 k_5 k_6)$. The inhibition constants for A, B, P, Q, R are $K_{iA} = k_{-1} / k_1$, $K_{iB} = (k_{-2} k_3) / (k_2 (k_{-3} + k_3))$, $K_{iP} = k_6 / k_{-6}$, $K_{iQ} = k_5 / k_{-5}$, $K_{iR} = (k_3 k_4) / (k_4 (k_3 + k_{-3}))$. Use of the inhibition constants allows to redefine: $K_{PQ} = K_{iP} K_Q$ and $K_{QR} = K_{iQ} K_R$.

The equation 16 was employed to simulate the response curves and Eadie-Hofstee plots for the reagentless glutamate biosensors using the values of the Michaelis and inhibition constants found in the literature.³⁵

Figure 8 demonstrates the effect of the value of maximum flux of the electrochemical oxidation of NADH (Γk_{cat}) on the simulated response of the reagentless glutamate biosensors (at $A_t = 1$ mM). The Eadie-

Hofstee plots yield the straight line characteristic for the process limited by the enzymatic reduction of NAD^+ only when Γk_{cat} is infinitively high. The decrease in the value of Γk_{cat} leads to the decrease in the values of intercepts of the Eadie-Hofstee plots with the axis of j and their negative slopes i.e. the apparent maximum current densities and apparent Michaelis constants, respectively, become lower due to the limitation set by the flux of the electrochemical oxidation of NADH. The decrease in the value of Γk_{cat} also effects the shape of Eadie-Hofstee plots making them more concave. Hence the concavity of Eadie-Hofstee plots is diagnostic for reagentless glutamate biosensors limited by the rate of electrochemical NADH oxidation at the electrode surface.

Figure 9 represents the effect of mass transport rate on the response of biosensors limited by the rate of the electrochemical NADH oxidation. The decrease in the mass transfer coefficients leads to the drastic increase in the slope of Eadie-Hofstee plots, making the apparent Michaelis constants (measured using high concentrations of glutamate) higher than K_B of free GLDH. It can be concluded that the concave Eadie-Hofstee plots, giving the values of apparent Michaelis constant higher than the value of K_M of the free enzyme, are diagnostic for the reagentless glutamate biosensors limited by the rate of electrochemical NADH oxidation at the electrode surface and by the rate of mass transport.

The effect of the maximum flux of the enzymatic reduction of NAD^+ (LV_1) rate on the response of biosensors limited by the rate of the electrochemical NADH oxidation and mass transport is illustrated in Figure 10. The increase in LV_1 leads to the drastic increase in apparent current densities and the concavity of the Eadie-Hofstee plots, making the apparent Michaelis constants higher than K_B of free GLDH.

The response curve of the glutamate biosensors is shown in Figures 11 and their basic characteristics obtained from the Eadie-Hofstee plots are represented in Table II. The Eadie-Hofstee plots (Figure 10(B)) show concavity characteristic for the process limited by the rate of NADH oxidation at the electrode surface. The value of the apparent Michaelis constant (47 mM) is significantly higher than the literature value of that for mesophilic bovine GLDH (2.5 mM)³⁵ implying that the response of these glutamate sensors is limited by the rate of electrochemical NADH oxidation and the mass transfer between the lamellar phase and the external solution.

The glutamate biosensors prepared using immobilization in the lamellar phase layers have very short operational half-life time (30 min) and long response time 7-8 min. The loss of the response was caused by leaching of NAD^+ from the electrode surface. This was proven by the injection of NAD^+ at the end of operational stability study (when one half of the initial response to glutamate and 20% of Os-phendione-PVP were lost according to the data obtained by cyclic voltammetry. The injection of NAD^+ lead to the recovery of c.a. 80 % of the initial response current demonstrated by the biosensors operated in the presence of NAD^+ .

CONCLUSIONS

The new NADH oxidizing surfactant can be synthesized by complexation of $[\text{Os}(1,10\text{-phenanthroline-5,6-dione})_2\text{Cl}_2]$ with hydrophobic ligand and can be used for the formation of the aqueous lamellar phase which entraps NAD^+ dependent glutamate dehydrogenase and NAD^+ . The resulting lamellar phase suspension can be

immobilized by adsorption on graphite electrodes to yield reagentless glutamate biosensors operating at 150 mV vs. Ag/AgCl/KCl_{sat}. Their response is limited by the rate of electrochemical NADH oxidation and the mass transfer between the lamellar phase and the external solution. Their low operational stability is determined by leaching of NAD⁺.

ACKNOWLEDGEMENTS

This paper was supported by the grants of European Community, Industrial & Material Technologies Programme (Brite-EuRam III), project No. BE97-4511, the Spanish Ministry of Education and Culture Ref.: Acciones Especiales MAT98-1413.CE. V.P. acknowledges Ph. D. fellowship and the special grant Ref.:M3C99-80 from the Department of chemical engineering, University Rovira I Virgili.

LEGEND TO TABLE

Table I. Basic characteristics of the reagentless glutamate biosensors calculated from the Eadie-Hofstee plot.

LEGENDS TO FIGURES

Figure 1. Schematic diagram of the electron transfer steps for the mediated glutamate biosensors.

Figure 2. Synthetic route to the NADH oxidising tensoactive mediator Os-phendione-surfactant.

Figure 3. Surface pressure/area isotherm for Os-phendione-surfactant.

Figure 4. Cyclic voltammograms of reagentless glutamate biosensors based on the lamella phase layers and GLDH in the absence of glutamate and the presence 0.35 M glutamate. Scan rate 0.3 mV s⁻¹. Experimental conditions: E_{app} 150 mV vs. Ag/AgCl/KCl_{sat}, 0.1 M phosphate buffer (pH 7.4), temperature 30°C.

Figure 5. Effect of pH on maximum response of reagentless glutamate biosensors based on the lamellar phase. Experimental conditions: E_{app} 150 mV vs. Ag/AgCl/KCl_{sat}, 0.1 M phosphate buffer, temperature 30°C.

Figure 6. Effect of temperature on maximum response of reagentless glutamate biosensors based on the lamellar phase. Experimental conditions: E_{app} 150 mV vs. Ag/AgCl/KCl_{sat}, 0.1 M phosphate buffer (pH 7.4).

Figure 7. Reaction scheme for a reagentless glutamate biosensor.

Figure 8. Simulation of the Eadie-Hofstee plots for the reagentless glutamate biosensors with varying maximum fluxes of the electrochemical NADH oxidation (Γk_{cat}): a) 2.6×10^{-11} mol s⁻¹ cm⁻²; b) 1.04×10^{-10} mol s⁻¹ cm⁻²;

c) $4.15 \times 10^{-10} \text{ mol s}^{-1} \text{ cm}^{-2}$; d) $8.3 \times 10^{-10} \text{ mol s}^{-1} \text{ cm}^{-2}$; e) $1.7 \times 10^{-9} \text{ mol s}^{-1} \text{ cm}^{-2}$; f) $1.3 \times 10^{-8} \text{ mol s}^{-1} \text{ cm}^{-2}$; g) $5.178 \times 10^{-8} \text{ mol s}^{-1} \text{ cm}^{-2}$; h) ∞ . The values of other parameters are: $A_t=1 \text{ mM}$; $k'_B \rightarrow \infty$; $k'_Q \rightarrow \infty$; $k'_R \rightarrow \infty$; $LV_1=3.63 \times 10^{-10} \text{ mol s}^{-1} \text{ cm}^{-2}$; $K_M = 0.8 \text{ mM}$; $K_A = 0.23 \text{ mM}$; $K_B = 2.5 \text{ mM}$; $K_{AB} = 0.3 \text{ mM}^2$; $K_{iA} = 10 \text{ mM}$; $K_{iB} = 11 \text{ mM}$; $K_R = 20 \text{ mM}$; $K_Q = 0.25 \text{ mM}$; $K_P = 0.04 \text{ mM}$; $K_{iR} = 9 \text{ mM}$; $K_{iQ} = 1.6 \text{ mM}$; $K_{iP} = 0.03 \text{ mM}$.

Figure 9. Simulation of the Eadie-Hofstee plots for the reagentless glutamate biosensors with varying mass transfer coefficients (k'_B, k'_Q, k'_R): a) $5.18 \times 10^{-12} \text{ cm s}^{-1}$; b) $2.6 \times 10^{-11} \text{ cm s}^{-1}$; c) $5.18 \times 10^{-11} \text{ cm s}^{-1}$; d) $1.03 \times 10^{-10} \text{ cm s}^{-1}$; e) $2.6 \times 10^{-10} \text{ cm s}^{-1}$; f) ∞, ∞ . The values of other parameters are: $A_t=1 \text{ mM}$; $LV_1 = 3.63 \times 10^{-10} \text{ mol s}^{-1} \text{ cm}^{-2}$; $I k_{cat} = 8.3 \times 10^{-10} \text{ mol s}^{-1} \text{ cm}^{-2}$; $K_M = 0.8 \text{ mM}$; $K_A = 0.23 \text{ mM}$; $K_B = 2.5 \text{ mM}$; $K_{AB} = 0.3 \text{ mM}^2$; $K_{iA} = 10 \text{ mM}$; $K_{iB} = 11 \text{ mM}$; $K_R = 20 \text{ mM}$; $K_Q = 0.25 \text{ mM}$; $K_P = 0.04 \text{ mM}$; $K_{iR} = 9 \text{ mM}$; $K_{iQ} = 1.6 \text{ mM}$; $K_{iP} = 0.03 \text{ mM}$.

Figure 10. Simulation of the Eadie-Hofstee plots for the reagentless glutamate biosensors with varying maximum flux of enzymatic reduction of NAD^+ (LV_1): a) $1.55 \times 10^{-10} \text{ mol s}^{-1} \text{ cm}^{-2}$; b) $3.63 \times 10^{-10} \text{ mol s}^{-1} \text{ cm}^{-2}$; c) $6.22 \times 10^{-10} \text{ mol s}^{-1} \text{ cm}^{-2}$; d) $1.24 \times 10^{-9} \text{ mol s}^{-1} \text{ cm}^{-2}$; e) $2.49 \times 10^{-9} \text{ mol s}^{-1} \text{ cm}^{-2}$. The values of other parameters are: $k'_B = 2.6 \times 10^{-11} \text{ cm s}^{-1}$; $k'_Q = 2.6 \times 10^{-11} \text{ cm s}^{-1}$; $k'_R = 2.6 \times 10^{-11} \text{ cm s}^{-1}$; $A_t=1 \text{ mM}$; $I k_{cat} = 8.3 \times 10^{-10} \text{ mol s}^{-1} \text{ cm}^{-2}$; $K_M = 0.8 \text{ mM}$; $K_A = 0.23 \text{ mM}$; $K_B = 2.5 \text{ mM}$; $K_{AB} = 0.3 \text{ mM}^2$; $K_{iA} = 10 \text{ mM}$; $K_{iB} = 11 \text{ mM}$; $K_R = 20 \text{ mM}$; $K_Q = 0.25 \text{ mM}$; $K_P = 0.04 \text{ mM}$; $K_{iR} = 9 \text{ mM}$; $K_{iQ} = 1.6 \text{ mM}$; $K_{iP} = 0.03 \text{ mM}$.

Figure 11. Dependence of the steady apparent current density on L-glutamate concentration (**A**) and the Eadie-Hofstee plots (**B**) for reagentless biosensors based on the lamellar phase. Experimental conditions: $E_{app} 150 \text{ mV}$ vs. Ag/AgCl/KCl_{sat} , 0.1 M phosphate buffer (pH 7.4), temperature 30°C .

REFERENCES

- (1) Sprintschik, G.; Sprintschik, H. W.; Kirsch, P. P.; Whitten, D. G. *J. Am. Chem. Soc.* **1976**, *98*, 2337-2338.
- (2) Gaines, G. L.; Behnken, P. E.; Valenty, S. J. *J. Am. Chem. Soc.* **1978**, *100*, 6549-6559.
- (3) Saudan, P.; Zakeeruddin, S. M.; Malavallon, M. A.; Grätzel, M.; Fraser, D. M. *Biotechnol. Bioengin.* **1994**, *44*, 407-418.
- (4) Zakeeruddin, S. M.; Grätzel, M.; Fraser, D. M. *Biosens. Bioelectron.* **1996**, *11*, 305-315.
- (5) Fraser, D. M.; Zakeeruddin, S. M.; Grätzel, M. *Biochim. Biophys. Acta* **1992**, *1099*, 91-101.
- (6) Ryabov, A. D.; Amon, A.; Gorbatoeva, R. K.; Ryabova, E. S.; Gnedenko, B. B. *J. Phys. Chem.* **1995**, *99*, 14072-14077.
- (7) Sackmann, E. *Science*, **1996**, *271*, 43-48.
- (8) Miller, C.; Cuendet, P.; Grätzel, M. *J. Electroanal. Chem.* **1990**, *278*, 175-192.
- (9) Florin E. L.; Gaub, H. E. *Biophys. J.* **1993**, *64*, 375-383.
- (10) Kuhn, H.; Möbius H. D.; Bücher, H. In *Physical Methods of Chemistry*, Part IIIB, Weissenberger, A.; Rossiter, B. M. Eds.; Wiley: New York, 1972; pp. 577-578.
- (11) Egger, M.; Heyn, S. P.; Gaub, H. E. *Biophys. J.* **1990**, *57*, 669-673.

- (12) Kalb, E.; Frey, S.; Tamm, L. K. *Biochim. Biophys Acta* **1992**, *1103*, 307-316.
- (13) Bayerl, Th. M.; Bloom, M. *Biophys. J.* **1990**, *58*, 357-362.
- (14) Duschl, C.; Liley, M.; Lang, H.; Ghandi, A.; Zakeeruddin, S. M.; Stahlberg, H.; Dubochet, J.; Nemetz, A.; Knoll, W.; Vogel, H. *Mater. Sci. Eng. C* **1996**, *4*, 7-18.
- (15) Salamon, Z.; Hazzard, J. T.; Tollin, G. *Proc. Natl. Acad. U.S.A.* **1993**, *90*, 6420-6423.
- (16) Lindholm-Sethson, B.; Gonzalez, J. C.; Puu, G. *Langmuir* **1998**, *14*, 6705-6708.
- (17) Naumann, R.; Schmidt, E. K.; Jonczyk, A.; Fendler, K.; Kadenbach, B.; Liebermann, T.; Offenhäusser, A.; Knoll, W. *Biosens. Bioelectron.* **1999**, *14*, 651-662.
- (18) Bunjes, N.; Schmidt, E. K.; Jonczyk, A.; Rippmann, F.; Beyer, D.; Ringsdorf, H.; Gräber, P.; Knoll, Naumann, W.; R. *Langmuir*, **1997**, *13*, 6188-6194.
- (19) Schmidt, E. K.; Liebermann, T.; Kreiter, M.; Jonczyk, A.; Naumann, R.; Offenhäuser, A.; Neumann, E.; Kukol, A.; Maelicke, A.; Knoll, W. *Biosens. Bioelectron.* **1998**, *13*, 585-591.
- (20) Taylor, M. A.; Jones, M. N.; Vadgama, P.; Higson, S. P. J. *Biosens. Bioelectron.* **1995**, *10*, 251-260.
- (21) Taylor, M. A.; Jones, M. N.; Vadgama, P.; Higson, S. P. J. *Biosens. Bioelectron.* **1997**, *12*, 467-477.
- (22) Engelsens, B. *J. Neurochem.* **1986**, *47*, 1634-1641.
- (23) Greenamyre, J. T. *Arch. Neurol.* **1986**, *43*, 1058-1063.
- (24) Rietz, B.; Guilbault, G. G. *Anal. Chim. Acta* **1975**, *77*, 191-198.
- (25) Amouyal, E.; Homsy, A.; Chambron, J.-C.; Sauvage, J.-P. *J. Chem. Soc., Dalton Trans.* **1990**, 1841-1845.
- (26) Lay, P. A.; Sargeson, A. M.; Taube, H. In *Inorganic Synthesis*; Shreeve J. M., Ed.; John Wiley: New York, 1986; Vol 24; pp. 293-295.
- (27) Wu, Q.; Maskus, M.; Pariente, F.; Tobalina, F.; Fernandez, V. M.; Lorenzo, E.; Abruña, H. D. *Anal. Chem.* **1996**, *68*, 3688-3696.
- (28) Goss, C. A.; Abruña, H. D. *Inorg. Chem.* **1985**, *24*, 4263-4267.
- (29) Popescu, I. C.; Dominguez, E.; Narvaez, A.; Pavlov, V.; Katakis, I. *J. Electroanal. Chem.* **1999**, *464*, 208-214.
- (30) Pavlov, V.; Rincón, O.; Solé, S.; Narváez, A.; Domínguez, E.; Katakis I. Submitted to *Anal. Chem.*
- (31) Smith, E. L.; Austen, B. M.; Blumenthal, M. K.; Nyc, J. F. In *The Enzymes*; Boyer, P. D., Ed.; Academic Press: New York, 1975, volume XI, pp. 359-360.
- (32) Yamamura, A.; Sakaguchi, T.; Murakami, Y.; Yokoyama, K.; Tamiya, E. *Biochem. J.* **1999**, *125*, 760-769.
- (33) O'Flaherty, M.; McMahon, M.; Forde, J.; Mulcahy, P. *Prot. Express. Purif.* **1999**, *16*, 276-297.
- (34) Albery, W. J.; Bartlett, P. N.; Cass, A. E. G.; Sim, K. W. *J. Electroanal. Chem.* **1987**, *218*, 127-134.
- (35) Fahien, L. A.; Strmecki, M. *Arch. Biochem. Biophys.* **1969**, *130*, 468-477.

Table I

| J_{\max}, $\mu\text{A cm}^{-2}$ | RSD, % | Response time, s | K_M, mM | Operational half-life time, h |
|--|---------------|-------------------------|-----------------------------|--------------------------------------|
| 3.5 | 25.0 | 220 | 47 | 0.5 |

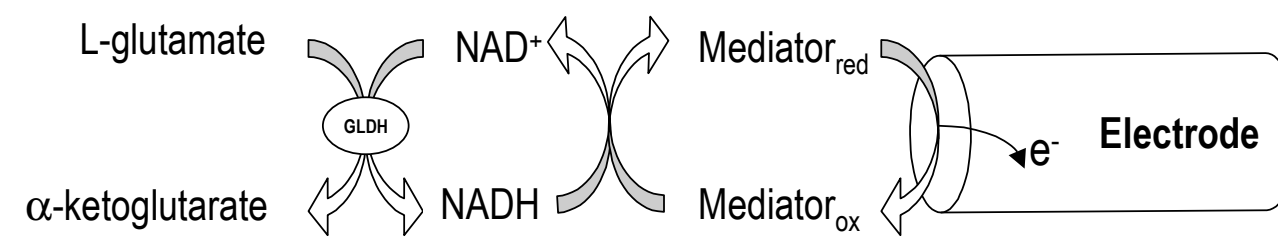


Figure 1

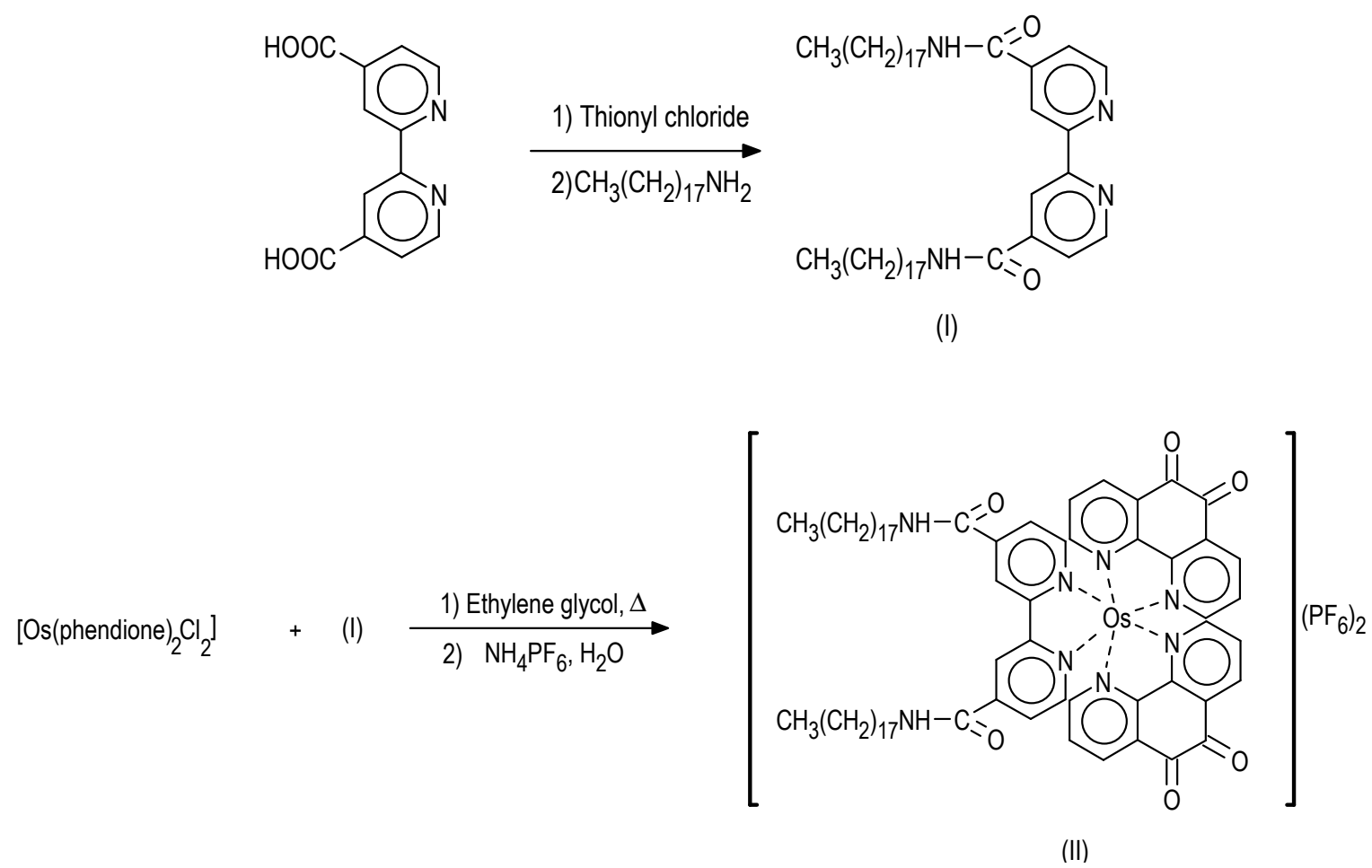


Figure 2

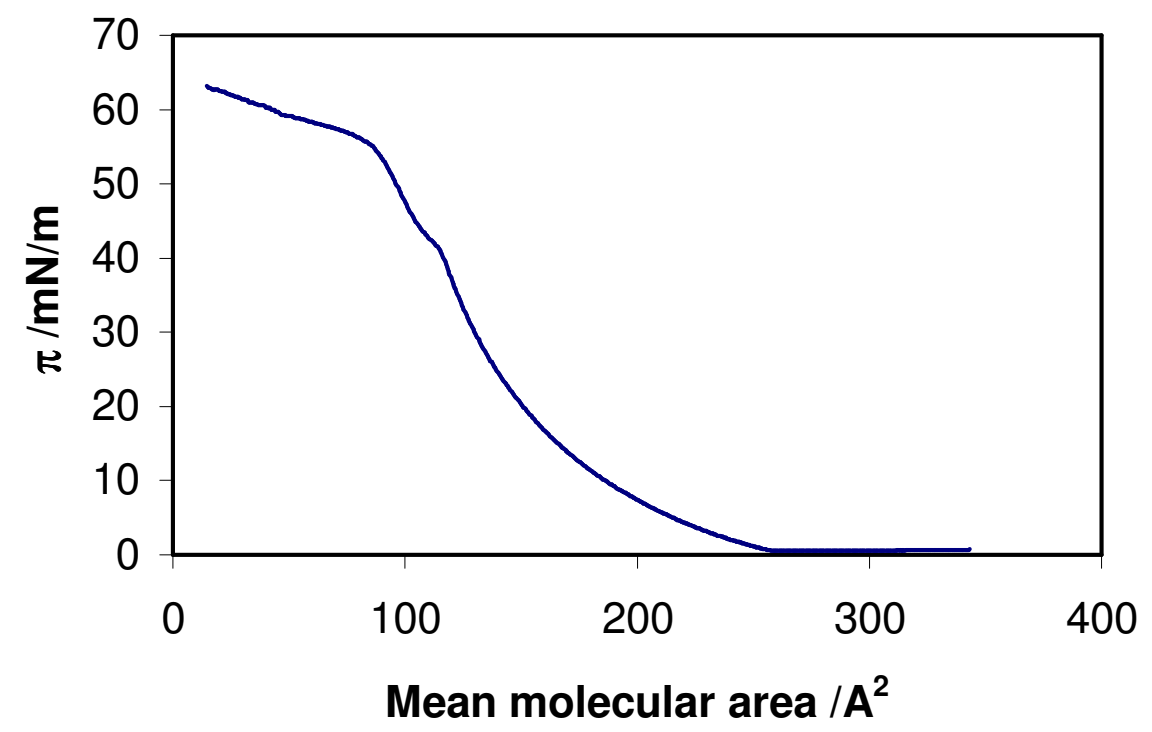


Figure 3

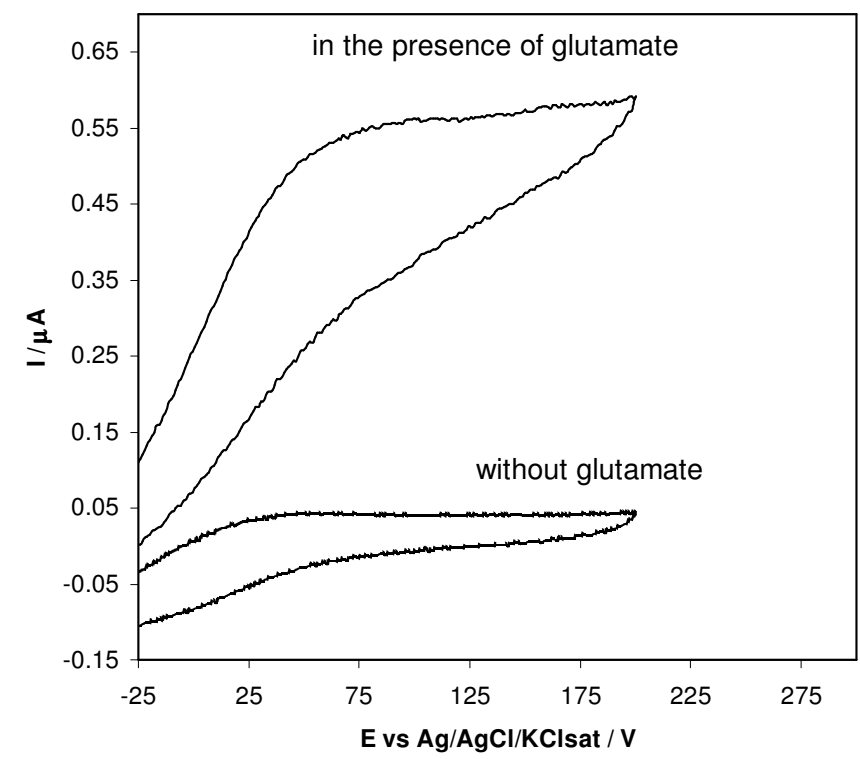


Figure 4

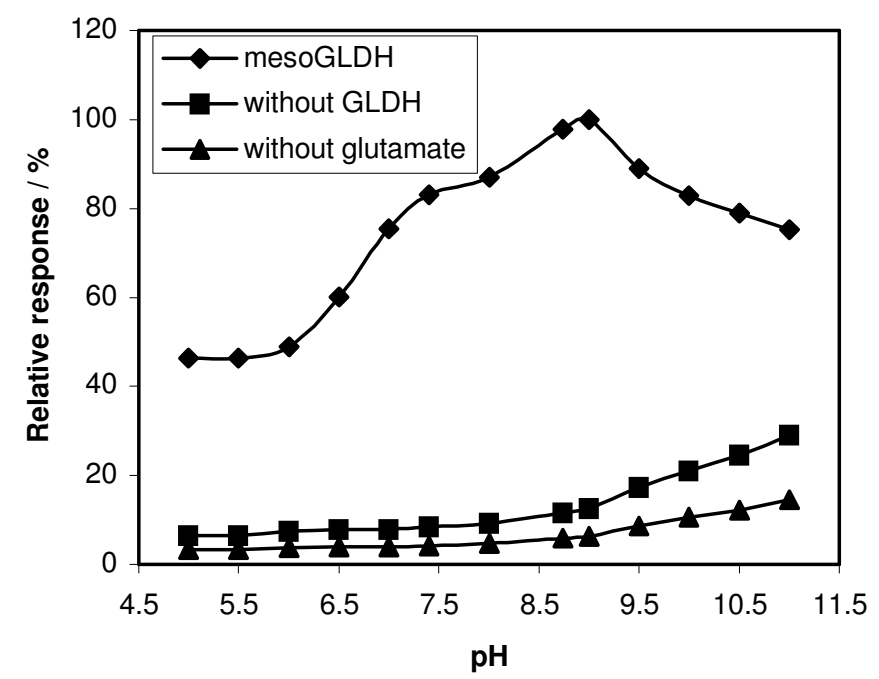


Figure 5

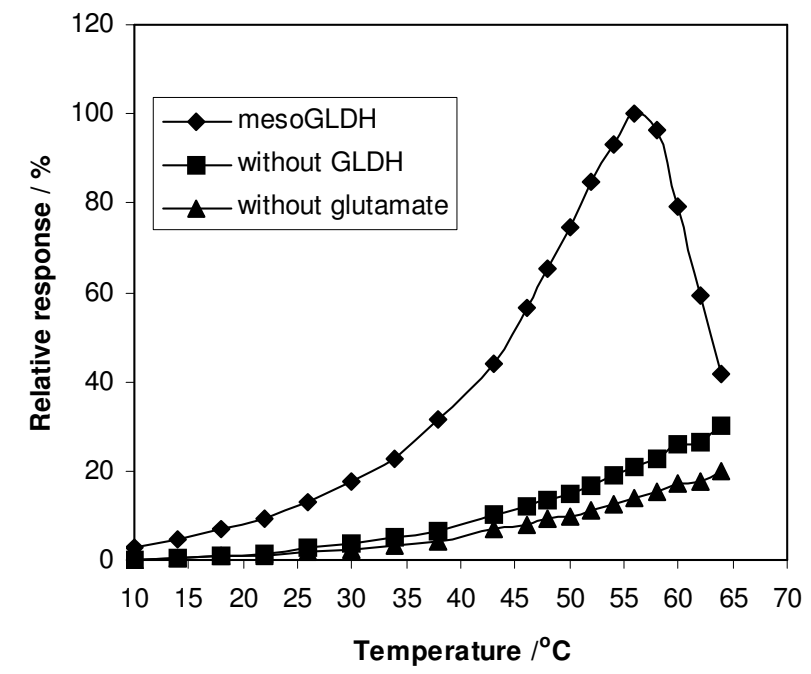


Figure 6

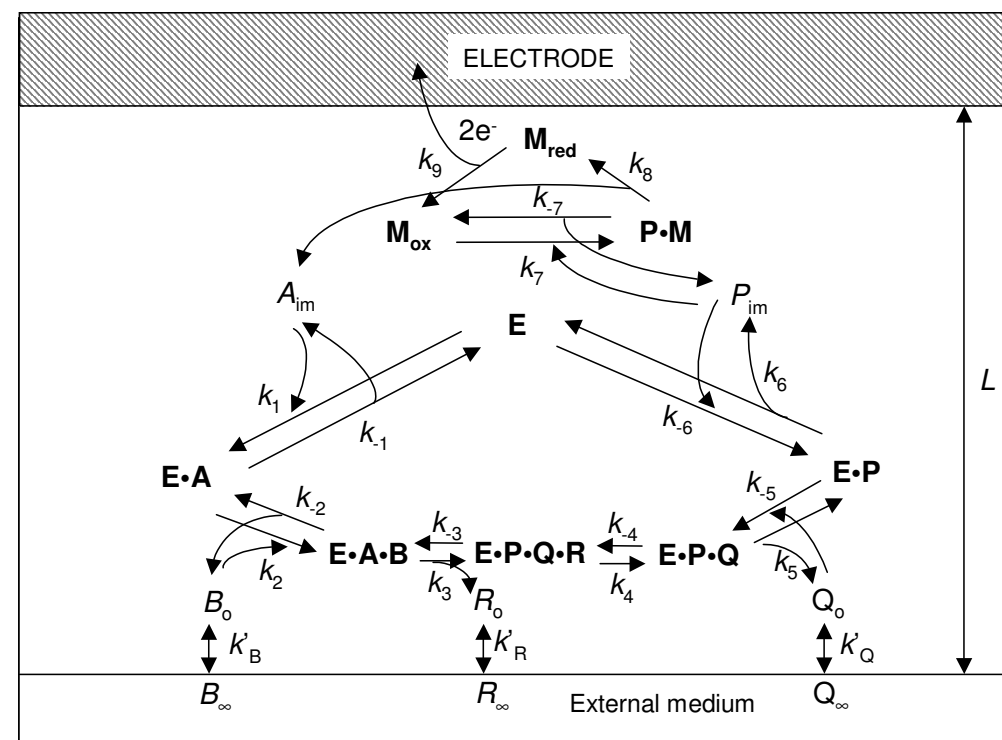


Figure 7

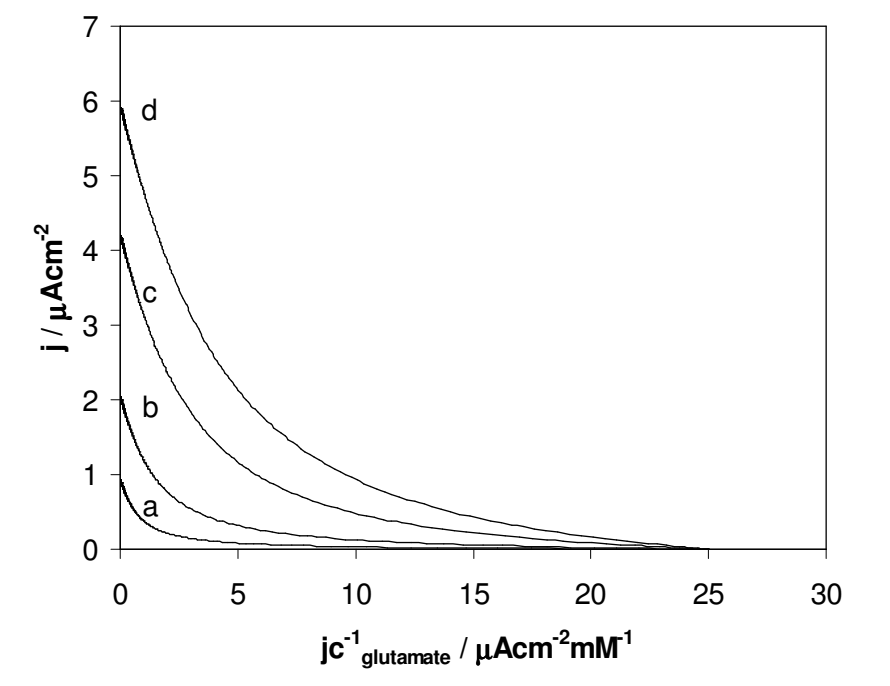
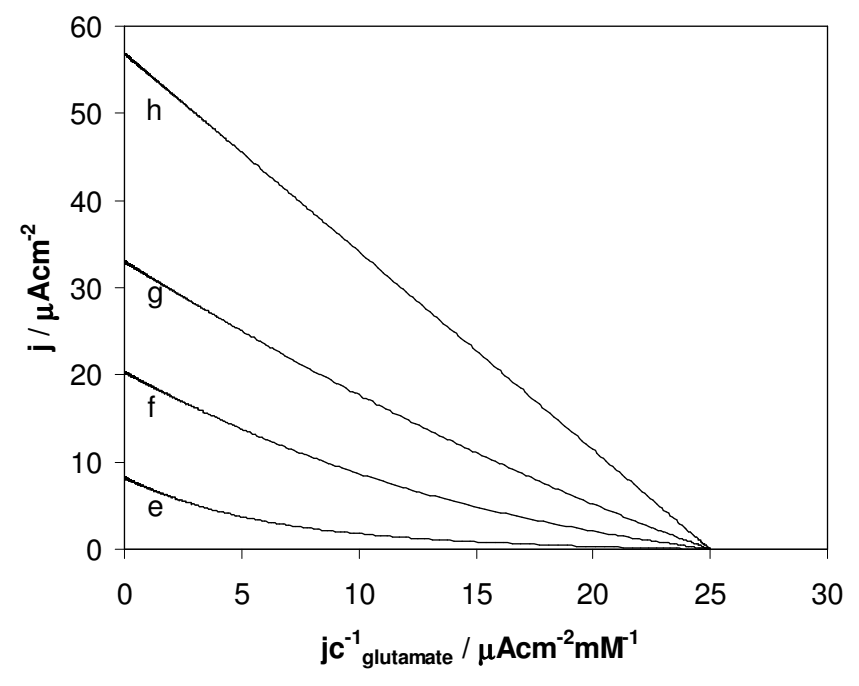


Figure 8

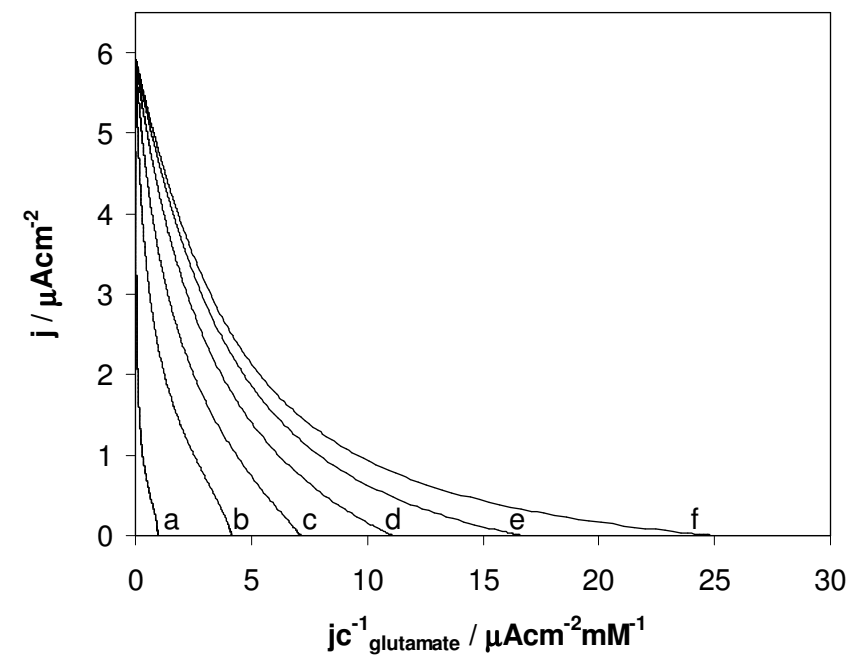


Figure 9

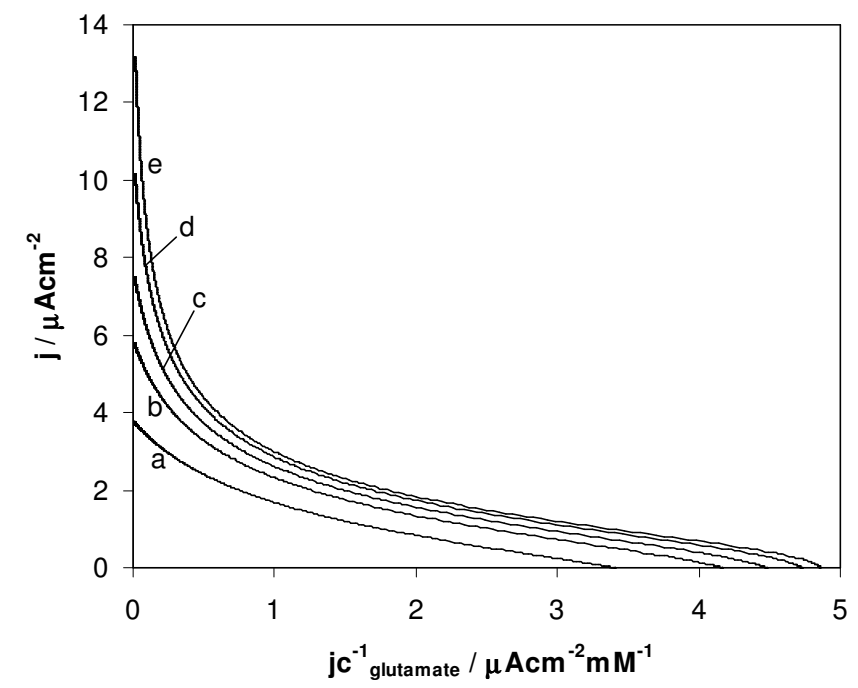
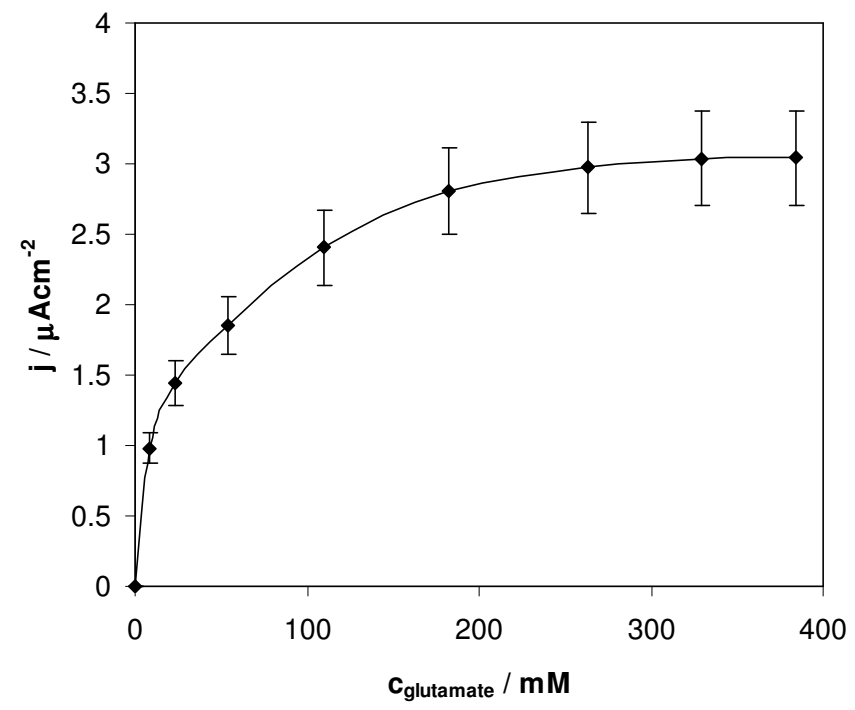
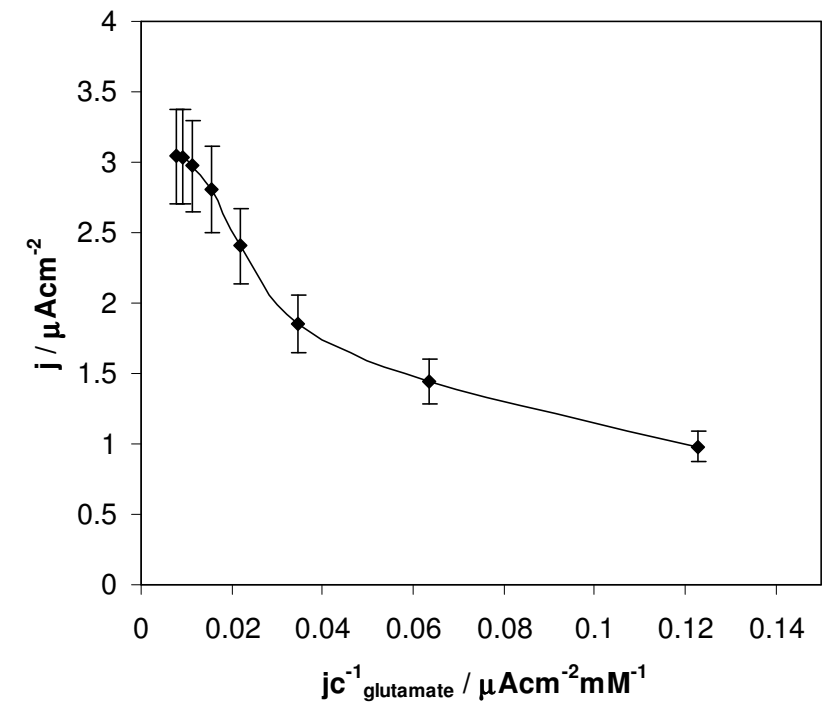


Figure 10



(A)



(B)

Figure 11



Escola Tècnica Superior d'Enginyeria Química

Departament d'Enginyeria Química

**New techniques for the fabrication of
biosensors based on NAD(P)⁺ dependent
dehydrogenases**

Memòria presentada per:

Valeri (Valery) Pavlov

Per optar al grau de

Doctor en Enginyeria Química

Treball dirigit per:

Dr. Ioanis Katakis

Departament d'Enginyeria Química

Tarragona, 2004

**Thesis presented by
Valeri (Valery) Pavlov
In fulfilment of the requirements for the degree
of Philosophy Doctor of Chemical Engineering
Tarragona, 2004**

El Dr. Ioanis Katakis, Profesor Titular del Departamento de Ingeniería Química de la Universidad Rovira i Virgili, director del trabajo de investigación realizado por el Sr. Valeri Pavlov titulado:

**NEW TECHNIQUES FOR THE FABRICATION OF BIOSENSORS BASED ON
NAD(P)⁺ DEPENDENT DEHYDROGENASES**

para optar al grado de Doctor en Ingeniería Química por la Universidad Rovira i Virgili,

HACE CONSTAR:

Que el citado trabajo es original y que todos los resultados presentados y los análisis realizados son fruto de su investigación.

Y para vuestro conocimiento y a los efectos que correspondan, firmo este documento.

Tarragona, Noviembre de 2004

Dr. Ioanis Katakis

ACKNOWLEDGEMENTS

I would like to thank all the persons who helped me to carry out the present study:

First of all, the members of my dissertation committee, for their kind agreement to participate in it and to read this thesis.

Dr. Ioanis Katakis, my scientific advisor, for his strong support, for giving me hope and showing “the light at the end of a tunnel” in difficult moments during the development of this work.

The members of Bioengineering and Bioelectrochemistry Group of the University Rovira I Virgili Dr. Ciara O’Sullivan, Mònica Campàs, Mònica Mir, Gemma Just and Gemma Cristòfol for creating a very friendly psychological environment in our research laboratory.

Dr. Britta Lindholm-Sethson for giving me the opportunity to work during 6 weeks in her laboratory at the Department of Chemistry in the University of Umeå (Sweden), where the study of tensoactive compounds was performed.

Professor Leonidas G. Bachas for being the host of my 6 week stay at the Department of Chemistry in the University of Kentucky (USA), where the biosensors based on thermophilic Glucose-6-phosphate dehydrogenase were constructed with the help of Ramesh B. Iyer.

Dr. Elena Domínguez from the Department of Analytical Chemistry in the University of Alcalá (Spain) and the members of her group Dr. Arántzazu Narváez, Estrella Maestre, Oscar Rincón for their collaboration with me during the work on my thesis.

Dr. Servé Kengen from the Wageningen Agricultural University (Netherlands) for providing me with thermophilic glutamate dehydrogenase and the profound comments on the resulting article.

Dr. Christophe Bengoa for the perfect organisation of my trips to Sweden and the USA.

DINAMIC Technology Innovation Centre for the generous help in the publication of this thesis.

Finally I wish to add that my work in Spain was made possible with the financial support of the European Commission under the Industrial & Materials Technologies Programme (PROMOFILM, Brite-EuRam Programme) project No. BE97-4511, the Spanish Ministry of Education and Culture

Ref.: MAT98-1413.CE, the Ph. D. fellowship from the Department of Chemical Engineering, University Rovira i Virgili and the special grant Ref.: M3C99-80 covering my travelling expenses to Sweden from the University Rovira i Virgili.

RESUMEN DE LA TESIS EN CASTELLANO

Antecedentes

Un avance importante en el campo de química analítica se hizo por Clark y Lyons en los años setenta. Ellos propusieron acoplar la especificidad de la enzima glucosa oxidasa con la transducción electroquímica de la señal en “biosensores”. En general, los biosensores son artefactos integrados autocontenidos, capaces de proporcionar información analítica, cuantitativa utilizando un elemento biológico de reconocimiento (receptor bioquímico) que se retiene en contacto espacial directo con un elemento de transducción. Posteriormente, los primeros biosensores de glucosa, basados en la detección amperométrica de peróxido de hidrógeno generado por glucosa oxidasa en la presencia de oxígeno fueron introducidos en el mercado por la empresa estadounidense Yellow Spring Instrument Co. (Ohio, EE. UU.) en 1975.

La respuesta de biosensores electroquímicos basados en el uso de oxígeno como cosustrato para oxidasas se ve desviada por la presencia de interferencias que pueden contribuir a la corriente. Por lo tanto la superficie de electrodo debe estar protegida por una membrana no permeable por sustancias que pueden interferir con la señal. Para evitar corrientes que perjudican la selectividad de los biosensores, el potencial aplicado puede ser aminorado usando electrocatalizadores difusionales (“mediadores”) en lugar de oxígeno, con un potencial redox controlable. Pero la respuesta de estos sensores también depende de la concentración de oxígeno porque este compite con los mediadores, para la reoxidación de las oxidasas. Un inconveniente adicional del uso de mediadores difusionales artificiales en biosensores es la baja estabilidad de los mismos debida al escape de mediadores desde la superficie del electrodo cuando esto se usa en línea. Se puede aliviar este problema creando enlaces covalentes entre los mediadores y la superficie del electrodo o usando polímeros redox que se adsorben fuértemente en la superficie del electrodo.

Una de las posibles maneras para disminuir la influencia del oxígeno a la corriente de la respuesta de biosensores es el uso de las deshidrogenasas dependientes de la pareja redox NAD^+/NADH . El potencial estándar redox de esta pareja es -0.56 V vs. SCE pero para conseguir la oxidación de NADH en la superficie de electrodos de carbono un sobrepotencial de $+0.5\text{ V vs. SCE}$ debe aplicarse. Bajo estas condiciones los electrodos tienen tiempo de vida corto debido a la adsorción de los productos de oxidación en su superficie ya que la oxidación de NADH no es reversible químicamente. Por otro lado estos electrodos sufren por la oxidación no específica de

interferencias a estos potenciales de operación. Los electrodos modificados químicamente por mediadores pueden oxidar NADH a potenciales más bajos. Sin embargo, muchos de los mediadores mencionados en la bibliografía no son estables o/y no forman NAD^+ enzimáticamente activo. Un problema adicional de los sistemas analíticos basados en deshidrogenasas dependientes de NAD^+ es la necesidad de añadir este cofactor, que tiene alto coste y es inestable, en las muestras. Se puede inmovilizar NAD^+ en la superficie de electrodos para producir biosensores capaces de funcionar en muestras que no contienen NAD^+ , biosensores *reagentless* (sin necesidad de adición de reactivos). Los métodos descritos en la bibliografía para la fabricación de biosensores *reagentless* se basan en cinco estrategias: (1) la inmovilización en hidrogeles formados *in situ*; (2) la inmovilización por una membrana; (3) la inmovilización en películas preparadas por electropolimerización; (4) la inmovilización en una pasta de carbono; (5) la inmovilización en monocapas auto ensambladas. Sólo los electrodos preparados con la estrategia (4) son biosensores *reagentless* con estabilidad operacional relativamente alta. Las demás estrategias no resultan en biosensores con suficiente estabilidad operacional por culpa de la pérdida del mediador, de NAD^+ o de la deshidrogenasa. Sin embargo la estrategia basada en electrodos de pasta de carbono no permite su aplicación a la producción de microsensores (electrodos con diámetro de menos de 10 μm) para su uso *in vivo*.

Metodología

El objetivo principal de esta tesis es el desarrollo de nuevas estrategias para la fabricación de biosensores *reagentless* basados en deshidrogenasas dependientes de NAD^+ con características mejoradas respecto a la densidad de la corriente, de la estabilidad operacional y de almacenamiento.

Para cumplir el objetivo se han sintetizado dos nuevos mediadores para la oxidación de NADH: un polímero insoluble en agua $[\text{Os}(1,10\text{-fenantrolina-5,6-diona})_2(\text{PVP})_4\text{Cl}]\text{Cl}$, (Os-fendiona-PVP) y un complejo anfifílico $[\text{Os}(1,10\text{-fenantrolina-5,6-diona})_2 4,4'-(n\text{-C}_{18}\text{H}_{37}\text{NHCO})_2\text{bpi}](\text{PF}_6)_2$ (Os-fendiona-surfactante). El polímero Os-fendiona-PVP fue producido vía la derivatización de poli(vinilpiridina) (peso molecular 50000) con $[\text{Os}(1,10\text{-fenantrolina-5,6-diona})_2\text{Cl}_2]$. El estudio electroquímico de este polímero redox adsorbido en electrodos de grafito se realizó por voltametría cíclica a distintas velocidades de barrido para evaluar el número de protones y electrones que participan en la reacción redox, la influencia del pH a su potencial estándar formal, y la constante de la transferencia heterogénea de los electrones k_s . Bajo bien definidas condiciones hidrodinámicas se realizaron estudios para encontrar la constante de la interacción con NADH $k_{[\text{NADH}] = 0}$. Os-fendiona-surfactante fue producido por la complejación de $[\text{Os}(1,10\text{-fenantrolina-5,6-diona})_2]\text{Cl}_2$ con el ligando hidrófobo octadodecilamida del ácido 2,2'-Bipiridina-4,4'-dicarboxílico. Las monocapas de Langmuir-Blodgett de Os-fendiona-surfactante y las de su análogo $[\text{Os}(\text{bpi})_2 4,4'-(n\text{-C}_{18}\text{H}_{37}\text{NHCO})_2\text{bpi}](\text{PF}_6)_2$ fueron estudiados en un equipo de Langmuir-Blodgett.

Os-fendiona-surfactante fue aplicado a la construcción de biosensores *reagentless* del glutamato vía la inmovilización de glucosa deshidrogenasa y de NAD^+ entre las bicapas en la fase lamelar formada por Os-fendiona-surfactante y el lípido 1,2-dioleilo-sn-glicero-3-fosfatidilcolina. Dos métodos adicionales para la fabricación de los biosensores *reagentless* de glutamato y glucosa basados en deshidrogenasas fueron desarrollados. Los electrodos del grafito fueron modificados con Os-fendiona-PVP y utilizados para (a) la inmovilización de deshidrogenasa y de NAD^+ en un hidrogel formado por entrecruzamiento de poli(vinilpiridina) modificado por grupos amino con el éter diglicidil de poli(etilenglicol); (b) la inmovilización por adsorción de la deshidrogenasa y del ácido alginico modificado por NAD^+ . Se ha hecho un estudio de los biosensores *reagentless* para calcular sus constantes de Michaelis, el efecto del pH y de la temperatura en su respuesta y su estabilidad operacional. Además se ha comparado la estabilidad operacional a temperaturas elevadas de biosensores de la configuración (a) usando glutamato, glucosa y glucosa-6-fosfato deshidrogenasas termófilas y mesófilas. Por otro lado se han estudiado métodos nuevos para mejorar la estabilidad durante el almacenamiento de sensores de glutamato. Con este fin, se han preparado electrodos utilizando glutamato deshidrogenasa mesófila y termófila con varios estabilizadores.

Conclusiones

1. El polímero $[\text{Os}(1,10\text{-fenantrolina-5,6-diona})_2(\text{PVP})_4\text{Cl}]\text{Cl}$, (Os-fendiona-PVP) para la oxidación de NADH se puede sintetizar por la complejación de $[\text{Os}(1,10\text{-fenantrolina-5,6-diona})_2\text{Cl}_2]$ con poli(vinilpiridina). La adsorción física de este polímero sobre los electrodos de grafito desde su solución en etilenglicol resulta en la formación de una monocapa de este polímero redox en la superficie del electrodo.
2. El proceso redox de este mediador es casi-reversible e implica 4 electrones y 4 protones dentro del rango del pH de 3-6.5. El mediador pierde su estabilidad química en valores de pH más altos que 6.5. Tres ramas lineales en el diagrama de $E^{0'}$ frente a pH con diversas pendientes se observan.
3. La constante heterogénea de la velocidad de transferencia de electrones (k_s) de Os-fendiona-PVP es del mismo orden de magnitud que la de otros mediadores capaces de oxidar NADH mencionados en la bibliografía ($k_s = 18 \pm 2 \text{ s}^{-1}$).
4. Os-fendiona-PVP es un electrocatalizador eficiente para la oxidación del NADH. La modificación de los electrodos del grafito con Os-fendiona-PVP conduce a la disminución del sobrepotencial para la oxidación electroquímica del NADH desde +0.33 V vs. Ag/AgCl/KCl_{sat} para los electrodos no modificados hasta +0.11 V vs. Ag/AgCl/KCl_{sat}. La constante cinética para la interacción del polímero redox con el NADH ($k_{1,[\text{NADH}]=0} = (1.9 \pm 0.2) \times 10^3 \text{ s}^{-1} \text{ M}^{-1}$) coincide prácticamente con la de

Os-fendiona que sugiere que el número de los ligandos de fendiona en los complejos del osmio es proporcional a la corriente de la respuesta al NADH pero no afecta a las constantes cinéticas electroquímicas.

5. El mediador anfifílico para la oxidación del NADH se puede sintetizar con la complejación del complejo $[\text{Os}(1,10\text{-fenantrolina-5,6-diona})_2\text{Cl}_2]$ con el ligando hidrofóbico octadodecilamida del ácido 2,2'-Bipiridina-4,4'-dicarboxílico.

6. El mediador anfifílico para la oxidación NADH forma monocapas de Langmuir-Blodgett estables en la interfaz de agua-aire. Multicapas de este compuesto depositado en la superficie sólida de electrodos por la técnica de Langmuir-Blodgett pierden la actividad electroquímica de 1,10-fenantrolina-5,6-diona probablemente debido a las limitaciones del transporte de protones a través de las monocapas formadas por las cadenas alifáticas hidrófobas.

7. Las características anfifílicas del análogo del compuesto antedicho, que no lleva el ligando del fenantrolina, se han estudiado también. El análogo forma monocapas estables en la interfaz de agua-aire y puede ser depositado en un electrodo sólido con la pérdida parcial de las propiedades electroquímicas del átomo del osmio, debido a la alta hidrofobicidad de las multicapas.

8. Tres nuevas configuraciones, basadas en estos mediadores, fueron desarrolladas para la fabricación de biosensores *reagentless* de glucosa y L-glutamato basados en deshidrogenasas. Las primeras dos configuraciones se basan en la adsorción de Os-fendiona-PVP en la superficie de los electrodos de grafito, seguida por la adsorción de la deshidrogenasa y del ácido algínico modificado con NAD^+ (NAD-alginato) o por la inmovilización de deshidrogenasa y de NAD^+ en un hidrogel formado por poli(vinilpiridina) que lleva grupos amino. La tercera configuración emplea la inmovilización de la enzima y de la coenzima en la fase lamelar creada por una mezcla de mediador anfifílico y un lípido en soluciones acuosas.

9. Se puede mejorar la estabilidad operacional de biosensores a temperaturas elevadas mediante el uso de enzimas termófilas en vez de mesófilas. Esto fue demostrado comparando el funcionamiento de los sensores de glutamato y de glucosa-6-fosfato preparados usando deshidrogenasas mesófilas y termófilas. El uso de enzimas termófilas también permite mejorar drásticamente la estabilidad de almacenamiento de biosensores. Esto se puede explicar en términos de la estabilidad intrínseca más alta de las enzimas termófilas. Algunos estabilizadores como el copolímero de vinilo-pirrolidón y de dimetilamino etil metacrilato denominado como Gafquat[®] HS100 pueden aumentar la estabilidad de almacenamiento de biosensores formando un complejo proteína-polielectrolito.

ABSTRACT

The objective of this work was the development of new configurations of reagentless biosensors based on NAD^+ dependent dehydrogenases. These configurations are based on the immobilisation of enzyme, cofactor and the electrochemical catalyst used for its regeneration. In addition to being reagentless these configurations yielded biosensors with improved current density and operational stability compared to the state of the art.

To achieve the objective two new NADH oxidising mediators were synthesised: a water insoluble polymer $[\text{Os}(1,10\text{-phenanthroline-5,6-dione})_2(\text{PVP})_4\text{Cl}]\text{Cl}$ (Os-phendione-PVP) and an amphiphilic complex $[\text{Os}(1,10\text{-phenanthroline-5,6-dione})_2 4,4'-(n\text{-C}_{18}\text{H}_{37}\text{NHCO})_2\text{bpy}](\text{PF}_6)_2$ (Os-phendione-surfactant). The electrochemical study of Os-phendione-PVP has revealed a rate constant for the heterogeneous electron transfer of the phendione redox couple $k_s = 25 \pm 2 \text{ s}^{-1}$, and a second order rate constant for NADH oxidation $k_{[\text{NADH}] = 0} = (1.1 \pm 0.1) \times 10^3 \text{ M}^{-1} \text{ s}^{-1}$. These constants are higher or of the same order of magnitude as those of previously described NADH oxidising mediators. The tensoactive mediators Os-phendione-surfactant and its analogue $[\text{Os}(\text{bpy})_2 4,4'-(n\text{-C}_{18}\text{H}_{37}\text{NHCO})_2\text{bpy}](\text{PF}_6)_2$ (Os-bpy-surfactant) form very stable monolayers at the air-water interface collapsing at the surface pressure $60\text{-}65 \text{ mN m}^{-1}$.

The Os-phendione-surfactant was used for the construction of reagentless glutamate biosensors via the immobilisation of dehydrogenase and NAD^+ between bilayers in lamellar phase formed by Os-phendione-surfactant and the lipid 1,2-dioleoyl-sn-glycero-3-phosphatidylcholine. The resulting glutamate biosensors demonstrated maximum current density of $3.5 \mu\text{A cm}^{-2}$ (RSD=25%), apparent Michaelis constant of 47 mM, and operational half life of 0.5 h. In addition graphite electrodes were modified by Os-phendione-PVP and utilised for (a) immobilisation of dehydrogenase and NAD^+ in a hydrogel formed by crosslinking of poly(vinylpyridine) carrying amino groups with polyethylene glycol diglycidyl ether and (b) immobilisation of dehydrogenase and an NAD^+ -alginate derivative by adsorption. The configuration (a) yielded glutamate sensors with maximum current density of $8.7 \mu\text{A cm}^{-2}$ (RSD=5%), apparent Michaelis constant of 9.1 mM, operational half life of 12 h and glucose sensors with maximum current density of $37 \mu\text{A cm}^{-2}$ (RSD=14%), apparent Michaelis constant of 4.2 mM, the operational half life of 1 h. The glutamate sensors based on the configuration (b) showed maximum current density of $15.8 \mu\text{A/cm}^2$ (RSD=21%), apparent Michaelis constant of 17.6 mM and operational half life of 1.5 h.

Glucose, glucose-6-phosphate, and glutamate biosensors were prepared and characterised. The employment of the thermophilic enzymes helps to dramatically increase the operational stability of biosensors at elevated temperatures higher than 60°C . The shelf life of glutamate electrodes built with the use of thermophilic dehydrogenase was eleven times longer than this of electrodes modified with the mesophilic enzyme. The addition of the copolymer of vinyl-pyrrolidone and dimethylamino ethyl methacrylate termed as Gafquat HS100 to the enzyme also significantly improved shelf life.

TABLE OF CONTENTS

| | |
|---|--------------|
| 1. INTRODUCTION | 1-32 |
| 1.1 Biosensors..... | 1 |
| 1.2 Coenzymes I and II..... | 2 |
| 1.3 Reactions with participation of NAD(P) ⁺ and dehydrogenases..... | 3 |
| 1.4 Some applications of enzymes..... | 6 |
| 1.5 Chemical regeneration of NAD(P) ⁺ | 7 |
| 1.6 Electrochemical regeneration of NAD(P)H..... | 8 |
| 1.6.1 Direct oxidation of NAD(P)H on bare electrode surfaces..... | 8 |
| 1.6.2 Oxidation of NAD(P)H via enzymes..... | 9 |
| 1.6.3 Oxidation of NAD(P)H by soluble mediators..... | 10 |
| 1.6.4 Oxidation of NAD(P)H on chemically modified electrode surfaces..... | 12 |
| 1.7 Dehydrogenase electrodes..... | 18 |
| 1.8 Thermostable enzymes..... | 25 |
| 1.9 Application of Langmuir-Blodgett techniques for electrode modification..... | 27 |
| 1.10 Challenges..... | 30 |
| 2. EXPERIMENTAL METHODS..... | 33-38 |
| 2.1 The synthesis of new mediators for the oxidation of NADH..... | 33 |
| 2.2 Electrochemical measurements in bulk solution..... | 33 |
| 2.3 Shelf life study of glutamate biosensors..... | 35 |
| 2.4 Glutamate dehydrogenase (GLDH) assay method..... | 36 |
| 2.5 Glucose-6-phosphate dehydrogenase (G6PDH) assay method..... | 37 |
| 2.6 Instrumentation used for the study of amphiphilic compounds..... | 37 |
| 3. GENERAL OVERVIEW OF THE PRESENTED PAPERS..... | 39-47 |
| 4. GENERAL OVERVIEW OF THE PAPERS NOT INCLUDED IN THE THESIS..... | 48-50 |
| 5. CONCLUSIONS..... | 51-53 |
| 6. FUTURE WORK..... | 54-55 |
| 7. BIBLIOGRAPHY..... | 56-62 |
| 8. ARTICLES | |
| 8.1 Electrocatalytic Oxidation of NADH at Graphite Electrodes Modified with Osmium Phenanthroline-dione | |
| 8.2 A Novel [Os(1,10-phenanthroline-5,6-dione) ₂ (PVP) ₄ Cl]Cl Redox Polymer for Electrocatalytic Oxidation of NADH and its Application to the Construction of reagentless β-D-glucose Biosensors | |
| 8.3 New Reagentless Glutamate Biosensors Based on Mesophilic and Thermophilic Glutamate Dehydrogenases | |

8.4 The Use of Lipid Bilayers for the Construction of Reagentless Biosensors Based on NAD⁺ Dependent Glutamate Dehydrogenase

8.5 Amperometric Sensing at High Temperature with a “Wired” Thermostable Glucose-6-phosphate Dehydrogenase from *Aquifex aeolicus*

LIST OF FIGURES

| | |
|---|----|
| Figure 1. Structure of NAD ⁺ and NADP ⁺ | 2 |
| Figure 2. Redox transformation of NAD(P) ⁺ | 3 |
| Figure 3. Schematic diagram of a system for electrochemical NADH recycling based on a mediator..... | 11 |
| Figure 4. Reactions resulting in deactivation of ortho-quinone mediators..... | 13 |
| Figure 5. Observed dependence of reaction rate with NADH on structure of a mediator..... | 15 |
| Figure 6. Proposed mechanistic scheme for NADH oxidation by reaction with a redox mediator..... | 15 |
| Figure 7. Different strategies for the fabrication of reagentless biosensors based on NAD(P) ⁺ dependent dehydrogenases..... | 24 |
| Figure 8. Diagrammatic representation of Langmuir-Blodgett trough..... | 28 |
| Figure 9. Deposition of Langmuir-Blodgett films on a solid substrate..... | 29 |
| Figure 10. The electrochemical cell employed in electrochemical experiments..... | 35 |
| Figure 11. Screen printed electrode used for the preparation of disposable glutamate biosensors..... | 36 |

Figures of the article Electrocatalytic Oxidation of NADH at Graphite Electrodes Modified with Osmium Phenanthroline-dione

| | |
|---|-----|
| Figure 1. Consecutive cyclic voltammograms for phendione of the Os-phendione complex, adsorbed on spectrographic graphite..... | 210 |
| Figure 2. Electrocatalytic oxidation of NADH on Os-phendione modified graphite electrode..... | 211 |
| Figure 3. Levich plot of the steady state electrocatalytic response for an Os-phendione modified graphite RDE at different NADH concentrations..... | 212 |
| Figure 4. Dependence of Log $k_{[NADH]=0}$ on the formal standard potential ($E^{0'}$) for some phenoxazine dyes..... | 214 |

Figures of the article A Novel [Os(1,10-phenanthroline-5,6-dione)₂(PVP)₄Cl]Cl Redox Polymer for Electrocatalytic Oxidation of NADH and its Application to the Construction of reagentless β -D-glucose Biosensors

| | |
|---|----|
| Figure 1. Consecutive cyclic voltammograms at 50 mVs ⁻¹ of Os-phendione-PVP adsorbed on spectrographic graphite..... | 20 |
| Figure 2. Cyclic voltammetry of an electrode modified with Os-phendione-PVP..... | 21 |

| | |
|--|------|
| Figure 3. Cyclic voltammetry of: (a) bare electrode in buffer; (b) bare electrode in 2.4 mM of NADH; (c) electrode modified with Os-phendione-PVP (surface coverage $(1.1\pm 0.2)\times 10^{-10}$ mol/cm ²) in buffer; (d) electrode modified with Os-phendione-PVP (coverage $(1.1\pm 0.2)\times 10^{-10}$ mol/cm ²) in 2.4 mM of NADH..... | 22 |
| Figure 4. Schematic representation of the electron transfer steps for the glucose sensor based on Os-phendione-PVP polymer, NAD ⁺ , and glucose dehydrogenase..... | 23 |
| Figure 5. Cyclic voltammetry of a reagentless glucose biosensor..... | 24 |
| Figure 6. The effect of pH on the response of glucose biosensors | 25 |
| Figure S-1. The synthetic route to Os-phendione-PVP..... | S-11 |
| Figure S-2. The effect of pH on the ratio of phendione peak area to that of osmium atom in cyclic voltammetry | S-11 |
| Figure S-3. The effect of scan rate on the anodic peak current of phendione..... | S-12 |
| Figure S-4. The effect of scan rate on the cathodic peak current of phendione. | S-12 |
| Figure S-5. pH dependence of the formal potential of Os-phendione-PVP for 1,10-phenanthroline-5,6-dione couple..... | S-13 |
| Figure S-6. Variation of ΔE_p as a function of pH..... | S-13 |
| Figure S-7. Experimental variations of E_p as a function of $\log \nu$ for Os-phendione-PVP..... | S-14 |
| Figure S-8. Koutecky-Levich plot of steady state electrocatalytic response for an Os-phendione-PVP modified graphite RDE at different NADH concentrations..... | S-14 |
| Figure S-9. Plot of k^{-1} vs. concentration of NADH for the electrooxidation of NADH at Os-phendione-PVP modified electrodes..... | S-15 |
| Figure S-10. Reaction scheme for a reagentless glucose biosensor..... | S-15 |
| Figure S-11. Simulation of calibration curves (A) and Eadie-Hofstee plots (B) for the reagentless glucose biosensors with varying loading of NAD ⁺ in the hydrogel..... | S-16 |
| Figure S-12. Simulation of calibration curves (A) and Eadie-Hofstee plots (B) for the reagentless glucose biosensors with varying mass transfer coefficient | S-17 |
| Figure S-13. Simulation of calibration curves (A) and Eadie-Hofstee plots (B) for the reagentless glucose biosensors at $A_t \rightarrow \infty$ with varying maximum fluxes of the electrochemical NADH oxidation..... | S-18 |
| Figure S-14. Simulation of calibration curves (A) and Eadie-Hofstee plots (B) for the reagentless glucose biosensors at A_t equal to 20 mM with varying maximum fluxes of the electrochemical NADH oxidation | S-19 |
| Figure S-15. Simulation of calibration curves (A) and Eadie-Hofstee plots (B) for the reagentless glucose biosensors at A_t equal to 2 mM with varying maximum fluxes of the electrochemical NADH oxidation..... | S-20 |

| | |
|---|------|
| Figure S-16. Simulation of calibration curves (A) and Eadie-Hofstee plots (B) for the reagentless glucose biosensors at A_t equal to 0.1 mM with varying maximum fluxes of the electrochemical NADH oxidation..... | S-21 |
| Figure S-17. Simulation of calibration curves (A) and Eadie-Hofstee plots (B) for the reagentless glucose biosensors at $A_t \rightarrow \infty$ with varying maximum fluxes of the enzymatic reduction of NAD^+ | S-22 |
| Figure S-18. Simulation of calibration curves (A) and Eadie-Hofstee plots (B) for the reagentless glucose biosensors at A_t equal to 20 mM with varying maximum fluxes of the enzymatic reduction of NAD^+ | S-23 |
| Figure S-19. Simulation of calibration curves (A) and Eadie-Hofstee plots (B) for the reagentless glucose biosensors at A_t equal to 2.0 mM with varying maximum fluxes of the enzymatic reduction of NAD^+ | S-24 |
| Figure S-20. Simulation of calibration curves (A) and Eadie-Hofstee plots (B) for the reagentless glucose biosensors at A_t equal to 0.1 mM with varying maximum fluxes of the enzymatic reduction of NAD^+ | S-25 |
| Figure S-21. Simulation of calibration curves (A) and Eadie-Hofstee plots (B) for the reagentless glucose biosensors at k'_B equal to $2.591 \times 10^{-11} \text{ cm s}^{-1}$ and $A_t \rightarrow \infty$ with varying maximum fluxes of the enzymatic reduction of NAD^+ | S-26 |
| Figure S-22. Simulation of calibration curves (A) and Eadie-Hofstee plots (B) for the reagentless glucose biosensors at k'_B equal to $2.591 \times 10^{-11} \text{ cm s}^{-1}$ and A_t equal to 20 mM with varying maximum fluxes of the enzymatic reduction of NAD^+ | S-27 |
| Figure S-23. Simulation of calibration curves (A) and Eadie-Hofstee plots (B) for the reagentless glucose biosensors at k'_B equal to $2.591 \times 10^{-11} \text{ cm s}^{-1}$ and A_t equal to 2.0 mM with varying maximum fluxes of the enzymatic reduction of NAD^+ | S-28 |
| Figure S-24. Simulation of calibration curves (A) and Eadie-Hofstee plots (B) for the reagentless glucose biosensors at k'_B equal to $2.591 \times 10^{-11} \text{ cm s}^{-1}$ and A_t equal to 0.1 mM with varying maximum fluxes of the enzymatic reduction of NAD^+ | S-29 |
| Figure S-25. Simulated and experimental calibration curves (A) and Eadie-Hofstee plots (B) for the biosensors prepared using varied loading of GDH per electrode..... | S-30 |
| Figure S-26. Simulated and experimental calibration curves (A) and Eadie-Hofstee plots (B) for the biosensors operating in the reagentless mode prepared using varied loading of GDH per electrode..... | S-31 |
| Figure S-27. The effect of temperature on the response of glucose biosensors..... | S-32 |

Figures of the article New Reagentless Glutamate Biosensors Based on Mesophilic and Thermophilic Glutamate Dehydrogenases

| | |
|--|------|
| Figure 1. Schematic diagram of the electron transfer steps for the mediated glutamate biosensors..... | 22 |
| Figure 2. Cyclic voltammograms of reagentless glutamate biosensors fabricated with the use of mesophilic bovine GLDH based on NAD ⁺ -alginate (A) and the “ binder “ polymer | 23 |
| Figure 3. Effect of pH on maximum response of reagentless glutamate biosensors based on NAD-alginate fabricated with the use mesophilic and thermophilic GLDH..... | 24 |
| Figure 4. Effect of pH on maximum response of reagentless glutamate biosensors based on binder polymer fabricated with the use of mesophilic and thermophilic GLDH..... | 25 |
| Figure 5. Effect of temperature on maximum response of reagentless glutamate biosensors based on NAD ⁺ -alginate fabricated with the use of mesophilic and thermophilic GLDH..... | 26 |
| Figure 6. Effect of temperature on maximum response of reagentless glutamate biosensors based on binder polymer fabricated with the use of mesophilic and thermophilic GLDH..... | 27 |
| Figure S-1. Synthetic route to NADH oxidizing polymer Os-phendione-PVP..... | S-11 |
| Figure S-2. Structure of NAD ⁺ -alginate..... | S-12 |
| Figure S-3. Sketch of a screen printed disposable electrode utilised in the shelf life stability study of glutamate biosensors..... | S-12 |
| Figure S-4. Reaction scheme for a reagentless glutamate biosensor..... | S-13 |
| Figure S-5. Simulation of calibration curves (A) and Eadie-Hofstee plots (B) for the reagentless glutamate biosensors with varying loading of NAD ⁺ in the hydrogel..... | S-14 |
| Figure S-6. Simulation of calibration curves (A) and Eadie-Hofstee plots (B) for the reagentless glutamate biosensors at $k_{cat} \rightarrow \infty$ with varying mass transfer coefficients..... | S-15 |
| Figure S-7. Simulation of calibration curves (A) and Eadie-Hofstee plots (B) for the reagentless glutamate biosensors with varying maximum fluxes of the electrochemical NADH oxidation..... | S-16 |
| Figure S-8. Simulation of calibration curves (A) and Eadie-Hofstee plots (B) for the reagentless glutamate biosensors at $\Gamma_{k_{cat}}$ equal to $8.3 \times 10^{-10} \text{ mol s}^{-1} \text{ cm}^{-2}$ with varying mass transfer coefficients..... | S-18 |
| Figure S-9. Simulation of calibration curves (A) and Eadie-Hofstee plots (B) for the reagentless glutamate biosensors with varying maximum flux of enzymatic reduction of NAD ⁺ | S-19 |
| Figure S-10. Dependence of the apparent current density on L-glutamate concentration (A) and Eadie-Hofstee plots (B) for reagentless biosensors fabricated with the use of mesophilic GLDH based on NAD ⁺ -alginate and binder polymer..... | S-20 |
| Figure S-11. Dependence of the apparent current density on L-glutamate concentration (A) and Eadie-Hofstee plots (B) for reagentless biosensors fabricated with the use of thermophilic GLDH based on NAD ⁺ -alginate and binder polymer..... | S-21 |

| | |
|--|------|
| Figure S-12. Dependence of response current to 0.6 M glutamate, 0.6 M glutamate containing 0.18 M of NAD^+ , and buffer on time obtained in shelf life study for the biosensors based on mesophilic and thermophilic GLDH..... | S-22 |
| Figure S-13. Effect of NAD^+ on the response of graphite electrode in steady-state modified with osmium complex $[\text{Os}(4,4'\text{-dimethyl-2,2'\text{-bipyridine}})_2(1,10\text{-phenanthroline-5,6-dione})](\text{PF}_6)_2$ | S-23 |
| Figure S-14. Koutecky-Levich plot of steady-state electrocatalytic response for graphite RDE modified with $[\text{Os}(4,4'\text{-dimethyl-2,2'\text{-bipyridine}})_2(1,10\text{-phenanthroline-5,6-dione})](\text{PF}_6)_2$ in the presence of 20 mM NAD^+ at different NADH concentrations..... | S-23 |

Figures of the article The Use of Lipid Bilayers for the Construction of Reagentless Biosensors Based on NAD^+ Dependent Glutamate Dehydrogenase.

| | |
|---|------|
| Figure 1. Schematic diagram of the electron transfer steps for the mediated glutamate biosensors..... | 10 |
| Figure 2. Surface pressure/area isotherm for Os-phendione-surfactant..... | 11 |
| Figure 3. Cyclic voltammograms of reagentless glutamate biosensors in the absence of glutamate and the presence 0.35 M glutamate..... | 12 |
| Figure 4. Effect of pH on maximum response of reagentless glutamate biosensors..... | 13 |
| Figure 5. Effect of temperature on maximum response of reagentless glutamate biosensors..... | 14 |
| Figure 6. Dependence of the steady apparent current density on L-glutamate concentration (A) and the Eadie-Hofstee plots (B) for reagentless biosensors..... | 15 |
| Figure S-1. Synthetic route to the NADH oxidizing tensoactive mediator Os-phendione-surfactant..... | S-6 |
| Figure S-2. Reaction scheme for a reagentless glutamate biosensor..... | S-7 |
| Figure S-3. Simulation of the Eadie-Hofstee plots for the reagentless glutamate biosensors with varying maximum fluxes of the electrochemical NADH oxidation..... | S-8 |
| Figure S-4. Simulation of the Eadie-Hofstee plots for the reagentless glutamate biosensors with varying mass transfer coefficients..... | S-9 |
| Figure S-5. Simulation of the Eadie-Hofstee plots for the reagentless glutamate biosensors with varying maximum flux of enzymatic reduction of NAD^+ | S-10 |

Figures of the article Amperometric Sensing at High Temperature with a “Wired” Thermostable Glucose-6-phosphate Dehydrogenase from *Aquifex aeolicus*

| | |
|--|------|
| Figure 1. Reaction scheme for the mediated electrodes and chemical structure of the Os-phendione-PVP mediator..... | 3899 |
|--|------|

| | |
|--|------|
| Figure 2. Cyclic voltammograms of immobilized Os-phenadione-PVP at 70 °C in 0.100 M Na ₂ HPO ₄ /HCl, 0.500 M NaCl, pH 7.00 containing (a) no NADH (b) 2.4 mM NADH (c) 4.7mM NADH, and (d) 6.9 mM NADH..... | 3900 |
| Figure 3. Calibration curve for tG6PDH-based biosensing system in 0.100 M Na ₂ HPO ₄ /HCl, 0.500 M NaCl containing 30 mM NAD, pH 6.80 at 70 °C..... | 3900 |
| Figure 4. Response curve of tG6PDH and mG6PDH biosensors as a function of temperature..... | 3900 |

LIST OF TABLES

| | |
|---|----|
| Table I. Immobilized NADH oxidizing small molecules reported in literature | 14 |
| Table II. Immobilized NADH oxidizing polymers reported in literature | 17 |
| Table III. Configurations of reagentless electrodes based on NAD(P) ⁺ dependent dehydrogenases | 21 |

Tables of the article Electrocatalytic Oxidation of NADH at Graphite Electrodes Modified with Osmium Phenanthroline-dione

| | |
|---|-----|
| Table 1. Results of data interpretation for electrocatalytic NADH oxidation at an Os-phenadione Modified RDE..... | 213 |
| Table 2. pH dependence of the rate constant for the NADH electrocatalytic oxidation at an Os-phenadione modified graphite electrode (Koutecky-Levich interpretation)..... | 213 |

Tables of the article A Novel [Os(1,10-phenanthroline-5,6-dione)₂(PVP)₄Cl]Cl Redox Polymer for Electrocatalytic Oxidation of NADH and its Application to the Construction of reagentless β-D-glucose Biosensors

| | |
|---|------|
| Table I. Effect of pH on the peak width at half peak height E_{fwhm} | 17 |
| Table II. Results of data interpretation for electrocatalysis of NADH oxidation at Os-phenadione-PVP modified RDE at pH 6.0 and 5.0..... | 17 |
| Table S-I. Characteristics of glucose biosensors operating in the presence of 26 mM NAD ⁺ calculated from Eadie-Hofstee plots and fitting by the non-linear regression analysis..... | S-10 |
| Table S-II. Characteristics of glucose biosensors operating in reagentless mode calculated from Eadie-Hofstee plots and fitting by the non-linear regression analysis..... | S-10 |

Tables of the article New Reagentless Glutamate Biosensors Based on Mesophilic and Thermophilic Glutamate Dehydrogenases

| | |
|---|------|
| Table I. Activation energies of the reagentless glutamate biosensors calculated from Arrhenius plots..... | 16 |
| Table II. Basic characteristics of reagentless glutamate biosensors calculated from Eadie-Hofstee plots. | 17 |
| Table S-I. Effect of maximum flux of the electrochemical NADH oxidation on apparent Michaelis constants and maximum current densities given by simulated Eadie-Hofstee plots in the range of high glutamate concentrations..... | S-10 |
| Table S-II. Effect of mass transfer constants on the apparent Michaelis constants and maximum current densities given by simulated Eadie-Hofstee plots in the range of high glutamate concentrations. | S-10 |
| Table S-III. Effect of the maximum flux of the enzymatic reduction of NAD^+ (LV_1) on apparent Michaelis constants and maximum current densities given by simulated Eadie-Hofstee plots in the range of high glutamate concentrations..... | S-10 |
| Table S-IV. Data of shelf life study of glutamate biosensors..... | S-11 |

Tables of the article The Use of Lipid Bilayers for the Construction of Reagentless Biosensors Based on NAD^+ Dependent Glutamate Dehydrogenase

| | |
|--|---|
| Table I. Basic characteristics of the reagentless glutamate biosensors calculated from the Eadie-Hofstee plot..... | 9 |
|--|---|

LIST OF ABBREVIATIONS

| | |
|----------------------------|---|
| Ag/AgCl/KCl _{sat} | standard silver/silver chloride electrode |
| bpy | 2,2'-bipyridine |
| B | base |
| DH | dehydrogenase |
| 3,4-DHB | 3,4-dihydroxybenzaldehyde |
| E | enzyme |
| Gafquat [®] HS100 | copolymer of vinyl-pyrrolidone and dimethylamino ethyl methacrylate |
| GDH | glucose dehydrogenase |
| GLDH | glutamate dehydrogenase |
| G6P | glucose-6-phosphate |
| LB | Langmuir-Blodgett |
| M _{ox} | oxidised form of a mediator |
| M _{red} | reduced form of a mediator |
| NAD ⁺ | nicotinamide adenine dinucleotide |
| NADP ⁺ | nicotinamide adenine dinucleotide phosphate |
| NADH | reduced form of nicotinamide adenine dinucleotide |
| NADPH | reduced form of nicotinamide adenine dinucleotide phosphate |
| P | product |
| PVP | poly(4-vinylpyridine) |
| PVI | poly(vinylimidazole) |
| PQQ | pyrroloquinolinequinone |
| phenanthroline | 1,10-phenanthroline-5,6-dione |
| Q | quinone |
| RDE | rotating disk electrode |
| S | substrate |
| SCE | standard calomel electrode |
| UV | ultra violet |

LIST OF SYMBOLS

| | |
|----------------------------------|---|
| A | the electrode surface area (cm^2) |
| c_{NADH} | concentration of NADH (M) |
| C | concentration (M) |
| D | diffusion coefficient ($\text{cm}^2 \text{s}^{-1}$) |
| $E^{0'}$ | formal standard potential (V) |
| E_{pa} | anodic peak potential (V) |
| E_{pc} | cathodic peak potential (V) |
| ΔE_{p} | peak-to-peak potential separation (V) |
| $[E_{\text{t}}]$ or e_{Σ} | total enzyme concentration (mM) |
| I_{pa} | anodic peak current (A) |
| I_{pc} | cathodic peak current (A) |
| I_{cat} | the current of electrocatalytical NADH oxidation at the electrodes modified with the mediator (A) |
| j_{el} | the flux ($\text{mol cm}^{-2} \text{s}^{-1}$) |
| K_{M} | Michaelis-Menten constant (mM) |
| K_{i} | formal Michaelis-Menten constant for substrate i (mM) |
| K_{eq} | equilibrium constant (mM) |
| K_{ij} | inhibition constant for substrate j (mM) |
| k_{S} | heterogeneous electron transfer rate constant (s^{-1}) |
| k_1 | the rate constant of the reaction between NADH oxidizing mediator and NADH ($\text{M}^{-1} \text{s}^{-1}$) |
| k_{-1} | the rate constant of the decomposition of the mediator-NADH complex into NADH and the oxidized mediator (s^{-1}) |
| k_2 | the rate constant of the decomposition of mediator-NADH complex into the reduced mediator and NAD^+ (s^{-1}) |
| k_1', k_2', k_3' | rate constants of the enzymatic reactions in forward direction ($\text{M}^{-1} \text{s}^{-1}$, s^{-1} , and s^{-1} respectively) |
| $k_{-1}', k_{-2}', k_{-3}'$ | rate constants of the enzymatic reactions in backward direction (s^{-1} , s^{-1} , and $\text{M}^{-2} \text{s}^{-1}$ respectively) |
| k'_i | mass transfer rate coefficient for the substrate i (cm s^{-1}) |
| L | thickness (cm) |
| n | number of electrons |
| Q | charge (C) |

| | |
|-------|--|
| t | time (s) |
| v | overall reaction rate (M s^{-1}) |
| V_1 | maximum velocity in the forward direction (M s^{-1}) |
| V_2 | maximum velocity in the backward direction (M s^{-1}) |

Greek letters

| | |
|------------|--|
| α | transfer coefficient |
| Γ | surface coverage (mol cm^{-2}) |
| Π | surface pressure (N m^{-1}) |
| ν | hydrodynamic viscosity ($\text{cm}^2 \text{s}^{-1}$) |
| ω | rotation speed (rad s^{-1}) |
| υ | scan rate (V s^{-1}) |

1. INTRODUCTION

1.1 Biosensors

Analytical chemistry plays an important role in our everyday life because almost every sector of industry and public service relies on quality control. The majority of chemical analysis methods are time-consuming and heavily employ expensive reagents and equipment in order to achieve high selectivity and low detection limits. A serious breakthrough in this field was announced by professor Leland C. Clark in 1962 at a New York Academy of Sciences symposium who described the concept of construction of electrochemical devices for the rapid, cheap, selective, and sensitive glucose analysis produced by the immobilisation of the enzyme glucose oxidase in the vicinity of an electrochemical oxygen sensor [Clark and Lyons, 1962]. Then, having significantly improved the design of this sensor, Updike and Hicks [1967] reported the first functional biosensor for glucose.

According to the latest definition by IUPAC [Thevenot et al., 1999] an electrochemical biosensor is a self-contained integrated device, which is capable of providing specific quantitative or semi-quantitative analytical information using a biological recognition element (biochemical receptor) which is retained in direct spatial contact with an electrochemical transduction element. Biosensors which do not need any additional reagents in a sample solution for the detection of an analyte, because they have all the components necessary for the reaction sequence, are called reagentless biosensors.

The first commercially available glucose biosensors, based on the amperometric detection of hydrogen peroxide generated by glucose oxidase, were delivered on the market by the Yellow Springs Instruments Company (Ohio, USA) in 1975. Since then many serious players in the field of medical diagnostics, such as Bayer, Boehringer Mannheim, Eli Lilly, Lifescan, DKK Corporation etc., invested in the development and the mass scale production of biosensors, which are utilised in health care [Alcock and Turner, 1994], environmental monitoring [Dennison and Turner, 1995], food and drink [Kress-Rogers, 1996], the process industries [White and Turner, 1997], defense and security.

Electrochemical biosensors employ redox enzymes as recognition elements. The use of oxidases and dehydrogenases has been extensively demonstrated in the literature. The biggest class of dehydrogenases includes dehydrogenases dependent on coenzymes I and II.

1.2 Coenzymes I and II

The full structure of codehydrogenase I was discovered by von Euler with coworkers [von Euler et al., 1936, von Euler et al., 1937] by hydrolysis that gave D-ribose-phosphoric acid, adenine and nicotinamide. The establishment of the constituents of codehydrogenase II was completed by Kornberg and Pricer [Kornberg and Pricer, 1950] through enzymatic degradation yielding adenosine-2',5'-diphosphate and nicotinamide nucleotide. Therefore the Enzyme Commission of the International Union of Biochemistry and Biological Chemistry Nomenclature Commission of the International Union of Pure and Applied Chemistry recommended the name nicotinamide adenine dinucleotide (NAD^+) for codehydrogenase I and nicotinamide adenine dinucleotide phosphate (NADP^+) for codehydrogenase II [Dixon, 1960]. The structure of NAD^+ and NADP^+ is depicted in Figure 1.

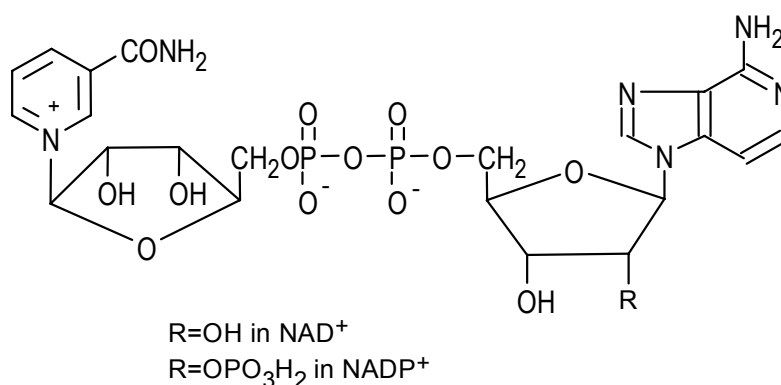


Figure 1. Structure of NAD^+ and NADP^+ .

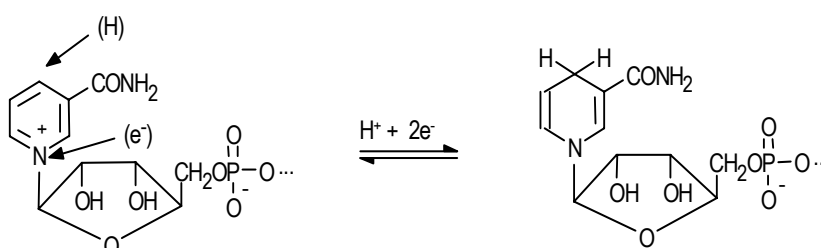
Many apoenzymes (dehydrogenases) combine with these coenzymes, performing the dehydrogenation of a great number of substrates. The structure of every apoenzyme controls the specificity of the reaction between NAD(P)^+ and corresponding substrate. More than 300 NAD(P)^+ dependent dehydrogenases have been discovered [Nomenclature Committee of the International Union of Biochemistry, 1984] and every year this list is extended.

All animal and plant cells, metabolising carbohydrates, contain NAD^+ . For example the concentration of NAD^+ in fresh yeast is 0.5 g per kg. The heart muscle of man contains about 0.4 g of NAD^+ per kg. NADP^+ occurs in all living cells in association with NAD^+ and the ratio of these coenzymes depends on the type of tissue. Yeast cells contain very small amount of NADP^+ , but there are animal tissues containing up to 80 μg of NADP^+ per g [Adler et al., 1939].

The study of the redox mechanism explaining the inter-convertibility of NAD(P)^+ and NAD(P)H was carried out by Karrer and coworkers [Karrer and Warburg, 1936; Karrer et al., 1936; Karrer and Benz, 1936; Karrer et al., 1937]. Their goal was to test the working hypothesis

INTRODUCTION

that the redox behaviour of the two cofactors is caused by the presence of nicotinamide moiety. For that purpose a number of nicotinamide derivatives were synthesised as model compounds and their UV adsorption spectra were compared with these of coenzymes in oxidised and dihydro form. It was found that only the dihydropyridine derivatives with an sp^3 hybridised nitrogen atom in the ring and dihydro coenzymes have UV spectra with two absorption peaks at 260 and 340 nm, meanwhile the oxidised derivatives carrying an sp^2 hybridised nitrogen atom in the aromatic pyridine ring and oxidised cofactors had only one peak at 260 nm. The group of Karrer arrived to the conclusion that the reduction of the coenzymes occurs in ortho position. Later, when deuterium was used as a tracer it was established that the reduction of $NAD(P)^+$ takes place in the para rather



than in the ortho position [Pullman et al., 1954] and can be represented according to Figure 2.

Figure 2. Redox transformation of $NAD(P)^+$.

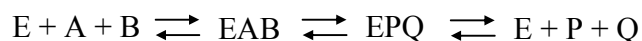
The reduction of $NAD(P)^+$ to $NAD(P)H$ requires two reducing agents per molecule: one electron (e^-) and one hydrogen atom ($H=H^+ + e^-$), which together can be regarded as a hydride ion (H^-). The redox properties of NAD^+ and $NADP^+$ are identical but in nature they act as coenzymes for enzymes participating in different metabolic pathways: $NADP^+$ is normally used by apoenzymes playing anabolic function, whereas enzymes reducing NAD^+ participate in catabolic transformations and the produced $NADH$ serves as an energy source.

1.3 Reactions with participation of $NAD(P)^+$ and dehydrogenases

$NAD(P)^+$ dependent dehydrogenases need for operation a coenzyme, which can be regarded as enzymatic substrate, and at least one more substrate, hence the theory of two-substrate reactions can be applied here. Two substrate reactions can be divided into two categories.

(1). *Reactions with the participation of a ternary complex, containing enzyme and both substrates*

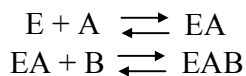
These reactions can be represented as follows



This mechanism, can be further subdivided:

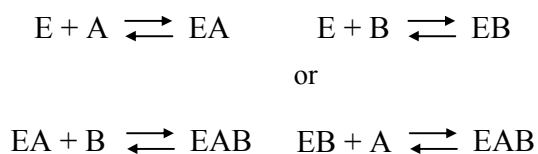
INTRODUCTION

(1a). The reactions in which the ternary complex is formed in ordered manner. For example the substrate B can bind to the enzyme only if the substrate A had bound before:

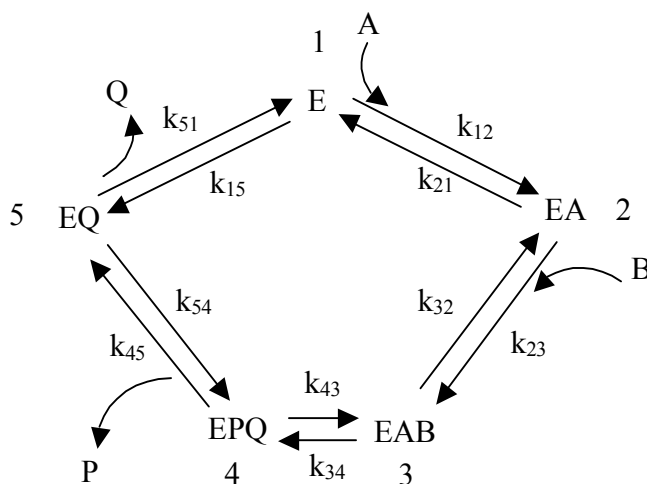


For example, the oxidation of L-lactate by NAD^+ dependent lactate dehydrogenase. It was found that when NAD^+ binds to the enzyme there is no detectable binding of lactate, hence it was concluded that NAD^+ binding precedes that of lactate [Holbrook et al., 1975]. Binding of NAD^+ to the enzyme precedes also in the oxidation of L-malate by malate dehydrogenase, this fact was discovered by isotope labelling of NAD^+ with ^{14}C [Silverstein and Sulebele, 1969].

(1b). The reactions in which either substrate can bind first i.e. the ternary complex is formed in a random manner



The reactions catalysed by NAD^+ dependent alcohol dehydrogenase from yeast proceed via random ternary complex mechanism [Fromm, 1979].



For the ordered ternary complex mechanism the following equation the overall reaction rate v can be derived:

$$v = \frac{V_1([A][B] - [P][Q]/K_{eq})}{K_{ia}K_b + K_b[A] + K_a[B] + [A][B] + K_{ia}K_b[P]/K_{ip1} + K_{ia}K_b[Q]/K_{iq} + K_b[A][P]/K_{ip1} + K_a[B][Q]/K_{iq} + K_{ia}K_b[P][Q]/K_pK_{iq} + [A][B][P]/K_{ip2} + K_a[B][P][Q]/(K_{ip3}K_{iq})}$$

INTRODUCTION

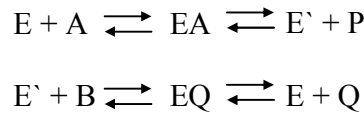
Where: the Michaelis constants for the substrates A and B are $K_a = k_{34}k_{45}k_{51}/(k_{12}(k_{34}k_{45} + k_{34}k_{51} + k_{45}k_{51} + k_{43}k_{51}))$, $K_b = k_{51}(k_{32}k_{45} + k_{34}k_{45} + k_{32}k_{43})/(k_{23}(k_{34}k_{45} + k_{34}k_{51} + k_{45}k_{51} + k_{43}k_{51}))$, for the products P and Q $K_p = k_{21}(k_{32}k_{45} + k_{32}k_{43} + k_{34}k_{45})/(k_{54}(k_{21}k_{32} + k_{21}k_{34} + k_{21}k_{43} + k_{32}k_{43}))$, $K_q = k_{21}k_{32}k_{43}/(k_{15}(k_{21}k_{32} + k_{21}k_{34} + k_{21}k_{43} + k_{32}k_{43}))$, the maximum velocity in the forward direction $V_1 = k_{33}k_{45}k_{51}[E_t]/(k_{34}k_{45} + k_{34}k_{51} + k_{45}k_{51} + k_{43}k_{51})$, $[E_t]$ is total enzyme concentration, the equilibrium constant $K_{eq} = k_{12}k_{23}k_{34}k_{45}k_{51}/(k_{15}k_{21}k_{32}k_{43}k_{54})$, the inhibition constants for A, Q and P are $K_{ia} = k_{21}/k_{12}$, $K_{iq} = k_{51}/k_{15}$, $K_{ip1} = k_{51}(k_{32}k_{45} + k_{34}k_{45} + k_{32}k_{43})/(k_{32}k_{43}k_{54})$, $K_{ip2} = (k_{34}k_{45} + k_{34}k_{51} + k_{51}k_{45} + k_{51}k_{43})/(k_{34}k_{54} + k_{43}k_{54})$, $K_{ip3} = k_{34}k_{45}/(k_{54}k_{34} + k_{54}k_{43})$

The initial rate of reaction (in the absence of P and Q) is:

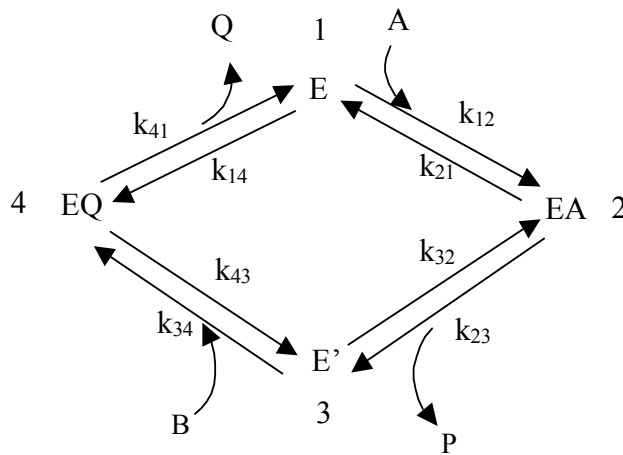
$$v = \frac{V_1[A][B]}{K_{ia}K_b + K_b[A] + K_a[B] + [A][B]}$$

(2). Reactions which do not involve a ternary complex

These reactions are governed by enzyme substitution or ping-pong mechanisms. The second substrate interacts with the enzyme, which has been modified by the first substrate:



The rate equation for this reaction can be derived on the basis of the following mechanism:



$$v = \frac{V_1([A][B] - [P][Q]/K_{eq})}{K_b[A] + K_a[B] + [A][B] + K_{ia}K_b[P]/K_{ip} + K_aK_{ib}[Q]/K_{iq} + K_b[A][P]/K_{ip} + K_a[B][Q]/K_{iq} + K_aK_{ib}(P)(Q)/K_pK_{iq}}$$

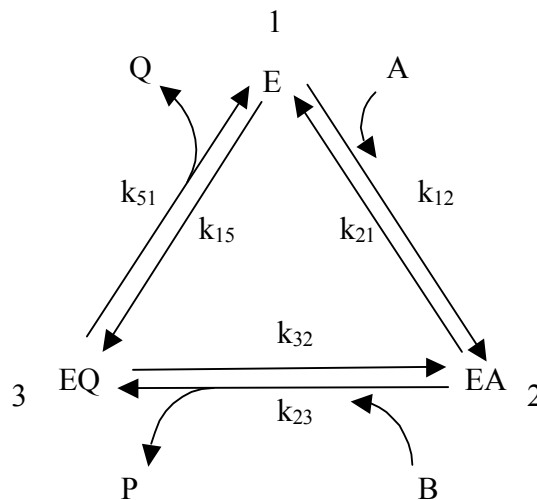
INTRODUCTION

Where: the Michaelis constants for the substrates A and B are $K_a = (k_{21}k_{34}k_{41} + k_{23}k_{34}k_{41} + k_{12}k_{23}k_{43}) / (k_{12}k_{23}k_{34} + k_{12}k_{23}k_{41})$, $K_b = k_{41} / (k_{34} + k_{41})$, for the product P $K_p = (k_{21}k_{43} + k_{23}k_{43}) / (k_{21}k_{32} + k_{32}k_{43})$, the maximal velocity in the forward direction $V_1 = k_{34}k_{41}[E_t] / (k_{34} + k_{41})$, $[E_t]$ is total enzyme concentration, the equilibrium constant $K_{eq} = k_{12}k_{23}k_{34}k_{41} / (k_{14}k_{21}k_{32}k_{43})$, the inhibition constants for A, B, Q and P are $K_{ia} = k_{21} / k_{12}$, $K_{ib} = k_{43} / k_{34}$, $K_{iq} = (k_{21}k_{34}k_{41} + k_{23}k_{34}k_{41} + k_{12}k_{23}k_{43}) / (k_{14}k_{21}k_{34} + k_{14}k_{23}k_{34})$, $K_{ip} = k_{41}k_{23} / (k_{32}k_{41} + k_{32}k_{43})$.

In this case the initial rate of reaction becomes:

$$v = \frac{V_1[A][B]}{K_b[A] + K_a[B] + [A][B]}$$

Another reaction in which no central complex is formed at all proceeds through the mechanism proposed by Theorell and Chance for the oxidation of ethanol by NAD^+ dependent alcohol dehydrogenase from horse liver [Theorell and Chance, 1951; Dalzier and Dickinson, 1966]:



The reaction rate of a reaction governed by this mechanism follows:

$$v = \frac{(k_{12}k_{23}k_{31}[A][B] - k_{21}k_{32}k_{13}[P][Q])[E_t]}{k_{21}k_{31} + k_{12}k_{31}[A] + k_{23}k_{31}[B] + k_{12}k_{23}[A][B] + k_{21}k_{32}[P] + k_{21}k_{13}[Q] + k_{32}k_{13}[P][Q] + k_{12}k_{32}[A][P] + k_{23}k_{13}[B][Q]}$$

Or in the absence of P, Q

$$v = \frac{k_{12}k_{23}k_{31}[A][B][E_t]}{k_{21}k_{31} + k_{12}k_{31}[A] + k_{23}k_{31}[B] + k_{12}k_{23}[A][B]}$$

$$k_{21}k_{31} + k_{12}k_{31}[A] + k_{23}k_{31}[B] + k_{12}k_{23}[A][B]$$

1.4 Some applications of enzymes

In nature enzymes allow chemical reactions to occur within the homeostasis constraints of living systems operating as organic catalysts and enzymes are substrate specific. These properties make enzymes very useful in many areas of human activity.

The specificity of enzymes is widely exploited in analytical chemistry for quantitative and qualitative analyses. The capacity of enzymes to catalyse chemical reactions under mild conditions can be exploited in chemical reactors and fuel cells where enzymes or whole living cells are utilised as catalysts. The highest specific activity, in terms of weight of enzyme and support is desirable in enzyme reactors. The employed support also should perform the function of separation, because if this takes place simultaneously with reaction unfavourable equilibria can be displaced. Possible supports are molecular sieves, glass, silica; membranes of Celite, Bentonite, alumina, graphite and titanium oxide. Changes in physical and chemical properties of the immobilised enzymes have been seen. The stability of enzymes can either increase or decrease on insolubilisation, depending on whether the carrier and the procedure for the immobilisation denatures or stabilizes the proteins.

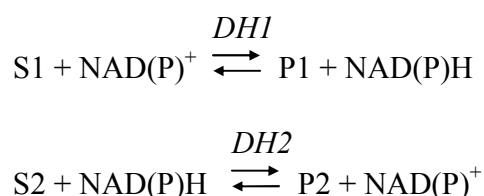
The specific activity of an enzyme usually decreases upon insolubilisation because of denaturation of the enzymic proteins. The apparent Michaelis constants of the immobilised enzymes are affected by the diffusion limitation of the substrate and normally are higher than those of free enzymes in a solution, but if a substrate has opposite charge to the carrier matrix then the apparent Michaelis constants of immobilised enzymes decrease. In some cases diffusional limitation may be an advantage, because the immobilised enzymes may be protected by inhibitor molecules.

1.5 Chemical regeneration of NAD(P)⁺

In order to use the selective advantages of NAD(P)⁺ dependent enzymes in bioreactors it was essential to solve the practical problem of coenzyme recycling. For example, it is known that the carbonyl group is one of the most significant functionalities in synthesis. The control of chirality of the reaction product in the course of reduction or oxidation of ketones and aldehydes is obviously very important. To achieve this goal the methods of classical organic synthesis use bulky groups in reagents with the purpose to hinder approach from one of the two enantiotropic faces of the carbonyl group. The use of enzymes could simplify the synthetic routes thanks to the presence of the proteic three-dimensional structure which controls the direction of attack but

dehydrogenases require quite expensive cofactors. Coenzyme recycling can be accomplished by use of added chemical oxidising or reducing agents. In case of need of NAD(P)H for the enzymatic reduction it can be regenerated by sodium dithionate. If NAD(P)⁺ is required for the enzymatic oxidation then N-(2,3,4,6-tetraacetyl-D-glycopyranosidyl)-3-carbamoylpyridinium bromide, N-(2,3,4,6-tetraacetyl-β-D-glucopyranosidyl)-3-acetylpyridinium bromide, N-(2,6-dichlorobenzyl)-3-nitropyridinium bromide, N-(4-nitrobenzyl)-3-nitropyridinium bromide, N-benzoylmethyl-3-nitropyridinium bromide, and N-methyl-3,5-dinitropyridinium flourosulfonate can be applied to recycling [Jones and Beck, 1976; Jones and Taylor, 1976].

Recycling of NADH also can be performed by coupling the enzymatic reaction producing NAD(P) (where the substrate S1 is oxidised by NAD(P)⁺ through the dehydrogenase *DH1* to give the product P1 and the reduced coenzyme NAD(P)H) with another enzymatic reaction which consumes NAD(P)H (where the substrate S2 is reduced by NAD(P)H through the dehydrogenase *DH2* to give the product P2 and the oxidised coenzyme NAD(P)⁺ according to the scheme:

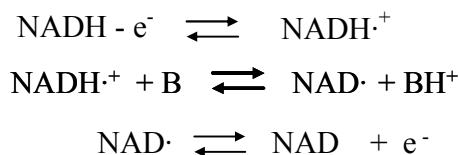


For example galactose dehydrogenase, alanine dehydrogenase, and dextran bound NAD⁺ were immobilised in a bioreactor, which produced alanine and galactonate from pyruvate and galactose [Davies and Mosbuch, 1974]. Another reactor containing rabbit muscle lactate dehydrogenase, horse liver alcohol dehydrogenase and poly(ethylene glycol)-bound NAD⁺ was used for the production of lactate and acetic aldehyde from pyruvate and ethanol [Katayama et al., 1983].

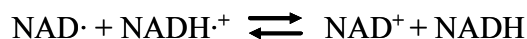
1. 6 Electrochemical regeneration of NAD(P)H

1.6.1 Direct oxidation of NAD(P)H on bare electrode surfaces

An alternative to chemical and enzymatic regeneration of NAD(P)H in organic synthesis and enzymatic analysis is the electrochemical oxidation. The formal redox potential of the NAD⁺/NADH couple is -0.56 V vs. SCE (at pH 7.0) but the first intents of direct NADH oxidation on solid carbon electrodes [Moiroux and Elving, 1979a; 1979b; 1980] demonstrated that very high overpotential must be applied (+0.5 - 0.7 V vs. SCE). The speculated mechanism [Blankespoor and Miller, 1984; Hapiot et al., 1990; Fukusumi et al., 1987] of the oxidation reaction on bare electrodes is:

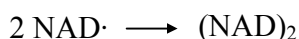


It is very possible that a disproportionation reaction also takes place:



where **B** is a base and $\text{NADH}^{\cdot+}$ and NAD^{\cdot} are the intermediate radicals.

It is thought that the direct oxidation of NADH yields enzymatically active NAD^+ [Bonnefoy et al., 1988; Fassouane et al., 1990]. The solid carbon electrodes showed short lifetime due to fouling caused by adsorption of $(\text{NAD})_2$ dimers (formed by the following reaction) on the electrode surface when the NADH concentration is more than 0.5 mM [Jaegfeldt et al., 1981].

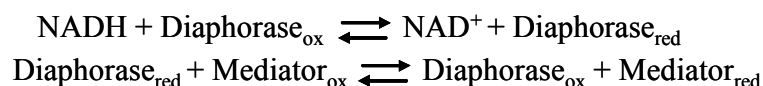


Another probable reason for this deactivation is the formation of stable adducts between surface species and reaction radical intermediates [Jaegfeldt et al., 1983]. Probably the reason for the yields of NADH oxidation less than 100% and generally, the main limiting factor in the systems based on NADH recycling, is the low stability of this reduced cofactor due to its hydrolysis in aqueous solutions at low values of pH. It was shown that the half life time of NADH in solution at pH 6.0 is 9 hours [Hedemno et al., 1996] meanwhile at pH 7.5 half life-time is 17 hours [Wong and Whitesides, 1981; Bonnefoy et al., 1988].

The necessity to apply high overpotential is a real drawback for applications of carbon and platinum electrodes in biosensors because of the presence of interferents, having low redox potentials, in real samples. The use of silver as the electrode material helps to decrease the potential of direct NADH oxidation to +0.23 V vs. SCE [Li et al., 1996]. It is also reported that screen printed thick-film gold electrodes can be utilised for NADH detection at relatively low overpotential of +0.145 V vs. SCE with minimised fouling [Silber et al., 1995], but it has not reported if the reaction product, generated by silver or thick-film gold electrodes, retains enzymatic activity.

1.6.2 Oxidation of NAD(P)H via enzymes

One of the options for lowering the applied potential for NAD(P)H oxidation is to employ enzymatic recycling of reduced cofactors by diaphorases or NADH oxidases according to the following sequence of reactions:



and, finally, the reoxidation of a mediator on the electrode surface:



The formation of enzymatically active NAD(P)^+ is secured by the fact that enzymatic NADH oxidation is the natural way for recycling of coenzymes.

The use of diaphorase in biosensors for NADH oxidation has been demonstrated for the first time in sensors incorporating glutamate and lactate dehydrogenase together with dextran bound NAD^+ in the 70's [Davies and Mosbach, 1974]. Next, an alcohol sensor based on alcohol dehydrogenase and diaphorase was reported [Smith and Olson, 1975].

NADH oxidases also proved to be suitable for construction of biosensors. NADH oxidase was immobilised in poly(vinyl alcohol) [Leca and Marty, 1997] or poly(4-styrene sulfonate) [Mizutani et al., 2000] to yield the system in which hydrogen peroxide, resulting from NADH oxidation, was detected. Thermostable NADH oxidase was immobilised on a immobilon AV membrane [Compagnone et al., 1995] by poly(vinylalcohol) bearing photocrosslinkable terminal groups on a carbon paste electrode and used as NADH sensor [Noguer et al., 1999] through the detection of hydrogen peroxide.

Not only NADH diaphorases and oxidases were used in biosensors. The electropolymerisation of flavin reductase-amphiphilic pyrrole ammonium mixture provides NADH biosensors based on the oxidation at 0.1 V vs. SCE of enzymatically generated dihydroriboflavin [Cosnier et al., 1997]. In another system NADH was oxidised by salicylate hydroxylase in an oxygen and salicylate dependent reaction, and the consumption of oxygen was monitored with a Clark electrode [Chen et al., 2000].

The use of diaphorases and oxidases is very promising if they become more widely available, stable and cheaper.

1.6.3 Oxidation of NAD(P)H by soluble mediators

Another possible solution to the problem of high overpotential is to introduce into the system homogeneous or heterogeneous catalysts for the oxidation of NADH. They increase the rate of processes by introducing new pathways (mechanisms) with lower activation energies mediating the transfer of electrons from NAD(P)H to the electrode surface and are referred as mediators which operate according to Figure 3. The function of a mediator is to serve as a catalyst for

INTRODUCTION

NAD(P)H oxidation. NAD(P)H is oxidised by the mediator, and the mediator is oxidised in its turn on the electrode surface at low applied potential. It is desirable to use selective mediators for NADH oxidation in biosensors to avoid the oxidation of interfering substances. Another important requirement for them is their long lifetime.

The first reported water soluble mediators suitable for NADH oxidation in bulk solution were small organic molecules carrying aromatic moieties such as quinones, phenylene diimines, indophenols, phenazines and phenoxazines [Gorton, 1986].

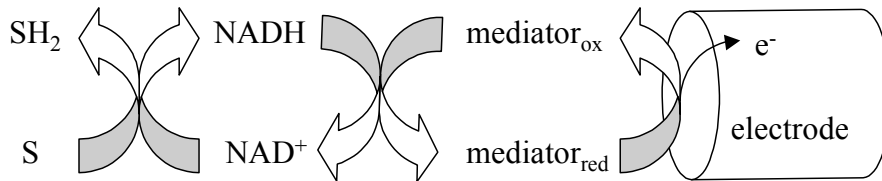
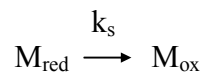


Figure 3. Schematic diagram of a system for electrochemical NADH recycling based on a mediator.

It is suggested that the NADH oxidation reaction proceeds via the formation of a mediator-NAD(P)H complex [Gorton, 1986; Katakis and Dominguez, 1997]. The mechanism of this reaction is represented in the following scheme:



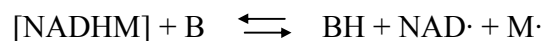
Which is followed by the reoxidation of mediator at the electrode surface:



Oxygen molecules can compete with an electrode for the mediator reoxidation [Katakis and Dominguez, 1997] leading to a decrease in oxidation current in case of biosensors and fuel cells:



At high pH another undesirable reaction occurs which adds to electrode fouling:

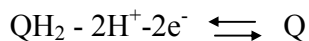


where **B** is a base. In case of ortho and para quinones (**Q**) and aromatic diamines the oxidation reaction goes through a net hydride transfer [Kitani et al., 1981; Jaegfeldt et al., 1983; Fukuzumi et al., 1984a; 1984b; 1989]:

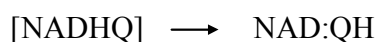




and the reoxidation of the mediator



The high rate of the interaction between quinoid structures and NADH is caused by the formation of stabilised transition state complex [NADHQ]. Unfortunately this complex can decompose through a side reaction leading to poisoning of the catalyst.



1.6.4 Oxidation of NAD(P)H on chemically modified electrode surfaces

The main disadvantage of homogenous mediators is the necessity to introduce them into a sample solution, therefore a good alternative is to find a way to modify the electrode surface with the objective to lower the applied potential for NAD(P)H oxidation.

One method is the modification of the electrode surface by pretreatment in order to achieve its activation. In a number of works it was shown that the drastic oxidation of a carbon electrode leads to the modification of its surface with ortho-quinone groups. The resulting electrodes showed NADH oxidation capacity at decreased applied potentials [Blaedel and Jenkins, 1975; Laval et al., 1984; Ravichandran and Baldwin, 1984]. Electrochemical pretreatment was combined with a novel polishing method for carbon fibre electrodes [Hayes and Khur, 1999] which generated a decreased overpotential and a high faradaic current of NADH oxidation. In another method the adenine moiety in NAD^+ was oxidised at carbon paste electrodes to modify carbon particles with redox active products capable of NADH oxidation at +0.05 V vs. Ag/AgCl/KCl_{sat} [Alvarez et al., 2000], the surface of carbon fibre electrode also can be activated by electrochemical oxidation of NADH followed by exposure to ascorbic acid [Nowal and Kuhr, 1995] or peroxide [Nowall and Kuhr, 1997]. Another approach is to use new conducting materials for electrode preparation such as boron-doped chemical vapour deposited diamond film [Sarada et al., 1999; Fujishima et al., 1999; Rao et al., 1999]. Nothing was reported on enzymatic activity of NAD^+ produced at the surface of diamond electrodes.

The second method is the adsorption of water soluble or insoluble organic molecules, mediating NADH oxidation, onto the electrode surface. Electrochemical catalysis of NADH by mediators adsorbed on the electrode surface has been reported (Table I). The majority of mediators presented in the table suffer from short operational life time. Ortho-quinone is not stable in the process of NADH oxidation because it leads to the formation of a stable complex which poisons

INTRODUCTION

and blocks the surface of the electrodes, which lose the capacity to oxidise NADH after several oxidative cycles [Jaegfeldt et al., 1983], and in many cases nothing was reported on the enzymatic activity of the oxidation product.

Electrodes covered with phenazine methosulphate are not stable in a stirred buffer solution and lost 60% of this mediator over 2 h due to desorption, the stability study in the presence of NADH by cyclic voltammetry has demonstrated consecutive decrease of the anodic current [Torstensson and Gorton, 1981] without showing enzymatic activity of the oxidation product. Electrodes modified with phenoxazinium salt, Meldola Blue in the oxidised form showed maximal half life-time of 12 h at neutral pH in the absence of NADH [Gorton et al., 1984], no data were presented on the NADH oxidising operational stability and enzymatic activity of resulting NAD^+ . 1,2-benzophenoxazine-7-one modified electrodes showed higher stability than those modified with Meldola Blue [Gorton et al., 1985]. Toluidine blue, methylene blue, and brilliant cresyl blue are not stable at pH higher than 7, for example toluidine blue adsorbed on glassy carbon demonstrated half life-time of 10 h at pH 8 [Chi and Dong, 1995]. The majority of the above mentioned mediators are not stable at high pH due to the side reactions of oxidation intermediates with hydroxyls, an example of side polymerisation reaction for ortho-quinone is represented in Figure 4 [Katakis and Dominguez, 1997]. Phenoxazine dyes as well proved to be unstable in alkaline solutions [Huck, 1994].

The complexation of ortho-quinoid structures with transition metals leads to mediators having higher chemical stability in alkaline solutions. Graphite electrodes modified with complexes $[\text{Re}(1,10\text{-phenanthroline-5,6-dione})(\text{CO})_3\text{Cl}]$, $[\text{Fe}(1,10\text{-phenanthroline-5,6-dione})_3(\text{PF}_6)_2]$, $[\text{Ru}(1,10\text{-phenanthroline-5,6-dione})(\text{vinylbipyridine})_2](\text{PF}_6)_2$ [Wu et al., 1996] and $[\text{Os}(4,4'\text{-dimethyl-2,2'-bipyridine})_2(1,10\text{-phenanthroline-5,6-dione})](\text{PF}_6)_2$ [Popescu et al., 1999], the latter yielding enzymatically active NAD^+ [Hedemno et al., 1996], showed electrocatalytic oxidation of NADH at potentials from 0.0 to +0.15 V vs. $\text{Ag}/\text{AgCl}/\text{KCl}_{\text{sat}}$.

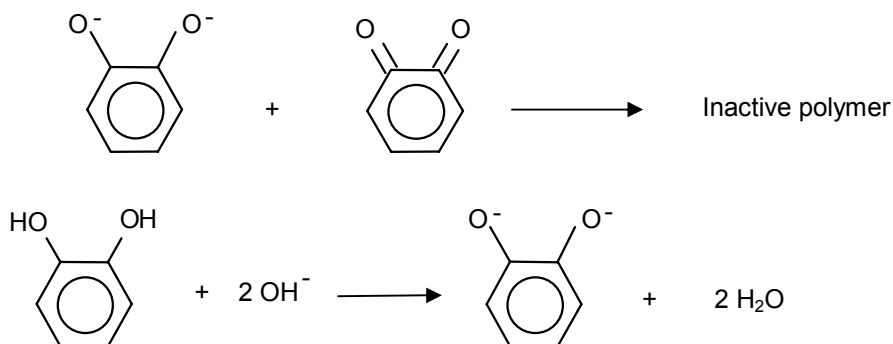


Figure 4. Reactions resulting in deactivation of ortho-quinone mediators.

INTRODUCTION

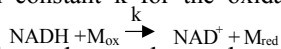
One of probable explanations for the higher stability of complexed quinoid ligands is the greater delocalisation of the possible radical electrons on a positively charged central atom [Katakis and Domínguez, 1997]. Another example of stabilisation by complexation are complexes of terpyridine bearing catechol functionality with Co, Cr, Fe, Ni, Ru, Os for NADH oxidation [Storrier et al., 1999].

Table I. Immobilised NADH oxidising small molecules reported in the literature

| Mediator | Working potential | $k_{[NADH]=0}/M^{-1} s^{-1} *$ | Reference |
|--|---------------------|---|---|
| ortho-quinone | +0.1 V vs. SCE | 1×10^4 | Jaegfeldt et al., 1981, 1983 |
| phenazine methosulphate | -0.05 V vs. SCE | | Torstensson and Gorton, 1981 |
| phenazine ethosulphate | -0.1 V vs. SCE | | Torstensson and Gorton, 1981 |
| meldola blue (phenoxazine) | -0.175 V vs. SCE | 2.7×10^4 | Gorton et al., 1984, Nagy et al., 1995 |
| 3- β -naphtoyl-nile blue | -0.22 V vs. SCE | | Huck et al., 1982 |
| 1,2-benzophenoxazine-7-one | -0.21 V vs. SCE | 1.2×10^3 | Gorton et al., 1985 |
| methylene blue | +0.3 V vs. SCE, | 340 | Chi and Dong, 1995 |
| toluidine blue | +0.3 V vs. SCE, | 320 | Chi and Dong, 1995 |
| brilliant cresyl blue | +0.4 V vs. SCE | 180 | Chi and Dong, 1995 |
| methylene green | +0.1 V vs. SCE, | | Han, et al., 1995, Chen et al., 1995 |
| catechol violet | +0.1 V vs. SCE | | Zhu et al., 1995 |
| cobalt hexacyanoferrate | +0.18 V vs. SCE, | | Cai et al., 1995 |
| nickel hexacyanoferrate | +0.2 V vs. SCE, | 1.2×10^3 | Cai et al., 1995b |
| ferrocene derivatives | +0.6 V vs. Ag/AgCl | 4.68×10^3 | Tian and Dong, 1995 |
| 2,6-dichlorophenolindo-phenol salts | +0.06 V vs. Ag/AgCl | | Florou et al., 1998 |
| nitro-fluorenone derivatives | -0.05 V vs. Ag/AgCl | | Mano and Kuhn, 1999 |
| riboflavin combined with zirconium phosphate | + 0.25-0 V vs. SCE | | Malinauskas et al., 1999 |
| pyrocatechol sulfonephtalein | +0.3 V vs. SCE | | Cai et al., 2000 |
| phenothiazine derivatives | | | Dicu et al., 2000 |
| [Re(1,10-phenanthroline-5,6-dione) ₃](PF ₆), [Fe(1,10-phenanthroline-5,6-dione) ₃](PF ₆), [Ru(1,10-phenanthroline-5,6-dione) ₃](PF ₆), | +0.15 vs. Ag/AgCl | 2.7×10^3 6.8×10^3 4.3×10^3 | Goss and Abruña, 1985; Wu et al., 1996 |
| [Os(4,4'-dimethyl-2,2'-bi-pyride)(1,10-phenanthroline-5,6-dione)](PF ₆) ₂ | +0.15 vs. Ag/AgCl | 0.9×10^3 | Popescu et al., 1999 |

INTRODUCTION

* $k_{[\text{NADH}] = 0}$ is the value of the overall reaction constant k for the oxidation of NADH by the mediator extrapolated to zero NADH concentration.



The rate of reaction with NADH depends greatly on the mediator structure and Meldola Blue proved to be the fastest mediator. The dependence of reaction rate on the structure is represented in Figure 5 [Gorton, 1986]. Taking into consideration the mechanistic scheme for

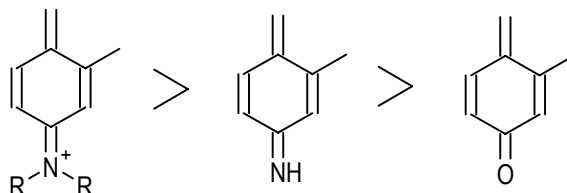


Figure 5. Observed dependence of reaction rate with NADH on structure of a mediator.

NADH oxidation (Figure 6) proposed by Bartlett with coworkers [Bartlett et al., 1997], it can be concluded that the mediators bearing positive amino groups demonstrated higher reaction rates because they have higher formal standard potential (which is the thermodynamic driving force for electron exchange) on the other hand nitrogen atom accepts a hydride more readily than oxygen.

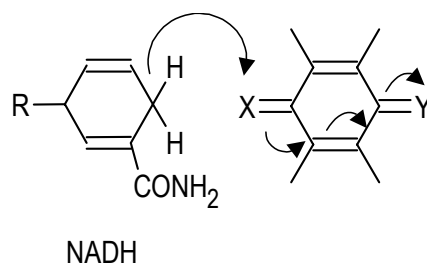


Figure 6. Proposed mechanistic scheme for NADH oxidation by reaction with a redox mediator. X is a group capable of accepting a hydride, Y is an electron-deficient group.

The most important disadvantage of electrodes modified with small molecules by adsorption is the leaching of the mediator from the electrode surface to the bulk solution. Hence different methods of mediator immobilisation via formation of chemical bonds with molecules of the electrode material have been developed. Ortho-quinone was chemically immobilised on the surface of solid carbon electrodes through covalent bonds [Tse and Kuwana, 1978; Ueda et al., 1982], toluidine blue was covalently attached to monolayers of cystamine or 3-mercaptopropionic acid on gold electrodes oxidising NADH at -0.1 V vs. Ag/AgCl/KCl_{sat} [Schlereth et al., 1994], phenoxazine and phenothiazine derivatives were attached to monolayers of cystamine and cysteine [Schlereth et al., 1995], the imine derived from 3,4-dihydroxybenzaldehyde and 4-aminopyridine was adsorbed onto polycrystalline platinum electrodes through the pyridine nitrogen [Lorenzo et al., 1995], dopamine was covalently bound to self-assembled cysteamine monolayers on gold electrodes oxidising NADH at +0.15 V vs. SCE [Sun et al., 1997], thionine was attached to self-assembled cysteamine monolayer on gold to oxidise NADH at about 0 V vs. SCE [Chen et al.,

1997], graphite particles were exfoliated and subsequently covalently functionalised with toluidine blue [Ramesh and Sampath, 2000].

Another way to decrease leaching of mediators from the electrode surface is to boost the adsorption by using electroactive (redox) polymers for coating which contain the equivalent of many monomolecular layers. The electrodes modified with the redox polymer have much more electroactive sites per area, and in volume terms the concentration of electroactive sites in the polymer is higher therefore the electrocatalytic response to NADH of redox polymers can be much higher than this for monolayers of redox molecules due to the “volume effect” [Murray, 1984]. Two main methods for immobilisation of redox polymers on electrodes, which are adsorption of pre-synthesised polymer and electropolymerisation *in situ* of monomeric mediators, have been shown in literature. Examples of NADH oxidising polymers are reviewed in table II.

Study of charge propagation in quinoid polymers over electrode surfaces has shown that only the inner sublayer of the polymer is readily oxidised, whereas the outer sublayers are oxidised only very slowly. This phenomenon was explained in terms of slow charge propagation through polymeric films of quasi-reversible two-electron redox couples, so only the first monolayer of redox polymers is effective in NADH oxidation. Poly(dopaquinone) proved to be very unstable on the electrode surface and about 70% of hydroquinone-quinone couples were inactivated after 22 consecutive cyclic voltammograms at neutral pH because of the low stability of the oxidised form [Fukui et al., 1982]. Electropolymerised films of 3,4-dihydroxybenzaldehyde (3,4-DHB) showed higher stability, with 30% of redox couples lost after 30 min of continuous scanning. Electrodes modified with polymeric form of Meldola Blue showed high stability measured by repeated redox cycling and poor NADH sensitivity due to low permeability of NADH molecules through the polymeric film [Persson, 1995]. Electrodes bearing films of poly(ortho-phenylenediamine) were not stable immediately after preparation [Lobo et al., 1996]. Electropolymerisation of azure I gave electrodes which were losing their activity during 500 repetitive scans but after 6 h stabilisation was reached [Cai and Xue, 1996].

In general most polymeric mediators showed lower rate constants of reaction with NADH than the corresponding monomers because of “capping” by the polymer backbone of the active redox sites, oriented towards the electrode surface [Persson et al., 1995]. The majority of monomeric and polymeric mediators has pH dependent redox potential and rate of interaction with NADH. Both of them increase when pH decreases because protons participate in the redox conversion of NAD(P)^+ and many mediators and facilitate hydride transfer to accepting groups of the mediators.

Polymeric mediators proved to adhere more than small molecules on the electrode surface, but inherit from their corresponding monomers low chemical and hence operational stability at elevated values of pH, which is not convenient because the majority of the known NAD(P)^+

INTRODUCTION

dependent dehydrogenases have optimal activity at pH higher than 7.0.

The reversible electrochemical oxidation of NADH to its enzymatically active form is the key to the application of mediators in reagentless biosensors. For example, the enzymatic activity of the product of NADH oxidation by [Os(4,4'-dimethyl-2,2'-bipyridine)(1,10-phenanthroline-5,6-dione)] has been demonstrated [Hedemno et al., 1996] though in the majority of the published works on NADH oxidising mediators the enzymatic activity of the resulting oxidation products has not been studied. Such regeneration can be questioned in many cases, for example, it is very doubtful that electrodes modified with [Os(bpy)₂(PVI)₁₀Cl]Cl convert NADH to active NAD⁺ [Ju and Leech, 1997].

Table II. Immobilised NADH oxidising polymers reported in literature

| Polymer | Method of immobilisation | Working potential | $k_{\text{NADH} =0}/\text{M}^{-1}\text{s}^{-1}$ | Reference |
|---|---|---------------------|---|---|
| poly(dopamine) | covalent coupling with poly(methacryloyl chloride) followed by adsorption on glassy carbon | +0.2 V vs. SCE | | Degrad and Miller, 1980; Fukui et al., 1982 |
| poly(toluidine blue) | inclusion in carbon paste | +0.2 V vs. SCE | | Dominguez et al., 1993 ^a |
| poly(3,4- dihydroxybenzaldehyde) | electropolymerisation on glassy carbon | +0.2 V vs. SCE | 4.3×10^3 | Pariante et al., 1994; 1997 |
| poly(meldola blue) | covalent coupling with poly(methylsiloxane) followed by adsorption on graphite | NADH at 0 V vs. SCE | 2.9×10^3 | Persson et al., 1995 |
| poly(orthophenylenediamine) | electropolymerisation on carbon paste | +0.15 V vs. Ag/AgCl | | Lobo et al., 1996 |
| poly(orthoaminophenol) | electropolymerisation on carbon paste | +0.15 V vs. Ag/AgCl | | Lobo et al., 1996 |
| poly(azure I) | electropolymerisation on glassy carbon electrodes | +0.1 V vs. SCE | 2×10^3 | Cai and Xue, 1997 |
| poly(toluidine blue) | covalent coupling with poly(styrene) or poly(etheleneimine) followed by adsorption on graphite | 0-+0.05 V vs. SCE | | Huan et al., 1996 |
| poly(methylene green) | electropolymerisation on glassy carbon | +0.1 V vs. SCE | | Zhou et al., 1996 |
| poly(methylene blue) | Electropolymerisation on gold | +0.2 V vs. Ag/AgCl | | Silber et al., 1996 |
| [Os(bpy) ₂ (PVI) ₁₀ Cl]Cl | complexation of [Os(bpy) ₂ Cl ₂] with poly(vinylimidazol) followed by adsorption on carbon fiber | +0.5 V vs. Ag/AgCl | | Ju and Leech, 1997 |
| poly(nile blue A) | electropolymerisation on glassy carbon | +0.02 V vs. SCE | 800 | Cai and Xue, 1997; Malinauskas et |

INTRODUCTION

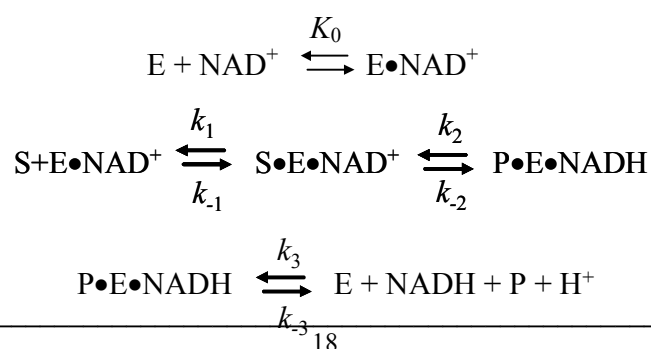
| | | | | |
|---------------|--|----------------|--|-----------------------|
| | | | | al., 2000 |
| poly(aniline) | electropolymerisation on glassy carbon | +0.1 V vs. SCE | | Bartlett et al., 1997 |

Table II. (continued)

| Polymer | Method of immobilisation | Working potential | $k_{[NADH]=0}/M^{-1} s^{-1}$ | Reference |
|---|---|---------------------|------------------------------|-------------------------------|
| poly(aniline) | electropolymerisation on poly(acrylic acid) film | +0.05 V vs. SCE | | Bartlett and Simon, 2000 |
| poly(1,2-, 1,3-, 1,4-diaminobenzene) | Electropolymerisation in the presence of PQQ on Pt, Au and graphite | +0.2 V vs. SCE | | Curulli et al., 1997 |
| poly(1,2-, 1,3-, 1,4-diaminobenzene) | Electropolymerisation in the presence of PQQ on Pt, Au and graphite | +0.2 V vs. SCE | | Curulli et al., 1997 |
| poly(4-aminobiphenyl) | electropolymerisation in the presence of PQQ on Pt, Au and graphite | +0.2 V vs. SCE | | Curulli et al., 1997 |
| poly(3-methyl-thiophene) | electropolymerisation on carbon fibre | +0.45 V vs. Ag/AgCl | | Jaraba et al., 1998 |
| poly(naphtol green B) | electropolymerisation on glassy carbon | +0.1 V vs. SCE | | Cai and Xue, 1998 |
| poly(toluidine blue O) | electropolymerisation on glassy carbon | +0.15 V vs. SCE | | Cai and Xue, 1998b |
| poly(caffeic acid) | electropolymerisation on glassy carbon | +0.2 V vs. SCE | | Zare and Golabi, 2000 |
| poly(1,4-bis(3,4-dihydroxyphenyl)-2,3-dimethylbutane) | electropolymerisation on glassy carbon | +0.3 V vs. Ag/AgCl | 3.4×10^3 | Ciszewski and Milczarek, 2000 |

1.7 Dehydrogenase electrodes

The reaction of electrochemical oxidation of NAD(P)H can be coupled with the reaction of enzymatic oxidation by dehydrogenases to yield a great number of possible configurations applicable to the construction of biosensors, bioreactors and fuel cells. The following kinetic model for the conversion of substrate S to product P by a dehydrogenase modified electrode has been developed by Albery with co-workers [1987]:



The final step is the oxidation of NADH at the electrode:



For each step in this scheme

$$K_n = k_n/k_{-n}$$

The constant K_{TD} serves to describe the overall equilibrium between $\text{S} + \text{NAD}^+$ and $\text{P} + \text{NADH} + \text{H}^+$

$$K_{\text{TD}} = K_0K_1K_2K_3$$

The transport of S and P in the enzyme layer having the thickness L , is described by the mass transfer rate coefficients k'_s and k'_p .

Assuming that there is no product in the external bulk solution and the kinetics of binding of the enzyme to NAD^+ are rapid the following expression for the flux, j can be obtained:

$$\begin{aligned} \frac{e_{\Sigma}}{j} = & \frac{1}{Lk_{\text{cat}}} \left(1 - \frac{j}{k'_s s_{\infty}} \right) + \frac{K_M}{Lk_{\text{cat}} s_{\infty}} + \frac{je_{\Sigma}}{k'_p s_{\infty} k' K_{\text{TD}} [\text{NAD}^+]} \\ & + \frac{j^2}{Lk'_p s_{\infty} k' K_{\text{TD}} [\text{NAD}^+]} \left(\frac{1}{k_{-1}'} + \frac{K_2}{k_{-1}'} + \frac{1}{k_{-2}'} \right) + \frac{e_{\Sigma}}{k'_s s_{\infty}} \end{aligned}$$

where s_{∞} is the substrate concentration in the external medium, e_{Σ} is the total enzyme concentration.

$$e_{\Sigma} = [\text{E} \cdot \text{NAD}^+] + [\text{S} \cdot \text{E} \cdot \text{NAD}^+] + [\text{P} \cdot \text{E} \cdot \text{NADH}]$$

$$1/k_{\text{cat}} = 1/k_2' + 1/(K_2 k_3') + 1/k_3'$$

$$K_M/k_{\text{cat}} = 1/k_1' + 1/(K_1 k_2') + 1/(K_1 K_2 K_3)$$

Many electrodes operating in the presence of enzymes, cofactors and mediators in a sample solution have been demonstrated in the literature, but the number of dehydrogenase electrodes which can detect an analyte without addition of any reagent to a sample solution, so called reagentless electrodes, is limited. Some reagentless electrodes based on dehydrogenases are represented in Table III. Most of these electrodes were produced by immobilisation of enzymes, NAD^+ and mediator for the coenzyme reoxidation on the surface of an electrode. Five strategies for the coenzyme immobilisation have been shown: (a) entrapment in hydrogels formed *in situ* by polymeric macromolecules, (b) adsorption onto pre-prepared polymeric membranes, (c)

INTRODUCTION

entrapment in electropolymerised films, (d) entrapment in carbon paste, and (e) immobilisation in self-assembled monolayers.

a. Entrapment in hydrogels formed in situ by macromolecules

An attempt to entrap NAD^+ in gels formed by gelatine and poly(lysine) yielded very unstable biosensors for glycerol [Laurinavicius et al., 1996].

b. Immobilisation of NAD^+ under preprepared membranes

NAD^+ was crosslinked on a cellulosic dialysis membrane by glutaraldehyde to yield unstable lactate biosensors [Blaedel and Jenkins, 1976]. Polymeric form of NAD^+ (NAD^+ -dextran) was entrapped in the hydrogel formed by poly(vinyl alcohol) bearing styrylpyridinium groups and finally covered by a cellophane membrane to yield ethanol biosensors. The authors claim that they observed a good operational stability though they do not report the detailed results of their operational stability study [Leca and Marty, 1997]. Malate biosensors have been prepared by adsorption of NAD^+ onto nitrocellulose and cellulose acetate membranes which rapidly lost activity with time because of coenzyme leaching [Maines et al., 2000].

c. Entrapment of NAD^+ in electropolymerised films

An L-lactate biosensor based on NAD^+ entrapment in poly(pyrrole) electropolymerised on a platinum electrode [Ikariyama et al., 1990] showed poor stability and low sensitivity.

d. Entrapment of NAD^+ in carbon paste

L-lactate biosensors were fabricated on the bases of carbon paste, but nothing was reported on their operational stability [Yoon and Kim, 1996], glucose biosensors showed very high stability and lost 6-8% in their response during 3-8 h [Hedemno et al., 1996], alcohol biosensors protected with dialysis membrane [Lobo et al., 1996b] were stable during one day. Glutamate biosensors covered with poly(*o*-phenylenediamine) lost $\frac{1}{2}$ of the initial response after 2 days of operation [Alvarez et al., 1997].

e. Immobilisation in self-assembled monolayers

This strategy has been pioneered by the group of Itamar Willner which reported L-lactate biosensors produced by attachment of NAD^+ to a self-assembled PQQ monolayer [Katz et al., 1998].

Biosensors in which NAD^+ was entrapped in hydrogels formed *in situ* have good sensitivities because of very easy transport of analyte to the enzyme, but suffer from low stability in the reagentless mode of operation due to easy desorption of the coenzyme and the enzyme. When NAD^+ was entrapped in electropolymerised films and pre-prepared membranes the sensitivity was bad due to the limited transport of analyte. The most stable biosensors were produced on the basis of carbon paste in which a “reserve pool” of the coenzyme was created, at the same time their sensitivity was high hence the local coenzyme concentration was high as well. Unfortunately it is not possible to opt for carbon paste configurations to fabricate miniaturised

INTRODUCTION

sensors.

Table III. Configurations of reagentless electrodes based on NAD(P)⁺ dependent dehydrogenases

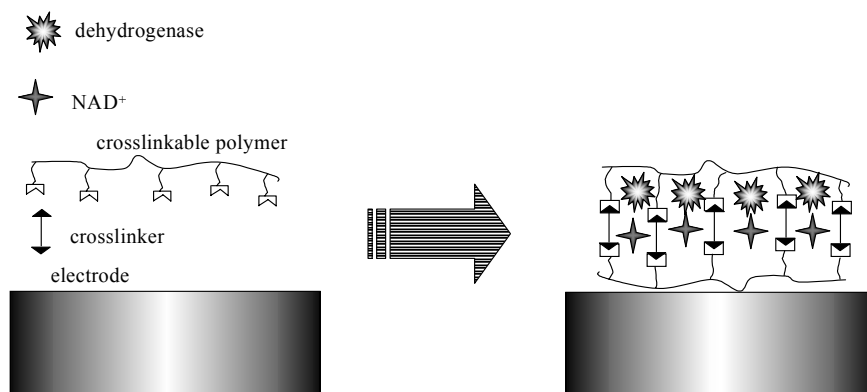
| Analyte | Cofactor immobilisation | Dehydrogenase | Method of NADH oxidation / E _{app} | Time of operation without regeneration | Reference |
|-----------|--|---|--|--|----------------------------|
| L-lactate | NAD ⁺ crosslinked on a cellulosic dialysis membrane by glutaraldehyde | lactate dehydrogenase crosslinked on a cellulosic dialysis membrane by glutaraldehyde | direct oxidation on glassy carbon +0.45 vs. Ag/AgCl | Response decreased over several hours by 20% | Blaedel and Jenkins, 1976 |
| L-lactate | NAD ⁺ covalently attached to agarose | lactate dehydrogenase immobilised behind a dialysis membrane | direct oxidation on glassy carbon +0.45 vs. Ag/AgCl | Response almost unchanged over several hours | Blaedel and Jenkins, 1976 |
| ethanol | NAD ⁺ immobilised by Schiff base | alcohol dehydrogenase in carbon paste | direct oxidation on carbon paste +0.4 V vs. SCE | unstable | Yao et al., 1979 |
| L-lactate | NAD ⁺ immobilised by Schiff base | lactate dehydrogenase in carbon paste | direct oxidation on carbon paste +0.4 V vs. SCE | unstable | Yao et al., 1979 |
| malate | NAD ⁺ immobilised in a dialysis membrane | malate dehydrogenase under dialysis membrane | direct oxidation on platinum electrode +0.875 V vs. SCE | | Blaedel and Engstrom, 1980 |
| L-lactate | NAD ⁺ in electropolymerised poly-(pyrrole) | lactate dehydrogenase in electropolymerised poly(pyrrole) | Methylene blue on platinum electrode +0.3 V vs. Ag/AgCl | unstable | Ikariama et al., 1990 |
| glucose | NAD ⁺ in Eastman AQ TM | glucose dehydrogenase in carbon paste | Cresyl blue 0.0 V vs. Ag/AgCl | | Gorton et al., 1991 |
| ethanol | NAD ⁺ in carbon paste | alcohol dehydrogenase in carbon paste | direct oxidation on carbon paste +0.58 V Ag/AgCl | | Wang and Liu, 1993 |
| ethanol | NAD ⁺ with poly(ethyleneimine) in carbon paste | alcohol dehydrogenase in carbon paste | poly(toluidine blue) +0.1 V vs. Ag/AgCl | | Dominguez et al., 1993b |
| glucose | NAD ⁺ entrapped in ionic polymers on graphite | glucose dehydrogenase | toluidine blue on graphite 0 V vs. Ag/AgCl | | Boguslavsky et al., 1995 |
| glycerol | NAD ⁺ in gelatine or polylysine crosslinked with glutaraldehyde | glycerol dehydrogenase and lipase in gelatine or polylysine crosslinked with glutaraldehyde | meldola blue, Nile blue, toluidine blue adsorbed on carbon 0 V vs. Ag/AgCl | | Laurinavicius et al., 1996 |

Table III. (continued)

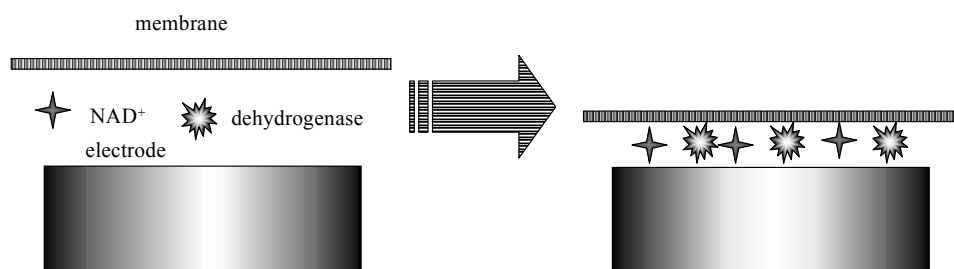
| Analyte | Cofactor immobilisation | Dehydrogenase | Method of NADH oxidation / E_{app} | Time of operation without regeration | Reference |
|-------------|---|---|---|--|--|
| L-lactate | NAD ⁺ in carbon ink of screen printed electrodes | L-lactate dehydrogenase over carbon ink | meldola blue in carbon ink 0 V vs. Ag/AgCl | | Sprules et al., 1996 |
| glucose | NAD ⁺ in carbon paste | glucose dehydrogenase in carbon paste | [Os(4,4'-dimethyl-2,2'-bipyridine) ₂ (1,10-phenanthroline-5,6-dione)](PF ₆) ₂ in carbon paste +0.15 V vs. Ag/AgCl | loss of 6-8 % of response in 3-8 h | Hedemno et al., 1996 |
| ethanol | NAD ⁺ in carbon paste | alcohol dehydrogenase in carbon paste | toluidine blue in carbon paste +0.05 V vs. Ag/AgCl | response is constant for 1 day, half life is 2 days. | Lobo et al., 1996b |
| L-lactate | NAD ⁺ in carbon ink of screen printed thick film | L-lactate dehydrogenase in carbon ink of screen printed thick film | thick film carbon electrode +0.35 V vs. Ag/AgCl | | Yoon and Kim, 1996 |
| L-lactate | NAD ⁺ in carbon paste | L-lactate dehydrogenase and glutamic pyruvic transaminase in carbon paste | poly(orthophenylenediamine) electropolymerised on carbon paste +0.15 V vs. Ag/AgCl | response is constant for one day, 10 measurements | Lobo et al., 1997a |
| ethanol | NAD ⁺ in carbon paste | alcohol dehydrogenase | poly(orthophenylenediamine) electropolymerised on carbon paste +0.15 V vs. Ag/AgCl | useful time is 3 days provided periodic recalibration is performed | Lobo et al., 1997b |
| L-lactate | NAD ⁺ covalently attached to PQQ molayer | L-lactate dehydrogenase | PQQ monolayer on gold +0.1 V vs. SCE | | Bardea et al., 1997; Katz et al., 1998 |
| ethanol | NAD ⁺ in carbon paste | alcohol dehydrogenase | poly(orthophenylenediamine) electropolymerised on carbon paste +0.15 V vs. Ag/AgCl | useful time is 3 days provided periodic recalibration is performed | Lobo et al., 1997b |
| L-glutamate | NADP ⁺ in carbon wax | thermophilic L-glutamate dehydrogenase in carbon wax | poly(toluidine blue O) on carbon wax | response was constant during 4 days in the FIA system | Pasco et al., 1999 |

Table III. (continued)

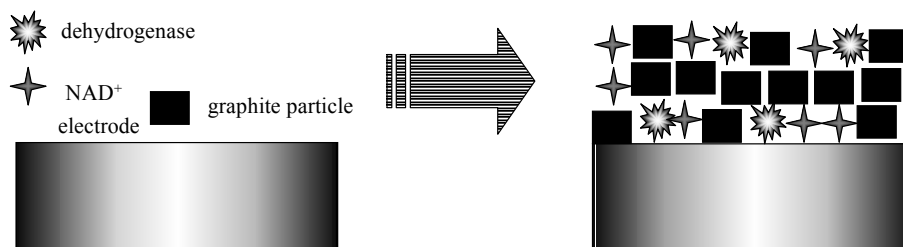
| Analyte | Cofactor immobilisation | Dehydrogenase | Method of NADH oxidation / E_{app} | Time of operation without regeneration | Reference |
|--|---|---|---|---|-----------------------|
| L-lactate | NAD ⁺ in carbon paste | L-lactate dehydrogenase in carbon paste | toluidine blue O in carbon paste 0.0 V vs. Ag/AgCl | this electrode in a flow cell retains 98% after 45 successive injections of L-lactate | Ramirez et al., 1999 |
| ethanol | NAD ⁺ in carbon paste | alcohol dehydrogenase in carbon paste | [Fe(1,10-phenanthroline -5,6-dione) ₃](PF ₆) ₂ or [Re(1,10-phenanthroline -5,6-dione)(CO) ₃ Cl] in carbon paste 0 V vs. SCE | response was constant during 8 days of operational stability study | Tobalina et al., 1999 |
| ethylene-bis(dithiocarbamate) fungicides | NAD ⁺ in screen printed carbon ink | aldehyde dehydrogenase in screen printed carbon ink | NADH oxidase in poly(vinylalcohol) bearing styryl-pyridinium group | | Noguer et al., 1999 |
| ethanol | NAD ⁺ in carbon ink | alcohol dehydrogenase in carbon ink | bare thick film carbon electrode +0.47 V vs. Ag/AgCl | disposable sensors | Park et al., 1999 |
| glycerol | NAD ⁺ in carbon paste under poly(ortho-phenylenediamine) | glycerol dehydrogenase in carbon paste under poly-(<i>o</i> -phenylene diamine) | Products of NAD ⁺ oxidation in carbon paste +0.15 V vs. Ag/AgCl | the signal is steady during 2 days | Alvarez et al., 2000 |
| D-sorbitol | NAD ⁺ in carbon paste under poly(ortho-phenylenediamine) | D-sorbitol dehydrogenase in carbon paste under poly-(<i>o</i> -phenylenediamine) | products of NAD ⁺ oxidation in carbon paste 0.0 V vs. SCE | slope of calibration graph decreased by 15% and 40% during after 48 and 72h correspondingly | Saidman et al., 2000 |
| malate | NAD ⁺ entrapped under ester cellulose membrane | malate dehydrogenase in ester cellulose membrane in conjunction with a PVC outer membrane | diaphorase mediated by hexacyanoferrate (III) or 2,4-dichlorophenolindophenol +0.05 V vs. Ag/AgCl | this sensor retained almost 80% of its initial activity after 3 h | Maines et al., 2000 |



a. Entrapment in hydrogels formed *in situ* by macromolecules



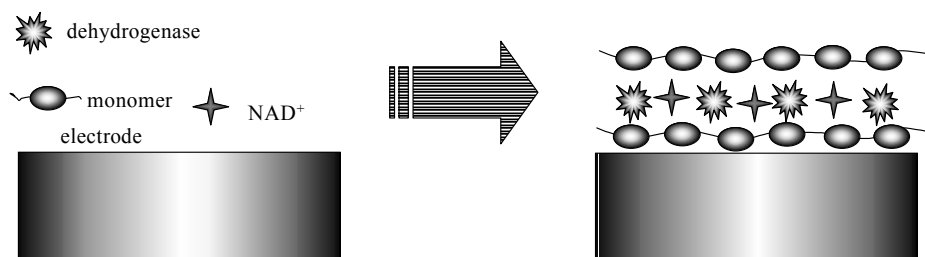
b. Immobilisation of NAD⁺ under pre-prepared membranes



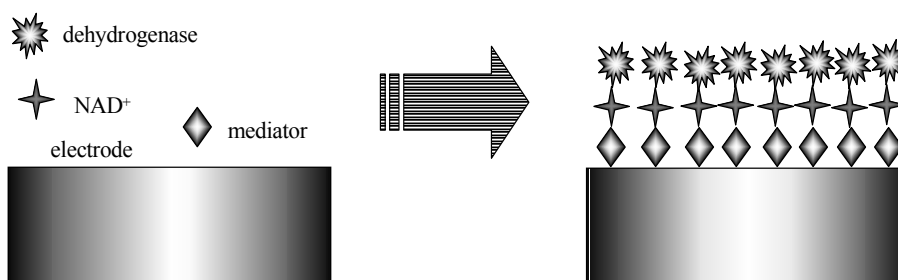
c. Entrapment in electropolymerised films

Figure 7. Different strategies for the fabrication of reagentless biosensors based on NAD(P)⁺ dependent

dehydrogenases



d. Entrapment in carbon paste



e. Immobilisation in self-assembled monolayers

Figure 7. (continued)

1.8 Thermostable enzymes

The majority of enzymes utilised in organic synthesis and bioanalysis are obtained from organisms which live and reproduce optimally at temperatures below 45°C, so called mesophilic species or mesophiles. On the other hand a wide variety of natural habitats exist, including boiling or superheated springs and submarine volcanoes where the temperature of water is equal or higher than 100°C, inhabited by micro organisms termed as thermophilic species or thermophilies. The three main groups of thermophilic species were proposed by Farrell and Campbell [1969]:

- (1) strict or obligate thermophiles, which have optimal growth at 65°C to 70°C but do not grow below 40°C
- (2) facultative thermophiles having a maximal growth temperature between 50°C and 65°C

INTRODUCTION

which are able to reproduce at room temperature

(3) thermotolerant bacteria having growth maxima at 45°C to 50°C, and grow at room temperature too

The first reports on enzymes extracted from thermophiles appeared as early as in 1949 when Militzer et al. demonstrated the thermostability at 65°C for 2 h of malate dehydrogenase from an obligate thermophile. It was found that the enzymes from the thermophile *Bacillus stearothermophilus* were significantly more resistant to heat inactivation than the homologous enzymes from the mesophile *Bacillus cereus* [Amelunxen and Lins, 1968]. The experiments comparing the 6-phosphogluconate dehydrogenase from the thermophile *Clostridium thermosacchrolyticum* and the mesophile *Clostridium pasteurianum* have shown greater thermostability of the enzyme extracted from the thermophile [Howell et al., 1969]. Different hypotheses explaining the elevated stability of enzymes from thermophiles have been proposed and tested.

The hypothesis of transferable protective factors suggested that those factors are present in thermophilic cells and impart thermostability to thermophilic enzymes and was tested by Koffler and Gale (1957). In these experiments they measured the extent of coagulation after heat treatment of free extracts from thermophiles, mesophiles and mixtures of both to find out that stabilising factors are non-transferable.

The hypothesis of rapid resynthesis of thermophilic macromolecules was based on a suggestion that thermophiles can very rapidly synthesise proteins in order to counteract thermal deactivation which was supported by the fact that the rates of protein and nucleic acid synthesis and turnover are higher in *B. stearothermophilus* than in *E. coli*. [Bubela and Holdsworth, 1966a, b].

Another group of hypotheses claims that the thermostability of thermophilic enzymes can be explained in terms of greater intrinsic stability of macromolecules in thermophiles. Physicochemical studies have demonstrated great homology between thermophilic and mesophilic proteins. Although there are some structural differences between very stable thermophilic and mesophilic enzymes, there is no pattern of systematic structural differences [Daniel and Cowan, 2000] but thermophilic proteins undergo only small conformational changes without denaturation when heated, in contrast to the mesophilic ones denaturing at about 60°C. The conformational changes are responsible for a break in the Arrhenius plot of many thermophilic enzymes [Ljungdahl and Sherod, 1976]. The secondary structure of proteins in aqueous environment is formed by hydrogen bonds, salt linkages, and hydrophobic interactions. Increase in temperature leads to a decrease in salt linkages and hydrogen bonding and an increase in hydrophobic interactions because of the increase of dielectric constant of water with temperature. It was estimated that hydrophobic interactions for large side-chains increase rapidly up to 75°C and then

slowly decrease [Brandts, 1967], therefore hydrophobic interactions could play a great role in the stabilisation of thermophilic enzymes. Nevertheless the calculations of relative hydrophobicity of thermophilic and mesophilic enzymes gave no correlation between hydrophobicity and thermostability [Singleton and Amelunxen, 1973; Bull and Breese, 1973]. The attempts to explain the thermostability in terms of hydrogen bonding also failed when no difference in hydrogen bonding was found in the secondary structure of thermophilic and mesophilic enzymes [Suzuki and Imahori, 1974; Cass and Stellwagen, 1975]. Other effort to understand the stability of thermophilic enzymes concentrated on finding a correlation between thermostability and secondary structure of globular proteins, particularly the helical and β -structure but spectropolarimetric measurements found no difference between the mesophilic and thermophilic proteins [Hibino et al., 1974; Hasegawa et al., 1976].

The hypothesis, connecting a decrease in cysteine content i.e. decrease of ancillary sulphhydryl groups, subjected to oxidation, with enzymatic thermostability of glyceraldehyde-3-phosphate dehydrogenase from *Thermus aquaticus* seems to be more promising [Hocking and Harris, 1976]. Some thermophilic enzymes also have fewer sulphhydryl groups, for example, phosphoglycerate kinase [Suzuki and Imahori, 1974] and adenosine triphosphatase [Yoshida et al., 1975], nevertheless the content of cysteine in thermophilic phosphofructokinase is much higher than in the mesophilic analogue [Cass and Stellwagen, 1975].

Another hypothesis relates thermostability with the increased number of acidic carboxyl moieties in thermophilic proteins [Singleton, 1976]. It is suggested that carboxyl groups can be protonated and form two hydrogen bonds with other groups, form an ion-dipole interaction with the phenolic hydroxyl of tyrosine, and a salt-linkage, therefore increasing the stability of the tertiary structure. Some other proposed factors contributing to the thermal stability of proteins are: increased number of ion pairs [Hennig et al., 1995], aromatic interactions in aromatic pairs and clusters [Burley and Petsko, 1985], stabilisation of the dipoles of the α -helices [Nicholson et al., 1988], high internal packing, and reducing the area of water accessible hydrophobic surface [Wigley et al., 1987]. Finally it can be concluded that there is not a unique way to obtain protein stability at elevated temperatures, every thermostable enzyme is individually adapted to environmental conditions by the combination of the above mentioned factors.

1.9 Application of Langmuir-Blodgett techniques films for electrode modification

The techniques allowing to form ordered monolayers and multilayers of molecules find wide applications in electronics and bioelectronics. One of the methods for building such layers is based on transferring them from the liquid-gas interface onto a solid substrate.

Monolayers of many insoluble compounds on liquid-gas interface can be created by

INTRODUCTION

spreading their solutions in a volatile solvent over another liquid. The first systematic study of monolayers of insoluble compounds at the water-air interface was carried out by Langmuir [1917]. In his work he described a trough for creation and study of such films (Figure 8).

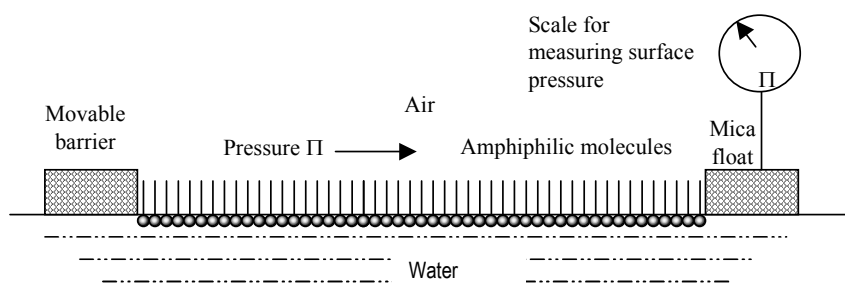


Figure 8. Diagrammatic representation of Langmuir-Blodgett trough in which the movable barrier compresses the insoluble monolayer. The scale, connected to the mica float by wire suspension, measures the surface pressure.

Typical representatives of amphiphilic compounds capable to form the above mentioned monolayers are aliphatic carboxylic acids which have two distinct moieties in the molecule: a hydrophilic headgroup ($-\text{COOH}$) and a hydrophobic long alkyl chain ($\text{C}_n\text{H}_{2n+1}$, where $n \geq 5$). If the distance between amphiphilic molecules on the surface of water is large then their interactions are small hence they can be regarded as forming a two-dimensional gas, having almost no effect on the surface tension. When a barrier system reduces the area of available surface for the monolayer molecules start to exert a repulsive effect on each other leading to the necessity to introduce the two-dimensional analogue of a pressure termed as the surface pressure Π , which is equal to the difference between the surface tension in the absence of a monolayer and that with the monolayer present.

The maximum value of the surface pressure for a monolayer of any amphiphilic compound at the water-air interface at room temperature is less than 73 mN/m . On compressing the surface areas beyond the limit of monolayer compressibility, the phenomenon of collapse takes place, which is explained in terms of breaking the monolayers with the formation of disordered multilayers.

A method for transferring multilayers of long chain carboxylic acids on solid substrate was invented by Blodgett [1934] who added to the trough of Langmuir a device, which lowers a solid substrate beneath a monolayer at the water-air interface and then withdraws it, therefore the resulting layers, deposited on the substrate, are referred to as the Langmuir-Blodgett (LB) films. An example of deposition of amphiphilic molecules on a hydrophilic substrate is shown in Figure 9.

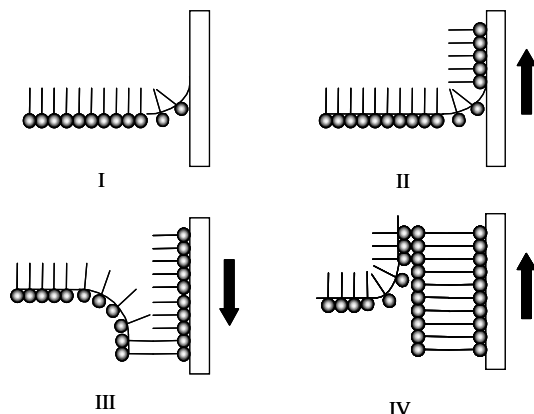


Figure 9. Deposition of Langmuir-Blodgett films on a solid substrate: (I) first dipping, (II) first withdrawal, (III) second dipping, (IV) second withdrawal.

During the first dipping (I) water wets the hydrophilic substrate's surface with no deposition at this stage because the meniscus is turned up. Only during the first withdrawal the first monolayer is being deposited in which hydrophilic tails are orientated toward the hydrophilic substrate. The second dipping (III) leads to the deposition of the second layer because the resulting surface now is hydrophobic and the meniscus is turned down.

The Langmuir-Blodgett (LB) technique is widely used to immobilise redox amphiphilic compounds on solid electrodes yielding photo-current generating devices, chemical sensors and biosensors. For example, photo-cells were produced by immobilisation of LB layers of pyrrolidinofullerene derivatives [Sheng et al., 2000], or amphiphilic stilbazolium dye dimer [Li et al., 2001] on a semiconducting transparent indium-tin-oxide.

Amphiphilic molecules also can be employed for the immobilisation of enzymes. The pioneering work demonstrating that enzymes retain their activity when entrapped into reversed micelles of surfactants were published in the beginning of the 80's [Martinek et al., 1981; Khmel'nitskii et al., 1982]. Next a novel LB method was developed for producing and transferring a uniform protein thin film – a layer of a protein sandwiched between layers of a lipid [Vakula et al., 1995; Troitsky et al., 1996a,b; Berzina et al., 1996]. A glucose sensor was made on the basis of adsorbed layers of glucose oxidase on LB monolayers of N, N-dimethyl-acetylacetylmethacryloyl ethyl on platinum [Zaitsev et al., 1995]. Choline oxidase was inserted in a hydrophilic or hydrophobic environment of behenic acid LB films and the biosensing layer was directly coated on an especially designed amperometric transducer to yield a choline biosensor [Girardegrot et al., 1998]. An electroactive film was self assembled upon which a solution of

proteoliposomes was fused, the oxidation of reduced cytochrome c by the membrane bound cytochrome c oxidase being transduced to a gold electrode via a mediator bound to the polymer cushion where the lipid membrane rested [Lindholm-Sethson, 1998]. A glucose biosensor was fabricated by LB deposition of a phospholipid analogous vinyl polymer together with glucose oxidase [Yasuzawa et al., 2000]. LB films containing butyrylcholinesterase were fabricated to produce an enzymatic field effect transistor for the detection of organophosphorus pesticides in water [Wan et al., 2000].

The advantages of LB films deposition technique in the fabrication of biosensors are :

- (a) creation of multilayered structure which allows to deposit all the components of a biosensor by one standard procedure leading to easy automation of the industrial production
- (b) easy inclusion of protein layers in the desired position of the layered structure
- (c) deposition of enzymes without any contact with air which allows to avoid protein denaturation
- (d) minimisation of the amount of tensoactive materials consumed for the production of biosensors
- (e) high stability in aqueous solutions of the deposited tansoactive bilayers

At the same time this technique suffers from:

- (a) long time of deposition
- (b) limitations of the transport of matter between hydrophobic chains of the deposited lipid bilayers, which in some cases can deactivate mediators requiring protons or hydroxyls for their reactions

1.10 Challenges

Nowadays a growing interest is demonstrated towards the development of *in-vivo* sensors for biomedical applications. These sensors should satisfy at least three requirements: to be oxygen independent; to be stable at temperatures of 36-40°C; and to be miniaturisable. It can be seen that thermophilic NAD(P)⁺ dependent dehydrogenases are the enzymes of choice for the construction of miniaturised biosensors provided that an efficient, simple and reagentless system for harnessing NAD(P)⁺ dependent dehydrogenases is developed. Neither the carbon paste configurations nor the configurations based on the adsorption of NAD⁺ onto pre-prepared membranes are applicable because of size limitations. Only the strategies of entrapment of NAD⁺ in electropolymerised films, self-assembled monolayers and the entrapment in hydrogels formed *in situ* are applicable for the fabrication of biosensors operating *in-vivo*.

The main problems that should be solved in this field are (i) low response currents, (ii) low

operational and shelf stability of the resulting electrodes caused by three factors: (a) loss of $\text{NAD(P)}^+/\text{NAD(P)H}$ redox couple, (b) loss of mediators for NAD(P)H oxidation, (c) loss of enzyme activity. How can these challenges be addressed?

(i) Low response currents can be increased by achieving an excess of NAD^+ using oxidising mediators with high rate of NADH oxidation and/or using an NADH oxidising redox polymer. The majority of reported NADH oxidising polymers are not stable at high pH and their capacity to produce enzymatically active NAD^+ has never been confirmed, consequently we opted for the synthesis and detailed characterisation of a novel NADH oxidising polymer (Os-phendione-PVP) by the complexation of $[\text{Os}(1,10\text{-phenanthroline-5,6-dione})_2\text{Cl}_2]$ with poly(4-vinyl pyridine).

(ii) The reported reagentless dehydrogenase biosensors [Laurinavicius et al., 1996] produced by the entrapment of NAD(P)^+ in gelatine and poly(lysine) matrix showed low operational and shelf stability life because of the following three factors:

(a) Leaching of $\text{NAD(P)}/\text{NAD(P)H}$ redox couple from the electrode surface which was very rapid in the previously reported reagentless sensors hence in the course of this thesis we developed a novel hydrogel matrix: poly(vinylpyridine) modified with amino groups which can be crosslinked with NAD(P)^+ by polyethylene glycol diglycidyl ether. Another type of gel was prepared by us on the basis of NAD^+ immobilised on alginic acid [Nakamura, et al., 1996]. It was also opted for creating highly organised layered architectures on the electrode surface. Many biosensors based on the organised layered architecture where an enzyme was sandwiched between lipid bilayers, have been reported in the literature but to our knowledge a reagentless dehydrogenase biosensor of this configuration has never been reported, probably due the absence of good amphiphilic mediators for the effective NADH oxidation at low working potential. Therefore a new NADH oxidising amphiphilic mediator having 1,10-phenanthroline-5,6-dione ligands has been synthesised and used for the fabrication of a reagentless glutamate biosensor of the ordered architecture. The analogue of this surfactant carrying bipyridine ligands instead of 1,10-phenanthroline-5,6-dione was synthesised too and its tensoactive properties were compared with those of the NADH oxidising surfactant.

(b) Low operational stability due to the loss of the NADH oxidising mediator can be amended: by covalent bonding of the mediator to the electrode surface or the macromolecules of the matrix; utilisation of redox polymers, and by employment of mediator with high chemical stability. The new NADH oxidising mediators, polymer Os-phendione-PVP and amphiphilic complex Os-phendione-surfactant were used in this work for the production of reagentless biosensors based on the three above mentioned

configurations.

(c) The poor operational and shelf stability due to the loss of the enzyme and its deactivation could be ameliorated by the formation of covalent bonds between the enzymes and the electrode surface and the macromolecules of a matrix, utilisation of stabilising additives and/or by utilisation of more stable thermophilic enzymes. Still, no detailed comparison of the operational and shelf stability of thermophilic and mesophilic enzyme based biosensors was published in the literature, so in the course of the present work such a study was performed using thermophilic and mesophilic glutamate dehydrogenases immobilised together with different additives, and glucose-6-phosphate dehydrogenases. For the first time biosensors based on thermophilic enzymes were applied to the detection of glutamate and glucose-6-phosphate at the temperatures higher than 60°C.

2. EXPERIMENTAL METHODS

2.1 The synthesis of new mediators for the oxidation of NADH

The synthesis of the redox amphiphilic and polymeric mediators was performed by the introduction of polymeric and amphiphilic ligands into osmium complexes [Os(1,10-phenanthroline-5,6-dione)₂Cl₂] or [Os(2,2'-bipyridine)₂Cl₂]. These reactions were performed at high temperatures (above 180°C) using reflux in ethylene glycol in a round bottom glass flask connected to a condenser. The structures of the resulting surfactants were established on the basis of ¹H NMR study in CDCl₃ using tetramethylsilane as a standard. NMR data confirmed the presence of long alkane chains: 1.29 p. p. m. (m) 1.26 (m) , 0.88 (t).

2.2 Electrochemical measurements in bulk solution

In the course in this work a three-electrode conventional thermostabilised cell (3 ml) equipped with an Ag/AgCl/KCl_{sat} reference electrode, a platinum auxiliary electrode, and a graphite electrode modified according to one of the above mentioned methods as working electrode. The buffer, (0.1 M sodium phosphate containing 0.15 M sodium chloride) served as supporting electrolyte. The electrochemical measurements were performed in a three-electrode thermostabilised electrochemical cell (Figure 10) connected to the potentiostat Autolab PGSTAT 10 (Eco chemie, Holland) controlled by a computer.

Surface coverage of electroactive species was determined by linear potential sweep cyclic voltammetry in which the under peak areas served to calculate the charge. Taking into account the number of exchanged electrons per redox molecule and the Faraday's constant the surface concentration was calculated. The peak current I_p is a function of scan rate ν , charge diffusion coefficient D_0 , number of exchanged electrons n , surface concentration of redox active species C_0^* , surface coverage Γ , electrode surface area A , temperature T , Faraday's constant F and gas constant R according to the equations:

$$I_p = 0.4463(nF)^{3/2}(RT)^{-1/2}AC_0^*\nu^{1/2}D_0^{1/2} \text{ (for a thick film of redox species)}$$

$$I_p = n^2F^2\Gamma A\nu(4RT)^{-1} \text{ (for a monolayer of redox species)}$$

Therefore in order to minimise the influence of charge diffusion limitations through the film of electroactive species on the surface low scan rates not exceeding 4 mV/s should be used for surface coverage measurements. Another factor affecting the credibility of surface coverage measurements is the reliability of determination of the electrode surface area.

In the course in the present work potential step chronocoulometry based on the Anson equation was employed to find the electrode surface area from the charge(Q) vs. time(t)

EXPERIMENTAL METHODS

dependence in the presence of redox species with known concentration C :

$$Q=2nFAD^{1/2}C\pi^{-1/2}t^{1/2}$$

It is important to note that in any potential step experiment, there is a delay in attaining the step potential due to the finite rise time of the potentiostat. This non-ideal behaviour affects the validity of the data points measured during this delay time, and hence these data are discarded when calculating the slope and intercept. On another, hand the Anson equation is valid only within very short time periods hence in this study the pulse width not larger than 300 ms was used.

Linear potential sweep cyclic votammety was employed also for the determination of heterogeneous rate constant k_s and the transfer coefficient α between the electrode surface and adsorbed redox mediators accordind to the Laviron equations:

$$E_{pc}-E^{0'}=(2.303RT/cnF)\log[cnFv/(RTk_s)]$$

$$E_{pa}-E^{0'}=(2.303RT/(1-\alpha)nF)\log[(1-\alpha)nFv/(RTk_s)]$$

Where E_{pc} and E_{pa} are cathodic and anodic peak potentials, $E^{0'}$ is the formal redox potential, v is the scan rate, F is Faraday's constant, n is the number of electron. These equations are applicable only if the difference $(E_{pa} - E_{pc})/n$ is larger than 200 mV. In the case of quasi-reversible redox couple this condition can be satisfied by running cyclic voltammograms of an immobilised redox monolayer at scan rates higher than 10 V s⁻¹.

Chronoamperometric measurements with a rotating disk electrode were employed in the determination of rate constants of the reaction between NADH and mediators adsorbed on graphite using a solution having the volume of at least 10 mL. In order to eliminate the influence of oxygen on the response the modified rotating electrodes all solutions of NADH used in the measurements were deaerated with argon. The estimation of rate constants for the reaction between NADH and a mediator was based on the hypothesis that in thin polymeric films (which were obtained by the deposition of only one monolayer of a mediator) diffusional transport of both charge and NADH can be neglected and the substrate-mediator complex is formed in this interaction according to the following scheme:



The model proposed by Gorton to calculate the dependence of the catalytic current (I_{cat}) on experimental parameters in terms of a Michaelis-Menten like kinetic model were utilised in this work.

$$1/I_{cat}=1/(nFA\Gamma k c_{\text{NADH}}) + [1/(0.62nFAD^{2/3} c_{\text{NADH}} v^{-1/6})](1/\omega^{1/2})$$

$$1/I_{cat}=1/(nFA\Gamma k_2) + [K_M/(nFA\Gamma k_2) + 1/(0.62nFAD^{2/3} v^{-1/6} \omega^{1/2})](1/c_{\text{NADH}})$$

$$K_M=(k_{-1}+k_2)/k_1$$

where D ($\text{cm}^2 \text{s}^{-1}$) is the diffusion coefficient of NADH, ν ($\text{cm}^2 \text{s}^{-1}$) the hydrodynamic viscosity, ω (rad s^{-1}) the speed of rotation of an electrode, A (cm^2) the electrode surface area, Γ (mol cm^{-2}) the surface coverage, c_{NADH} (M) the concentration of NADH, and k ($\text{M}^{-1} \text{s}^{-1}$) the rate coefficient of the formal overall chemical reaction:

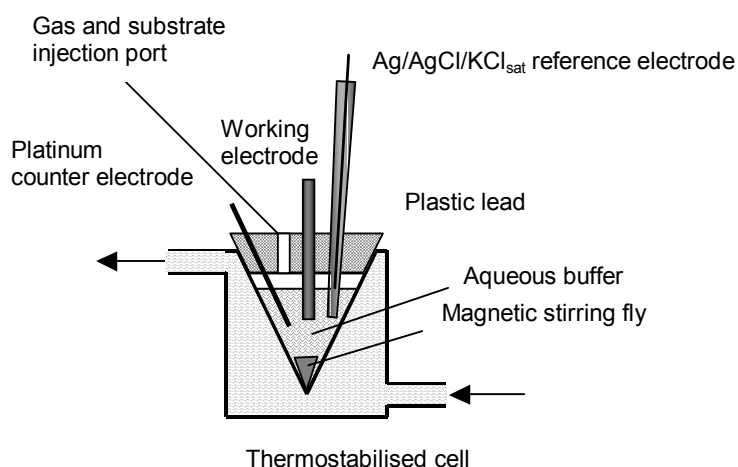
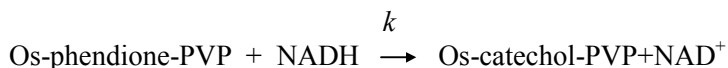


Figure 10. The electrochemical cell employed in electrochemical experiments

2.3 Shelf life study of glutamate biosensors

Disposable glutamate electrodes were prepared by deposition of the aqueous solution of mesophilic or thermophilic GLDH, NAD^+ , water soluble mediator $[\text{Os}(4,4'\text{-dimethyl-2,2'\text{-bipyridine}})_2(1,10\text{-phenanthroline-5,6-dione)]\text{Cl}_2$ and an additive on screen printed electrodes depicted in Figure 11. A disposable glutamate biosensor was connected to the potentiostat Autolab PGSTAT 10 by the following way: the carbon electrode was connected to the working lead and Ag/AgCl reference electrode to the reference and auxiliary leads, next the biosensor was fixed during 5 min on a glass heat exchanger thermostabilised at 40°C . In order to determine the response of the sensor $0.5 \mu\text{L}$ of a sample solution was deposited and after 20 s a potential of $+0.2 \text{ V}$ vs. Ag/AgCl electrode was applied to the working electrode.

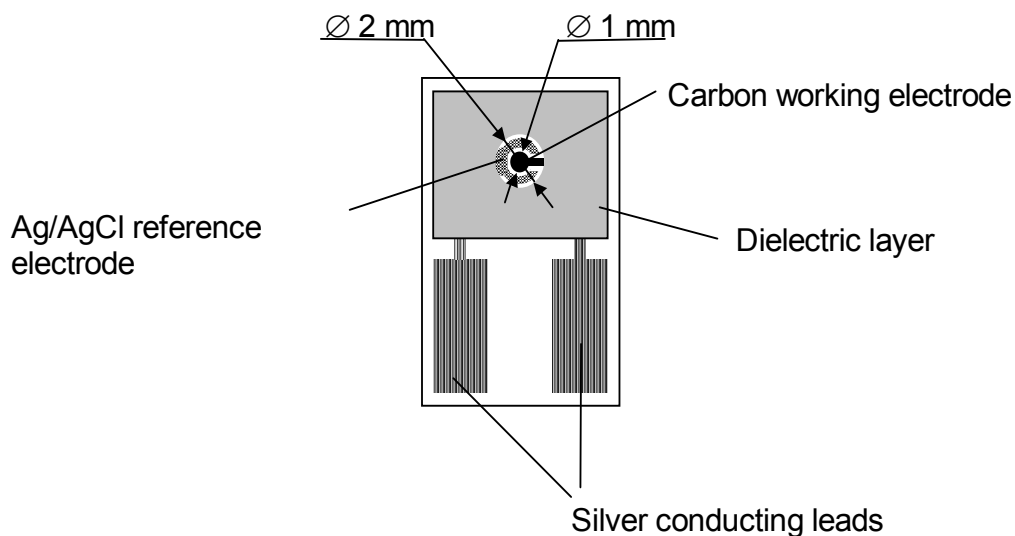


Figure 11. Screen printed electrode used for the preparation of disposable glutamate biosensors.

The value of current after 30 s (starting from the moment of applying the potential) was recorded for every electrode. From three to five sensors were used for measurements at every point. All sensors were assayed by depositing three different samples: 0.1 M Tris buffer, pH 7.4 (containing 0.15 M NaCl), or 0.6 M glutamate solution in this buffer, or 0.6 M glutamate solution with 0.18 M NAD^+ in the buffer.

2.4 Glutamate dehydrogenase (GLDH) assay method

Both mesophilic and thermophilic GLDH were tested spectrophotometrically by following the increase in absorbance at 340 nm at 30°C or 40°C. The following reagents were prepared: (A) 0.1 M sodium phosphate buffer, pH 7.4, containing 0.15 M sodium chloride; (B) 0.1 M $\beta\text{-NAD}^+$ sodium salt solution in reagent A; (C) 0.3 M L-glutamic acid monosodium salt solution in reagent A; (D) mesophilic or thermophilic GLDH solution in reagent A. Next the following reagents : 884 μL of A, 33 μL of C, 33 μL of D were pipetted into a suitable 1 mL cuvette, mixed and equilibrated to 30 or 40°C. Then 50 μL of B were injected, mixed by inversion and the increase in A_{340} was recorded for 2 min. The ΔA_{340} (Au/min) was obtained using the maximal linear rate for both the test and blank (without enzyme) mixtures. The activity was calculated by the equation:

$$\text{Units/ml}_{\text{enzyme stock solution}} = \frac{\Delta A_{340} / \text{min Test} - \Delta A_{340} / \text{min Blank}}{\varepsilon_{\text{NADH}} (\text{ml}_{\text{enzyme stock solution}} / \text{ml}_{\text{RM}})}$$

Where $\varepsilon_{\text{NADH}}=6.22 \text{ mM}^{-1} \text{ cm}^{-1}$ extinction coefficient of β -NADH, $\text{ml}_{\text{enzyme stock solution}}/\text{ml}_{\text{RM}}$ is amount of ml of stock enzyme solution per 1 ml of reaction mixture in a cuvette. One unit of GLDH oxidises 1 μmol of L-glutamate per minute at pH 7.4 at 30 or 40°C. Protein concentration was determined spectrophotometrically at A_{280} using an absorbance coefficient of $0.973 \text{ cm}^2 \text{ mg}^{-1}$.

2.5 Glucose-6-phosphate dehydrogenase (G6PDH) assay method

Both mesophilic and thermophilic G6PDH were tested spectrophotometrically by following the increase in absorbance at 340 nm. For the G6PDG assay the following reagents were prepared: (A) 0.12 mM sodium phosphate buffer, pH 7.0, containing 0.5 M sodium chloride; (B) 0.025 M β -NAD⁺ sodium salt solution in reagent A; (C) 0.025 M glucose-6-phosphate solution in reagent A; (D) mesophilic or thermophilic G6PDH solution in reagent A. Next the following reagents: 650 μL of A, 50 μL of D, were pipetted into 1 mL cuvettes, mixed and equilibrated to 25°C (in case of mesophilic G6PDH) or 70°C (in case of thermophilic G6PDH) in the presence of a rotating micro-stirrer. Next 50 μL of C and 50 μL of B were injected and the increase in A_{340} was recorded for 2 min. The ΔA_{340} (Au/min) was obtained using the maximal linear rate for both the test and blank (without enzyme) mixtures. The activity was calculated by the equation mentioned in the description of the GLDH activity assay.

2.6 Instrumentation used for the study of amphiphilic compounds

A KSV 5000 film deposition system (KSV Instruments Ltd., Finland) was used for the preparation of the Langmuir-Blodgett films and the equipment was supervised with a KSV multitasking software package LB 5000 version 3.7. The area of the Teflon trough was 85 426 mm^2 and the surface pressure was monitored with a 20 mm wide Wilhelmy platinum plate suspended from a KSV microbalance. The Langmuir trough was extensively cleaned on a daily basis, which comprised soaking trough and barrier in 96 % ethanol, wiping them with Techni-Cloth texwipes, and rinsing for at least 20 min in ultrapure water. All electrochemical experiments on the transferred films were conducted at room temperature *in situ* in the Langmuir trough with a computer controlled (BAS, Bioanalytical Systems, West Lafayette, IN) CV-50W voltammographic analyser. A conventional three-electrode set up was employed involving a platinum wire counter electrode, a Ag/AgCl/KCl_{sat} double junction reference electrode, and a planar gold working

EXPERIMENTAL METHODS

electrode. The thin gold film electrodes (thickness ≈ 80 nm and electrode area 0.50 cm^2 connected with a 1 mm wide strip to a contact pad) were deposited by electron gun evaporation in ultra high vacuum onto glass slides using (3-mercaptopropyl)-trimethoxy silane as a molecular glue between glass and glass and the gold working electrode.

3. GENERAL OVERVIEW OF THE PRESENTED PAPERS

The work performed in the course of elaboration of the present thesis was aimed at the development of new techniques for the fabrication of electrodes modified with dehydrogenases dependent on NAD(P)⁺. The results of this investigation are presented in the following manuscripts:

1. **Electrocatalytic Oxidation of NADH at Graphite Electrodes Modified with Osmium Phenanthroline-dione.**

I. C. Popescu, E. Domínguez, A. Narváez, V. Pavlov, I. Katakis
J. Electroanal. Chem. 464 (1999) 208-214.

2. **A Novel [Os(1,10-phenanthroline-5,6-dione)₂(PVP)₄Cl]Cl Redox Polymer for Electrocatalytic Oxidation of NADH and its Application to Construction of β-glucose Biosensors.**

V. Pavlov, O. Rincon, S. Sole, A. Narváez, E. Dominguez, I. Katakis
Submitted for publication in *Anal. Chem.*

3. **New Reagentless Glutamate Biosensors Based on Mesophilic and Thermophilic Glutamate Dehydrogenases.**

V. Pavlov, S. Kengen, I. Katakis
Submitted for publication in *Anal. Chem.*

4. **The Use of Lipid Bilayers for the Construction of Reagentless Biosensors Based on NAD⁺ Glutamate Dependent Dehydrogenase.**

V. Pavlov, B. Lindholm-Sethson, G. Lindblom, I. Katakis
Submitted for publication in *Langmuir*.

5. **Amperometric Sensing at High Temperature with a “Wired” Thermostable Glucose-6-Phosphate Dehydrogenase from *Aquifex aeolicus*.**

R. Iyer, V. Pavlov, I. Katakis, L. G. Bachas
Anal. Chem. 75 (2003) 3898-3901.

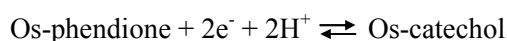
In brief these articles can be summarized as follows:

Article 1. Electrocatalytic Oxidation of NADH at Graphite Electrodes Modified with Osmium Phenanthroline-dione.

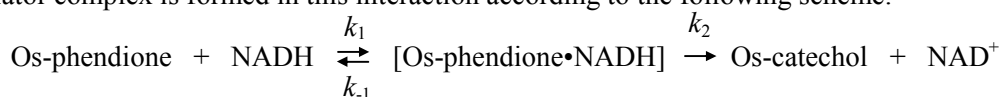
OBJECTIVES: The investigation described in this article was carried out with the purpose to study the electrochemical behaviour of [Os(4,4'-dimethyl-2,2'-bipyridine)₂(1,10-phenanthroline-5,6-dione)](PF₆)₂ (Os-phendione) and assess its capacity to serve as a mediator for NADH oxidation.

METHODS: This compound was synthesised through complexation of [Os(4,4'-dimethyl-2,2'-bipyridine)₂]Cl₂ with 1,10-phenanthroline-5,6-dione (phendione) by refluxing in ethylene glycol and converted into water insoluble form by ion exchange of the anions, next it was adsorbed on the surface of graphite electrodes. Cyclic voltammetry at in aqueous solutions at different scan rates and pH values was utilised to assess the number of protons and electrons participating in the redox process of Os-phendione. By evaluating the change in peak potentials with the potential scan rate the rate constant of heterogeneous electron transfer was calculated. Chronoamperometry using graphite rotating disk electrodes poised at +0.2 V vs. Ag/AgCl/KCl_{sat} was used for measurement of the second order rate constant of electrocatalytic oxidation of NADH.

MAIN RESULTS AND CONCLUSIONS: The redox potential of the complexed phendione was pH dependent because of the participation of protons according to the reaction:

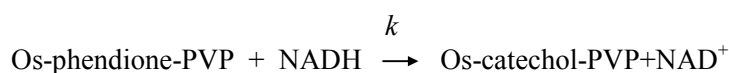


So at pH 6.0 the formal standard potential ($E^{0'}$) was +0.08 V vs. Ag/AgCl/KCl_{sat}, the voltammetric wave being quasi-reversible. The rate constant of heterogeneous electron transfer between the graphite electrode and adsorbed mediator was estimated to be 20.1 s⁻¹, the value was two times higher than this reported for Meldola Blue (10 s⁻¹). Voltammetric study of electrodes modified with Os-phendione in the presence of NADH in a solution at pH 6.0 demonstrated a dramatic enhancement of the anodic current indicating the electrocatalytic oxidation starting from +0.06 V vs. Ag/AgCl/KCl_{sat}. This potential was much lower than that for the NADH oxidation at bare graphite electrodes. The estimation of rate constants for the reaction between NADH and Os-phendione was based on the hypothesis that in a monolayer of the mediator adsorbed on a graphite surface the diffusional transport of both charge and NADH can be neglected and substrate-mediator complex is formed in this interaction according to the following scheme:



The second order rate constants of electrocatalytic oxidation of NADH ($k_{[\text{NADH}]=0}$) were measured at different pH, and proved to be 3.1 x10³, 1.9x10³, and 0.9 x10³ M⁻¹ s⁻¹, at pH 5.5, 6.1, and 7.0

respectively.



The value of $k_{[\text{NADH}]=0}$ was lower than the corresponding value for Meldola blue at pH 7.0. It was observed that the linear correlation between $E^{0'}$ and $\log k_{[\text{NADH}]=0}$ found for phenoxazine derivatives, extends to Os-phendione too. This mediator reversibly oxidises NADH through the formation of a charge transfer complex.

Article 2. A Novel [Os(1,10-phenanthroline-5,6-dione)₂(PVP)₄Cl]Cl Redox Polymer for Electrocatalytic Oxidation of NADH and its Application to Construction of β -glucose Biosensors.

OBJECTIVES: This investigation was performed in order to synthesise new NADH oxidising polymeric mediator [Os(1,10-phenanthroline-5,6-dione)₂(PVP)₄Cl]Cl where every fourth pyridine is complexed to osmium, (Os-phendione-PVP), to study its electrochemical behaviour, its capacity towards the electrocatalytic oxidation of NADH, and the possibility of its use in reagentless biosensors based on glucose dehydrogenase (GDH).

METHODS: The polymer (Os-phendione-PVP) was produced via derivatisation of poly(vinyl pyridine), having molecular weight of 50000, with [Os(1,10-phenanthroline-5,6-dione)₂Cl₂] by reflux in ethylene glycol. The electrochemical study of this redox polymer adsorbed on graphite electrodes was performed by cyclic voltammetry at different values of scan rate and pH to assess the number of protons and electrons participating in the redox reaction, the influence of pH on its formal standard potential, and the rate constant of heterogeneous electron transfer. Amperometric experiments with graphite rotating disk electrodes poised at +0.2 V vs. Ag/AgCl/KCl_{sat} were performed to find the rate constant for the interaction with NADH $k_{[\text{NADH}]=0}$. An electrochemical conversion experiment was carried out by the bulk oxidation of NADH at graphite electrodes modified with Os-phendione-PVP poised at +0.15 V vs. Ag/AgCl/KCl_{sat}. Spectrophotometry at 340 nm was used for measuring the depletion of the NADH concentration. The resulting NAD⁺ solution was used as a cosubstrate of GDH and the recovery of the original NADH concentration was monitored spectrophotometrically at 340 nm. Next reagentless glucose biosensors were built by the immobilisation of different amounts of glucose dehydrogenase and NAD⁺ in the new hydrogel matrix formed by crosslinking of polyvinyl pyridine bearing amino groups with poly(ethylene glycol) diglycidyl ether.

MAIN RESULTS AND CONCLUSIONS: The wave of phendione in Os-phendione-PVP is quasi reversible and pH dependent, the formal redox potential being equal to +0.04 V vs. Ag/AgCl/KCl_{sat} at pH 6.0. Cyclic voltammetry demonstrated also the voltammetric waves of Os^{II/III}

redox couple at +0.407 V vs. Ag/AgCl/KCl_{sat}, as expected for osmium atom coordinated with five pyridine ligands and one Cl⁻. The comparison of peak areas of osmium and phendione indicated that two phendione moieties exchanged four electrons and four protons in the redox process at pH values lower than 6.5 according to the reaction:



confirming the suggested structure of the new polymer. The cyclic voltammetry performed at high scan rates at pH 5, 6 and 7 demonstrated linear anodic and cathodic peak current (I_p) versus scan rate (v) plots at scan rates up to 0.5 V s⁻¹ which indicates that there are no limitations of charge propagation within the thin layer of Os-phendione-PVP adsorbed on the electrode surface. The heterogeneous electron transfer rate constant k_s (18.7 s⁻¹ at pH 6.0), was very close to this measured for monomeric Os-phendione. Cyclic voltammetry performed with Os-phendione-PVP modified graphite electrodes in the presence of NADH in the bulk solution at pH 6.0 showed great increase in the oxidation current to show electrocatalytic NADH oxidation starting from the potential +0.07 V vs. Ag/AgCl/KCl_{sat}. This potential is much lower than that for NADH oxidation at bare electrodes (+0.33 V vs. Ag/AgCl/KCl_{sat}) under the same conditions.

The rate constant for the interaction with NADH $k_{[\text{NADH}]=0}$ was $(1.9 \pm 0.2) \times 10^3 \text{ M}^{-1}\text{s}^{-1}$ at pH 6.0, which is practically equal to that Os-phendione because the standard potentials of both mediators are close. According to the data of the electrochemical conversion experiment, electrodes modified with Os-phendione-PVP generated 100% enzymatically active NAD⁺ hence the new NADH oxidising polymer is suitable for the fabrication of reagentless biosensors based on NAD⁺ dependent dehydrogenases.

Reagentless glucose biosensors were built using graphite electrodes modified with Os-phendione-PVP and a new hydrogel for the immobilisation of enzyme and cofactor. The response of glucose biosensors was dependent on the amount of immobilised enzyme and the amount of NAD⁺. The maximum response current shown in reagentless mode of operation was 35.6 $\mu\text{A cm}^{-2}$ and in the presence of saturating NAD⁺ concentration 92 $\mu\text{A/cm}^2$. The effect of pH on the response of reagentless and non reagentless glucose biosensors demonstrated the increase in the response current with pH until the value of 9.0. This data corroborates well with the effect of pH on the activity of free GDH. The kinetic analysis based on the equation relating the response current with the construction parameters of biosensors has demonstrated that the response current of all reagentless biosensors is limited by the amount of immobilised NAD⁺. Thus new NADH oxidising polymeric mediator has been developed which generates enzymatically active coenzyme. This mediator is suitable for the construction of reagentless biosensors based on NAD⁺ dependent dehydrogenases which demonstrate high current densities.

Article 3. New Reagentless Glutamate Biosensors Based on Mesophilic and Thermophilic Glutamate Dehydrogenases.

OBJECTIVES: This investigation was carried out to develop two new methods for the construction of reagentless biosensors based on NAD^+ dependent dehydrogenases and to compare the performance of resulting glutamate sensors prepared using mesophilic and thermophilic glutamate dehydrogenases (GLDH).

METHODS: Graphite electrodes were modified with a monolayer of new NADH oxidising polymer Os-phendione-PVP and utilised for the fabrication of reagentless glutamate biosensors by two methods. The first one consisted the immobilisation of mesophilic bovine GLDH or thermophilic GLDH from *Pyrococcus furiosus* in the hydrogel matrix formed by crosslinking of polyvinyl pyridine bearing amino groups (“binder” polymer) with poly(ethylene glycol) diglycidyl ether. The second method based on physical adsorption of polymeric form of NAD^+ , alginate carrying NAD^+ moieties (NAD^+ -alginate), together with thermophilic or mesophilic GLDH. The response curves, the effect of temperature and pH on the response current, and operational stability were studied. The second part of investigation was the accelerated shelf stability (at 40°C) study of disposable glutamate biosensors prepared using thermophilic and mesophilic enzymes mixed together with different polymeric and monomeric additives, NAD^+ , and mediator [Os(4,4'-dimethylbipyridine)₂(1,10-phenanthroline-5,6-dione)]Cl₂. The chronoamperometric response of disposable biosensors to analyte was determined by spreading 0.5 µl of sample solution on working carbon and Ag/AgCl/KCl_{sat} reference electrodes.

MAIN RESULTS AND CONCLUSIONS:

Cyclic voltammetry of the reagentless glutamate biosensors fabricated by the two above mentioned methods demonstrated clear electrocatalytic waves achieving almost a plateau at potentials more negative than 0.2 V vs. Ag/AgCl/KCl_{sat} in the presence of glutamate in sample solutions.

The effect of pH on the maximal response current of the glutamate biosensors was studied. The biosensors based on NAD-alginate prepared from mesophilic and thermophilic GLDH have maximum response at pH 9.0. This result is in good agreement with the pH optimum of 9.0 for glutamate oxidation by free bovine GLDH and GLDH from *Pyrococcus furiosus*. The biosensors based on immobilisation by crosslinking with “binder” polymer constructed using mesophilic and thermophilic GLDH achieved maximal response currents at pH 9.5 probably because of increased enzymatic stability caused by crosslinking. The study of the effect of temperature on the response to glutamate was also performed. The thermophilic enzyme based biosensors, independently of the immobilisation procedure, have shown increase in response to L-glutamate up to the maximum temperature of 88°C achieved in the thermostated electrochemical cell, this temperature value corroborates with optimal temperature of 95°C for free thermophilic GLDH. Mesophilic

biosensors based on NAD-alginate showed the lowest optimal temperature of 52°C, “binder” polymer biosensors had the highest optimal temperature 56°C. This data is in good agreement with the published thermostability study of bovine GLDH according to which this enzyme starts to lose activity from the temperature of 52°C. The use of thermophilic GLDH instead of the mesophilic enzyme allowed to increase the operational stability of “binder” polymer based biosensors at 65°C, which showed the half life time of 16 min (in the presence of NAD⁺ in a sample). In the reagentless mode of operation at 30°C the mesophilic enzyme based biosensors prepared using “binder” polymer demonstrated the half-life ($\tau_{1/2}$) of 12 h which is higher by 9 times than $\tau_{1/2}$ of the biosensors based on simple adsorption of NAD⁺-alginate (1.5 h) due to better immobilisation of the biosensor components by forming covalent bonds.

The accelerated study of shelf life of mesophilic and thermophilic glutamate biosensors demonstrated that thermophilic dehydrogenase based sensors demonstrated the expansion of shelf half life by about 11 times in comparison with that of the mesophilic biosensors. The effect of different additives on the shelf life was studied too, to reveal that the best results were achieved by addition of the copolymer of vinyl-pyrrolidone and dimethylamino ethyl methacrylate termed as Gafquat[®] HS100 which enhanced the stability of mesophilic sensors by 4.6 times, and of thermophilic sensors by 3.3 times. This polyelectrolyte, promoting electrostatic interactions, forms a protein-polyelectrolyte adduct apparently stabilizing the enzyme.

With the purpose to take into consideration the loss of response to glutamate due to the decomposition of NAD⁺ in biosensors during the shelf life study the controlled samples of glutamate containing fresh NAD⁺ were utilised in the investigation but the response to pure glutamate proved to be higher by 1.5 times. The same phenomenon was encountered if NADH was used instead of glutamate i.e. the response to pure NADH samples was higher by 1.5 times than that to NADH samples containing NAD⁺. This was related with the hypothesis of the formation of a parasite complex between NAD⁺ and the mediator. According to the kinetic analysis the effect of NAD⁺ on the response to NADH can be observed at high NAD⁺ concentration and low rate of oxidation of the reduced mediator at the electrode surface.

Finally it can be concluded that two new methods for the fabrication of reagentless biosensors based on NAD⁺ dependent dehydrogenases have been developed which can be utilised in miniaturised sensors. The advantages of using thermophilic glutamate dehydrogenase instead of mesophilic enzyme is the improvement of operational stability at extreme temperatures and the extension of shelf life. The operational stability of the resulting sensors at temperatures more than 40°C is limited by leaching of NAD⁺.

Article 4. The Use of Lipid Bilayers for the Construction of Reagentless Biosensors Based on NAD⁺ Dependent Glutamate Dehydrogenase.

OBJECTIVES: The study described in this work was performed to synthesise a new tensoactive mediator for the electrochemical oxidation of NADH, asses its tensoactive properties, include it in lamellar phase, and use it for the construction of reagentless biosensors based on NAD⁺ dependent bovine glutamate dehydrogenase (GLDH).

METHODS: A novel NADH oxidising surfactant [Os(1,10-phenanthroline-5,6-dione)₂4,4'-(n-C₁₈H₃₇NHCO)₂bpy)](PF₆)₂ (Os-phendione-surfactant) was produced by complexation of [Os(1,10-phenanthroline-5,6-dione)₂]Cl with the hydrophobic ligand 4,4'-(n-C₁₈H₃₇NHCO)₂bpy under reflux in ethylene glycol. Its structure was confirmed by ¹H NMR investigation. Langmuir-Blodgett (LB) monolayers of Os-phendione-surfactant were studied in a Langmuir-Blodgett trough. The redox surfactant together with NAD⁺ and GLDH was included into a lamellar phase based on the lipid 1,2-dioleoyl-sn-glycero-3-phosphatidylcholine and ³¹P NMR investigation proved the presence of lipid multilayers. Reagentless biosensors were constructed by adsorption of the lamellar phase on graphite electrodes. The effect of analyte concentration, temperature, and pH was studied.

MAIN RESULTS AND CONCLUSIONS:

Surfactant for the NADH oxidation can be produced by the complexation of a hydrophobic ligand with redox active head group bearing 1,10-phenanthroline-5,6-dione leading to Os-phendione-surfactant.

This surfactant forms Langmuir-Blodgett monolayers in the air-water interface. The surface pressure vs. area per molecule isotherm showed a take off surface pressure at 240-250 Å² per molecule, and the monolayer collapsed at 78-80 mN m⁻¹. The results obtained from this isotherm point out to the mean molecular area of 190 Å². This high value can be explained by the presence of bulky phenanthroline ligands. Some reorganisation of the monolayer takes place starting from surface pressure value of 40 mN m⁻¹. LB layers of this compound can be deposited on gold planar electrodes but the redox reactions at the phendione moiety are passivated due to the limitation on the transport of protons through the layers of hydrophobic tails. The mixture of this mediator with 1,2-dioleoyl-sn-glycero-3-phosphatidylcholine forms a lamellar phase, (confirmed by the presence of a broad peak from -7 to -15 ppm in ³¹P NMR spectra) in which phendione retains electrochemical activity. NAD⁺ and GLDH can be included in this lamellar phase to give the suspension which is adsorbed on graphite electrodes to yield reagentless glutamate biosensors which showed clear electrocatalytic cyclic voltammograms in the presence of glutamate. Their response time was 7-8 min, and was limited by the diffusion of analyte through the lamellar phase. The operational half-life was 30 min, because of leaching of GLDH or NAD⁺.

Therefore Os-phendione-surfactant can be utilised to create a lamellar phase in the presence of a “helper” lipid at room temperature. The resulting lamellar phase can include NAD^+ and dehydrogenase offering a new method for the fabrication of reagentless biosensors. Their response is limited the rate of the NADH oxidation at the electrode surface and by the transport of the analyte and the reaction products through the layers of hydrophobic aliphatic tail groups. In order to be useful for the construction of biosensors this new technique needs to improve the entrapment of NAD^+ and enzyme and the stability of the lamellar phase.

Article 5. Amperometric Sensing at High Temperature with a “Wired” Thermostable Glucose-6-Phosphate Dehydrogenase from *Aquifex aeolicus*.

OBJECTIVES: This investigation was performed with the purpose to develop the system operating at temperatures up to 83°C for enzymatic sensing based on NAD^+ dependent dehydrogenase and to study the advantages of biosensors based on thermophilic glucose-6-phosphate dehydrogenase over the mesophilic enzyme.

METHODS: Graphite electrodes were modified with NADH oxidising polymer [Os(1,10-phenanthroline-5,6-dione)₂(PVP)₄Cl]Cl. Then thermophilic glucose-6-phosphate dehydrogenase (tG6PDH) from *Aquifex aeolicus* and the mesophilic analogue from *Leuconostoc mesenteroides* (mG6PDH) together with NAD^+ were immobilised on the modified electrodes through crosslinking with poly(ethylene glycol) diglycidyl ether in a hydrogel matrix formed by poly(vinylpyridine) bearing amino groups. The response of the resulting biosensors to glucose-6-phosphate in the presence of NAD^+ at temperatures ranging from 25 to 83 °C was measured by chronoamperometry at applied potential +0.15 V vs. Ag/AgCl/KCl_{sat}.

MAIN RESULTS AND CONCLUSIONS: The resulting glucose-6-phosphate biosensors based on the thermophilic enzyme showed Michaelis-Menten type response with an apparent K_M of 2.9 mM for glucose-6-phosphate (the free enzyme shows K_M of 0.18 mM in homogenous solution at 70 °C). The increase in the apparent K_M of the immobilised enzyme can be explained by transport limitations. The current densities at 0.05 M concentration of glucose-6-phosphate reached a plateau of 390 $\mu\text{A cm}^{-2}$ at 70 °C. Biosensors based on mG6PDH had an apparent K_M of 6.1 mM (free mG6PDH showed K_M of 0.069 mM in a homogenous solution at 25 °C) with current densities reaching a plateau of 120 $\mu\text{A cm}^{-2}$ at 0.05 M glucose-6-phosphate concentrations at 25 °C. Electrodes based on tG6PDH showed clear electrocatalytic activity up to 83 °C, proving that the enzyme exhibits high thermostability. In contrast, when mG6PDH was used, maximum activity at the temperature of 50 °C was observed above which there was a steady drop in current densities due to enzyme denaturation. The operational half life of tG6PDH immobilised system was 2 h at

60°C whereas the biosensors based on mG6PDH did not show any response to glucose-6-phosphate at this temperature due to total enzyme denaturation.

In summary, a robust system demonstrating the possibility of recycling of NAD^+ at extreme temperatures for using in conjunction with a recombinant thermophilic G6PDH from *Aquifex aeolicus* was developed. The scheme of mediation reported here can be used for many thermostable dehydrogenases that use the co-factors β -nicotinamide adenine dinucleotide (NAD^+) and β -nicotinamide adenine dinucleotide phosphate (NADP^+) thereby opening a wide spectrum of applications at high temperatures in biosensing and bioreactors.

4. GENERAL OVERVIEW OF THE PAPERS NOT INCLUDED IN THE THESIS

Summary of the articles about the use the NADH oxidising complexes of osmium and 1,10-phenanthroline-5,6-dione)₂Cl₂ in electrochemical biosensors: (Parellada et al., 1998), (Hedemno et al., 1996), (Fernández et al., 1998).

OBJECTIVES: These investigations concentrated on the development of phosphate biosensors and glucose biosensors in which electrocatalytic oxidation of NADH was performed using complexes of osmium containing 1,10-phenanthroline-5,6-dione.

METHODS: The phosphate sensors were prepared by the immobilisation under membrane of glassy carbon electrodes of the composition containing [Os(1,10-phenanthroline-5,6-dione)₂Cl₂], NAD⁺, glucose-6-phosphate dehydrogenase, glycogen, phosphorylase A, phosphoglucomutase, Oxidation current was monitored at +0.2 V vs. SCE.

The glucose biosensors were fabricated using electrodes based on carbon paste containing [Os(4,4'-dimethyl-2,2'-bipyridine)₂(1,10-phenanthroline-5,6-dione)](PF₆)₂, glucose dehydrogenase and NAD⁺. The sensors were operated at the applied potential of +0.15 V vs. Ag/AgCl/KCl_{sat}.

MAIN RESULTS AND CONCLUSIONS: The resulting phosphate electrodes were based on the trienzymatic configuration consisting of phosphorylase A (enzyme that produces glucose 1-phosphate from glycogen), phosphoglucomutase (glucose 1-phosphate gives glucose 6-phosphate) and glucose 6-phosphate dehydrogenase (that oxidises glucose 6-phosphate in the presence of NAD⁺ producing NADH). This cofactor is reoxidised electrocatalytically by the mediator [Os(1,10-phenanthroline-5,6-dione)₂Cl₂] at the applied potential of +0.2 V vs. SCE. The optimised phosphate sensors demonstrated maximum current densities of 1.97 μA cm⁻² and the detection limit of 6 μM. The phosphate biosensors showed a catalytic current that is independent of the pH between pH 6.5 and 7.5. and the optimal temperature of operation of 41°C. When an Arrhenius plot is made of the temperature data, an activation energy of 84.5 kJ mol⁻¹ can be calculated. This high value shows that a kinetic step, probably the phosphoglucomutase reaction, limits the overall response of the system.

The use of [Os(4,4'-dimethyl-2,2'-bipyridine)₂(1,10-phenanthroline-5,6-dione)](PF₆)₂ mediator helped to achieve a more than 0.5 V lowering of the overpotential for NADH oxidation at carbon paste electrodes allowing to use the potential of +0.15 V vs. Ag/AgCl/KCl_{sat}. Electrochemical conversion experiments yielded a 100% conversion of NADH into enzymatically active NAD⁺. The reagentless glucose biosensors were based on the electrocatalytic oxidation through the above mentioned mediator of NADH generated by glucose dehydrogenase. The optimised reagentless glucose sensors demonstrated maximum current density of 469.8 μA cm⁻²

which was limited by enzyme kinetics. The operational stability study of these biosensors showed a loss of 6-8% in their response in 3-8 h. The stability was so good due to the creation of a 'pool' of NAD^+ and mediator in the carbon paste.

Summary of the article about electrochemical and spectroscopic characterization of a Langmuir-Blodgett film based on an $\text{Os}(\text{bpy})_3$ surfactant mediator: (Maestre et al., article in preparation).

OBJECTIVES: The investigation presented in the article was aimed at characterisation of the redox surfactant $[\text{Os}(\text{bpy})_2 4,4'-(\text{n}-(\text{C}_{18}\text{H}_{35})_{17}\text{NHCO})_2\text{bpy}](\text{PF}_6)_2$ (Os-bpy-surfactant) by studying its monolayers at the water-air interface, and Langmuir-Blodgett (LB) multilayers on solid electrodes.

METHODS: Os-bpy-surfactant was produced by complexation of $[\text{Os}(\text{bpy})_2]\text{Cl}_2$ with hydrophobic ligand $4,4'-(\text{n}-(\text{C}_{18}\text{H}_{37}\text{NHCO})_2\text{bpy})$ under reflux in ethylene glycol. Its structure was confirmed by ^1H NMR investigation. A monolayer Os-bpy-surfactant in the air-water interface was obtained by spreading its solution in chloroform on water surface. For electrochemical studies by cyclic voltammetry in the LB trough layers of this mediator were transferred on planar gold electrodes pre-modified with self-assembled monolayer of 3-mercaptopropyltrimethoxysilane.

For spectroscopic characterisation layers of Os-phendione-surfactant were deposited on glass slides modified with a monolayer of 3-mercaptopropyltrimethoxysilane. The thickness and organization of the Os-surfactant film on the substrate were estimated by the electron density projection (EDP) method using the molecular electron density surface.

MAIN RESULTS AND CONCLUSIONS:

Os-bpy-surfactant forms Langmuir-Blodgett layer at the water-air interface. The surface pressure vs. area per molecule isotherm demonstrated a take off surface pressure at 160-170 \AA^2 per molecule, and the collapse of the monolayer at the surface pressure 65 mN m^{-1} , the largest estimate of the mean molecular area being 150 \AA^2 . The treatment of data according to MacDonald and Simon has indicated the organisation of the monolayer in a perfectly fluid liquid expanded phase with all head groups solvated in the aqueous phase. Cyclic voltammograms showed that the formal standard potential of the mediator was affected by the value of surface pressure used for the deposition, so when the layers were deposited at 30 mN m^{-1} E_o' was +0.827 V vs. $\text{Ag}/\text{AgCl}/\text{KCl}_{\text{sat}}$ meanwhile at surface pressures higher than 40 mN m^{-1} the potential was more positive +0.845 V vs. $\text{Ag}/\text{AgCl}/\text{KCl}_{\text{sat}}$. The ratio of electroactive mediator in multilayers decreases with surface pressure and hence with the surface coverage, due to increase in hydrophobicity within the layers.

Spectroscopic measurements based on Beer-Lambert law allowed to find the surface concentration of Os-phendione-surfactant in LB layers deposited on glass slides. The average orientation and thickness of the first layer were estimated by the EDP method. Assuming a uniform

film and that the chosen Fe-derivative resembles the Os-surfactant optimised geometry, the fitted projection of the EDP onto the surface indicates a dense monolayer, where the individual molecules are slightly oriented away from the surface normal. If the amide functionalities are used as a reference for the orientation, the average tilt of the molecules should then be around 20° from the surface normal at 30 mN m^{-1} and the thickness can be estimated to be about 32 \AA .

It can be concluded that the Os-surfactant can form stable electroactive films on gold and glass surfaces modified with LB technique. The described redox system might provide a new transduction design permitting a rigorous surface control for incorporation in bioelectronic configurations.

5. CONCLUSIONS

1. The NADH oxidising polymer $[\text{Os}(1,10\text{-phenanthroline-5,6-dione})_2(\text{PVP})_4\text{Cl}]\text{Cl}$ (Os-phendione-PVP) can be synthesised by the complexation of $[\text{Os}(1,10\text{-phenanthroline-5,6-dione})_2\text{Cl}_2]$ with poly(vinyl pyridine) in ethylene glycol. The physical adsorption of this polymer onto graphite electrodes from its solution in ethylene glycol leads to the formation of a thin film without limitations on charge propagation.
2. The quasi-reversible redox process of this mediator involves 4 electrons and 4 protons within the pH range of 3-6.5. The mediator loses its chemical stability at pH values higher than 6.5. Three different linear parts in the plot of $E^{0'}$ vs. pH with different slopes having two breaking-points are caused by the fact that pK of pyridine moieties is pH 4.5 and pK of Os-catechol-PVP is 6.4.
3. The heterogeneous electron transfer rate constant (k_s) of Os-phendione-PVP is higher or of the same order of magnitude as that of other reported NADH oxidising mediators ($k_s = 18 \pm 2 \text{ s}^{-1}$).
4. Os-phendione-PVP is an efficient electrocatalyst for the oxidation of NADH. The modification of graphite electrodes with Os-phendione-PVP leads to the decrease in overpotential for the electrochemical oxidation of NADH from +0.33 V vs. Ag/AgCl/KCl_{sat} for bare electrodes to +0.11 V vs. Ag/AgCl/KCl_{sat}. Measurement of the kinetic rate constant for the interaction of the oxidised redox polymer with NADH by rotating disk electrodes gave the value of $k_{1, [\text{NADH}] = 0}$ equal to $(1.9 \pm 0.2) \times 10^3 \text{ M}^{-1} \text{ s}^{-1}$ at pH 6. This value practically coincides with that for Os-phendione suggesting that the number of phendione ligands of the osmium complex changes proportionally the response current to NADH but does not effect the electrochemical kinetic constants.
5. The amphiphilic mediator for NADH oxidation can be synthesised by the interaction of $[\text{Os}(1,10\text{-phenanthroline-5,6-dione})_2\text{Cl}_2]$ with 4,4'-[CH₃(CH₂)₁₇NHCO]₂bpy.
6. This amphiphilic NADH oxidising mediator forms stable Langmuir-Blodgett monolayers at the water-air interface. Multilayers of this compound deposited on the solid electrode surface by Langmuir-Blodgett technique lose electrochemical activity of 1,10-phenanthroline-5,6-dione due to the transport limitations of protons through bilayers formed by hydrophobic aliphatic chains.

7. The analogue of the above mentioned compound, which does not bear phenanthroline ligand, forms stable monolayers at the water-air interface and can be deposited on a solid electrode with partial loss of electrochemistry of the osmium atom, possibly, due to high hydrophobicity of the resulting multilayers.
8. Three new configurations, based on these mediators, were developed for the fabrication of reagentless dehydrogenase biosensors for glucose and L-glutamate. The first two fabrication methods rely on the adsorption of Os-phendione-PVP on the surface of graphite electrodes, followed by either adsorption of dehydrogenase and alginic acid modified with NAD⁺ moieties (NAD-alginate) or by the entrapment of dehydrogenase and NAD⁺ in a hydrogel formed by poly(vinyl pyridine) bearing amino groups. The third fabrication method relies on the entrapment of enzyme and coenzyme in lamellar phase created by a mixture of the NADH oxidising amphiphilic mediator and a lipid in aqueous solutions.
9. Reagentless glucose biosensors were fabricated by the immobilisation of biosensor's components in the above mentioned hydrogel deposited on graphite electrodes modified with a thin film of Os-phendione-PVP. The response to glucose of these sensors bearing different amount of glucose dehydrogenase in reagentless mode of operation was governed by the kinetics of the cycling of the E·NAD⁺.
10. Reagentless glutamate biosensors were built by the three above mentioned methods using thermophilic and mesophilic glutamate dehydrogenase. Mesophilic reagentless glutamate biosensors, fabricated with the use of NAD-alginate showed J_{\max} 14.26 $\mu\text{A cm}^{-2}$, apparent K_M 14.3 mM, and $\tau_{1/2}$ 1.5 h, glutamate biosensors produced on the basis of the hydrogel demonstrated J_{\max} 7.8 $\mu\text{A cm}^{-2}$, K_M 10.1 mM, and $\tau_{1/2}$ 12 h, glutamate sensors based on vesicle showed showed J_{\max} 3.5 $\mu\text{A cm}^{-2}$, K_M 47.0 mM, and $\tau_{1/2}$ 0.5 h. Thermophilic glutamate biosensors based on the adsorption together with NAD-alginate demonstrated J_{\max} 13.0 $\mu\text{A cm}^{-2}$, apparent K_M 39 mM and the sensors constructing using the hydrogel had shown J_{\max} 19.1 $\mu\text{A cm}^{-2}$, apparent K_M 55 mM. In general the biosensors having higher maximal response current demonstrated the higher apparent Michaelis constants. The response of those biosensors was determined by the rate of electrochemical oxidation of NADH by the mediator and diffusional limitations.

CONCLUSIONS

11. The response of lamellar phase based biosensors was determined by the rate of electrochemical oxidation NADH and diffusional limitations.
12. The use of the hydrogel helps to increase the operational stability of produced reagentless sensors by improving enzyme and NAD^+ immobilisation through formation of covalent bonds between the enzyme proteins, NAD^+ and amino group born by modified poly(vinyl pyridine).
13. The effect of pH on the response of the present glutamate and glucose biosensors is defined by the kinetics of enzymatic reaction but not by the kinetics of NADH oxidation as one can see from the plots of response currents vs. pH.
14. The operational stability of biosensors at elevated temperatures can be improved by the use of thermophilic enzymes instead of mesophilic ones. It was proved by comparing performance of glutamate and glucose-6-phosphate prepared using mesophilic and thermophilic dehydrogenases in the presence of NAD^+ in the external solution. The use of thermophilic enzymes also allows to improve drastically the shelf stability of biosensors as it was shown by comparing shelf half-life time of glutamate biosensors constructed with the use of mesophilic and thermophilic glutamate dehydrogenases. This can be explained in terms of higher intrinsic stability demonstrated by the thermophilic enzymes. Some additives such as a copolymer of vinyl-pyrrolidone and dimethylamino ethyl methacrylate termed as Gafquat[®] HS100 can extend the shelf life of biosensors by forming a protein-polyelectrolyte complex which mimicks aqueous environment of enzymes in dry state. Other tested additives such as glycerol, trehalose and poly(ethylene imine) proved to be useless for the improvement of shelf life because they fail to form the protective complex with the enzyme
15. The presence of NAD^+ in a sample solution can decrease the response of disposable glutamate biosensors to glutamate and NADH because of the formation of the parasite com-plex between the mediator and NAD^+ . This effect is evident if the concentration of the reduced cofactor is high and/or the rate of reoxidation of the mediator is low.

6. FUTURE WORK

This work, although demonstrated that the reagentless biosensors based on NAD^+ dependent dehydrogenases can be constructed with the use of new NADH oxidizing mediators and methods for the NAD^+ immobilization, leaves open questions that could be answered with the following types of studies:

1. The possibility to apply Os-phendione-PVP and the “binder” polymer to the construction of the reagentless glutamate microsensors should be investigated. The resulting microsensors can be employed to detect glutamate anions in the vicinity of axons of living neurons.
2. The rotating disk electrode (RDE) should be used to evaluate the response of the reagent glutamate biosensors to glutamate in order to assess experimentally the influence of the controlled mass transport on the shapes of the Eadie-Hofstee plots and the resulting values of the Michaelis constants. This study could further confirm the mathematical model describing the effect of different factors on the response of the biosensors to their analytes.
3. The detailed study of the electrochemical behavior of Os-phendione-surfactant adsorbed on graphite electrodes should be carried out with cyclic voltammetry at different scan rates and pH values to determine the rate constant for the heterogeneous electron transfer of the phendione redox couple in this new complex. Next the rotating disk electrode should be employed to evaluate the second order rate constant for NADH oxidation.
4. The above-mentioned investigation should be also performed with Os-phendione-surfactant in the lamellar phase immobilized on the electrode surface.
5. The inhibiting effect of NAD^+ on the NADH oxidation by $[\text{Os}(4,4'\text{-dimethyl-2,2'\text{-bipyridine})}_2(1,10\text{-phenanthroline-5,6\text{-dione})](\text{PF}_6)_2$, Os-phendione-PVP, and Os-phendione-surfactant can be studied in details by varying concentrations of NAD^+ and NADH in the electrolyte to determine the constants of inhibition. Next, the effect of the pH values on those inhibition constants can be investigated.
6. An interesting additional study can be carried out by using Os-phendione-surfactant as the redox catalyst for the reduction of AuCl_4^- anions by NADH leading to the formation of colloidal gold in the enzymatic reaction of dehydrogenases with their substrates and NAD^+ . Theoretically, this amphiphilic mediator is capable of forming stabilizing micelles

FUTURE WORK

around the resulting gold nanoparticles.

7. BIBLIOGRAPHY

- E. Adler, H. von Euler, G. Gunther, M. Plass, *Biochem. J.*, **1939**, 33, 1028.
- W. J. Albery, P. N. Bartlett, A. E. G. Cass, K. W. Sim, *J. Electroanal. Chem.*, **1987**, 218, 127.
- S. J. Alcock, A. P. E. Turner, *IEEE Engin. Med. Biol.*, **1994**, 319.
- S. L. Alvarez, M. J. Lobo, A. J. Miranda, P. Tuñón, *Biosens. Bioelectron.*, **1997**, 12, 739.
- M. I. Alvarez, S. A. Saidman, M. J. Lobo, A. J. Miranda, P. Tunon, *Anal. Chem.*, **2000**, 72, 520.
- R. E. Amelunxen, M. Lins, *Arch. Biochem. Biophys.*, **1968**, 125, 765.
- A. Bardea, E. Katz, A. F. Buckmann, I. Willner, *J. Am. Chem. Soc.*, **1997**, 119, 9114.
- P. N. Bartlett, P. R. Birkin, E. N. K. Wallace, *J. Chem. Soc., Faraday Trans.*, **1997**, 93, 1951.
- P. N. Bartlett, E. Simon, *Phys. Chem. Chem. Phys.*, **2000**, 2, 2599.
- T. S. Berzina, V. I. Troitsky, A. Petrigliano, D. Alliata, A. Yu. Tronin, C. Nicolini, *Thin Solid Films*, **1996**, 284/285, 757.
- R. L. Blankespoor, L. L. Miller, *J. Electroanal. Chem.*, **1984**, 171, 231.
- W. J. Blaedel and R. C. Engstrom, *Anal. Chem.*, **1980**, 52, 1691.
- W. J. Blaedel and R. A. Jenkins, *Anal. Chem.*, **1975**, 47, 1337.
- W. J. Blaedel and R. A. Jenkins, *Anal. Chem.*, **1976**, 48, 1240.
- K. B. Blodgett, *J. Am. Chem. Soc.*, **1934**, 56, 495.
- L. I. Boguslavsky, L. Geng, I. P. Kovalev, S. K. Sahni, Z. Xu, T. A. Skotheim, *Biosens. Bioelectron.*, **1995**, 10, 693.
- J. Bonnefoy, J. Moiroux, J. -M. Laval. C. Bourdillon, *J. Chem. Soc., Faraday Trans.*, **1988**, 84, 941.
- J. F. Brandts, *In Thermobiology*, Ed. A. H. Rose, Academic Press, New York and London, **1967**, pp. 25.
- B. Bubela, E. S. Holdsworth, *Biochim. Biophys. Acta*, **1966a**, 123, 364.
- B. Bubela, E. S. Holdsworth, *Biochim. Biophys. Acta*, **1966b**, 123, 376.
- H. B. Bull, K. Breese, *Arch. Biochem. Biophys.*, **1973**, 158, 681.
- S. K. Burley, G. A. Petsko, *Science*, **1985**, 229, 23.
- C. X. Cai, H. X. Ju, H. Y. Chen, *Anal. Chim. Acta*, **1995a**, 310, 145.
- C. X. Cai, H. X. Ju, H. Y. Chen, *J. Electroanal. Chem.*, **1995b**, 397, 185.
- C. X. Cai, K. H. Xue, *J. Electroanal. Chem.*, **1997a**, 427, 147.
- C. X. Cai, K. H. Xue, *Anal. Chim. Acta*, **1997b**, 343, 69.
- C. X. Cai, L. H. Yin, K. H. Xue, *J. Mol. Catalysis, A. Chem.*, **2000**, 152, 179.
- C. X. Cai, K. H. Xue, *Microchem. J.*, **1998a**, 58, 197.
- C. X. Cai, K. H. Xue, *Talanta*, **1998b**, 47, 1107.

BIBLIOGRAPHY

- K. H. Cass, E. Stellwagen, *Arch. Biochem. Biophys.*, **1975**, *171*, 682.
- H. Y. Chen, A. M. Yu, J. L. Han, Y. Z. Mi, *Anal. Lett.*, **1995**, *28*, 1579.
- H. Y. Chen, D. M. Zhou, J. J. Xu, H. Q. Fang, *J. Electroanal. Chem.*, **1997**, *422*, 21.
- Q. Chi, S. Dong, *Electroanalysis*, **1995**, *7*, 147.
- A. Ciszewski, G. Milczarek, *Anal. Chem.*, **2000**, *72*, 3203.
- L. C. Clark, C. Lyons, *Ann. N. Y. Acad. Sci.*, **1962**, *102*, 29.
- D. Compagnone, C. J. McNeil, D. Athey, C. Dillio, G. G. Guilbault, *Enz. Micr. Techn.*, **1995**, *17*, 472.
- S. Cosnier, M. Fontecave, C. Innocent, V. Niviere, *Electroanalysis*, **1997**, *9*, 685.
- A. Curulli, I. Carelli, O. Trischitta, G. Palleschi, *Biosens. Bioelectron.*, **1997**, *12*, 1083.
- K. Dalzier, F. M. Dickinson, *Biochem. J.*, **1966**, *100*, 34.
- R. M. Daniel, D. A. Cowan, *Cell. Mol. Life Sci.*, **2000**, *57*, 250.
- P. Davies, K. Mosbach, *Biochim. Biophys. Acta.*, **1974**, *370*, 329.
- C. Degrand, L.L. Miller, *J. Am. Chem. Soc.*, **1980**, *102*, 5728.
- M.J. Dennison, A. P. F. Turner, *Biotechnol. Adv.*, **1995**, *13*, 1.
- J. G. Dewan and D. E. Green, *ibid.*, **1937**, *31*, 1074.
- D. Dicu, L. Muresan, I. C. Popescu, C. Cristea, I. A. Silberg, P. Brout, *Electrochim. Acta*, **2000**, *45*, 3951.
- M. Dixon, *Nature*, **1960**, *188*, 464.
- E. Domínguez, H. L. Lan, Y. Okamoto, P. D. Hale, T. A. Skotheim, L. Gorton, *Biosens. Bioelectron.*, **1993a**, *8*, 167.
- E. Domínguez, H. L. Lan, Y. Okamoto, P. D. Hale, T. A. Skotheim, L. Gorton, B. Hahn-Hägerdal, *Biosens. Bioelectron.*, **1993b**, *8*, 229.
- H. von Euler, P. Karrer, B. Becker, *Helv. Chim. Acta*, **1936**, *19*, 1060.
- H. von Euler, F. Schlenk, R. Vestin, *Naturwiss.*, **1937**, *25*, 318.
- H. von Euler, E. Bauler, *Ber.*, **1938**, *71*, 411.
- J. Farrell, L. L. Campbell, *Adv. Microbial Physiol.*, **1969**, *3*, 83.
- A. Fassouane, J. -M. Laval, J. Moiroux, C. Bourdillon, *Biotechnol. Bioeng.*, **1990**, *35*, 935.
- J. J. Fernández, J. R. López, X. Correig, I. Katakis, *Sens. Actators*, **1998**, *47*, 13.
- A. B. Florou, M. I. Prodromidis, M. I. Karayannis, S. M. Tzouera-Karayanni, *Electroanalysis*, **1998**, *10*, 1261.
- H. J. Fromm, *Methods Enzymol.*, **1979**, *63*, 42.
- A. Fujishima, T. N. Rao, E. Popa, B. V. Sarada, I. Yagi, D. A. Tryk, *J. Electroanal. Chem.*, **1999**, *473*, 179.
- M. Fukui, A. Kitani, C. Degrand, L. L. Miller, *J. Am. Chem. Soc.*, **1982**, *104*, 28.

BIBLIOGRAPHY

- S. Fukuzumi, Y. Kando, T. Tanaka, *J. Chem. Soc. Perkin Trans. II*, **1984a**, 4, 673.
- S. Fukuzumi, N. Nishizawa, T. Tanaka, *J. Org. Chem.*, **1984b**, 49, 3571.
- S. Fukuzumi, S. Koumitsu, K. Hironaka, T. Tanaka, *J. Am. Chem. Soc.*, **1987**, 109, 305.
- S. Fukuzumi, S. M. Ishikawa, T. Tanaka, *J. Chem. Soc. Perkin. Trans. II*, **1989**, 11, 1811.
- A. P. Girardegrot, R. M. Morelis, P. R. Coulet, *Bioelectrochem. Bioenerg.*, **1998**, 46, 39.
- L. Gorton, *J. Chem. Soc., Faraday Trans.*, **1986**, 82, 1245.
- L. Gorton, G. Bremle, E. Csöregi, G. Jönsson-Pettersson, *Anal. Chim. Acta*, **1991**, 249, 43.
- L. Gorton, A. Torstensson, H. Jaegfeldt, G. Johansson, *J. Electroanal. Chem.*, **1984**, 161, 103.
- L. Gorton, G. Johansson, A. Torstensson, *J. Electroanal. Chem.*, **1985**, 196, 81.
- C. A. Goss, H. D. Abruña, *Inorg. Chem.*, **1985**, 24, 4263.
- D. E. Green, J. G. Dewan, L. F. Leloir, *Biochem. J.*, **1937**, 31, 934.
- J. L. Han, A. M. Yu, H. Y. Chen, *Acta Chim. Sinica*, **1995**, 53, 362.
- P. Hapiot, J. Moiroux, J. -M. Savient, *J. Am. Chem. Soc.*, **1990**, 112, 1337.
- D. C. Harrison, *ibid.*, **1931**, 25, 1016.
- J. P. Hart, A. K. Abass, D. C. Cowell, A. Chappel, *Electroanalysis*, **1999**, 11, 406.
- A. Hasegawa, N. Miwa, T. Oshima, K. Imahori, *J. Biochem.*, **1976**, 79, 34.
- M. A. Hayes, W. G. Kuhr, *Anal. Chem.*, **1999**, 71, 1720.
- M. Hedemno, A. Narváez, E. Dominguez, I. Katakis, *Analyst*, **1996**, 121, 1891.
- M. Hennig, B. Darimont, R. Sterner, K. Kirshner, J. N. Jansonius, *Structure*, **1995**, 3, 1295.
- Y. Hibino, Y. Nosoh, T. Samejima, *J. Bioche.*, **1974**, 75, 553.
- J. D. Hocking, J. I. Harris, *FEBS Lett.*, **1973**, 34, 280.
- J. J. Holbrook, A. Liljas, S. J. Steindel, M. G. Rossmann, *Enzymes*, **1975**, 11, 281.
- N. Howell, J. M. Akagi, R. H. Himes, *Can. J. Microbiol.*, **1969**, 15, 461.
- Zh. Huan, B. Persson, L. Gorton, S. Sahni, T. Skotheim, P. Bartlett, *Electroanalysis*, **1996**, 8, 575.
- H. Huck, *Fresenius J. Anal. Chem.*, **1982**, 313, 548.
- H. Huck, *Fresenius J. Anal. Chem.*, **1994**, 350, 599.
- Y. Ikariyama, T. Ishizuka, H. Sinohara, M. Aizawa, *Denki Kagaku*, **1990**, 58, 1097.
- H. Jaegfeldt, *Bioelectrochem. Bioenerg.*, **1981**, 8, 935.
- H. Jaegfeldt, A. B. C. Torstensson, L. Gorton, G. Johansson, *Anal. Chem.*, **1981**, 53, 1979.
- H. Jaegfeldt, T. Kuwana, G. Johansson, *J. Am. Chem. Soc.*, **1983**, 105, 1805.
- P. Jaraba, L. Agui, P. Yañez-Sedeño, J. M. Pingarron, *Electrochim. Acta*, **1998**, 43, 3555.
- J. B. Jones, J. F. Beck, *Applications of Biochemical Systems in Organic Chemistry, Techniques of Organic Chemistry Series* (eds. J. B. Jones, C. J. Sih, D. Perlman), Wiley Interscience, New York, **1976**, p. 107.
- J. B. Jones. K. E. Taylor, *J. Am. Chem. Soc.*, **1976**, 98, 5689.

BIBLIOGRAPHY

- H. Ju, D. Leech, *Anal. Chim. Acta*, **1997**, 345, 51.
- P. Karrer, O. Warburg, *Biochem. Z.*, **1936**, 225, 297.
- P. Karrer, G. Schwarzenbach, F. Benz, U. V. Solmssen, *Helv. Chim. Acta*, **1936**, 19, 811.
- P. Karrer, F. Benz, *ibid.*, **1936**, 19, 1028.
- P. Karrer, G. Schwarzenbach, G. E. Utzinger, *ibid.*, **1937**, 20, 72.
- Y. Kashiwagi, Q. Pan, F. Kurashima, C. Kikuchi, J. Anzai, T. Osa, *Chem. Lett.*, **1998**, 143.
- I. Katakis, E. Dominguez, *Mikrochim. Acta*, **1997**, 126, 11.
- N. Katayama, I. Urabe, H. Okada, *Eur. J. Biochem.*, **1983**, 132, 403.
- E. Katz, V. Heleg, A. Bardea, I. Willner, H. K. Rau, W. Haehnel, *Biosens. Bioelectron.*, **1998**, 13, 741.
- A. Kitani, Y. H. So, L. L. Miller, *J. Am. Chem. Soc.*, **1981**, 103, 7636.
- I. L. Khmel'nitskii, A. V. Levashov, N. L. Kliachko, V. I. Cherniak, K. Martinek, *Biokhimiia*, **1982**, 47, 86.
- H. Koffler, G. O. Gale, *Arch. Biochem. Biophys.*, **1957**, 67, 249.
- A. Kornberg, W. E. Pricer, *J. Biol. Chem.*, **1950**, 186, 557.
- E. Kress-Rogers, "Handbook of Biosensors and Electronic Noses: Medicine, Food and the Environment", CRC Press, Boca Raton, USA, 1996.
- I. Langmuir, *J. Am. Chem. Soc.*, **1917**, 39, 1848.
- V. Laurinavicius, B. Kurtinaitiene, V. Gureviciene, L. Boguslavsky, L. Geng, T. Scotheim, *Anal. Chim. Acta.*, **1996**, 330, 159.
- J. M. Laval, C. Bourdillon, J. Moiroux, *J. Am. Chem. Soc.*, **1984**, 106, 4701.
- B. Leca, J. L. Marty, *Biosens. Bioelectron.*, **1997**, 12, 1083.
- G. X. Li, J. J. Zhu, H. Q. Fang, H. Y. Chen, D. X. Zhu, *J. Electroanal. Soc.*, **1996**, 143, L141.
- F. Y. Li, L. P. Jin, C. H. Huang, J. Zheng, J. Q. Gou, X. S. Zhao, T. T. Liu, *Chem. Mater.*, **2001**, 13, 192.
- B. Lindholm-Sethson, J.C. Gonzalez, G. Puu, *Langmuir*, **1998**, 14, 6705.
- L. G. Ljungdahl, D. Sherod, *In Extreme Environments: Mechanisms of Microbial Adaptation*, Ed. M. R. Heinrich, Academic Press, New York and London, p. 147.
- M. J. Lobo, A. J. Miranda, J. M. López-Fonseca, P. Tuñon, *Anal. Chim. Acta.*, **1996a**, 325, 33.
- M. J. Lobo, A. J. Miranda, P. Tunon, *Electroanalysis*, **1996b**, 8, 932.
- M. J. Lobo, A. J. Miranda, P. Tunon, *Anal. Chim. Acta*, **1997a**, 346, 165.
- M. J. Lobo, A. J. Miranda, P. Tuñon, *Biosens. Bioelectron.*, **1997b**, 12, 511.
- E. Lorenzo, L. Sanchez, F. Pariente, J. Tirado, H. D. Abruña, *Anal. Chim. Acta*, **1995**, 309, 79.
- A. Maines, M. I. Prodromidis, S. M. Tzouwara, M. I. Karayannis, D. Ashworth, P. Vadgama, *Anal. Chim. Acta*, **2000**, 408, 217.
- A. Malinauskas, T. Ruzgas, L. Gorton, *Bioelectrochem. Bioenerg.*, **1999**, 49, 21.

BIBLIOGRAPHY

- A. Malinauskas, G. Niaura, S. Bloxham, T. Ruzgas, L. Gorton, *J. Coll. Interface Science*, **2000**, 230, 122.
- N. Mano, A. Kuhn, *J. Electroanal. Chem.*, **1999**, 477, 79.
- K. Martinek, A. V. Levashov, N. L. Klyachko, V. I. Pantin, I. V. Berezin, *Biochim. Biophys. Acta*, **1981**, 657, 277.
- W. Miltzer, T. B. Sonderegger, L. C. Tuttle, C. E. Georgi, *Arch. Biochem.*, **1949**, 24, 75.
- F. Mizutani, Y. Sato, Y. Hirata, T. Sawaguchi, S. Yabuki, *Sens. Actuat. B Chem.*, **2000**, 65, 46.
- J. Moiroux; P. J. Elving, *J. Electroanal. Chem.*, **1979a**, 102, 93.
- J. Moiroux; P. J. Elving, *Anal. Chem.*, **1979b**, 51, 346.
- J. Moiroux; P. J. Elving, *J. Am. Chem. Soc.*, **1980**, 102, 6533.
- R. Murray, *Electroanal. Chem.*, **1992**, 13, 297.
- G. Nagy, I. Kapui, L. Gorton, *Anal. Chim. Acta.*, **1995**, 305, 65.
- Yo. Nakamura, S. Suye, J. Kira, H. Tera, I. Tabata, M. Senda, *Biochim. Biophys. Acta*, **1996**, 1289, 221
- H. Nicholson, W. J. Becktel, B. W. Matthews, *Nature*, **1988**, 336, 651.
- Nomenclature Committee of the International Union of Biochemistry, *Enzyme Nomenclature*, Academic Press, New York, 1984.
- T. Noguer, A. Gradinaru, A. Ciucu, J. L. Marty, *Anal. Lett.*, **1999**, 32, 1723.
- W. B. Nowal, W. G. Kuhr, *Electroanalysis*, **1997**, 9, 102.
- W. B. Nowal, W. G. Kuhr, *Anal. Chem.*, **1995**, 67, 3583.
- Y. Okamoto, T. Kaku, R. Shundo, *Pure & Appl. Chem.*, **1996**, 68, 1417.
- J. Parellada, A. Narváez, M. A. López, E. Domínguez, J. J. Fernández, V. Pavlov, I. Katakis, *Anal. Chim. Acta*, **1998**, 362, 47.
- F. Pariente, E. Lorenzo, H. D. Abruña, *Anal. Chem.*, **1994**, 66, 4337.
- F. Pariente, F. Tobalina, G. Moreno, L. Hernández, E. Lorenzo, H. D. Abruña, *Anal. Chem.*, **1997**, 69, 4065.
- J. K. Park, H. J. Yee, K. S. Lee, W. Y. Lee, M. C. Shin, T. H. Kim, S. R. Kim, *Anal. Chim. Acta.*, **1999**, 390, 83.
- N. Pasco, C. Jeffries, Q. Davies, A. J. Downard, A. D. Roddick-Lanzilotta, *Biosens. Bioelectron.*, **1999**, 14, 171.
- B. Persson, H. S. Lee, L. Gorton, T. Skotheim, P. Bartlett, *Electroanalysis*, **1995**, 7, 935.
- I. C. Popescu, E. Dominguez, A. Narvaez, V. Pavlov, I. Katakis, *J. Electroanal. Chem.*, **1999**, 464, 208.
- M. E. Pullman, A. San Pietro, S. P. Golowick, *J. Biol. Chem.*, **1954**, 206, 129.
- P. Ramesh, S. Sampath, *Anal. Chem.*, **2000**, 72, 3369.
- C. Ramirez, M. Boujtita, N. El-Murr, *Anal. Chim. Acta.*, **1999**, 401, 155.

BIBLIOGRAPHY

- K. Ravichandran, R. P. Baldwin, *Anal. Chem.*, **1984**, *56*, 1744.
- S. B. Saidman, M. J. Lobo, A. J. Miranda, P. Tunon, *Anal. Chim. Acta*, **2000**, *424*, 45.
- D. D. Schlereth, E. Katz, Schmidt, *Electroanalysis*, **1994**, *6*, 725.
- D. D. Schlereth, E. Katz, Schmidt, *Electroanalysis*, **1995**, *7*, 46.
- A. Silber, C. Brauchle, N. Hampp, *J. Electroanal. Chem.*, **1995**, *390*, 83.
- A. Silber, N. Hamp, W. Schuhmann, *Biosens. Bioelectron.*, **1996**, *11*, 215.
- E. Silverstein, G. Sulebele, *Biochemistry*, **1969**, *8*, 2543.
- R. Singleton, In *Extreme Environments: Mechanisms of Microbial Adaptation*, Ed. M. R. Heinrich, Academic Press, New York and London, **1976**, p. 189.
- Z. Sheng, L. B. Gan, C. H. Huang, *Chem. Phys. Lett.*, **2000**, *331*, 143.
- M. Hennig, B. Darimont, R. Sterner, K. Kirshner, J. N. Jansonius, *Structure*, **1995**, *3*, 1295.
- R. Singleton, R. E. Amelunxen, *Bacteriol. Rev.*, **1973**, *37*, 320.
- M. D. Smith, C. L. Olson, *Anal. Chem.*, **1975**, *47*, 1074.
- S. D. Sprules, J. P. Hart, R. Pittson, S.A. Wring, *Electroanalysis*, **1996**, *8*, 539.
- G. D. Storrier, K. Takada, H. D. Abruña, *Inorg. Chem.*, **1999**, *38*, 559.
- J. J. Sun, J. J. Xu, H. Q. Fang, H. Y. Chen, *Bioelectrochem. Bioenerg.*, **1997**, *44*, 45.
- K. Suzuki, K. Imahori, *J. Biochem.*, **1974**, *76*, 771.
- H. Theorell, B. Chance, *Acta Chem. Scand.*, **1951**, *5*, 1127.
- M. Tian, S. J. Dong, *Electroanalysis*, **1995**, *7*, 1995.
- D.R. Thevenot, K. Toth, R.A. Durst, and G.S. Wilason, *Pure Appl. Chem.*, **1999**, *71*, 2333.
- F. Tobalina, F. Pariente, L. Hernandez, H. D. Abruña, E. Lorenzo, *Anal. Chim. Acta*, **1999**, *395*, 17.
- A. Torstensson, L. Gorton, *J. Electroanal. Chem.*, **1981**, *130*, 199.
- V. I. Troitsky, T. S. Berzina, A. Petrigliano, C. Nicolini, *Thin Solid Films*, **1996a**, *284/285*, 122.
- V. I. Troitsky, M. Sartore, T. S. Berzina, D. Nardeli, C. Nicolini, *Rev. Sci. Instr.*, **1996**, *67*, 4216.
- D. C-S. Tse, T. Kuwana, *Anal. Chem.*, **1978**, *50*, 1315.
- B. Ueda, D. C-S. Tse, T. Kuwana, *Anal. Chem.*, **1982**, *54*, 850.
- S.J. Updike, J.P. Hicks, *Nature*, **1967**, *214*, 986.
- S. Vakula, V. Erokhin, C. Nicolini, P. Facci, F. Antolini, patent WO 9509058.
- K. Wan, J. M. Chovelon, N. Jaffrezic-Renault, *Talanta*, **2000**, *52*, 663.
- J. Wang, J. Liu, *Anal. Chim. Acta*, **1993**, *284*, 385.
- O. Warburg and W. Christian, *Helv. Chim. Acta*, **1936**, *19*, E79.
- D. B. Wigley, A. R. Clarke, C. R. Dunn, D. Barstow, T. Atkinson, W. Chia, H. Muirhead, J. Holbrook, *Biochim. Biophys. Acta*, **1987**, *916*, 145.
- S.F. White, A. P. F. Turner In: "Encyclopedia of Bioprocess Technology: Fermentation,

BIBLIOGRAPHY

Biocatalysis and Bioseparation"(Eds. M C Flickinger and S W Drew). Wiley, New York, USA, 1997.

C. H. Wong, G. M. Whitesides, *J. Am. Chem. Soc.*, **1981**, *103*, 4890.

Q. Wu, M. Maskus, F. Pariente, F. Tobalina, V. M. Fernandez, E. Lorenzo, H. D. Abruña, *Anal. Chem.*, **1996**, *68*, 3688.

T. Yao, S. Musha, *Anal. Chim. Acta*, **1979**, *110*, 203.

M. Yasuzawa, M. Hashimoto, S. Fujii, A. Kunugi, T. Nakaya, *Sens. Actuat. B Chem.*, **2000**, *65*, 241.

H. C. Yoon, H. S. Kim, *Anal. Chim. Acta*, **1996**, *336*, 57.

M. Yoshida, N. Sone, H. Hirata, Y. Kagawa, *J. Biol. Chem.*, **1975**, *250*, 7910.

S. Y. Zaitsev, *Sens. Actuat. B Chem.*, **1995**, *24*, 177.

H. R. Zare, S. M. Golabi, *J. Solid State Electrochem.*, **2000**, *4*, 87.

Z. Zheng, L.B. Gan, C. H. Huang, *Chem. Phys. Lett.*, **2000**, *331*, 143.

D. Zhou, H. Q. Fang, H. Chen, H. Ju, Y. Wang, *Anal. Chim. Acta*, **1996**, *329*, 41.

R. G. Zhu, J. L. Han, H. Y. Chen, *Chem. J. Chin. Univ.*, **1995**, *16*, 35.

Supporting Information

The Use of Lipid Bilayers for the Construction of Reagentless Biosensors Based on NAD⁺ Dependent Glutamate Dehydrogenase.

Valeri Pavlov,¹ Britta Lindholm-Sethson,² Goran Lindblom,² Ioanis Katakis^{*1}

¹Bioanalysis and Bioelectrochemistry Group, Chemical Engineering, Universitat Rovira i Virgili, E-43006, Tarragona (Catalonia), Spain. ²Department of Chemistry, Umeå University, Umeå, SE-901 87, Sweden.

* E-mail: ioanis.katakis@urv.net, Tel: +34 977 55 9655, Fax: +34 977 55 9667.

EXPERIMENTAL SECTION

Materials. GLDH (E.C. 1.4.1.3) from bovine liver, as suspension in saturated ammonium was purchased from Biozyme (UK), nicotinamide adenine nucleotide (NAD⁺), L-glutamic acid monosodium salt, dimethylformamid (DMF), *n*-C₁₈H₃₇NH₂, sodium dihydrogen phosphate, sodium hydroxide, *ortho*-phosphoric acid, sodium chloride, thionyl chloride, NH₄PF₆, 2,2'-bipyridine-4,4'-dicarboxylic acid, absolute 1,4-dioxane were obtained from Sigma-Aldrich (USA), K₂OsCl₆ was from Alfa (Spain), ethylene glycol and sodium dithionite were obtained from Pancreac (Madrid, Spain), 1,2-dioleoyl-sn-glycero-3-phosphatidylcholine from Larodan Fine Chemicals (Sweden), 1,10-phenanthroline-5,6-dione was prepared by the published procedure.²⁷

[Os(1,10-phenanthroline-5,6-dione)₂Cl₂] was synthesized according to the adapted method.²⁶ Generally the synthesis procedure involved refluxing of K₂OsCl₆ with 1,10-phenanthroline-5,6-dione in DMF under argon in the dark for 1 hr, followed by reduction with aqueous sodium dithionite solution.

Synthesis of 4,4'-[CH₃(CH₂)₁₇NHCO]₂bpy (I)

0.82 mmol of 2,2'-bipyridine-4,4'-dicarboxylic acid were refluxed during 24 h in 4 ml of thionyl chloride (Aldrich, USA), next thionyl chloride was evaporated under vacuum during 4 h. The reaction product was dissolved in 40 ml of absolute 1,4-dioxane. This solution was added dropwise to a solution 1.8 mmol of *n*-C₁₈H₃₇NH₂ in 200 ml of absolute 1,4-dioxane during 20 min, the reaction mixture was left to stay overnight. The next day the solid was filtered off, washed with 1,4-dioxane and air-dried to give compound I.

Synthesis of [Os(1,10-phenanthroline-5,6-dione)₂(4,4'-[CH₃(CH₂)₁₇NHCO]₂bpy)](PF₆)₂ (II) (Os-phendione-surfactant)

0.1468 mmol of [Os(1,10-phenanthroline-5,6-dione)₂Cl₂] and 0.1762 mmol of compound I were refluxed during 1 h in 5 ml of deaerated ethylene glycol under argon in the dark. Next the product was precipitated by mixing with a solution of 1 g of NH₄PF₆ in 100 ml of water. The solid was filtered off and washed with water, extracted with acetone and air dried to yield compound II. The synthesis route is presented in Figure S-1. ¹H NMR performed in CDCl₃ with a tetramethylsilane standard confirmed the presence of long alkane chains: 1.29 p. p. m. (m) 1.26 (m), 0.88 (t).

Preparation of bovine GLDH solution

In order to purify mesophilic bovine GLDH 4 ml of meso GLDH suspension in saturated ammonium sulphate solution were centrifuged during 10 min at 14000 RPM at 5°C. The precipitated enzyme was isolated from the ammonium sulfate solution and dissolved in 3 ml of 0.1 M sodium phosphate buffer (pH 7.4) containing 0.15 M sodium chloride, next the resulting enzyme solution was extensively dialyzed at 5°C against 200 ml of the same buffer during 24 h, the buffer solution being changed every two hours.

Preparation of graphite electrodes. Spectrographic graphite rods of 3 mm in diameter (Carbone of America, USA) were cut into pieces of 2 cm in longitude, introduced into heat-shrinkable PVC plastic tubes, shrunk by heating, wet polished on fine (grit 400 and 600) emery paper (Buehler, USA) and sonicated in water.

Preparation of reagentless glutamate biosensors based on immobilization between lipid bilayers. 1.5 mg of Os-phendione-surfactant and 10 mg of 1,2-dioleoyl-sn-glycero-3-phosphatidylcholine were dissolved in 0.5 mL of chloroform. Then this solution was evaporated under vacuum in a pear shaped flask to form the solid thin layer on the bottom. Next 1 mL of a solution containing 5.8 mg mL⁻¹ (38 U mL⁻¹ at 30°C) of bovine glutamate dehydrogenase and 40 mg of NAD⁺ in 0.1 M phosphate buffer pH 7.6 were stirred during 2 h to form the lamellar phase. The suspension was washed 6 times with 1 mL of 0.1 M phosphate buffer (pH 7.6), using centrifugation at 4000 rpm during 10 min every time. Next the volume of this suspension was adjusted to 1 mL and 5 µL of it was deposited per graphite electrode and air-dried during 1 h.

Electrochemical measurements. A three-electrode conventional thermostabilised cell (3 mL) equipped with an Ag/AgCl/KCl_{sat} reference electrode, a platinum auxiliary electrode, and a graphite electrode modified according to one of the above mentioned methods as working electrode. The buffer, pH 7.4 (0.1 M sodium phosphate containing 0.15 M sodium chloride) served as supporting electrolyte. The response to successive additions of stock glutamate solution was registered as steady state current on a three-electrode potentiostat Autolab PGSTAT 10 (Eco chemie, Holland) controlled by a computer. The working potential was 150 mV vs. Ag/AgCl/KCl_{sat} and the temperature of a thoroughly stirred solution was 30°C.

GLDH assay method. The activity of GLDH was tested spectrophotometrically by following the increase in absorbance at 340 nm, 30°C. The assay solution contained 5 mM NAD⁺ and 10 mM in 0.1 M

sodium phosphate buffer (pH 7.4). The ΔA_{340} (Au/min) was obtained using the maximum linear rate for both the test and blank (without the enzyme) mixtures. The activity was calculated using $\epsilon_{\text{NADH}}=6.22 \text{ mM}^{-1}\text{cm}^{-1}$ extinction coefficient of β -NADH. One unit of GLDH oxidizes 1 μmol of L-glutamate per minute at pH 7.4 at 30°C. Protein concentration was determined spectrophotometrically at A_{280} using an absorbance coefficient of $0.973 \text{ cm}^2 \text{ mg}^{-1}$.

Figure 2S illustrates the kinetic scheme for the operation of reagentless biosensors based on the enzyme glutamate dehydrogenase (E) catalyzing the reaction of immobilized NAD^+ (A) with a L-glutamate (B) to give immobilized NADH (P), α -ketoglutarate (Q), and NH_4^+ (R). Then a mediator (M), which can stay in reduced (M_{red}) and oxidized (M_{ox}) forms, immobilized on the electrode surface reoxidizes NADH to NAD^+ . A_{im} and P_{im} are the concentrations of immobilized A and P. B_o , Q_o , R_o are the concentrations of the substrate and the products in the lamellar phase B_∞ , Q_∞ and R_∞ are the concentrations of the substrate and the products in the external medium. k'_B , k'_Q and k'_R are mass transfer coefficients of the substrate and the products (cm s^{-1}), respectively. L is the thickness of the film in which the enzymatic reaction occurs. The following expressions for the flux of B to the electrode surface (j_{el}), which determines the current density of a biosensor (j) through the equation $j = nFj_{\text{el}}$, where n is the number of exchanged electrons and F is the Faraday's constant, can be obtained.

$$j_{\text{el}} = k'_B(B_\infty - B_o) \quad (\text{S-1})$$

$$j_{\text{el}} = L(k_1 A_{\text{im}} [E] - k_{-1} [E \cdot A]) \quad (\text{S-2})$$

$$j_{\text{el}} = L(k_2 B_o [E \cdot A] - k_{-2} [E \cdot A \cdot B]) \quad (\text{S-3})$$

$$j_{\text{el}} = L(k_3 [E \cdot A \cdot B] - k_{-3} [E \cdot P \cdot Q \cdot R]) \quad (\text{S-4})$$

$$j_{\text{el}} = L(k_4 [E \cdot P \cdot Q \cdot R] - k_{-4} [E \cdot P \cdot Q] Q_o) \quad (\text{S-5})$$

$$j_{\text{el}} = L(k_5 [E \cdot P \cdot Q] - k_{-5} [E \cdot P] Q_o) \quad (\text{S-6})$$

$$j_{\text{el}} = L(k_6 [E \cdot P] - k_{-6} [E] P_{\text{im}}) \quad (\text{S-7})$$

$$j_{\text{el}} = k'_Q Q_o \quad (\text{S-8})$$

$$j_{\text{el}} = k'_R R_o \quad (\text{S-9})$$

$$j_{\text{el}} = k_7 P_o \Gamma_{\text{Mox}} - k_{-7} \Gamma_{\text{M} \cdot \text{P}} \quad (\text{S-10})$$

$$j_{\text{el}} = k_8 \Gamma_{\text{M} \cdot \text{P}} \quad (\text{S-11})$$

$$j_{\text{el}} = k_5 \Gamma_{\text{Mred}} \quad (\text{S-12})$$

$$E_t = [E] + [E \cdot A] + [E \cdot A \cdot B] + [E \cdot P \cdot Q \cdot R] + [E \cdot P \cdot Q] + [E \cdot P] \quad (\text{S-13})$$

$$\Gamma_{\text{M}} = \Gamma_{\text{M} \cdot \text{P}} + \Gamma_{\text{Mox}} + \Gamma_{\text{Mred}} \quad (\text{S-14})$$

$$A_t = A_{\text{im}} + P_{\text{im}} \quad (\text{S-15})$$

Where Γ_{Mox} and Γ_{Mred} are the surface coverages of the mediator in oxidized and reduced forms, respectively. Γ_{M} is the total mediator surface coverage. $\Gamma_{\text{M} \cdot \text{P}}$ is the surface coverage of the intermediate complex between the mediator and NADH. A_t and E_t are the total concentrations of NAD^+ and the enzyme immobilized in the lamellar phase, respectively. The equations (S-2 – S-7, S-13) yield the equation for the enzymatic kinetics:

$$j_{\text{el}} = \frac{L(V_1 A_{\text{im}} B_o - (V_1 P_{\text{im}} Q_o R_o) / K_{\text{cq}})}{K_{\text{AB}} + K_{\text{B}} A_{\text{im}} + K_{\text{A}} B_o + A_{\text{im}} B_o + K_{\text{QR}} K_{\text{iA}} K_{\text{B}} P_{\text{im}} / (K_{\text{iP}} K_{\text{iQ}} K_{\text{R}}) + K_{\text{PQ}} K_{\text{iA}} K_{\text{B}} R_o / (K_{\text{iP}} K_{\text{iQ}} K_{\text{R}}) + K_{\text{P}} K_{\text{iA}} K_{\text{B}} Q_o R_o / (K_{\text{iP}} K_{\text{iQ}} K_{\text{R}}) + K_{\text{R}} K_{\text{iA}} K_{\text{B}} P_{\text{im}} Q_o / (K_{\text{iP}} K_{\text{iQ}} K_{\text{R}}) + K_{\text{iA}} K_{\text{B}} P_{\text{im}} Q_o R_o / (K_{\text{iP}} K_{\text{iQ}} K_{\text{R}}) + K_{\text{P}} K_{\text{iA}} K_{\text{B}} R_o P_{\text{im}} / (K_{\text{iP}} K_{\text{iQ}} K_{\text{R}}) + K_{\text{A}} B_o P_{\text{im}} / K_{\text{iP}} + K_{\text{A}} B_o P_{\text{im}} Q_o / (K_{\text{iQ}} K_{\text{iP}}) + K_{\text{iR}} K_{\text{P}} K_{\text{B}} A_{\text{im}} B_o Q_o / (K_{\text{iB}} K_{\text{iP}} K_{\text{iQ}} K_{\text{R}}) + K_{\text{P}} K_{\text{B}} A_{\text{im}} R_o Q_o / (K_{\text{iP}} K_{\text{iQ}} K_{\text{R}}) + K_{\text{PQ}} K_{\text{B}} A_{\text{im}} R_o / (K_{\text{iP}} K_{\text{iQ}} K_{\text{R}}) + K_{\text{P}} K_{\text{B}} A_{\text{im}} B_o Q_o R_o / (K_{\text{iB}} K_{\text{iP}} K_{\text{iQ}} K_{\text{R}}) + K_{\text{A}} B_o R_o P_{\text{im}} Q_o / (K_{\text{iR}} K_{\text{iP}} K_{\text{iQ}}) + K_{\text{PQ}} K_{\text{B}} A_{\text{im}} B_o R_o / (K_{\text{iB}} K_{\text{iP}} K_{\text{iQ}} K_{\text{R}}) \quad (\text{S-16})$$

Where the constant of equilibrium $K_{eq} = k_1k_2k_3k_4k_5k_6/(k_{-1}k_{-2}k_{-3}k_{-4}k_{-5}k_{-6})$. $V_1 = E_1(k_1k_2k_3k_4k_5k_6)/(k_1k_2k_3k_4k_5k_6k_{-3} + k_1k_2k_4k_5k_6 + k_1k_2k_3k_5k_6 + k_1k_2k_3k_4k_6 + k_1k_2k_3k_4k_5)$ and $V_2 = E_1(k_{-1}k_{-2}k_{-3}k_{-4}k_{-5}k_{-6})/(k_{-2}k_{-3}k_{-4}k_{-5}k_{-6} + k_{-1}k_{-3}k_{-4}k_{-5}k_{-6} + k_{-1}k_{-2}k_{-4}k_{-5}k_{-6} + k_3k_{-1}k_{-4}k_{-5}k_{-6})$ are the maximum velocities in forward and reverse directions, the Michaelis constants for A, B, P, Q, R are $K_A = (k_2k_3k_4k_5k_6)/(k_1k_2k_3k_4k_5k_6k_{-3} + k_1k_2k_4k_5k_6 + k_1k_2k_3k_5k_6 + k_1k_2k_3k_4k_6 + k_1k_2k_3k_4k_5)$, $K_B = (k_1k_5k_6k_{-2}k_{-3} + k_1k_4k_5k_6k_{-2} + k_1k_3k_4k_5k_6)/(k_1k_2k_3k_4k_5k_6k_{-3} + k_1k_2k_4k_5k_6 + k_1k_2k_3k_5k_6 + k_1k_2k_3k_4k_6 + k_1k_2k_3k_4k_5)$, $K_{AB} = (k_5k_6k_{-1}k_{-2}k_{-3} + k_4k_5k_6k_{-1}k_{-2} + k_{-1}k_3k_4k_5k_6)/(k_1k_2k_3k_4k_5k_6k_{-3} + k_1k_2k_4k_5k_6 + k_1k_2k_3k_5k_6 + k_1k_2k_3k_4k_6 + k_1k_2k_3k_4k_5)$, $K_P = k_{-1}k_{-2}k_{-3}k_{-4}k_{-5}/(k_{-2}k_{-3}k_{-4}k_{-5}k_{-6} + k_{-1}k_{-3}k_{-4}k_{-5}k_{-6} + k_{-1}k_{-2}k_{-4}k_{-5}k_{-6} + k_3k_{-1}k_{-4}k_{-5}k_{-6})$, $K_Q = k_{-1}k_{-2}k_{-3}k_{-4}k_{-6}/(k_{-2}k_{-3}k_{-4}k_{-5}k_{-6} + k_{-1}k_{-3}k_{-4}k_{-5}k_{-6} + k_{-1}k_{-2}k_{-4}k_{-5}k_{-6} + k_3k_{-1}k_{-4}k_{-5}k_{-6})$, $K_R = (k_{-1}k_{-2}k_{-3}k_{-5}k_{-6} + k_4k_{-1}k_{-2}k_{-5}k_{-6} + k_3k_4k_{-1}k_{-5}k_{-6})/(k_{-2}k_{-3}k_{-4}k_{-5}k_{-6} + k_{-1}k_{-3}k_{-4}k_{-5}k_{-6} + k_{-1}k_{-2}k_{-4}k_{-5}k_{-6} + k_3k_{-1}k_{-4}k_{-5}k_{-6})$, $K_{QR} = (k_5k_{-1}k_{-2}k_{-3}k_{-6} + k_4k_5k_{-1}k_{-2}k_{-6} + k_3k_4k_5k_{-1}k_{-6})/(k_{-2}k_{-3}k_{-4}k_{-5}k_{-6} + k_{-1}k_{-3}k_{-4}k_{-5}k_{-6} + k_{-1}k_{-2}k_{-4}k_{-5}k_{-6} + k_3k_{-1}k_{-4}k_{-5}k_{-6})$, $K_{PQ} = k_6k_{-1}k_{-2}k_{-3}k_{-4}/(k_{-2}k_{-3}k_{-4}k_{-5}k_{-6} + k_{-1}k_{-3}k_{-4}k_{-5}k_{-6} + k_{-1}k_{-2}k_{-4}k_{-5}k_{-6} + k_3k_{-1}k_{-4}k_{-5}k_{-6})$, $K_{PQR} = (k_5k_6k_{-1}k_{-2}k_{-3} + k_4k_5k_6k_{-1}k_{-2} + k_{-1}k_3k_4k_5k_6)/(k_{-2}k_{-3}k_{-4}k_{-5}k_{-6} + k_{-1}k_{-3}k_{-4}k_{-5}k_{-6} + k_{-1}k_{-2}k_{-4}k_{-5}k_{-6} + k_3k_{-1}k_{-4}k_{-5}k_{-6})$. The inhibition constants for A, B, P, Q, R are $K_{iA} = k_{-1}/k_1$, $K_{iB} = (k_{-2}k_{-3})/(k_2(k_{-3} + k_3))$, $K_{iP} = k_6/k_{-6}$, $K_{iQ} = k_5/k_{-5}$, $K_{iR} = (k_3k_4)/(k_4(k_3 + k_{-3}))$.

The equations (S-10 – S-12, S-14) give the equation (S-17) governing the kinetics of NADH oxidation at the electrode surface modified with the Os-phendione-surfactant mediator

$$j_{el} = \frac{\Gamma_M k_7 k_8 k_S P_o}{k_8 k_S + k_{-7} k_S + (k_7 k_8 + k_7 k_S) P_{im}} = \frac{\Gamma_M P_{im} k_7 k_8 k_S / (k_7 k_8 + k_7 k_S)}{(k_8 k_S + k_{-7} k_S) / (k_7 k_8 + k_7 k_S) + P_{im}} = \frac{k_{cat} \Gamma_M P_{im}}{k_M + P_{im}} \quad (S-17)$$

The Michaelis constant for the mediator M is $k_M = (k_8 k_S + k_{-7} k_S) / (k_7 k_8 + k_7 k_S)$ and $k_{cat} = k_8 k_S / (k_8 + k_S)$. On the basis of the equations (S-15) and (S-17) the concentrations of NAD^+ and $NADH$ (A_{im} and P_{im}) as well as B_o , Q_o and R_o from (S-1), (S-8) and (S-9) can be found: $P_{im} = j_{el} k_M / (k_{cat} \Gamma_M - j_{el})$, $A_{im} = A_t - P_{im} = A_t - j_{el} k_M / (k_{cat} \Gamma_M - j_{el})$, $B_o = B_\infty - j_{el} / k'_B$, $Q_o = j_{el} / k'_Q$, $R_o = j_{el} / k'_R$. Substitution of A_{im} , B_o , P_{im} , Q_o , R_o into the equation (S-16) yields the equation of the fourth order:

$$LV_1 \Gamma_M k_{cat} E_t A_t B_\infty = j_{el} [K_{AB} \Gamma_M k_{cat} + K_B \Gamma_M k_{cat} A_t + K_A \Gamma_M k_{cat} B_\infty + A_t \Gamma_M k_{cat} B_\infty + LV_1 (A_t + K_M) B_\infty + (LV_1 A_t \Gamma_M k_{cat}) / k'_B] + j_{el}^2 [(K_{PQ} K_B A_t \Gamma_M k_{cat}) / (K_{iP} K_{iQ} K_R k'_R) - LV_1 (A_t + K_M) / k'_B - K_{AB} - K_B (A_t + K_M) - K_A B_\infty + K_M K_{QR} K_{iA} K_B / (K_{iP} K_{iQ} K_R) - (A_t + K_M) B_\infty - A_t \Gamma_M k_{cat} / k'_B + \Gamma_M k_{cat} K_{PQ} K_{iA} K_B R_o / (K_{iP} K_{iQ} K_R k'_R) + K_A K_M B_\infty / K_{iP} + K_{iR} K_P K_B A_t B_\infty \Gamma_M k_{cat} / (K_{iB} K_{iP} K_{iQ} K_R k'_Q) + K_{PQ} K_B A_t B_\infty \Gamma_M k_{cat} / (K_{iB} K_{iP} K_{iQ} k'_R)] + j_{el}^3 [LV_1 K_M / (K_{eq} k'_Q k'_R) + K_A / k'_B + (A_t + K_M) / k'_B - K_{PQ} K_{iA} K_B / (K_{iP} K_{iQ} K_R k'_R) + \Gamma_M k_{cat} K_P K_{iA} K_B / (K_{iP} K_{iQ} K_R k'_Q k'_R) + K_M K_R K_{iA} K_B / (K_{iP} K_{iQ} K_R k'_Q) + K_M K_P K_{iA} K_B / (K_{iP} K_{iQ} K_R k'_R) - K_A K_M / (K_{iP} k'_B) + K_A K_M B_\infty / (K_{iQ} K_{iP} k'_Q) - K_{iR} K_P K_B (A_t + K_M) B_\infty / (K_{iB} K_{iP} K_{iQ} K_R k'_Q) - K_{iR} K_P K_B A_t \Gamma_M k_{cat} / (K_{iB} K_{iP} K_{iQ} K_R k'_B k'_Q) + K_P K_B A_t \Gamma_M k_{cat} / (K_{iP} K_{iQ} K_R k'_Q k'_R) - K_{PQ} K_B (A_t + K_M) / (K_{iP} K_{iQ} K_R k'_R) + K_P K_B A_t B_\infty \Gamma_M k_{cat} / (K_{iB} K_{iP} K_{iQ} K_R k'_Q k'_R) - K_{PQ} K_B B_\infty (A_t + K_M) / (K_{iB} K_{iP} K_{iQ} K_R k'_R) - A_t \Gamma_M k_{cat} K_{PQ} K_B / (K_{iB} K_{iP} K_{iQ} K_R k'_B k'_R)] + j_{el}^4 [K_{iA} K_B K_M / (K_{iP} K_{iQ} K_R k'_Q k'_R) - K_P K_{iA} K_B / (K_{iP} K_{iQ} K_R k'_Q k'_R) - K_A K_M / (K_{iQ} K_{iP} k'_B k'_Q) + K_{iR} K_P K_B (A_t + K_M) / (K_{iB} K_{iP} K_{iQ} K_R k'_B k'_Q) - K_P K_B (A_t + K_M) / (K_{iP} K_{iQ} K_R k'_Q k'_R) - K_P K_B B_\infty / (K_{iB} K_{iP} K_{iQ} K_R k'_Q k'_R) - K_P K_B A_t \Gamma_M k_{cat} / (K_{iB} K_{iP} K_{iQ} K_R k'_B k'_Q k'_R) + K_A B_\infty K_M / (K_{iR} K_{iP} K_{iQ} k'_Q k'_R) + K_{PQ} K_B (A_t + K_M) / (K_{iB} K_{iP} K_{iQ} K_R k'_B k'_R)] + j_{el}^5 [K_P K_B (A_t + K_M) / (K_{iB} K_{iP} K_{iQ} K_R k'_B k'_Q k'_R) - K_A K_M / (K_{iR} K_{iP} K_{iQ} k'_B k'_Q k'_R)] \quad (S-18)$$

Use of the inhibition constants allows to redefine: $K_{PQ} = K_{iP} K_{iQ}$ and $K_{QR} = K_{iQ} K_R$.

The model takes into consideration the general flux of glutamate to the biosensor from a bulk solution, the general flux of enzymatic oxidation of glutamate by NAD^+ to give $NADH$, the general flux of $NADH$ reoxidation by Os-phendione-surfactant, and the general flux of charges from reduced Os-phendione-

surfactant to the electrode surface. In steady state all these fluxes are equal to each other and to hence to j_{el} . The possible polarization of glutamate and the products of its oxidation due to their slow transport through the lipid bilayers can make individual fluxes of enzymatic NAD^+ reduction by glutamate, individual fluxes of NADH reoxidation by the mediator be dependent of the distance from the graphite electrode. This polarization is taken into consideration by using general apparent mass transfer coefficients k'_B , k'_Q and k'_R . Another kind of polarization can be caused by the slow transport of charges from reduced Os-phendione-surfactant in lipid bilayers to the electrode surface, but this fact is reflected in the values of the general apparent constants k_M and k_{cat} which are defined through the kinetic constants k_7 , k_{-7} , k_8 and k_S , where k_S is the apparent constant of the heterogeneous charge transfer between the electrode surface and Os-phendione-surfactant molecules distributed throughout the film. So, the model does not describe the distribution of individual fluxes and concentrations throughout the lipid bilayers, but it describes the general current generated by glutamate oxidation in the film using apparent general kinetic constants which actually consider lipid bilayers' geometry.

Figures and Figure Captions.

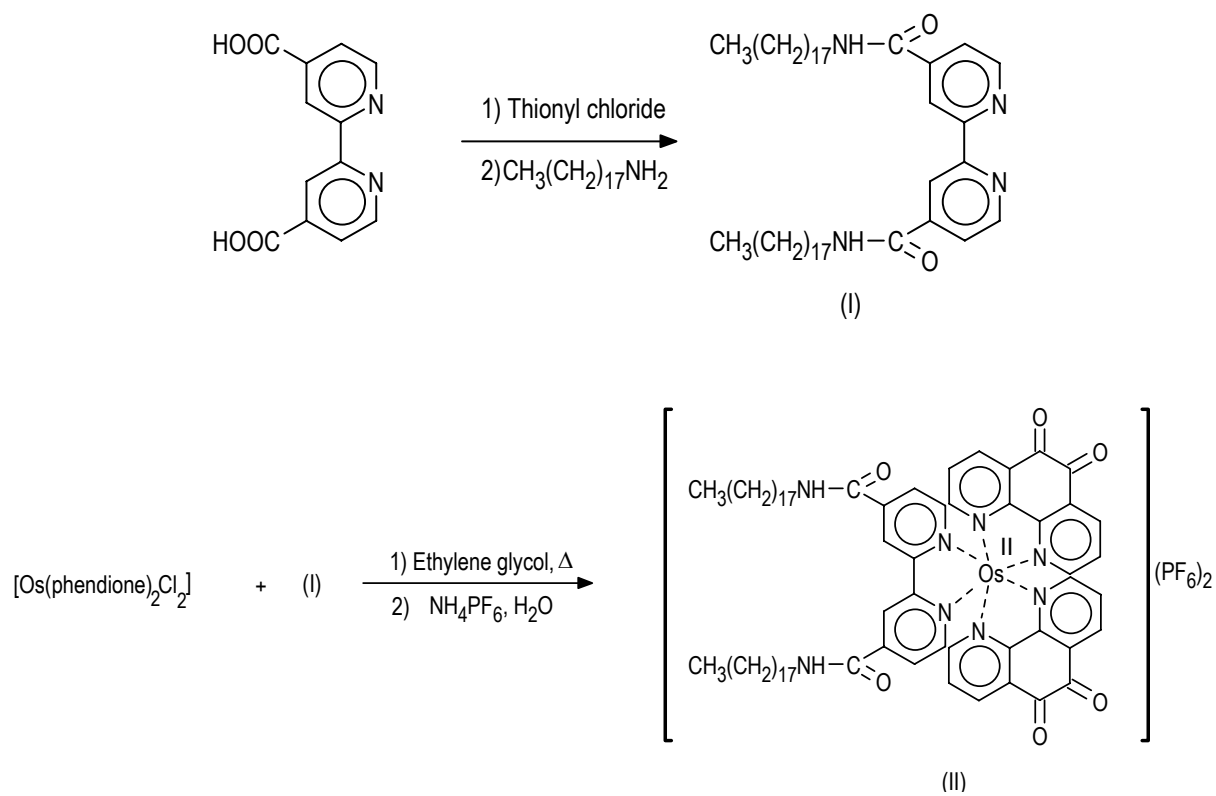


Figure S-1. Synthetic route to the NADH oxidizing tensoactive mediator Os-phendione-surfactant.

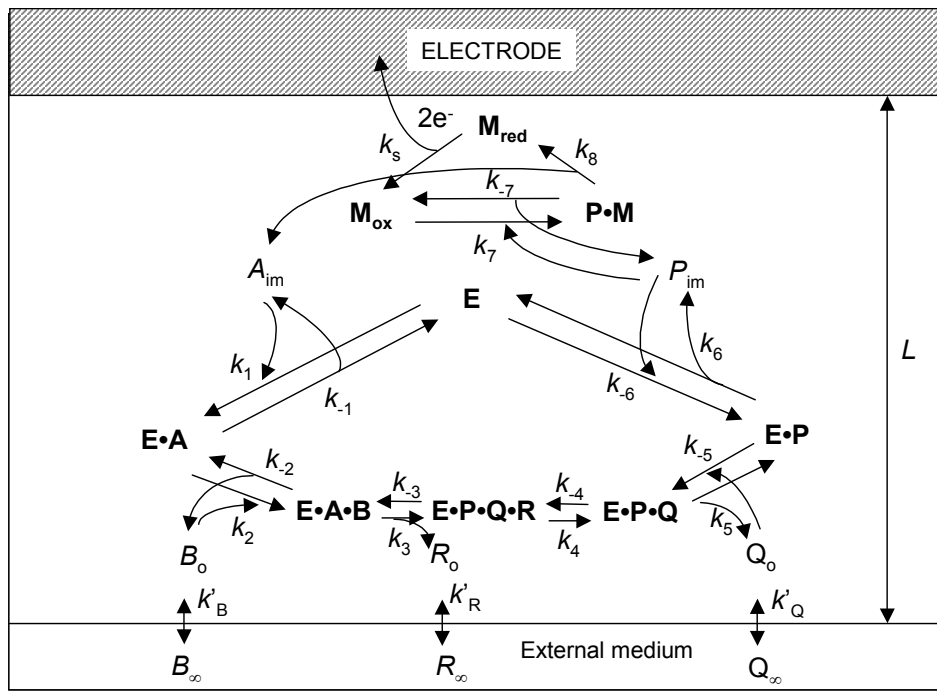


Figure S-2. Reaction scheme for a reagentless glutamate biosensor.

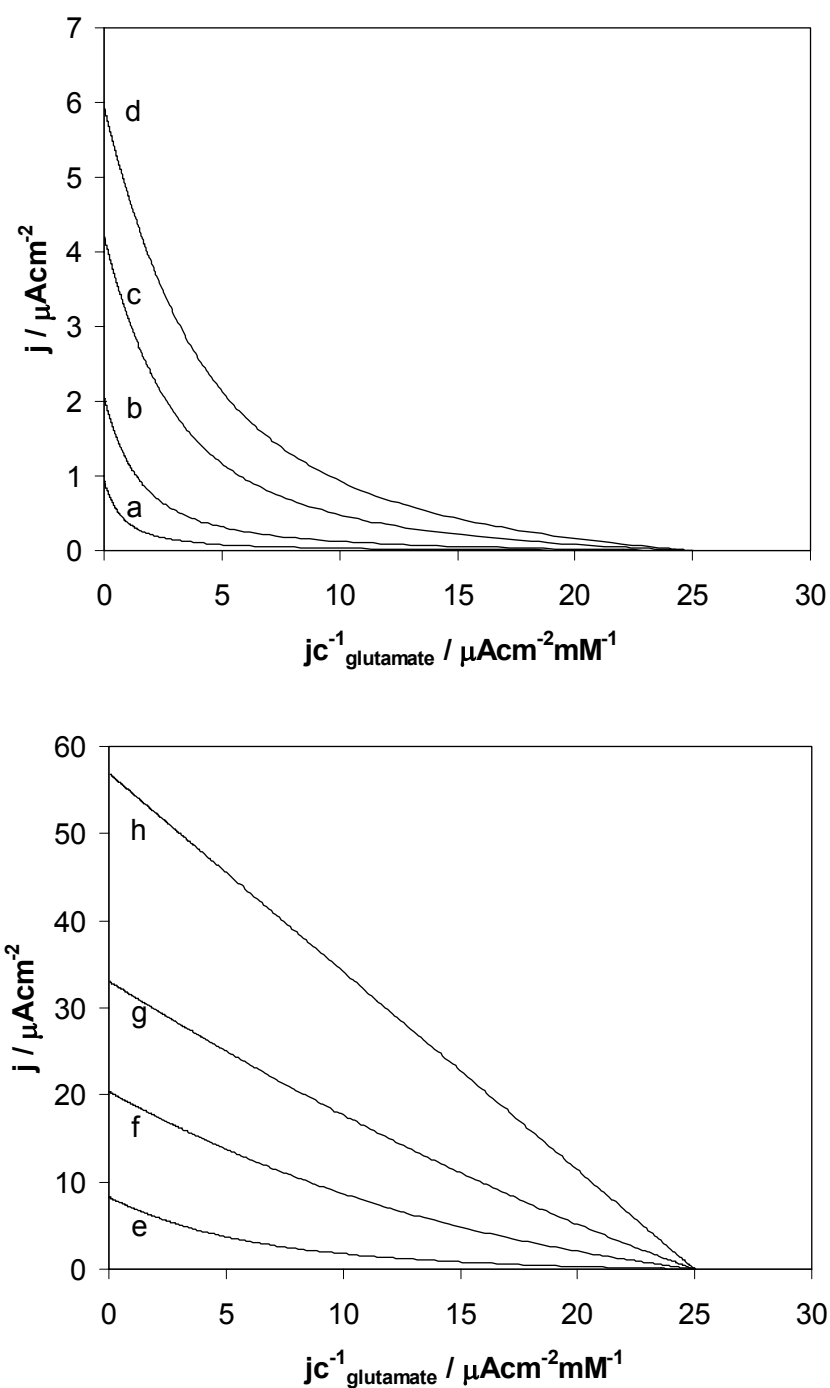


Figure S-3. Simulation of the Eadie-Hofstee plots for the reagentless glutamate biosensors with varying maximum fluxes of the electrochemical NADH oxidation (Γk_{cat}): a) $2.6 \times 10^{-11} \text{ mol s}^{-1} \text{ cm}^{-2}$; b) $1.04 \times 10^{-10} \text{ mol s}^{-1} \text{ cm}^{-2}$; c) $4.15 \times 10^{-10} \text{ mol s}^{-1} \text{ cm}^{-2}$; d) $8.3 \times 10^{-10} \text{ mol s}^{-1} \text{ cm}^{-2}$; e) $1.7 \times 10^{-9} \text{ mol s}^{-1} \text{ cm}^{-2}$; f) $1.3 \times 10^{-8} \text{ mol s}^{-1} \text{ cm}^{-2}$; g) $5.178 \times 10^{-8} \text{ mol s}^{-1} \text{ cm}^{-2}$; h) ∞ . The values of other parameters are: $A_t = 1 \text{ mM}$; $k'_B \rightarrow \infty$; $k'_Q \rightarrow \infty$; $k'_R \rightarrow \infty$; $LV_1 = 3.63 \times 10^{-10} \text{ mol s}^{-1} \text{ cm}^{-2}$; $K_M = 0.8 \text{ mM}$; $K_A = 0.23 \text{ mM}$; $K_B = 2.5 \text{ mM}$; $K_{AB} = 0.3 \text{ mM}^2$; $K_{iA} = 10 \text{ mM}$; $K_{iB} = 11 \text{ mM}$; $K_R = 20 \text{ mM}$; $K_Q = 0.25 \text{ mM}$; $K_P = 0.04 \text{ mM}$; $K_{iR} = 9 \text{ mM}$; $K_{iQ} = 1.6 \text{ mM}$; $K_{iP} = 0.03 \text{ mM}$.

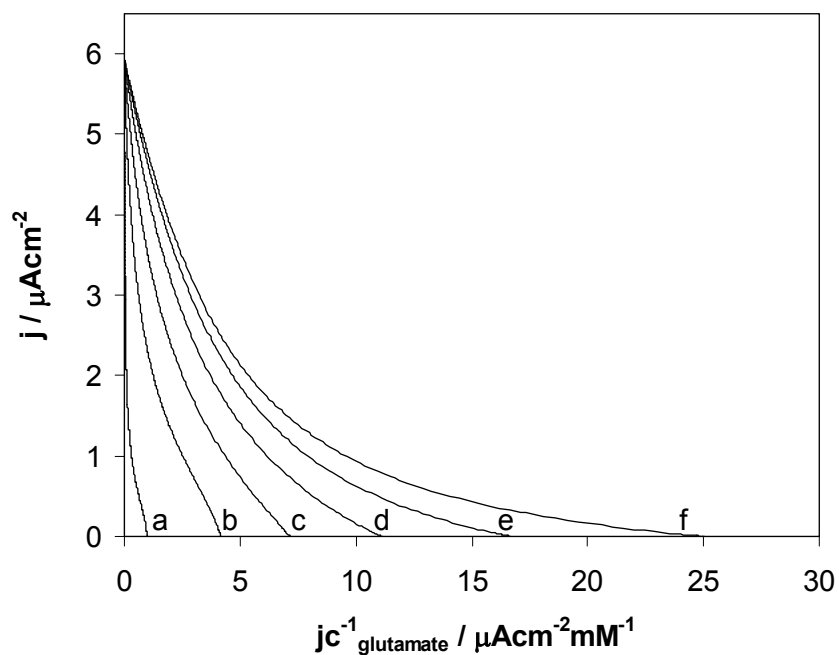


Figure S-4. Simulation of the Eadie-Hofstee plots for the reagentless glutamate biosensors with varying mass transfer coefficients (k'_B, k'_Q, k'_R): a) $5.18 \times 10^{-12} \text{ cm s}^{-1}$; b) $2.6 \times 10^{-11} \text{ cm s}^{-1}$; c) $5.18 \times 10^{-11} \text{ cm s}^{-1}$; d) $1.03 \times 10^{-10} \text{ cm s}^{-1}$; e) $2.6 \times 10^{-10} \text{ cm s}^{-1}$; f) ∞ . The values of other parameters are: $A_t = 1 \text{ mM}$; $LV_1 = 3.63 \times 10^{-10} \text{ mol s}^{-1} \text{ cm}^{-2}$; $\Gamma k_{\text{cat}} = 8.3 \times 10^{-10} \text{ mol s}^{-1} \text{ cm}^{-2}$; $K_M = 0.8 \text{ mM}$; $K_A = 0.23 \text{ mM}$; $K_B = 2.5 \text{ mM}$; $K_{AB} = 0.3 \text{ mM}^2$; $K_{iA} = 10 \text{ mM}$; $K_{iB} = 11 \text{ mM}$; $K_R = 20 \text{ mM}$; $K_Q = 0.25 \text{ mM}$; $K_P = 0.04 \text{ mM}$; $K_{iR} = 9 \text{ mM}$; $K_{iQ} = 1.6 \text{ mM}$; $K_{iP} = 0.03 \text{ mM}$.

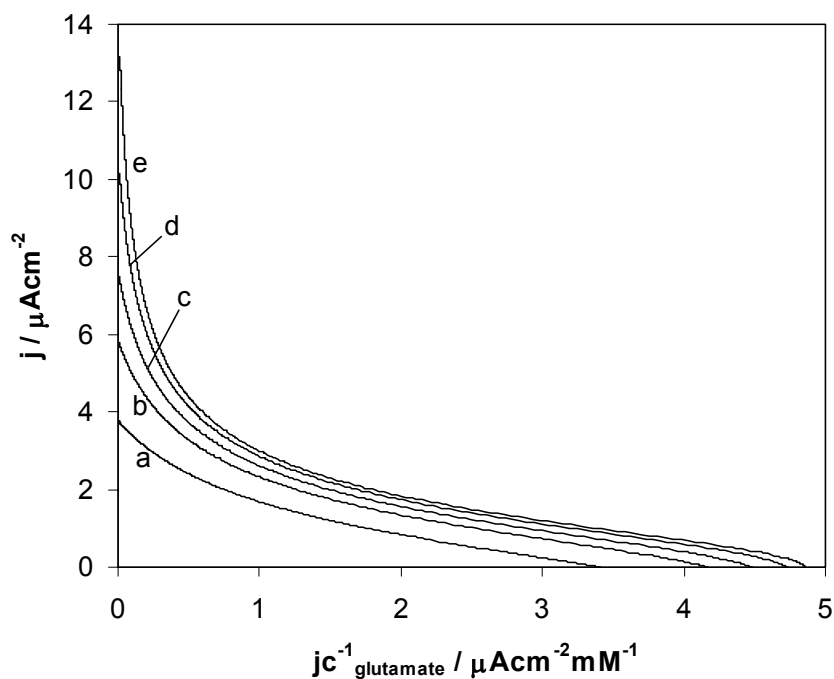


Figure S-5. Simulation of the Eadie-Hofstee plots for the reagentless glutamate biosensors with varying maximum flux of enzymatic reduction of NAD^+ (LV_1): a) $1.55 \times 10^{-10} \text{ mol s}^{-1} \text{ cm}^{-2}$; b) $3.63 \times 10^{-10} \text{ mol s}^{-1} \text{ cm}^{-2}$; c) $6.22 \times 10^{-10} \text{ mol s}^{-1} \text{ cm}^{-2}$; d) $1.24 \times 10^{-9} \text{ mol s}^{-1} \text{ cm}^{-2}$; e) $2.49 \times 10^{-9} \text{ mol s}^{-1} \text{ cm}^{-2}$. The values of other parameters are: $k'_B = 2.6 \times 10^{-11} \text{ cm s}^{-1}$; $k'_Q = 2.6 \times 10^{-11} \text{ cm s}^{-1}$; $k'_R = 2.6 \times 10^{-11} \text{ cm s}^{-1}$; $A_t = 1 \text{ mM}$; $I k_{\text{cat}} = 8.3 \times 10^{-10} \text{ mol s}^{-1} \text{ cm}^{-2}$; $K_M = 0.8 \text{ mM}$; $K_A = 0.23 \text{ mM}$; $K_B = 2.5 \text{ mM}$; $K_{AB} = 0.3 \text{ mM}^2$; $K_{iA} = 10 \text{ mM}$; $K_{iB} = 11 \text{ mM}$; $K_R = 20 \text{ mM}$; $K_Q = 0.25 \text{ mM}$; $K_P = 0.04 \text{ mM}$; $K_{iR} = 9 \text{ mM}$; $K_{iQ} = 1.6 \text{ mM}$; $K_{iP} = 0.03 \text{ mM}$.